The Calcium-Sensing Receptor (CaSR) as a Potential Mediator of Pollution-Induced Airway Cell Responses

Bethan Mansfield, BSc.

PhD Thesis 2022

SUMMARY

Exposure to ambient air pollution causes detrimental health effects and can sometimes be fatal, especially for those with lung diseases, such as asthma. Particulate matter (PM) forms a major component of ambient air pollution, drives acute exacerbations (worsening) of asthma symptoms, however, the cellular mechanisms underlying PM-induced asthma exacerbations are so far unclear.

The extracellular calcium-sensing receptor (CaSR) has been previously implicated in the development of asthma-like features in a range of *in vivo* models of asthma. Importantly, a negative allosteric modulator at the CaSR (CaSR NAM) reduces asthma-like features in these models. However, whether the CaSR plays a role in PM-induced airway cell responses was unclear. Therefore, during my thesis I investigated the role of the CaSR in PM-induced functions of airway and blood derived structural and immune cells. My principal discoveries are:

1. PM directly activates the CaSR in human embryonic kidney 293 cells (HEK293) which stably express the human CaSR (HEK-CaSR) cells, by increasing intracellular Ca^{2+}, an effect which can be abolished by co-treatment with NAM and that is not observed in control, vector-transfected (HEK-0) cells, which lack the CaSR
2. The CaSR is expressed at the protein level in airway epithelial cells and lung- and blood-derived immune cells, involved in sensing and responding to inhaled PM, and in the pathogenesis of lung diseases which are exacerbated by exposure to PM
3. The CaSR plays a key role in PM- and pro-inflammatory cytokine-induced maturation of dendritic cells (DC), and PM-induced cytokine secretion by DCs, effects which are reduced by CaSR NAM.

In addition to my novel findings:

4. Undifferentiated basal human bronchial epithelial cells are characterised by low functional expression of the CaSR, using intracellular Ca^{2+} as a biological readout for CaSR activation, therefore more work is required to establish a more suitable CaSR-expressing *in vitro* model of airway epithelial cells
5. Exposure of PM to "Healthy" alveolar macrophages (AMs) does not affect efferocytosis, a key resolving function of AMs, therefore, more work is required to better understand the effects of PM on key functions of AMs

Together, my findings promote the CaSR as one of the mechanisms behind PM-sensing and responding in the airways, which drives pro-inflammatory features associated with asthma exacerbations. Therefore, CaSR NAM have the potential to provide an effective "all-in-one" therapeutic for asthma to directly counteract exaggerated inflammatory responses to inhaled stimuli, such as PM.

ACKNOWLEDGEMENTS

First, I would like to thank the Knowledge Economy Skills Scholarships (KESS) 2 in partnership with Respiratory Innovation Wales (RIW) for funding my PhD position and providing me with opportunities to network and travel to collaborators laboratories and National and International Conferences to present my work. I give a special thanks to Prof. Kier Lewis of RIW for providing invaluable kindness, support, and opportunities throughout my PhD.

My biggest thanks goes to my supervisor Prof. Daniela Riccardi for your unending support, kindness, and belief in me throughout my PhD. I would also like to thank Professor Paul Kemp for the support and laughter you have provided since I was an undergraduate and throughout my PhD. I am so grateful for both your encouragement and support throughout my PhD and especially following my accident. Finally, I would also like to give a special thanks to Kasope Wolffs, for being such a good friend and PhD colleague, I am going to miss working closely with you. I would also like to thank Ping Huang, David Evans, Richard Bruce, and Petar Popov for providing such a friendly and supportive working environment and "Mexican Mondays" pre-COVID.

A huge thanks goes to all our collaborators who provided assistance with my work and contributed their expertise: Dr Polina Yarova, Prof Luzheng Xue, Dr Jian Luo, Dr Simon Scofield, Dr Zoë Prytherch, and Mr Mike O'Reilly. I would also like to give a massive thank you to those at numerous institutions who hosted me as a visiting scientist: Prof Luis Mur from Aberystwyth University, Prof. Catherine Hawrylowicz and Dr Tzer-Ren Ho from King's College London and Prof. David Thickett and Dr Sebastian Lugg from The University of Birmingham. Together, you have all helped to generate the data contained within my thesis and I am so grateful for my experiences working with you all.

Finally, I am immensely grateful for the support and love provided by my family, thanks Mum, Dad and Mike for your unending encouragement and belief in me throughout my life. Special thanks goes to Shaun for your faith in me during my PhD, I would not have been able to do this without you. In addition, I would like to thank all my friends outside of university for the kindness, support, and encouragement… I did it!!

TABLE OF CONTENTS

LIST OF ABBREVIATIONS

$1,25(OH)_2D_3$	Vitamin D3
A_{230}	Absorbance at 230 nm
A_{260}	Absorbance at 260 nm
A_{280}	Absorbance at 280 nm
A549	Lung Carcinoma Epithelial Cell Line
ABC	Avidin/Biotin Complex
ABDF	Antibody Dilution Fluid
ADH1	Autosomal Dominant Hypocalcaemia Type 1
ADIS	Agonist Driven Insertional Signalling
AHR	Airway Hyperresponsiveness
Akt	Protein Kinase B
ALI	Air-Liquid Interface
AM	Alveolar Macrophage
AMR	ATP Monitoring Reagent
ANOVA	Analysis of Variance
APC	Allophycocyanin
ASM	Airway Smooth Muscle
ATP	Adenosine Triphosphate
BALF	Broncho Alveolar Lavage Fluid
BCA	CD1c biotin
BLAST	Basic Local Alignment Search Tool
BR	Broad Range
BSA	Bovine Serum Albumin
cAMP	Cyclic Adenosine Monophosphate
CaSR	Calcium-Sensing Receptor
CBA	Cytometric bead array
CD	Cluster of Differentiation

CD4	T helper cell
CD8	Cytotoxic T cell
CDC	Centre for Disease Control and Prevention
cDC	Myeloid/Conventional Dendritic Cell
COPD	Chronic Obstructive Pulmonary Disease
CRTH2	Prostaglandin D 2 Receptor
CS	Cigarette Smoke
CSE	Cigarette Smoke Extract
CT	Cycle Threshold
cyt-D	Cytochalasin D
DAB	3,3'-Diaminobenzidine
DAG	Diacylglycerol
DAMP	Damage-associated Molecular Pattern
DAPI	4',6-Diamidino-2-Phenylindole
DC	Dendritic Cell
DEP	Diesel Exhaust Particle
DMEM	Dulbecco's Modified Eagle Medium
DMSO	Dimethyl Sulfoxide
dNTP	Deoxynucleoside Triphosphate
ECD	Extracellular Domain
ECP	Eosinophillic Cationic Protein
ECS	Extracellular Solution
EDTA	Ethylenediaminetetraacetic Acid
ERK	Extracellular Signal-Regulated Kinase
ERS	European Respiratory Society
FACS	Flow Assisted Cell Sorting
FBS	Fetal Bovine Serum
FDA	The Food and Drug Administration

FEV_1	Forced Expiratory Volume in the First Second
FITC	Fluorescein Isothiocyanate
fMLP	N-formyl-Met-Leu-Phe
FMO	Fluorescence Minus One
FSC	Forward Scatter
GAPDH	Glyceraldehyde-3-Phosphate
GC	Gas Chromatography
GM-CSF	Granulocyte Macrophage Colony Stimulating Factor
GPCR	G Protein-Coupled Receptor
GSH	Reduced Glutathione
GSSG	Oxidised Glutathione
GTP	Guanosine Triphosphate
HBEC	Human Bronchial Epithelial Cells
HBSS	Hanks' Balanced Salt Solution
HEK293	Human Embryonic Kidney Cell Line
HEPES	4-(2-Hydroxyethyl)-1-Piperazineethanesulfonic Acid
HI	Heat Inactivated
HLA-DR	Human Leukocyte Antigen
HLA-DR	Human Leukocyte Antigen
IARC	International Agency for Research on Cancer
ICP/MS	Inductively Coupled Plasma Mass Spectrometry
IFN-γ	Interferon-gamma
IHC	Immunohistochemistry
IL	Interleukin
ILC2	Type 2 Innate Lymphoid Cell
IP_3	Inositol Trisphosphate
IPF	Idiopathic Pulmonary Fibrosis
LABA	Long acting ß2 Adrenergic Receptor Agonist

LAMA	Long-acting Muscarinic Receptor Antagonist
LDH	Lactate Dehydrogenase
LPS	Lipopolysaccharide
M1	"Pro-inflammatory" Macrophage
M2	"Anti-inflammatory" Macrophage
MACS Buffer	2% FBS in 1X PBS with 8 µM EDTA
MAPK	Mitogen-activated Protein Kinase
MBP	Major Basic Protein
MDDC	Monocyte-Derived Dendritic Cell
MDM	Monocyte-Derived Macrophage
MerTK	MER proto-oncogene tyrosine kinase
MFI	Median Fluorescence Intensity
MHC	Major Histocompatibility Complex
MS	Mass Spectrometry
mTOR	Mammalian Target of Rapamycin
NAM	Negative Allosteric Modulator at the Calcium-Sensing Receptor
NCBI	National Centre for Biotechnology Information
NHBEC	Normal Human Bronchial Epithelial Cell
NIST	National Institute of Standards and Technology
NK	Natural Killer Cell
NLRP3	NOD-, LRR- and Pyrin Domain-Containing Protein 3
non-T2	Non-Type 2 Immune Response
NT	No-template
NTC	No-template Control
OCS	Oral Corticosteroid
OVA	Ovalbumin
PAH	Pulmonary Arterial Hypertension
PAM	Positive Allosteric Modulator at the Calcium-Sensing Receptor

PAMP	Pathogen Associated Molecular Pattern
PBMC	Human Peripheral Blood Mononuclear Cell
PBS	Phosphate Buffered Saline
PCR	Polymerase Chain Reaction
pDC	Plasmacytoid Dendritic Cell
PDL	Poly-D-Lysine
PE	Phycoerythrin
PFA	Paraformaldehyde
PI	Propidium Iodide
PI3K	Phosphoinositide 3-kinase
PKA,	Protein Kinase A
PKC	Protein Kinase C
PLA_2	Phospholipase A_2
PLC	Phospholipase C
PM	Particulate Matter
$PM_{0.1}$	Ultrafine Particulate Matter with Particles with a Diameter of <0.1 µm
PM_{10}	Coarse Particulate Matter with Particles with a Diameter of <10 µm
$PM_{2.5}$	Fine Particulate Matter with Particles with a Diameter of <2.5 µm
PMA	Phorbol 12-Myristate 13-Acetate
PMT	Photomultiplier Tube
PTH	Parathyroid Hormone
RBC	Red Blood Cell
REC	Research Ethics Committee
RIN^e	RNA Integrity Number
RMPI	Roswell Park Memorial Institute Culture Medium
ROS	Reactive Oxygen Species

RPS	Rapid Perfusion System
RT	Room Temperature
RT-qPCR	Real Time Quantitative Polymerase Chain Reaction
SABA	Short-Acting ß2 Adrenergic Receptor Agonist
SBP	Sulphobromophtalein
SD	Standard Deviation
SIM	Selective Ion Mode
SPME	Solid Phase Micro Extraction
SRM1648	Standard Reference Material of Urban Particulate Matter - 1648a
SRM2975	Standard Reference Material of Diesel Exhaust Particulates - 2975
SSC	Side Scatter
T2	Type 2 Immune Response
TAE	Tris-Acetate Buffer
TC	Tissue Culture Grade
Th17	T -helper 17 cells
THP	Human Leukaemia Monocytic Cell Line
TLR	Toll-like Receptor
TMD	Transmembrane Domain
TNF-α	Tumour Necrosis Factor-α
TSLP	Thymic Stromal Lymphopoietin
UDG	Uracil DNA Glycosylase
VC	Vehicle Control
VFT	Venus Flytrap
WHO	The World Health Organisation

LIST OF FIGURES AND TABLES

CHAPTER 1: INTRODUCTION.

1.1 Air Pollution:

The detrimental effects of poor air quality on public health have been reported as far back as Roman times, therefore ambient air pollution has afflicted the global population for thousands of years. For five days in 1952, a lethal smog covered the city of London, UK, culminating in an increased prevalence of chronic lung disease and ~12,000 deaths (Marsh 1963; Bell *et al.* 2004). As a result, by 1956, the UK Parliament enacted the UK Clean Air Act, outlining the need to reduce emission of harmful pollutants into the atmosphere, from urban sources. In 1968, the US Congress also enacted the US Clean Air Act, due to a similar lethal smog episode, in Donora, Pennsylvania. The UK and US Clean Air Acts both provided a framework for regulation of ambient air pollution levels, to improve Public Health.

Generally, these commitments to improve air quality have proved successful, with an overall reduction of ambient air pollution since the 1970's in the UK and US (Ritchie and Roser 2019). However, cities across the globe regularly exceed the regulatory levels of air pollution imposed by these acts through continued emission of ambient air pollution, mostly from urban environments. Globally the issue is regarded with a varying degree of importance and urgency, therefore there are large discrepancies in the amount of pollution deemed acceptable from country to country. As a result, The World Health Organisation (WHO) states that air pollution poses the world's largest environmental health risk with 9 out of every 10 people worldwide living in areas of poor air quality. Moreover, it is estimated that an annual excess of 8.8 million premature deaths occur globally, due to exposure to harmful levels of

air pollution (Lelieveld, Pozzer, Pöschl, *et al.* 2020). These figures highlight the importance of understanding the sources and components of ambient air pollution and their influence on the detrimental health effects induced by exposure.

1.2. The Effect of Ambient Air Pollution on Public Health:

Exposure to ambient air pollution, both short- and long-term, drives a range of adverse cardiopulmonary effects, which have been evidenced through the development of a large and robust literature base. The bioavailability of the components of ambient air pollution is dictated by the solubility and size fractions of the components. Conversely the toxicological aspects, of ambient air pollution, resulting in detrimental effects on health, are largely dictated by the source and chemical composition of ambient air pollution, especially at sites of deposition of pollution, such as the lungs (Kelly and Fussell 2015). The lungs provide the interface between inhaled components of ambient air pollution and associated downstream responses, which propose children, older people and those who suffer from heart or lung disease, as particularly susceptible to pollution-induced detrimental effects on lung development or heart/lung disease pathogenesis. There is increasing evidence that exposure to ambient air pollution drives abberant lung development in young subjects (between 10 and 18 years old), with chronically reduced lung growth rate, leading to lung function deficits, such as decreased forced expiratory volume in one minute (FEV_1), over time (Horak *et al.* 2002; Brauer *et al.* 2012; Mölter *et al.* 2013; Guo *et al.* 2018). Furthermore, chronic exposure to ambient air pollution is linked to airways remodelling, which culminates in chronic obstructions to airflow due to associated inflammation and mucus hypersecretion, associated with lung diseases, such as asthma (Churg *et al.*

2003). Finally, exposure to ambient air pollution drives acute exacerbations of disease symptoms, presentation to the emergency department, and subsequent hospitalisation for patients suffering with asthma (Zheng *et al.* 2015; Anenberg *et al.* 2018; Keet *et al.* 2018; Yang *et al.* 2021), chronic obstructive pulmonary disease (COPD) (Gan *et al.* 2013; Wang *et al.* 2019; Zhang *et al.* 2021), and more recently, idiopathic pulmonary fibrosis (IPF) (Winterbottom *et al.* 2018; Dales *et al.* 2020; Majewski and Piotrowski 2020).

1.2.1 Asthma Burden and Pathogenesis:

Asthma is one of the most prevalent chronic respiratory diseases, affecting ~ 300 million people worldwide and contributing to ~ 460,000 deaths during 2019, highlighting the global burden of this chronic disease (Global Burden of Disease 2019). Asthma is characterised by airway hyperresponsiveness (AHR), inflammation, and remodelling. The condition is acutely exacerbated upon exposure to inhaled stimuli, such as those contained within ambient air pollution, driven by type-2 (T2) or non-T2 responses, culminating in mainly eosinophilic (T2) or neutrophilic (non-T2) airways disease, with the latter sometimes termed severe or difficult-to-treat asthma, in patients who are unresponsive to any of the available treatments. These acute exacerbations upon exposure to ambient air pollution are referred to as "asthma attacks" which promote asthma pathogenesis and can sometimes prove fatal. Recently, under a landmark ruling, a coroner in the UK ruled that exposure to harmful levels of air pollution, generated by traffic, was the cause of death of nine-year-old asthma sufferer, Ella Kissi-Debrah, from London (Barlow 2021). This further highlights the danger to health posed by exposure to ambient air pollution in people with pre-existing chronic inflammatory lung diseases, such as asthma, resulting in a new clean air law in the UK, termed Ella's Law

(Vaughan 2021). However, the potential of exposure to ambient air pollution as a driver of the onset of asthma remains unclear. Some studies suggest that exposure to ambient air pollution can drive onset of childhood asthma, however, these findings are suggestive and require further investigation to fully understand and support the potential of pollution-induced onset of asthma (Bowatte *et al.* 2015; Khreis *et al.* 2017; Thurston *et al.* 2020).

1.3 Sources and Components of Ambient Air Pollution:

Ambient air pollution is generated and emitted from a wide range of anthropogenic and non-anthropogenic sources, resulting in primary and secondary components of air pollution. Air pollution which is emitted from a direct source such as diesel and petrol combustion engines, combustion of solid fuels such as coal, and more recently, the increase in wildfires seen across Europe, USA, Australia, and Southeast Asia, are classified as primary components of ambient air pollution. In addition to exposure to pollution emitted from diesel/petrol combustion engines, exposure to the pollution contained within wildfire smoke is also closely associated to increasing hospital admissions and acute exacerbations of the symptoms of lung diseases (Aguilera *et al.* 2021). Although efforts are being made to reduce levels of ambient air pollution from combustion of diesel and petrol, and solid fuels, the concurrent increase in the recent, devastating wildfires now evident across the globe, invokes fear that these interventions may be too late.

Secondary components of ambient air pollution result from the chemical reactions of gaseous pollutants, such as sulphur dioxide and oxides of nitrogen, which are emitted from combustion of sulphur-containing fossil fuels. Some ambient air pollution is made up of both primary and secondary

components, such as the particles produced from increased urbanisation, combustion of fossil fuels, cigarette smoking, diesel, and incineration of waste and sewage products (International Agency for Research on Cancer (IARC) 2016; Centers for Disease Control and Prevention (CDC) 2019). Together, these sources of pollution are emitted and produce solid and gaseous particles suspended in the air which aggregate together to form particulate matter (PM), one of the major components of air pollution. PM is thought to a major contributor to pollution-induced exacerbations of symptoms in chronic inflammatory lung diseases, such as asthma (World Health Organization, 2013).

1.4 Particulate matter:

Particulate Matter (PM) is a heterogeneous collection of different sized solid and/or liquid particles suspended in the air, ranging from 1 nm to 100 μm in diameter. PM is made up of both organic and inorganic constituents that are classified into size ranges, based on their aerodynamic diameters: $PM_{2.5}$ (fine PM), particulates that have a diameter ≤2.5 μm, while PM_{10} are particulates that have a diameter ≤10 μm. Finally, $PM_{0.1}$ (ultrafine PM) are particles with a diameter of <0.1 μm (Esworthy, 2014). Particles which are contained between the range of 2.5 and 10 μm in diameter ($PM_{2.5-10}$), is often referred to as the coarse mode of PM. Particulates obtained from combustion of petrol, diesel, oil, and wood produce much of the PM contained within this coarse fraction. Moreover, the coarse fractions of PM include dust from construction sites, landfills, agriculture, wildfires, industrial sources, and fragments of bacteria, highlighting the variety of sources and complexity of components of PM (Lelieveld *et al.* 2015; Guo *et al.* 2018). Each component of ambient air pollution in isolation and together, pose a significant risk for the development of

detrimental health effects for those exposed to ambient air pollution, especially for those suffering from lung diseases, such as asthma.

The WHO states that $PM_{2.5}$ and PM_{10} levels should not exceed an annual mean of 10 and 20 μg/m^3, respectively. However, the UK currently sets its levels for $PM_{2.5}$ and PM_{10} much higher at 25 and 40 μg/m^3, respectively. There is increasing evidence that adverse health effects occur from $PM_{2.5}$ exposure levels of 5-10 μg/m^3 (Næss *et al.* 2007; Ostro *et al.* 2007; Cesaroni *et al.* 2014), highlighting the necessity to regulate levels of PM exposure, to reduce detrimental health effects observed at high levels of PM exposure. Moreover, childhood exposure to an excess of PM ($PM_{2.5}$ at 65 μg/m^3, more than twice the limit set by the WHO) results in significant risk of developing respiratory symptoms related to asthma and increased use of asthma medication (Gold *et al.* 2000; Guaita *et al.* 2011). These health effects are often largely dependent on the size fraction, source, and chemical composition of PM, rendering it difficult to assess which components of PM drives adverse health effects, such as an exacerbation of asthma symptoms.

The size of PM particles has been directly implicated as the main driver of health-related issues regarding PM exposure (Brown *et al.* 2013). Generally, smaller particles contained within PM can penetrate the lungs on a deeper level than the larger particles, meaning that PM containing small and larger particles are deposited along the length of the respiratory tract, following inhalation. During nasal breathing, coarse PM is deposited and lodged in the trachea or in the bronchi (Atkinson et al. 2012), however, some of this is filtered out by the mucociliary escalator, which acts to move mucus (and therefore PM contained within it) out of the lungs where it can be expelled by coughing or swallowing (Cadelis *et al.* 2014; Bustamante-Marin and Ostrowski 2017)).

Therefore, particles which have the most impact on human health are <10 μm in diameter, due to their ability to penetrate deep into the lung and not be filtered by the mucociliary escalator, which results in deposition along the whole respiratory tract (Löndahl *et al.* 2007). Coarse PM particles that reside between 5 and 10 μm in diameter are deposited in the tracheobronchial tree, whereas smaller particles, such as those between 1 and 5 μm in diameter, are deposited in the respiratory bronchioles and alveoli, the site of gaseous exchange (Löndahl *et al.* 2007) (Figure 1.1, from Goossens et al. 2021). Finally, the ultrafine particles at <0.1 μm in diameter, penetrate deep into the lung, posing potential implications on gaseous exchange and systemic health effects due to passage of ultrafine PM into the circulation (Valavanidis *et al.* 2008).

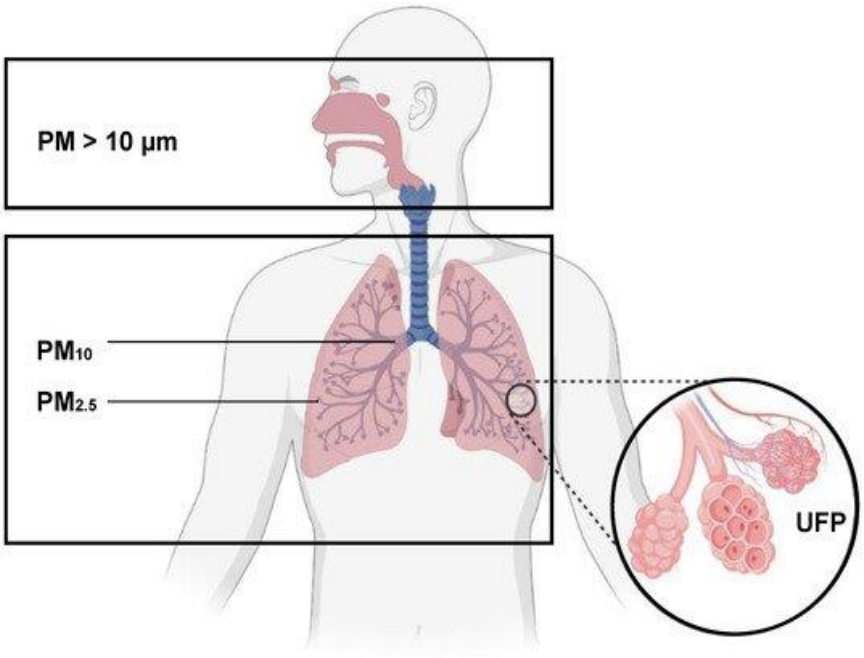

Figure 1.1: Particulate matter (PM) size and suggested deposition in the airways. PM consists of multiple particle sizes which deposits at distinct sites of the airways *in vivo*. PM at more than 10 µm in diameter (PM > 10 µm) accumulates in the upper airways and are filtered by the nose. PM at less than 10 µm in diameter (PM_{10}) penetrates deeper into the airways and is deposited in the tracheobronchial tree. PM <2.5 µm in diameter ($PM_{2.5}$) will also deposit here, however, accumulates deeper in the terminal bronchioles and alveoli. Finally, ultrafine particles (UFP), with diameters <0.1 µm, accumulate at the level of the alveoli and can diffuse into the systemic circulation. Figure from Goossens et al 2021.

PM induces effects on the cells it directly encounters, via inhaled or circulatory routes, and those that are activated indirectly by downstream mechanisms induced by other cells directly exposed to PM. These cells include the primary site for inhaled PM deposition, the airway epithelium, and immune cells, such as alveolar macrophages (AMs) and dendritic cells (DCs) which together, are directly activated by PM and form the first line of defence from inhaled stimuli, such as PM. These cells work together to orchestrate a variety of pro-inflammatory responses to PM exposure, via direct or indirect mechanisms, which are thought to culminate in cellular dysfunction and injury, and subsequent local and systemic inflammation. However, the mechanisms underpinning detrimental PM-induced airway effects, associated with exacerbations of asthma, remains poorly understood.

1.5 The Effects of Particulate Matter on Airway Structural and Immune Cells and Their Contribution to Asthma:

1.5.1 The Structure and Function of the Airway Epithelium:

The human respiratory tract is divided into the upper (nasal cavity, pharynx, and larynx) and lower, conducting zone of the airways (trachea and bronchi). The epithelial cells which line the whole respiratory tract form the barrier between the internal and external environment. Due to the often-polluted state of our external environment this barrier comprises the frontline of defence against air pollution. The airway epithelium is directly exposed to the external environment and therefore has a sensing capacity to determine components of inhaled air to initiate cellular responses to stimuli, such as PM.

The airway epithelium exists as a pseudostratified epithelium, made up of heterogeneous cell populations including basal cells, ciliated cells, club cells, and goblet cells. Basal cells are secured to the basement membrane of the

airway epithelium and comprise 6-31% of airway epithelial cells in humans, depending on their location in the airways (Boers *et al.* 2012; Crystal 2014). These cells are responsible for maintaining respiratory homeostasis, and most importantly, the ability to self-renew post-injury and differentiate into most other airway epithelial cells, such as club, ciliated and goblet cells (Hong *et al.* 2004; Hajj *et al.* 2007; Rock *et al.* 2009). Club cells, previously termed Clara cells, dominate the airway epithelium of the respiratory bronchioles (Boers *et al.* 1999). Club cells are one of the secretory cells, which also act as stem cells to facilitate epithelial repair, generation of ciliated and goblet cells, and can dedifferentiate into basal cells, if required, to repopulate basal cells under loss due to damage for example (Hong *et al.* 2001; Tata *et al.* 2013; Basil *et al.* 2020). Ciliated cells are terminally differentiated cells located throughout the airways and are descendants of club and goblet cells (Garcıá *et al.* 2019). Ciliated cells play a critical role in airways homeostasis by trapping, sensing, and expelling microorganisms, and inhaled particles, such as PM, through the rhythmic beating of cilia, via the mucociliary escalator mechanism (Bustamante-Marin and Ostrowski 2017). Goblet cells, which are derived from club cells, comprise the chief mucus secreting cells of the airways, contributing to the mechanism of mucociliary clearance, mentioned above (Whitsett 2018). Finally, in the alveolus, a simple squamous epithelium provides the physical barrier between the internal and external environment, made up of type I and II alveolar epithelial cells. This epithelium provides the surface for gas exchange, which makes up the respiratory zone of the airways. These cells also contribute to lung homeostasis, driven by the renewal capacity of type II alveolar epithelial cells (Guillot *et al.* 2013). The epithelial cells which line the airways are closely associated with specialised immune cells and work together to effectively

maintain airways homeostasis by rapid responses to inhaled stimuli, such as PM (Figure 1.2, taken from Invernizzi et al. 2020).

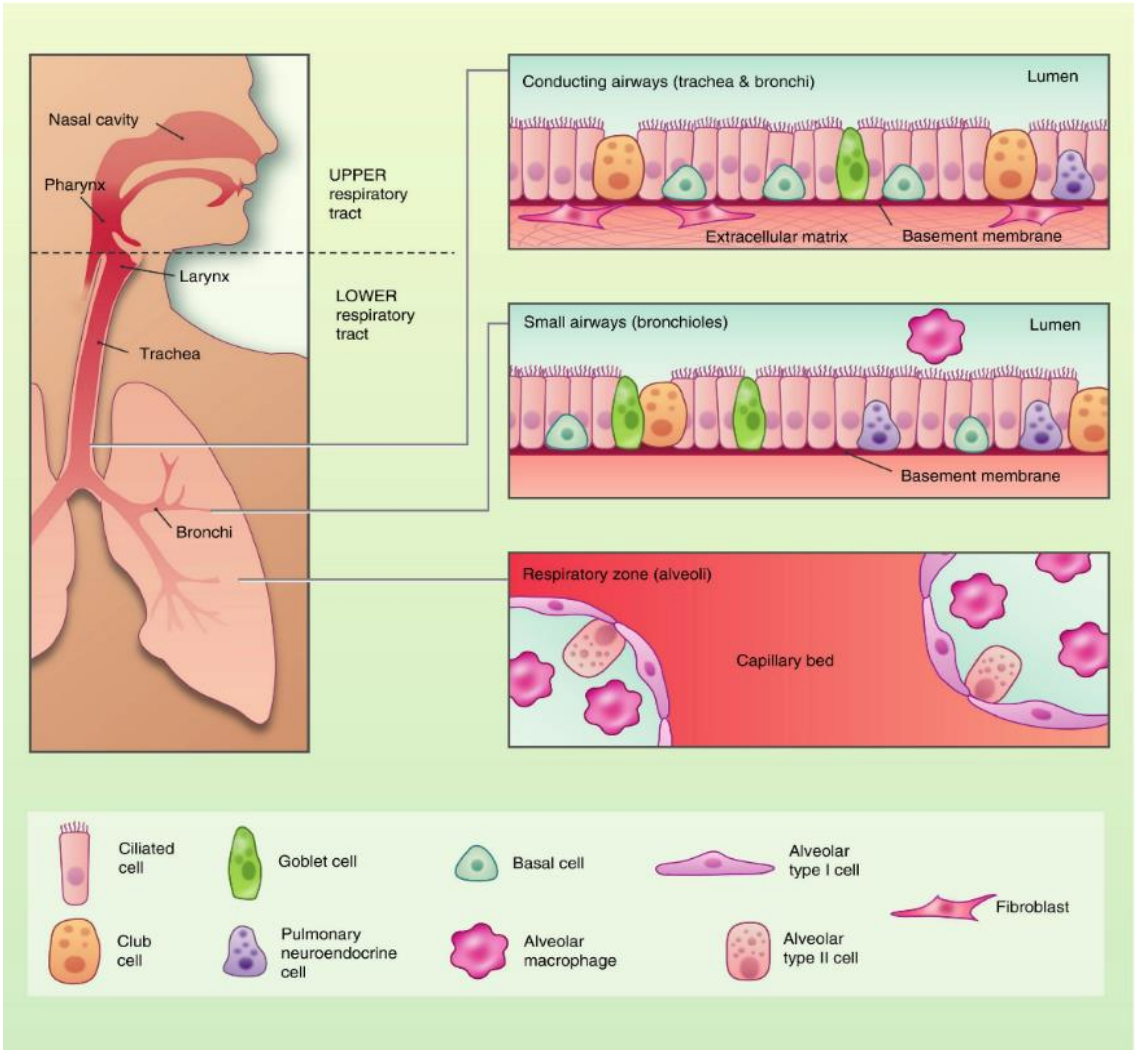

Figure 1.2: Composition of the respiratory epithelium. The respiratory tract is divided into the upper respiratory tract which includes the nasal cavity, pharynx, and larynx. The lower respiratory tract comprises the conducting airways (trachea and bronchi), the small airways (bronchioles) and the respiratory zone (alveoli). The trachea and large airways are made up of ciliated cells, goblet cells, neuroendocrine cells, and basal stem cells. Fibroblasts provide extracellular matrix which provide structural integrity and modulate airway epithelial cell turnover. The alveoli are comprised of type I and II alveolar cells (pneumocytes) and presence of alveolar macrophages. Image taken from review by Invernizzi et al (2020).

1.5.2 The Role of The Airway Epithelium in Response to Particulate Matter Exposure:

As mentioned above, the airway epithelium provides a physical barrier between the external and internal environments, and is therefore a prime target for inhaled stimuli, such as PM. Continued exposure to PM is generally thought to induce damage to the airway epithelium, which triggers release of damage associated molecular patterns (DAMPs), such as thymic stromal lymphopoietin (TSLP) and interleukin (IL)-33. These DAMPs are potent mediators of pro-inflammatory responses to inhaled noxious stimuli, such as PM. These effects have previously been investigated using *in vitro* models of human bronchial epithelial cells (HBECs) (Bleck *et al.* 2010). Furthermore, release of TSLP and IL-33 from HBECs has been shown to primarily drive T2 immune responses, where both mediate recruitment and modulation of innate immune cells, such as monocytes and neutrophils, and skews the immune response of DCs to a T2 phenotype and "allergic"-like responses (van Eeden et al. 2001; Bleck et al. 2008; Bleck et al. 2011; Matsuda Futamura et al. 2019). However, HBEC exposure to PM also induces secretion of pro-inflammatory cytokines such as IL-1ß, IL-6 and IL-8, which are associated with both T2 and non-T2 responses, highlighting the wide range of pro-inflammatory responses induced by PM exposure to HBECs *in vitro*. These pro-inflammatory cytokines go on to mediate recruitment of blood-derived inflammatory cells, such as monocytes and neutrophils, which further contribute to the pro-inflammatory effects induced by exposure to PM (Fujii *et al.* 2001; Ishii *et al.* 2005; Pfeffer, Ho, *et al.* 2018). These findings highlight the orchestration of immune responses by HBEC, through activation of a variety of cells, in response to exposure to inhaled stimuli, such as PM. Despite these findings, the

mechanisms underpinning PM-induced pro-inflammatory responses of the airway epithelium, remain poorly understood.

1.5.3 The Functions of Alveolar Macrophages:

AMs are the primary phagocytic cells of the lungs and therefore play an important role in maintaining lung homeostasis (Mitsi *et al.* 2018). AMs reside in the lining fluid of the alveolar space, where they are prepared to engulf infectious, toxic, or allergic particles or pathogens that have evaded the mechanical defences of the respiratory tract, such as the mucociliary escalator (Rubins 2003; Davidson and Patel 2014). AMs sample the inhaled environment via endocytic processes such as phagocytosis, macropinocytosis (engulfment of large amounts of extracellular fluid by budding vesicles) and efferocytosis (engulfment of apoptotic cells by cytoskeletal rearrangements). Following detection of inhaled particles or pathogens, such as PM, an inflammatory response may be initiated (Greenlee-Wacker 2016).

Generally, macrophages polarise to a pro-inflammatory, phagocytic phenotype (M1) or conversely, to an anti-inflammatory, wound healing, and remodelling macrophage phenotype (M2). Under chronic stimulation, M1 macrophages result in tissue damage and M2 macrophages result in pro-fibrotic responses, however, the switching of macrophages between phenotypes is dependent upon the cytokine milieu and therefore inflammatory status of the airways. M1 and M2 macrophages drive T2 and non-T2 responses respectively (Mills 2012; Mitsi *et al.* 2018), thus highlighting the differential roles of macrophages as key regulators of lung homeostasis, promoting pro- and anti-inflammatory balance. Whether AMs exhibit this clear dichotomy of polarisation, remains unclear, but it has been suggested that AMs express a hybrid phenotype. This supports the idea of AMs as key players

in both pro- and anti-inflammatory responses and therefore T2 and non-T2 inflammation (Mitsi *et al.* 2018).

Finally, AMs play an important role in both the secretion of pro-inflammatory cytokines, such as tumour necrosis factor-α (TNF-α), IL-1 and IL-6, and in the release of chemokines, such as IL-8. IL-8 is an important factor in the recruitment of neutrophils to sites of inflammation within the alveolar spaces to aid in phagocytosis and removal of pathogens and subsequent reduction of inflammation (Haslett *et al.* 1989). The potential of mediation of AM functions by PM, is poorly understood, however, the sentinel role of AMs in the airways highlights the potential of PM to negatively affect AM functions.

1.5.4 The Role of Alveolar Macrophages in Response to Particulate Matter Exposure:

AMs are able to remove inhaled PM through phagocytosis, to reduce the potential of pro-inflammatory responses induced by continued airways exposure to PM. AMs are long-lived in comparison to other innate immune cells, such as neutrophils, and are generally resistant to apoptotic stimuli. This highlights the need for proper functioning of AMs during the lifespan of a host, to promote lung homeostasis and prevent a persistent pro-inflammatory environment and contribution to chronic inflammatory lung diseases, such as asthma (Perlman *et al.* 1999; Murphy *et al.* 2012). Shorter-lived neutrophils undergo apoptosis at sites of inflammation and are then phagocytosed by AMs to prevent release of the potentially toxic internal environments of neutrophils, in a process termed efferocytosis (Henson *et al.* 2001; Greenlee-Wacker 2016) again emphasising the importance of AMs in lung homeostasis. However, the mechanisms responsible for PM-induced dysfunctional properties of AMs are so far unclear.

AMs obtained from the bronchoalveolar lavage fluid (BALF) of children living in London, indicate the presence of phagocytosed PM, as evidenced by carbon black clearly visible within the AMs under phase-contrast microscopy (Brugha and Grigg 2014). Additionally, AMs exposed to standard reference material of diesel exhaust particle extracts (DEP) from a fork-lift truck (SRM2975), display impaired expression of M1 and M2 markers, suggesting that PM exposure drives dysfunction to AMs (Jaguin *et al.* 2015). This data highlights that highly plastic AMs exposed to a variety of inhaled stimuli present in PM, such as lipopolysaccharide (LPS) and PM, could skew AMs to the M1 phenotype, resulting in promotion of inflammation and dysfunction of AMs (van Eeden et al. 2001; Becker et al. 2005). However, which components of PM drive skewed AM responses, resulting in persistence of AMs with a pro-inflammatory M1-like phenotype.

Potential PM-induced effects on AMs have been postulated in the review by Hiraiwa and Van Eeden (2013), where PM exposure drives M1-like AM stimulation. This results in production of pro-inflammatory cytokines associated with M1 responses, to recruit other blood-derived innate immune cells, such as neutrophils, to assist in the immune response. Both AMs and neutrophils phagocytose PM, a function that has been shown to be diminished in AMs from mice exposed to PM, highlighting the importance of proper AM functioning in the airways, to effectively clear the airways of apoptotic cells and prevent release of further pro-inflammatory inducing stimuli (Barlow *et al.* 2007). PM exposure appears to inhibit the switch from M1 to M2 macrophages, thereby leaving the lungs susceptible to persistent pro-inflammatory responses induced by accumulation of dead cells and PM within the airways (Figure 1.3). The effect of PM on these features of AMs, have been poorly

understood for some time, highlighting the need to assess these functions further and better understand the cellular mechanisms underpinning them.

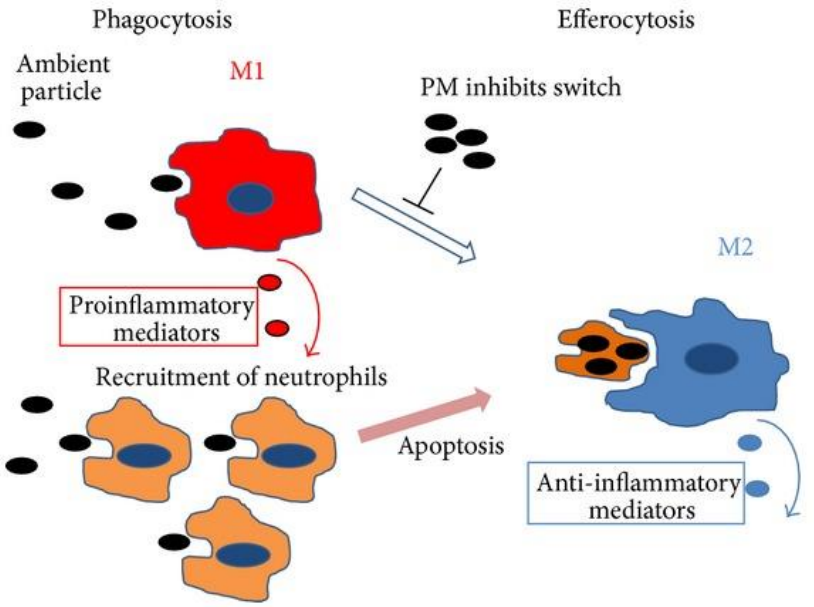

Figure 1.3: Alveolar Macrophage (AM) functions thought to be affected by exposure to particulate matter (PM). PM exposure to AMs, promotes phagocytosis, primarily by M1-like AMs, which results in release of M1-associated pro-inflammatory mediators. These act to attract and recruit blood-derived innate immune cells, such as neutrophils, to aid in the innate immune response to PM and removal of PM. Neutrophils are short-lived and therefore undergo apoptosis, which would promote M2-like AMs to engulf these cells via efferocytosis, however, PM exposure appears to inhibit the switch from M1 to M2, resulting in persistent inflammation in the lungs of people exposed to PM. Figure taken from Hiraiwa and Eeden (2013).

1.5.5 The Subtypes and Functions of Dendritic cells:

DCs act as the sentinels of the immune system and play an important role in bridging the innate and adaptive immune systems, as one of the key antigen presenting cells in the body, promoting activation of adaptive immune cells. DCs are therefore key in responding to and maintaining an immune response

to inhaled stimuli, such as PM (Matthews *et al.* 2016; Hilligan and Ronchese 2020). DCs sample their environment similarly to AMs, through functions such as endocytosis, phagocytosis and macropinocytosis (Liu and Roche 2015).

In contrast to AMs, the uptake of pathogens via these functions are not for clearance, but for processing and antigen presentation to cells of the adaptive immune system, such as naïve cytotoxic ($CD8^+$) T cells or helper ($CD4^+$) T cells by cross-presentation, aided by Major Histocompatibility complex (MHC) Class I or Class II, respectively, and co-stimulatory molecules (Hilligan and Ronchese 2020). Circulating immature DCs undergo frequent endocytosis and macropinocytosis, however, have low expression of MHC, so have limited interactions with adaptive immune cells. Upon exposure to environmental triggers, such as PM, DCs undergo cytoskeletal rearrangements and decrease their environmental sampling, increase expression of MHC and costimulatory molecules, such as CD80/CD86 and CD40, and present antigens to cells of the adaptive immune system in the lymph nodes, known as DC maturation. Upon migration to lymph nodes, mature DCs go on to activate antigen-specific T cells, initiating an adaptive T-cell-mediated immune response (Embgenbroich and Burgdorf 2018).

There are 3 major subsets of DCs which are derived from haematopoietic stem cells: plasmacytoid DC (pDC), myeloid/conventional DC1 (cDC1 and cDC2), which give rise to macrophage-dendritic cell progenitors. cDC and pDC derive from the common DC progenitor cells, however, under inflammatory conditions, bone marrow-derived monocytes infiltrate areas of inflammation and differentiate to DC to aid in mounting an appropriate inflammatory response (Collin and Bigley 2018). Lung DCs are often found in contact with the airway epithelium of the entirety of the respiratory tract, from the nostrils

to the alveolar spaces (Condon *et al.* 2011). Lung DCs (primarily cDC1 and lung-resident pDCs) can extend dendritic protrusions through tight junctions present within the airway epithelium and into the airway lumen, to acquire inhaled antigens (Jahnsen *et al.* 2006; Sung *et al.* 2006; Blank *et al.* 2007).

In contrast to AMs, which dominate the alveolar spaces, lung DCs are mainly associated with the larger airways, such as the bronchial epithelium. Larger PM particles are generally deposited in these larger airways, and it is these airways that are considered dysfunctional during asthma pathogenesis (Holt *et al.* 1990). Immature lung DCs survey the inhaled environment under steady-state conditions, to promote immunological homeostasis in the lungs. However, during inflammation, monocytes are recruited to the lungs via the vasculature and trafficked to sites of inflammation, where they differentiate into inflammatory monocyte-derived DC (Auffray *et al.* 2009) to promote inflammation (Collin and Bigley 2018).

1.5.6 The Role of Dendritic Cells in Response to Particulate Matter Exposure:

The constant sampling of the environment by DCs allows DCs to activate based on factors such as the size and composition of PM and the cytokine environment generated by other cells of the innate immune system (Bleck *et al.* 2011b). During innate inflammatory responses to inhaled substances such as PM, conventional and non-conventional (p)DCs, myeloid DCs and monocytes are recruited to the lungs from the circulation. This occurs in response to chemotactic agents released by the airway epithelium, AMs and pDCs and promotes a pro-inflammatory response (Newton and Dixit 2012; Chen *et al.* 2018). At sites of inflammation, monocytes differentiate into monocyte-derived DC when exposed to cytokines such as IL-4 and

granulocyte-macrophage colony-stimulating factor (GM-CSF) (Sander *et al.* 2017). In addition, PM exposure to DCs *in vitro* drives maturation of DCs - an effect that can be enhanced by co-treatment with GM-CSF and is associated with a pronounced increase in secretion of cytokines, culminating in enhanced proliferation and activation of naïve T cells to mount an adaptive immune response to specific stimuli (Matthews *et al.* 2016; Mann *et al.* 2017).

One prominent DC marker which is specifically upregulated by exposure to PM is CD83, a membrane bound molecule which has been demonstrated to be involved in T cell mediated immune responses (Kruse *et al.* 2000; Gras *et al.* 2017). In addition to maturation, PM-stimulated DCs also polarise $CD4^+$ T cells to a more pathogenic phenotype, including the expression of interferon-gamma (IFN-γ) and interleukin (IL)-17A (Acciani *et al.* 2013). Moreover, DCs exposed to PM drive secretion of pro-inflammatory cytokines, IL-6, and IL-23, which also play an important role in polarising T-helper 17 (Th17) cells. These are thought to contribute to development of neutrophilic inflammation and are associated with difficult-to-treat, severe asthma (Brandt *et al.* 2013; Mann *et al.* 2017). However, the underlying cellular mechanisms of potential PM-induced effects on DC functions remain unclear.

1.6 Mechanisms of action of Particulate Matter in the airways:

1.6.1 Toll-Like Receptor Signalling:

During physiology, TLR activation is one of the first defensive mechanisms to combat invading pathogens and repair damaged tissues. However, during pathophysiology, as in the lungs of patients with inflammatory lung diseases, such as asthma, dysregulated TLR signalling disrupts immune homeostasis due to sustained pro-inflammatory environments (Takeda *et al.* 2003; Beutler 2009;

Palm and Medzhitov 2009; Drexler and Foxwell 2010). TLRs play a key role in the innate immune system by recognition and response to pathogen-associated molecular patterns (PAMPs), leading to activation of an innate immune response, culminating in activation of intracellular signalling mediators associated with inflammation (Liu *et al.* 2013; Kawasaki and Kawai 2014; Tang *et al.* 2019a). PM contains pathogen associated molecular patterns (PAMPs), such as LPS which directly activates TLR4 which is thought to contribute to the innate immune response induced by exposure to PM (Bleck *et al.* 2010; Bleck *et al.* 2011b). However, mechanisms underpinning PM-induced cellular responses caused by other components such as the metals contained within PM, and their contribution to the exacerbation of asthma symptoms, are yet to be uncovered.

1.6.2 Reactive Oxygen Species Generation and Signalling:

Metals are contained within all fractions of PM, and these have been postulated as possible mediators of PM-induced airway injury and inflammation (Diociaiuti *et al.* 2001; González-Flecha 2004). Transition metals present within PM, have been shown to drive reactive oxygen species (ROS) generation *in vivo*, resulting in oxidative stress which induces or exacerbates inflammation (Hitzfeld *et al.* 1997; Kadiiska *et al.* 1997). Oxidative stress is therefore suspected as one of the major mechanisms of PM-induced cellular responses, however, the upstream mechanisms of PM-induced ROS generation are unclear.

Oxidative stress is defined as a depletion of reduced glutathione (GSH) in exchange for a rise in oxidised glutathione (GSSG), creating a decreased intracellular GSH/GSSG ratio (Rahman *et al.* 1999). Unpublished studies by our collaborators at King's College London indicate PM exposure to DCs drives

oxidative stress, however, DCs counter this by increasing cellular GSH. This illustrates the ability of DCs to modulate their response to oxidative stress, however, in pro-inflammatory environments generated through disease pathogenesis, continually counteracting oxidative stress this way induces a redox imbalance (Ho et al, unpublished observations). The upstream mechanisms driving this redox imbalance in airways cells upon exposure to PM are unclear and require further investigation.

Therefore, uncovering upstream mechanisms involved in the sensing and responding to inhaled stimuli, such as PM, is crucial for better understanding of the mechanisms underpinning PM-induced cellular responses. The current proposed mechanisms of PM-induced pro-inflammatory responses in airway epithelial cells are represented in Figure 1.4, adapted from De Grove et al. (2018). The figure also highlights the potential of alternative environmental sensors for inhaled PM in airway cells, such as G protein-coupled receptors (GPCRs) and their potential role in contributing to PM-induced pro-inflammatory responses associated with asthma.

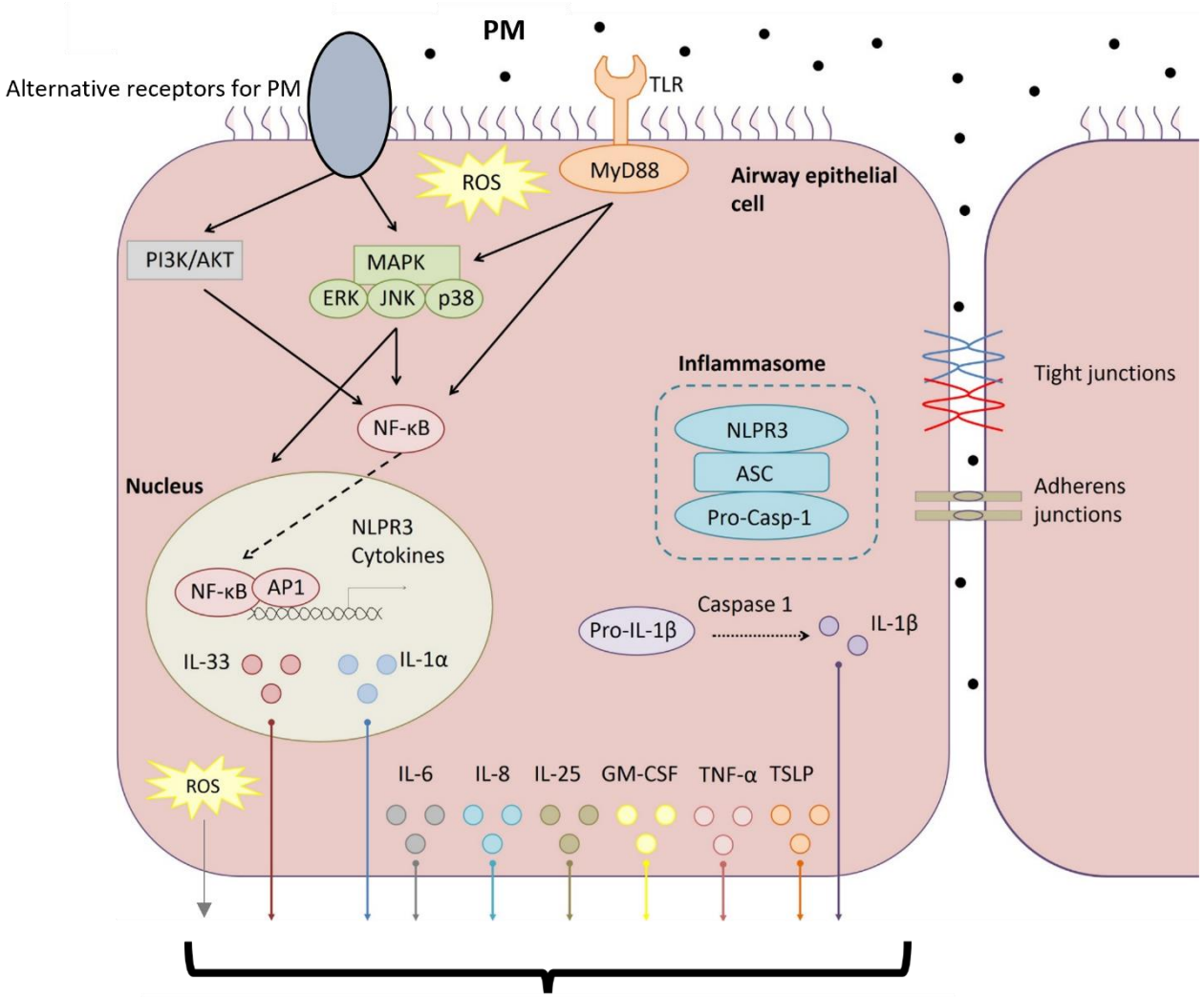

PRO-INFLAMMATORY RESPONSES

Figure 1.4: Current known mechanisms of particulate matter (PM)-induced inflammatory responses in the airway epithelium. Exposure to PM drives reactive oxygen species (ROS) generation and secretion and activation of toll-like receptors (TLR) and other potential receptors for PM. These drive activation of intracellular signalling pathways: Phosphoinositide 3-kinase (PI3K), mitogen-activated protein kinase (MAPK) and downstream effectors extracellular signal-related kinase (ERK), Jun-N-terminal kinase (JNK), and p38, which go on to activate nuclear factor kappa B (NF-κB). Downstream effectors of PM-induced intracellular signalling go on to drive inflammatory responses by transcription of pro-inflammatory cytokines such as interleukin (IL)-33 and IL1α in the nucleus. NF-κB undergoes translocation to the nucleus and drives transcription of NOD-, LRR- and pyrin domain-containing protein 3 (NLRP3) cytokines and formation of the inflammasome. The inflammasome is made up of NLRP3, the adaptor molecule apoptosis-associated speck-like protein containing a CARD (ASC) and pro-caspase-1 (Pro-Casp-1). Pro-Casp-1 is converted to Caspase-1 in the cytoplasm and causes cleavage of Pro-IL-1ß into IL-1ß. This is secreted from the airway epithelial cells along with other pro-inflammatory cytokines associated with the pathogenesis and acute exacerbations of asthma: IL-33, IL-1α, IL-6, IL-8, IL-25, granulocyte macrophage colony stimulating factor (GM-CSF), tumour necrosis factor-α (TNF-α) and thymic stromal lymphopoietin (TSLP). Arrows represent: → activation, ⇢migration, ↱ transcription, and ↓ release. Figure adapted from Grove et al 2018.

1.7 G Protein-Coupled Receptors as Environmental Trigger Integrators:

GPCRs are a superfamily of membrane-bound receptors, expressed throughout the body, which mediate responses to a wide array of stimuli, including small molecules (amino acids and ions), larger proteins (hormones and neurotransmitters), light, and odorants (Bockaert and Pin 1999). GPCRs interact with heterotrimeric G proteins, made up of an alpha (α), beta (ß), and gamma (γ) subunit; agonist binding at the GPCR induces α subunit dissociation from the ß and γ subunits. The α subunit of the G proteins comprise four families: $G\alpha_i$, $G\alpha_s$, $G\alpha_{12/13}$, and $G\alpha_q$, which drive a wide range of intracellular signal transduction, such as regulation of adenylyl cyclase activity ($G\alpha_i$ and $G\alpha_s$),

small GTPase families ($G\alpha_{12/13}$), and activation of phospholipase C (PLC) ($G\alpha_q$) (Neves *et al.* 2002). These G proteins influence downstream intracellular processes important in physiology, such as gene expression and proliferation ($G\alpha_i$ and $G\alpha_s$), cytoskeletal rearrangements ($G\alpha_{12/13}$), and intracellular calcium levels ($G\alpha_q$) (Neves *et al.* 2002). As a result, GPCRs have become attractive targets for drug development and ~ 34% of FDA approved drugs target GPCRs and their intracellular signalling machinery (Hauser *et al.* 2018; Sriram and Insel 2018). Since GPCRs are expressed in cells directly exposed to PM, such as the airway epithelium, these could provide suitable therapeutic targets as an upstream mechanism to directly counteract PM-induced cellular responses during the pathogenesis and acute exacerbations of asthma.

1.8 G Protein-Coupled Receptors as Therapeutic Targets for the Treatment of Asthma:

The mainstay for treatments of chronic obstructive lung diseases, such as asthma, have been previously targeted towards directly regulating airway constriction by inducing relaxation of airway smooth muscle (ASM) cells and reducing airways inflammation. Bronchodilators have long been used to induce ASM relaxation in the form of short- and long-acting ß2 adrenergic GPCR (ß2AR) agonists (SABA and LABA, respectively), for the treatment of asthma patients. These act by activation of the ß2AR, which goes on to activate the $G_{\alpha s}$ subunit of the associated heterotrimeric G protein, which stimulates adenylyl cyclase to catalyse the conversion of ATP into cAMP. The downstream effector of cAMP, PKA, mediates downregulation of intracellular Ca^{2+} levels as a mechanism to counteract ASM contraction (Penn 2008; Walker *et al.* 2011). Although SABA are regularly used for the maintenance of airway constriction in asthma patients, overuse of these have been associated with an increased

risk of acute exacerbations and mortality, due to promotion of airways inflammation and AHR, thereby increasing rather than alleviating symptoms of asthma (Nguyen *et al.* 2017; Nwaru *et al.* 2020). Therefore, there is a need to develop more effective, targeted therapeutics for patients with asthma.

Long-acting muscarinic antagonists (LAMA), such as Tiotropium, act at muscarinic receptors to block broncho constricting effects of acetyl choline, in asthma patients (Busse *et al.* 2016). Often, LABA and LAMA are used together to increase the efficacy on bronchoconstriction in asthma patients with severe symptoms (Kaplan *et al.* 2020). LAMAs are generally considered safe treatments at recommended doses in asthma. However, LAMAs can act to block muscarinic receptors on cholinergic airways nerves that usually function to decrease release of acetyl choline, resulting in a cough and paradoxical bronchoconstriction. This paradox is thought to be due to the ubiquitous expression of muscarinic receptors throughout the airways (Mann *et al.* 1984; Lee *et al.* 2008), again highlighting the need to develop more targeted therapeutic options for asthma patients.

In addition, inhaled or oral corticosteroid (ICS or OCS, respectively) treatment has been the mainstay for reducing airways inflammation observed in asthma patients (Barnes 1995; Rowe *et al.* 1999), however, these do not target GPCRs, do not target bronchoconstriction, and their efficacy for airways remodelling in asthma is unclear. ICS or OCS are thought to drive suppression of pro-inflammatory gene transcription, thereby inhibiting promotion of inflammation, by so far unclear mechanisms (Barnes 1995; Horwitz *et al.* 1996; Barnes 2011; Usmani *et al.* 2012). As a result, ICS are often used in combination with LABA in asthma patients and have been shown to provide a reduction in the risk of exacerbations and improvement of lung function and quality of life

than ICS or LABA alone (Barnes 2002; Usmani *et al.* 2012). Clinical trials have also been conducted in asthma patients using the triple inhaler therapy of LABA, LAMA and ICS, especially for those with severe, difficult-to-treat asthma (Virchow *et al.* 2019), however, there remains endotypes of asthma patients who are unresponsive to any of the available treatments, negatively affecting quality of life and leaving patients at a higher risk of mortality, due to a fatal "asthma attack".

Although most asthma patients respond well to steroid therapies targeting inflammatory symptoms, around 5-25% of asthma patients have poor sensitivity to treatment with steroids (severe, difficult-to-treat asthma patients) (Rhen and Cidlowski 2009; Barnes 2011). These patients have the greatest unmet clinical need in asthma management as they account for 50-80% of resources and healthcare costs for asthma ~$8 billion per year in Europe, USA, and Australia combined (Hansbro *et al.* 2017). This asthma endotype is characterised by neutrophilic airways inflammation through activation of non-T2 responses, as opposed to T2 cell responses observed in asthma patients with a primarily eosinophilic disease (Green *et al.* 2002; Bullens *et al.* 2006; Shannon *et al.* 2008). This endotype is associated with significant airways remodelling, such as basement membrane thickening and epithelial cell proliferation, which no treatment currently targets, highlighting the need to develop more targeted treatments for patients with severe, difficult-to-treat asthma (Bourdin *et al.* 2007; Cohen *et al.* 2007). Furthermore, exposure to PM drives both T2 and non-T2 asthma, however, no treatment currently directly targets this mechanism (Figure 1.5, taken from Israel and Reddel (2017).

In summary, although the mainstay treatments for asthma are effective for most patients, there are risks associated with the chronic use of some of these

treatments. In addition, specific endotypes of each disease are unresponsive to current available treatments, due in part to our poor understanding of the underlying disease mechanisms.

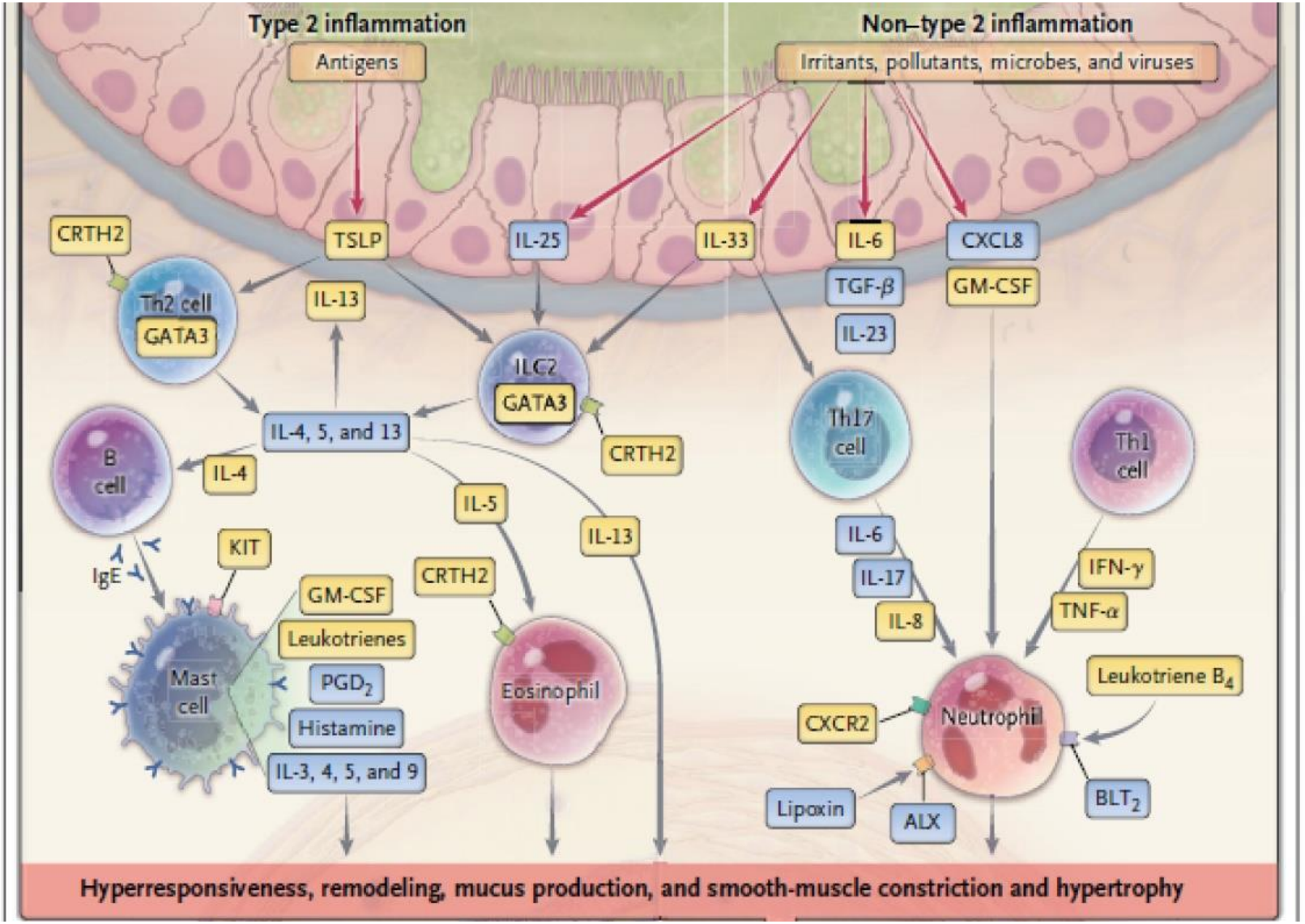
Type 2 inflammation
Non–type 2 inflammation
Antigens
Irritants, pollutants, microbes, and viruses
CRTH2
TSLP
IL-25
IL-33
IL-6
CXCL8
Th2 cell
GATA3
IL-13
TGF-β
GM-CSF
IL-23
ILC2
GATA3
Th17 cell
Th1 cell
IL-4, 5, and 13
CRTH2
B cell
IL-4
IL-5
IL-13
IL-6
IL-17
IL-8
IFN-γ
TNF-α
KIT
IgE
GM-CSF
Leukotrienes
PGD2
Histamine
IL-3, 4, 5, and 9
CRTH2
Mast cell
Eosinophil
Neutrophil
Leukotriene B4
CXCR2
Lipoxin
ALX
BLT2
Hyperresponsiveness, remodeling, mucus production, and smooth-muscle constriction and hypertrophy

Figure 1.5: The mechanisms of type 2 (T2) and non-T2 inflammation during asthma. T2 inflammation is initiated by exposure to recognised antigens, through the action of thymic stromal lymphopoietin (TSLP), which stimulates type 2 helper T (Th2) cells and type 2 innate lymphoid cells (ICL2) to differentiate and produce T2 cytokines: interleukin (IL)-4, IL-5, and IL-13, which is dependent on the GATA3 transcription factor. These cytokines result in the production of IgE and subsequent activation of mast cells (where survival is dependent on the KIT receptor) and eosinophils. IL-13 directly acts on smooth muscle to induce hyperresponsiveness and remodelling and on the airway epithelium to induce cytokine secretion and mucus production. This pathway can also be activated upon exposure to components present in the environment, through stimulation of the innate immune system, following secretion of IL-33, to stimulate ILC2 and Th2 cells, and directly recruit neutrophils to sites of inflammation. IL-33 can also activate non-T2 pathways such as type 17 helper T (Th17) cells, which release IL-6, IL-17, and IL-8, to induce neutrophil infiltration. Concurrently, Th1 cells are activated which can also directly activate neutrophil infiltration and cytokine release from the airway epithelium directly can stimulate neutrophilic inflammation. Substances in yellow have been or are currently being targeted for severe asthma. Lipoxin A4 receptor (ALX), leukotriene B4 receptor 2 (BLT2), CXC motif chemokine ligand 8 (CXCL8), CXC chemokine receptor 3 (CXCR3), granulocyte– macrophage colony-stimulating factor (GM-CSF), transforming growth factor β (TFG-β), and tumour necrosis factor α (TNF-α). Image adapted from Israel and Reddel (2017).

1.9 The Calcium-Sensing Receptor (CaSR):

In the mid-1980s, research began into the mechanisms regulating the release of parathyroid hormone (PTH), from parathyroid glands, where it was shown that elevated extracellular Ca^{2+} decreased PTH release by increasing intracellular Ca^{2+} levels (LeBoff *et al.* 1985; Nemeth and Scarpa 1986; Brown *et al.* 1987; Nemeth and Scarpa 1987; Brown and Chen 1989). These studies suggested a GPCR, functioning as a cell surface calcium-sensor was present in the parathyroid gland which subsequently led to the discovery - by expression cloning - of the calcium-sensing receptor (CaSR) (Brown *et al.* 1993). The CaSR has been shown to be expressed in other organs that contribute to

maintenance of extracellular Ca^{2+} (calciotropic tissues) such as kidney (Riccardi *et al.* 1995), bone and cartilage (Dvorak *et al.* 2004; Chang *et al.* 2008), intestine (Chattopadhyay *et al.* 1997), and non-calciotropic tissues, such as placenta (Bradbury *et al.* 2002), pancreas (Bruce *et al.* 1999; Rasschaert and Malaisse 1999), skin (Komuves *et al.* 2002), brain (Ruat *et al.* 1995), liver (Canaff *et al.* 2001), the vasculature (Bukoski 1998; Weston *et al.* 2005; Ziegelstein *et al.* 2006), and more recently, the lungs (Yarova *et al.* 2015; Wolffs *et al.* 2020). However, in contrast to the calciotropic tissues, the roles of the CaSR in the non-calciotropic tissues have not yet been fully uncovered.

Molecularly the CaSR exists as a functional homodimer (Bai *et al.* 1998; Ward *et al.* 1998; Pidasheva *et al.* 2005), where each subunit possesses the characteristic 7 transmembrane domain (TMD) of all GPCRs. In addition, the CaSR also contains a large N-terminal extracellular domain (ECD), comprised of a Venus flytrap (VFT) domain consisting of two lobe subdomains, and a cysteine rich domain (Figure 1.6). Each lobe of the VFT domain forms part of a ligand binding cleft, which binds orthosteric ligands of the CaSR, such as Ca^{2+} and other cations, L-amino acids, and polyamines (Kunishima *et al.* 2000; Tsuchiya *et al.* 2002; Muto *et al.* 2007). The 7TMD of the CaSR contains multiple allosteric binding sites for small molecule positive and negative allosteric modulators at the CaSR (PAMs and NAMs, respectively), demonstrating the functional diversity of the CaSR (Ray and Northup 2002; Petrel *et al.* 2003; Miedlich *et al.* 2004; Petrel *et al.* 2004; Hu *et al.* 2006; Bu *et al.* 2008; Gerspacher *et al.* 2010; Leach *et al.* 2016; Gregory *et al.* 2018; Keller *et al.* 2018; Josephs *et al.* 2020).

In the parathyroid gland, the primary role of the CaSR is extracellular Ca^{2+} homeostasis through suppression of parathyroid hormone (PTH) secretion

from chief cells of the parathyroid gland, which in turn inhibits cell proliferation, number, and size (Conigrave 2016; Fan *et al.* 2018). CaSR stimulation in parathyroid oxyphil cells also drives synthesis of $1,25(OH)_2D_3$, which is an inhibitor of PTH synthesis (Ritter *et al.* 2012). However, the ability of the CaSR to act as a multimodal chemosensor in other non-calciotropic tissues, such as the lungs, is key to understanding the role of the CaSR outside the control of total body mineral ion metabolism during physiology and disease.

1.9.1 The CaSR During Pulmonary Development and Disease:

During fetal development, the CaSR plays a crucial role in promoting expansion of lungs by branching morphogenesis and regulation of fluid secretion (Finney *et al.* 2008; Riccardi *et al.* 2013; Brennan *et al.* 2016). During the late stages of gestation, serum Ca^{2+} levels are increased, in comparison to adult physiological serum Ca^{2+} levels, highlighting the potential differential roles of the CaSR in the adult lung (Riccardi *et al.* 2013). So far, the CaSR has been demonstrated to be expressed on the mRNA level in a variety of lung-specific structural and immune cells, such as ciliated bronchial epithelial cells, macrophages, and DCs (Human Protein Atlas, available at: https://www.proteinatlas.org/ENSG00000036828-CASR/single+cell+type/lung). In addition, the CaSR has been shown to be functionally expressed in monocytes, monocyte-derived macrophages and dendritic cells (Canton *et al.* 2016) and human lung fibroblasts (Wolffs *et al.* 2020). To complement this, CaSR protein expression was demonstrated throughout the human and mouse airways (Yarova *et al.* 2015), however, our understanding of the roles of the CaSR in the adult lung, during physiology, are yet to be fully elucidated.

Expression of the CaSR throughout the lungs prompted studies from our laboratory to test the role of the CaSR during lung disease pathogenesis, such as in asthma. We have previously demonstrated that CaSR expression is increased in ASM cells from asthmatic patients, compared to healthy controls (Yarova *et al.* 2015). Furthermore, we have demonstrated that NAM is effective at reducing asthma-like features: AHR, inflammation, and some aspects of remodelling, in *in vivo* models of asthma (Yarova *et al.* 2015; Yarova *et al.* 2020). In addition to these findings, we have also demonstrated that NAM is effective at reducing both T2 (ovalbumin) and non-T2 (IL-33) asthma-like features in these models, such as AHR, inflammation, and some aspects of remodelling (Huang *et al.* 2019). These data highlight the potential of the CaSR as a therapeutic for asthma, including difficult-to-treat, severe asthma patients. However, whether the CaSR mediates pollution-induced exacerbations in these models, has not yet been investigated.

1.9.2 CaSR Ligands:

Extracellular Ca^{2+} is the main physiological ligand for the CaSR, however, the CaSR is activated by other polycations: Gd^{3+}, Al^{3+}, Mg^{2+}, Pb^{2+} and Cd^{2+}. Trivalent cations are generally more potent than divalent cations as orthosteric agonists at the CaSR (Handlogten *et al.* 2000a; Brown and Macleod 2001). Ca^{2+} and Mg^{2+} represent two physiologically relevant endogenous ligands of the CaSR, however, exogenous polycations may also activate the CaSR present in the lungs, as the main barrier surface from the outside environment. Furthermore, standard reference material (SRM, 1648a) PM derived from America between 1976 and 1977, contains a list of metals which could activate the CaSR present in the airway epithelium and immune cells, which come into direct contact with inhaled substances, such as PM (National Institute of

Standards & Technology 2020). In addition, endogenous polycations, such as eosinophilic cationic protein (ECP) and major basic protein (MBP, mimetic of poly-l-arginine), induce CaSR activation in human ASM cells *in vitro* (Yarova *et al.* 2015). Finally, synthetic analogues of endogenous polyamines, such as spermine and ornithine, comprise additional orthosteric agonists at the CaSR (Quinn *et al.* 1997), where polyamine-induced increases to intracellular Ca^{2+} were blocked by NAM in more recent studies with primary human lung fibroblasts, by my lab colleague Mrs Kasope Wolffs (Wolffs *et al.* 2020). These findings highlight the potential of the CaSR in mediating polyamine-induced cellular responses in the airways of asthma patients.

Blood polyamine levels are sustained in a ~5-10 μM range in humans and are increased in the BALF from human asthmatics and *in vivo* models of asthma, suggesting the role of polyamines in driving asthma pathogenesis (Jain 2018). However, whether the contribution of polyamines to asthma pathogenesis is mediated via the CaSR remains unknown. Polyamines, such as spermine, have been shown to drive airways constriction in precision cut lung slices of intralobular bronchi obtained from wild-type (WT) experimental animals; mice with genetic ablation of the CaSR, had no contraction response to extracellular spermine (Yarova *et al.* 2015). In addition, spermine-induced increases to intracellular Ca^{2+} were inhibited by co-treatment with a negative allosteric modulator (NAM) of the CaSR in HEK-CaSR cells, suggesting the potential of pharmacological ablation of the CaSR as a viable therapeutic to reduce polyamine-induced cellular responses associated with asthma, in airways cells.

In addition to responding to orthosteric ligands, the CaSR has several allosteric modulators that have been identified and are termed as such because they bind an alternative site on the CaSR to the orthosteric ligands. These allosteric

modulators bind in regions of the GPCR such as in the 7TMD region and extracellular loops of the CaSR. These are classified as positive and negative allosteric modulators (PAM & NAM) of the CaSR, which potentiate or dampen the affinity for an orthosteric ligand, respectively (Nemeth *et al.* 1998). PAM and NAM positively or negatively change GPCR affinity for their ligands and efficacy of the ligand-receptor complex for production of an intracellular response (Ehlert 2005; Kenakin 2017). These unique properties of CaSR PAMs and NAMs have therefore prompted investigation of these allosteric modulators as potential therapeutic approaches for a range of diseases.

The first PAM to be used in the clinic, Cinacalcet, is FDA-approved for the treatment of primary and secondary hyperparathyroidism, and for hypercalcemia in adults with parathyroid cancer (Block *et al.* 2004; Lindberg *et al.* 2005; Peacock *et al.* 2005; Quarles 2005; Pérez-Ricart *et al.* 2016). A second-generation PAM, Etelcalcitide was FDA-approved in 2017, and was shown to be more effective than Cinacalcet at reducing PTH concentrations in patients with secondary hyperparathyroidism (Block *et al.* 2017; Patel and Bridgeman 2018). In 2018, Evocalcet was also approved for treating secondary hyperparathyroidism in patients on dialysis in Japan (Yokoyama *et al.* 2019; Akizawa *et al.* 2020).

Owing to their ability to evoke short, sharp changes in plasma parathyroid hormone levels, a known bone anabolic stimulus, CaSR NAMs have been previously developed for the treatment of osteoporosis: Ronacaleret (Fitzpatrick *et al.* 2011; Fitzpatrick *et al.* 2012; Caltabiano *et al.* 2013), AXT914 (John *et al.* 2014), and JTT305 (Halse *et al.* 2014; Cosman *et al.* 2016). Each of these NAMs were tested in Phase 1 and 2 clinical trials, for the treatment of osteoporosis, however, further advancement of CaSR NAM for osteoporosis

was terminated, due to lack of efficacy for the disease indication (Gerspacher *et al.* 2010). CaSR NAM NPSP795 has also been tested in the clinic for treatment of Autosomal Dominant Hypocalcaemia Type 1 (ADH1) (Roberts *et al.* 2019; Hannan *et al.* 2020) and novel CaSR NAM Encaleret is currently undergoing clinical assessment for ADH1 (Gafni *et al.* 2021). Although NAM failed in clinical trials due to lack of efficacy against osteoporosis, there has been recent interest in repurposing these NAMs for other disease indications, such as clinical testing of NPSP795 for treatment of ADH1. Additionally, revealing a role of the CaSR during T2 and non-T2 asthma has led to pre-clinical testing of NAM by our laboratory, as a potential effective therapeutic for inflammatory lung diseases, such as asthma (Yarova *et al.* 2015; Huang *et al.* 2019; Yarova *et al.* 2020).

1.9.3 CaSR Signalling:

The CaSR signals through interactions with distinct heterodimeric G proteins, such as: Gαq/11, Gαi/o, Gα12/13 and Gαs (Ward 2004; Khan and Conigrave 2010; Mamillapalli and Wysolmerski 2010; Magno *et al.* 2011; Leach *et al.* 2020) which leads to activation of downstream effectors of a variety of intracellular signalling pathways (Figure 1.7). CaSR coupling to Gαq/11 is considered one of the primary CaSR-mediated intracellular signalling pathways that activates PLC to hydrolyse phosphatidylinositol 4,5-bisphosphate to the second messengers: inositol trisphosphate (IP_3) and diacylglycerol (DAG) (Brown *et al.* 1993). IP_3 triggers release of Ca^{2+} from intracellular sources, such as the endoplasmic reticulum (Shorte *et al.* 1995; Ward *et al.* 2002), whereas DAG in isolation, or in combination with intracellular Ca^{2+}, activates protein kinase C (Huang 1989; Berridge 1993). CaSR-mediated activation of Gαi/o intracellular signalling results in inhibition of adenylyl cyclase and subsequent inhibition of

the actions of cyclic AMP (cAMP) (Kifor *et al.* 2001). Gα12/13 coupling with the CaSR is thought to lead to activation of Rho family of small GTPases, however it is unclear whether this is due to coupling with Gα12/13 or Gαq/11 pathways, due to lack of effective inhibitors or functional readouts for Rho GTPase activity (Min *et al.* 2002). Stimulation of cAMP through activation of the Gαs signal transduction pathway is observed in malignant breast cells and in the AtT-20 pituitary tumour-derived cell line, however, not in HEK-CaSR cells (Mamillapalli *et al.* 2008; Mamillapalli and Wysolmerski 2010; Thomsen *et al.* 2012). This suggests that the CaSR could undergo molecular switching during disease, however the mechanisms behind this are unknown. Stimulation of these distinct intracellular signalling pathways leads to activation of a range of diverse downstream effectors of these pathways which play important roles in cell homeostasis and dysregulation of some of these pathways is associated with asthma pathogenesis (Athari 2019).

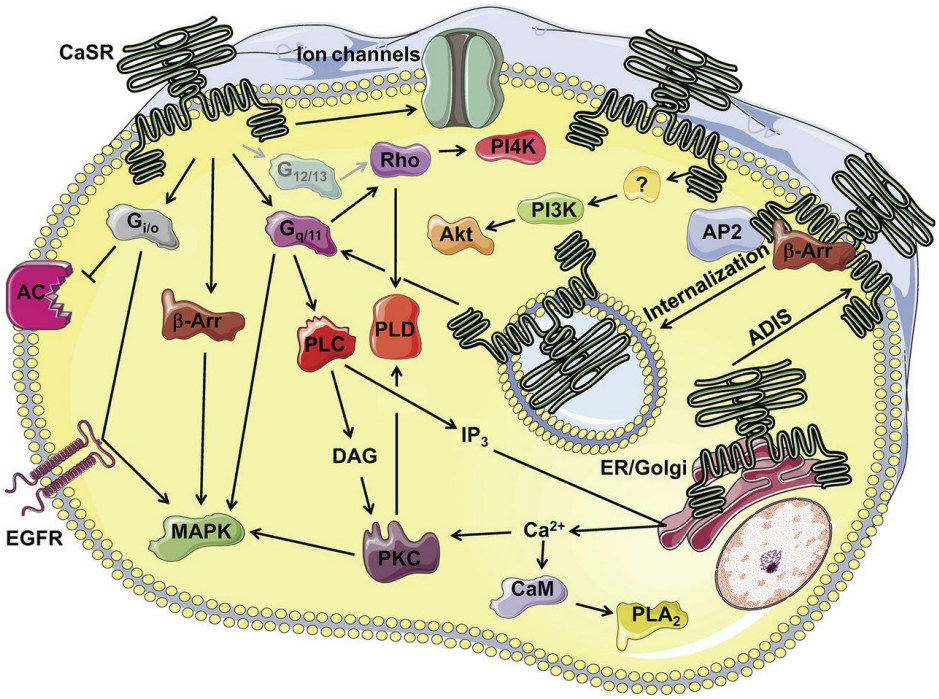

Figure 1.7: Signalling pathways downstream of calcium-sensing receptor (CaSR) activation. The CaSR receptor preferentially couples with Gαq/11 and Gαi/o heterotrimeric G proteins. The Gαq/11 heterotrimeric G proteins drive physiological responses, through activation of mitogen-activated protein kinases (MAPK), phospholipase C (PLC), and the second messengers: inositol trisphosphate (IP_3), diacylglycerol (DAG) and PKC. This culminates in increases to intracellular Ca^{2+}, leading to activation of calmodulin (CaM) and phospholipase A_2 (PLA_2), and activation of MAPK signalling cascades, and activation of phospholipase D (PLD). The Gαq/11 G protein also activates Rho associated kinases (Rho), which go on to activate PLD and phosphatidylinositol 4 kinase (PI4K). The CaSR-mediated activation of Gαi/o G protein induces inhibition of adenylyl cyclase (AC)and transactivation of the CaSR by the epidermal growth factor receptor (EGFR) leads to activation of MAPK signalling cascades. The CaSR has also been demonstrated to be linked with activation of ß-arrestin, which contributes to activation of MAPK signalling cascades. The CaSR also activates Gα12/13 proteins which go on to activate Rho and PI4K, and activation of phosphatidylinositol 3 kinase (PI3K) and protein kinase B (PKB) is driven by so far unclear mechanisms. Finally, the CaSR undergoes ß-arrestin dependent agonist-driven insertional signalling (ADIS) to sustain CaSR-mediated responses to chronic exposure to CaSR ligands, to prevent desensitisation. Figure taken from Leach et al (2020).

1.10 Hypothesis:

Given that; 1) the CaSR is expressed in airways cells and its activation has been implicated in the pathogenesis of asthma, 2) components of PM are potential activators at the CaSR, and 3) mediators of PM-induced intracellular signalling pathways are known to be downstream of CaSR activation, I hypothesise that the CaSR could represent one of the mechanisms of PM-induced responses in airways cells.

1.11 Aims and Objectives:

The specific aims and objectives of my project were to:

1. Determine whether PM directly activates the CaSR in a recombinant system in which HEK293 cells over-express the human CaSR (HEK-CaSR).
2. Determine the expression of the CaSR, at the protein level, in human airway cells involved in sensing and responding to PM.
3. Establish suitable *in vitro* models of basal human bronchial epithelial cells (HBECs), AMs and DCs, to begin to elucidate the role of the CaSR in mediating PM-induced cellular responses.

CHAPTER 2: METHODS.

Outlined below are the general principles of the methodological approaches used throughout my thesis, where detailed methods for each experiment are provided within each results chapter.

2.1 Fluorescent Intracellular Ca^{2+} Imaging:

Measurements of changes to intracellular Ca^{2+} in single cells in response to a variety of potential agonists at the CaSR was used as a method to determine CaSR activation, as changes to intracellular Ca^{2+} is one of the biological readouts for CaSR activation. Detailed methods regarding fluorescent intracellular Ca^{2+} imaging experiments are provided within Chapter 3, section 3.2.3 and Chapter 5, section 5.2.2.

2.1.1 Ca^{2+} Indicator – Fura-2AM:

Fluorescent intracellular Ca^{2+} imaging experiments were conducted using the fluorescent, ratiometric dye Fura-2AM to measure fluorescence of single-cells, using a monochromator-based fluorimeter system (OptoFluor; Cairn Research). The plasma membrane is permeable to Fura-2AM and upon entry into the cell, undergoes deesterification by cytosolic esterases, which cleave the AM group, resulting in active Fura-2, which is confined to the cell (Farley 1994). Fura-2 was used as a dual excitation Ca^{2+} indicator, which is excited at wavelengths of 340 and 380 nm, which represent the Ca^{2+} bound and unbound Fura-2, respectively. The emission for both wavelengths was measured at 510 nm, which allowed for the ratiometric measurement of changes to intracellular Ca^{2+} levels (340:380 ratio) (Zanin *et al.* 2019) (Figure 2.1). A ratiometric dye was used during these studies as these are advantageous for fluorescence imaging, due to factors such as artifacts due to uneven dye distribution, leakage of dye,

photo bleaching and unequal cell thickness being reduced compared to single wavelength dyes.

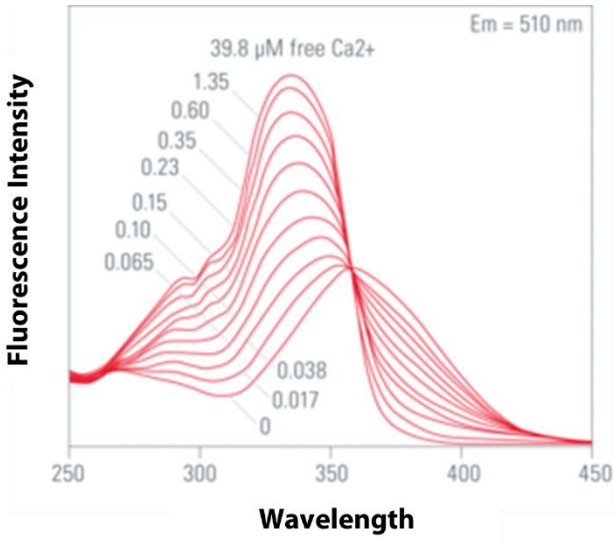

Figure 2.1: Fluorescence excitation spectra for Fura-2, in different Ca^{2+} concentrations. Demonstration of the fluorescence intensity for Fura-2, in solutions containing 0 to 39.8 µM free Ca^{2+}. As free Ca^{2+} concentration of the external solution increased, so did the fluorescence intensity after excitation at 340 nm, as Fura-2 is bound to the free Ca^{2+}. As free Ca^{2+} concentration decreased, unbound Fura-2 is excited at 380 nm. At 39.8 µM Ca^{2+}, there was maximal excitation at 340 nm, and no excitation at 380 nm as most fura-2 was bound to the free Ca^{2+}. At 0 Ca^{2+}, there was no excitation at 340 nm and maximal excitation at 380 nm, representing the maximal level of unbound Fura-2. Image adapted from https://www.leica-microsystems.com/science-lab/widefield-calcium-imaging-with-calcium-indicator-fura2/.

2.1.2 Measurements of Intracellular Ca^{2+}:

Cells used during each experiment were seeded on #1.5 glass coverslips (VWR, cat. #631-0150P) and loaded with Fura-2AM, in a loading buffer which was specific to the cell type used within each experiment. Coverslips containing

cells were placed in the perfusion chamber, mounted on an inverted microscope (Olympus IX71). Cells were continually perfused with a slow flow of baseline solutions which contained 0.5 or 2 mM Ca^{2+} + vehicle control (0.01% DMSO) or a NAM (NPS2143, 1, 3 & 10 μM) using a rapid perfusion system (RPS, Intracel, cat. #RSC160), where the equipment set up is demonstrated in Figure 2.2. The MetaMorph™ microscopy automation computer software system (Cairn Research) was used to manually select single cells from a pre-selected region of the coverslip, including a region which did not contain cells, to set the background fluorescence reading for the duration of each experiment. Cells were alternatively excited at 340 and 380 nm, through a 40x quartz, oil immersion objective and emission was measured at 510 nm using a charge-coupled device camera (Hamamastsu Orca), which converts electrical signals of each pixel, to generate an image, which were obtained every 2 seconds during each experiment. Figure 2.2 displays the fluorescent intracellular Ca^{2+} imaging equipment set up, where cells were exposed to pro-inflammatory stimuli at specific time-points during each experiment, controlled by the RPS system, to measure changes to intracellular Ca^{2+} levels in single cells, used as one of the biological readouts of CaSR activation, using the MetaMorph™ computer software (Cairn Research).

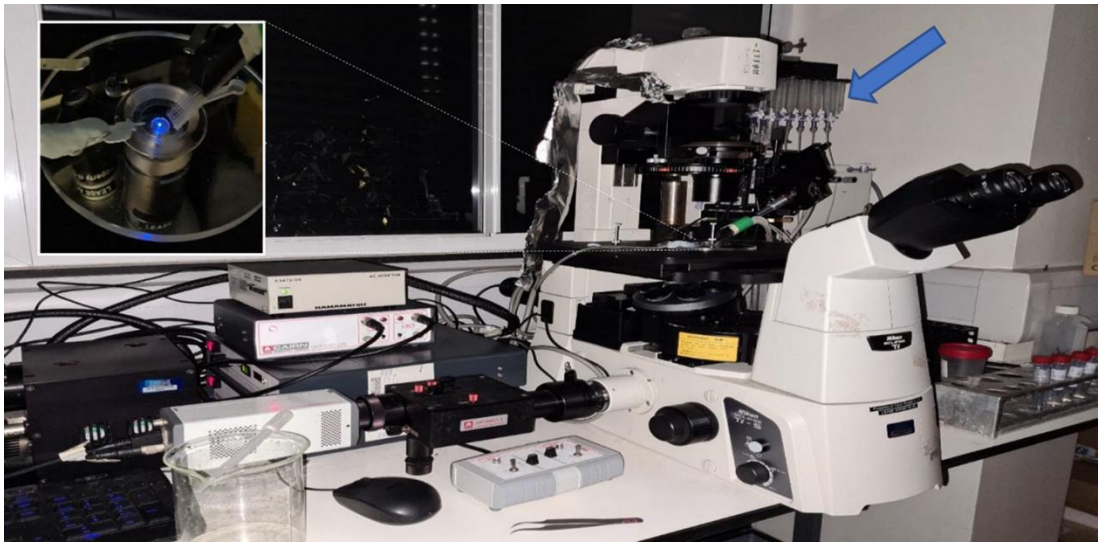

Figure 2.2 The fluorescent intracellular calcium imaging equipment set up. Cells seeded onto the centre of glass coverslips were placed in the perfusion chamber (inset), which was mounted on an inverted microscope (Olympus IX71) and continuously perfused with a slow flow of baseline solutions (either 0.5 or 2 mM Ca^{2+} + vehicle control (0.01% DMSO) or a negative allosteric modulator at the calcium-sensing receptor (NAM, NPS2143, 1, 3 and 10 μM) using a rapid perfusion system (blue arrow). The RSC system allows constant flow of different experimental solutions at times programmed into the RSC software. To the left of the perfusion chamber is a suction tube which slowly aspirates the solutions in chamber without disrupting the coverslip, allowing for exposure to a variety of stimuli, during one experiment, to monitor changes to intracellular Ca^{2+} levels over time, in response to a variety of stimuli. Image obtained from laboratory colleague, Mr Petar Popov.

Following acquisition of images and data generated by the MetaMorph™ computer software, data was analysed using an Excel based analysis programme, developed by a former laboratory colleague, Dr Martin Schepelmann. First, data were background-subtracted for each region defined on the MetaMorph™ software, then generation of the 340:380 ratio for each cell was performed ("cleaned" data). For generation of representative traces of Ca^{2+} imaging experiments, the "cleaned" values were transferred to Graphpad Prism 9.0 and representative traces of each cell per experiment were generated. From these "cleaned" data, maximum intracellular Ca^{2+} changes

were generated by determining the average maximum fold difference between the baseline and stimulated response for each coverslip analysed, minus the initial peak, due to potential artefacts from movement of the robotic arm. The data generated for each coverslip were transferred to GraphPad Prism 9.0 for figure preparation and statistical interrogation.

2.2 Immunohistochemistry (IHC):

IHC was used as a method to determine CaSR protein expression in human airways structural and immune cells involved in the sensing and responding to inhaled innocuous stimuli such as PM, and those involved in the pathogenesis of lung diseases such as asthma and COPD. Detailed methods regarding IHC experiments are provided within Chapter 4, section 4.2.6.

2.2.1 Antigen Staining:

IHC was used as a method to stain specific antigens of interest, such as the CaSR, used in these studies. First, endogenous peroxidase activity was quenched from cells before preparation and application of the primary antibody targeted towards the CaSR antigen was performed overnight, at 4 °C. The secondary antibody, which was targeted towards the species the primary antibody was raised in and the isotype of the primary antibody, and conjugated to biotin, was prepared, and applied to cells for 1 hr at RT. Both primary and secondary antibodies were dissolved in a buffer consisting of 0.1% Triton™X-100 (Sigma, cat. #X100), 3% Seablock (Thermofisher, cat. #37527) and 0.5 g bovine serum albumin in 50 ml 1X PBS.

2.2.2 Generation of the Avidin/Biotin Complex (ABC):

Once the CaSR had been targeted by specific primary and secondary antibodies, the VECTASTAIN® ABC kit was used to generate the avidin/biotin enzyme complex of horseradish peroxidase for downstream amplification and visualisation of CaSR distribution in a range of airway cell types.

2.2.3 Visualisation of CaSR distribution in airway cells:

The avidin/biotin enzyme complex required a specific substrate for visualisation of CaSR staining during IHCs contained within this Thesis. 3,3'-Diaminobenzidine (DAB) was used as the chromogenic substrate of horseradish peroxidase, which oxidises upon exposure to peroxidase enzymes, resulting in the development of a brown colour, which was indicative of positive CaSR staining. In IHC experiments, two negative controls were used: the primary antibody was omitted from the process, to assess in binding specificity of the secondary antibody, or an isotype control primary antibody was used, to assess non-specific background staining, where the isotype control lacks specificity to the antigen of interest but match the class and type

of the primary antibody. The processes described in the steps above are illustrated in Figure 2.3

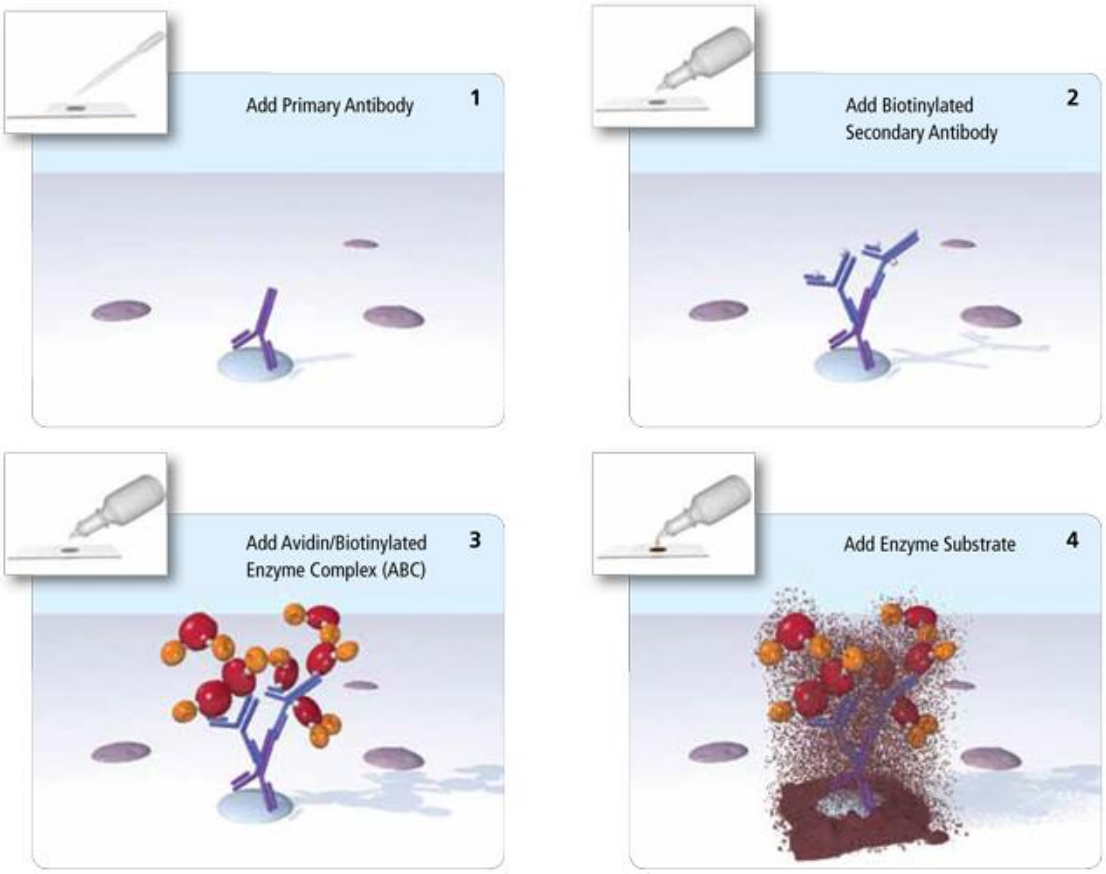

Figure 2.3: An illustration of the immunohistochemistry (IHC) process used. First, the antigen of interest was labelled using a specific primary antibody (1), then the biotinylated secondary antibody was applied to cells (2). Following this, the avidin/biotin enzyme complex was formed by utilisation of the VECTASTAIN® ABC kit (3), before addition of the 3,3'-Diaminobenzidine (DAB) as a chromogenic substrate of horseradish peroxidase, for visualisation of the expression of the antigen of interest (4). Image taken from https://vectorlabs.com/products/abc-kits/vectastain-abc-hrp-kit-standard.

2.2.4 Counterstaining and Mounting:

In each experiment, Harris Haematoxylin was used as a nuclear counterstain, which is a potassium alum haematoxylin which oxidises upon exposure to air.

Nuclear and non-nuclear structures were differentiated in stained cells by addition of acid alcohol and conversion of the initial soluble red colour of the haematoxylin to an insoluble blue colour was performed by addition of ammonia water.

Slides containing stained cells were dehydrated through a series of ethanol changes (70-100%) and through two changes of xylene. Slides were air dried and then VectaMount® was applied to the cells, to permanently preserve IHC stains. A #0 glass coverslip was carefully placed on top of the slide and left to air dry overnight. The following day, slides were sealed using clear nail varnish applied around the edges of the coverslip.

2.2.5 Image Acquisition:

An Objective Imaging Surveyor semi-automated slide scanning system, available in the Bioimaging Hub in The School of Biosciences at Cardiff University, was used to obtain high-quality images of IHC stains. The scanner consisted of an Olympus BX41 brightfield microscope equipped with 5x, 10x, 20x and 40x objectives, a QImaging QICAM Fast 1394 colour digital camera (with associated PC) and an OASIS motorised XYZ stage that can be controlled by a joystick or directly via the Surveyor software. 40x images were obtained of each sample and then images were then transferred to the IrfanView computer software for batch cropping, to ensure each image was of equal size, before a scale bar (50 μm) was added to each image for preparation of the final figure panels for each cell type.

2.3 Real-time quantitative Polymerase Chain Reaction (RT-qPCR):

RT-qPCR was used as a method to measure alterations to mRNA expression of alarmins as key mediators involved in the response to pro-inflammatory

stimuli in airway epithelial cells and contribute to the initiation and perpetuation of pro-inflammatory responses in lung diseases, such as asthma and COPD. Detailed methods regarding RT-qPCR experiments are provided within Chapter 5, section 5.2.3.

2.3.1 RNA Extraction and Analysis of Purity and Integrity:

High-quality total RNA was extracted from samples of primary normal human bronchial epithelial cells (NHBECs) using the TRIzol® (Thermofisher Scientific) method which consists of phenol and guanidine isothiocyanate, to isolate RNA, DNA, and protein content of biological samples. Chloroform was added to TRIzol® samples to promote phase separation of RNA, DNA, and protein from biological samples. Following refrigerated ultra-centrifugation using the Sigma 4K15 ultracentrifuge, RNA was removed from the sample before addition of isopropanol, to precipitate RNA. After washing the RNA with ethanol and air drying, RNA was resuspended in nuclease free H_2O and then subjected to treatment with DNase, to reduce potential DNA contamination of samples.

Purity analysis was conducted using the Nanodrop Spectrophotometer, which uses ultraviolet (UV) absorbance to measure RNA, DNA, and protein concentration of samples. Absorbance at a wavelength of 260 nm (A_{260}) was used for measurement of nucleic acid concentration of the samples and then a conversion factor was applied to the A_{260}, which is based on the extinction coefficient for RNA (40 µg/ml), to provide an accurate measurement of RNA concentration (performed within the Nanodrop computer software). The absorbance at 280 nm (A_{280}), on the other hand, was used to estimate the protein content of samples. From the A_{260} and A_{280} a ratio was formed, which was used to analyse purity of RNA samples. Pure RNA has a A_{260}:A_{280} ratio of

>1.8, and anything below this implies potential DNA or protein contamination of RNA. The absorbance at 230 nm (A_{230}) was also used as an indicator of other contaminants that may be present in the samples, such as guanidine thiocyanate, which is common in the nucleic acid purification method used in these studies.

Integrity analysis of RNA was carried out using the Agilent TapeStation 2200 or 4200 automated electrophoresis systems. This software generated a RIN[e] score for each sample, which demonstrated the integrity of RNA samples which was assessed on a scale of 1-10 and calculated using an algorithm which uses factors including total RNA ratio between 28S and 18S peaks. A score of 10 represented high quality RNA, with very little degradation, validating that samples were of sufficient quality to proceed with synthesis of cDNA from these RNA samples, for use as a template strand for RT-qPCR experiments.

2.3.2 RT-qPCR and Downstream Analysis:

First, intron-spanning primers were designed and validated to target specific genes of interest. RT-qPCR samples were prepared by addition of cDNA, primers, DNA polymerase, and Sybr Green, (double-stranded DNA-binding dye that intercalates non-specifically into double stranded DNA). Samples were added to Rotor-Gene and Rotor-Gene Q qPCR machines, in the laboratory of Dr Simon Scofield at Cardiff University. These machines are unique in that samples were spun during analysis, which minimised the optical and thermal variation often observed using plate formats, by preventing formation of bubbles or condensation. Set up of RotorGene machines is demonstrated in Figure 2.4, where tubes placed within the Rotor spin continuously throughout the duration of the PCR runs and each sample passes the LED light source. Upon excitation by the LED light source, Sybr green

fluorescence within each sample was emitted and filtered onto a photomultiplier tube (PMT) detector, to generate an electrical signal for each sample as it passes the detector, which were then converted into amplification curves on the RotorGene computer software (Arya *et al.* 2005).

Following RT-qPCR, sample data was interrogated using the Rotor-Gene software. As PCR products are yielded, Sybr green was incorporated into each double-stranded DNA molecule, until it reached a set threshold (cycle threshold, CT) of fluorescence intensity. The CT was set at 0.031622 ($\log 10^{-1.50}$) for each experiment which allowed for generation of a CT value for each sample, the cycle in which they crossed the CT. Normalisation of the data was performed using the Rotor-Gene computer software. The first step of normalisation was performed by dividing the raw sample data points by the by the background level (first 5 cycles of RT-qPCR) for all samples. Then the second derivative of each sample trace was taken to assess the curvature or concavity of each sample trace to determine positive or negative second derivative, respectively, to determine a starting point for each sample. The background level was then averaged from cycle 1 up to the starting point for each sample, as a method to precisely measure quantitation results (Dynamic Tube Normalisation). Additionally, to reduce potential noise generated by fluctuations in the background fluorescence of samples during progressive cycles, slope correction was performed, which uses a line of best fit to determine the level of noise, instead of an average, and normalises to that instead.

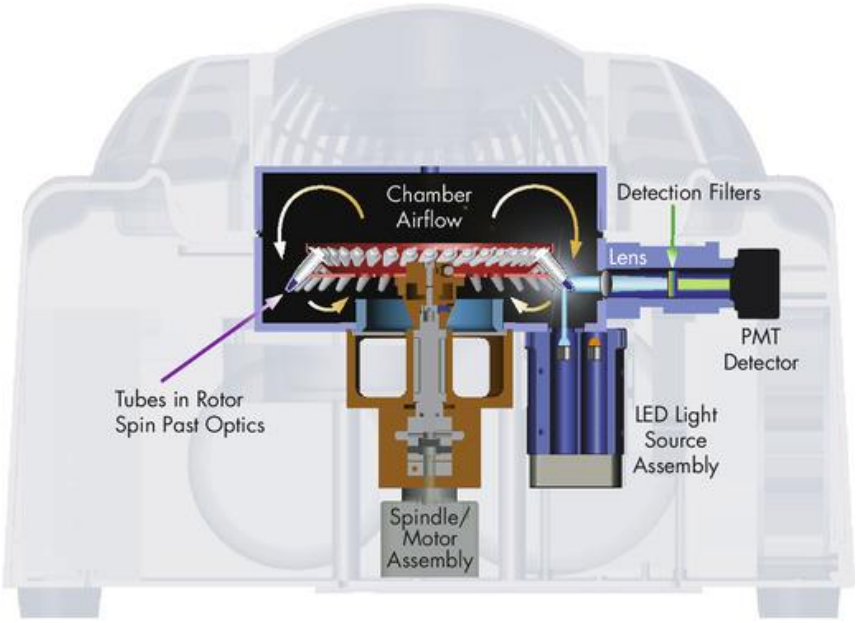

Figure 2.4: RotorGene real-time quantitative polymerase chain reaction (RT-qPCR) machine set up. Samples in tubes were placed in the rotor, which spin continuously during the PCR runs. These pass by an LED light source which shines light to excite the Sybr Green fluorescent intercalating dye. Photons emitted from each sample were focused through detection filters and finally onto the photomultiplier tube (PMT) detector, which converted the photon signal into an electrical signal, which is converted to a value for each sample and plotted as an amplification curve in the RotorGene computer software. Image taken from: https://www.qiagen.com/us/products/instruments-and-automation/pcr-instruments/rotor-gene-q-mdx-us/.

CT values for each technical replicate of samples from each treatment condition of the gene of interest and housekeeping gene were transferred to an Excel sheet. The technical repeats were averaged for each treatment condition and the average CT value for the gene of interest was subtracted from the average CT value for the housekeeping gene (ΔCT), of the same sample. Then, the ΔCT from the vehicle control treated cells was subtracted from the ΔCT from each treatment condition (ΔΔCT) before relative fold gene

expression was determined by calculating 2 to the power of negative ΔΔCT for each sample (2^-(ΔΔCT) (Livak and Schmittgen 2001).

2.4 Flow Cytometry:

Flow Cytometry was used as a method to characterise and purify a range of human blood and tissue-derived immune cells and to determine the effect of pro-inflammatory stimuli on key functions of airway immune cells. Detailed methods regarding flow cytometry experiments are provided within Chapter 4, sections 4.2.2.4, 4.2.3.11, 4.2.3.12, 4.2.4.3, and Chapter 5, sections 5.2.5.4 and 5.2.8.2.

2.4.1 Sample preparation:

Human immune cells were stained with fluorescently labelled antibodies specific to the cell-surface markers of each cell type of interest, an isotype control antibody or in an aliquot per sample, cells were not stained and acted as an unstained control, to ensure purity and to aid in characterisation of each sample, using flow cytometry. To determine purity of AMs isolated from human lung tissue, following resection surgery, primary AMs were stained with a panel of markers which included positive staining for Cluster of differentiation (CD)163, CD206, Human Leukocyte Antigen (HLA-DR), CD45, and CD33, and staining of CD14 and MerTK, with no difference in staining as the negative isotype or unstained controls. To determine purity of monocyte derived dendritic cells, from healthy human whole blood, cells at each stage of isolation and differentiation were analysed using specific markers. To analyse the purity of monocytes, CD14, CD11b, CD11c, HLA-DR, and CD86 were used as positive markers and CD1a, CD40 or CD83 were used as negative markers for these cells. iDCs showed positive staining for CD1a, CD11b, CD11c and

HLA-DR, but negative staining for CD14 and CD86 and mDCs purity were analysed by positive staining of CD83 in these cells. Finally, collection and processing of human peripheral blood mononuclear cells (PBMCs) allowed for purity analysis of ILC2 cells within the population by identifying lineage negative (Lin^-) (CD4/8/14/16/19/56/123 and FcεRI) $CD45^{high}CD127^+CRTH2^+$ ILC2 cells. All relevant antibodies used for phenotyping each cell type is provided within Chapter 4.

2.4.2 Flow cytometry principles:

The stained single cell suspension was applied to the flow cytometer, and the cell suspension underwent hydrodynamic focusing by sheath fluid. This resulted in injection of cells to the centre of the stream, at a slightly higher pressure, which aligns the cells into single file whilst they flow through the machine and through the path of the laser beam (Figure 2.5). The laser light source provided a light beam at a specific wavelength during the time at which each cell as passes through the machine and the light emitted and scattered from the cells was channelled by sets of filters and mirrors. The emitted or forward and side scattered (FSC or SSC) light was detected by specific PMTs, which converted the energy of a photon into an electric signal, which was plotted against time, using the FloJo analysis software (outlined in Figure 2.6). FSC and SSC correlate to cell size and granularity, respectively, therefore, cell populations were distinguished based on size and granularity alone, as used during Chapters 4 and 5 of my thesis, for characterisation and interrogation of experimental data. Photon emission over time was measured by the PMTs as a pulse and the total pulse height and area was measured, where the pulse area correlated directly to the intensity of fluorescence of each particle detected by the flow cytometer (termed as an event) (Figure 2.7). Once each

cell had run through the flow cytometer, per treatment condition, the results were interrogated using FloJo, where fluorescence intensity of each fluorochrome was converted to a log scale and the fluorescence intensity of each event were measured and compared to the isotype and unstained controls, to assess level of positive staining (Figure 2.8) (Adan *et al.* 2017).

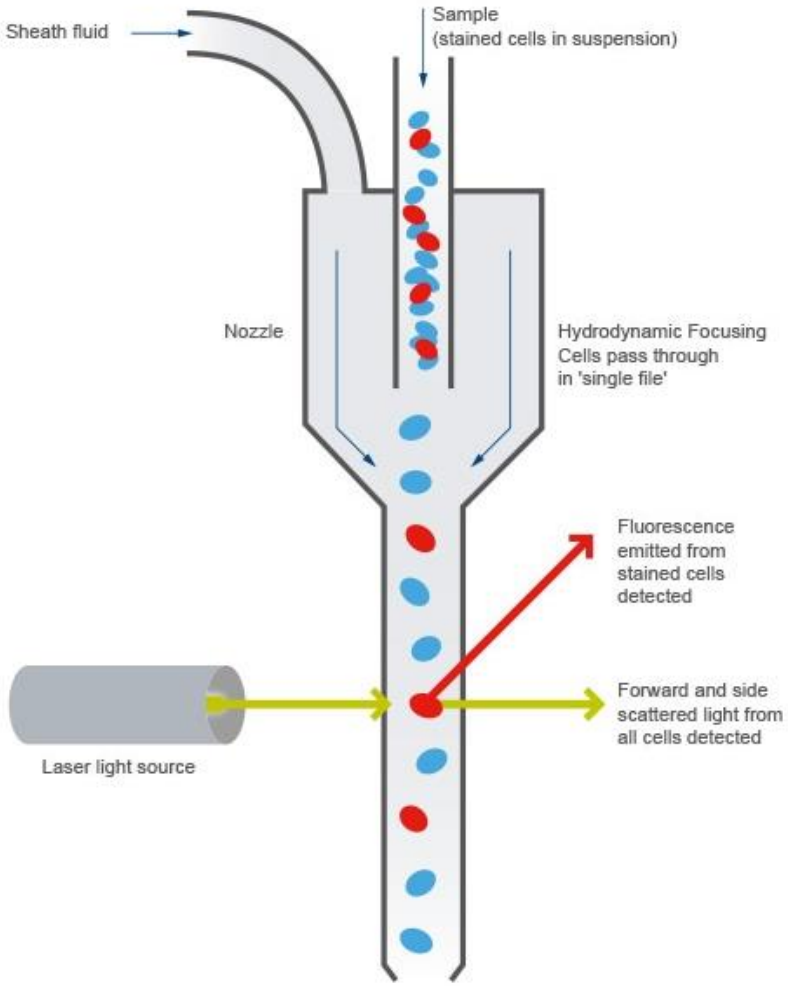

Figure 2.5: Simple outline of the process of flow cytometry. The stained single cell suspension was applied to the flow cytometer, before being hydrodynamically focussed by the sheath fluid. This resulted in injection of cells to the centre of the stream, at a slightly higher pressure, resulting in aligning of cells and single file flow direction through the machine. The laser light source provided light at a specific wavelength and the light which was emitted and scattered from each cell as it passed through the laser beam, was detected. Image taken from https://www.abcam.com/protocols/introduction-to-flow-cytometry.

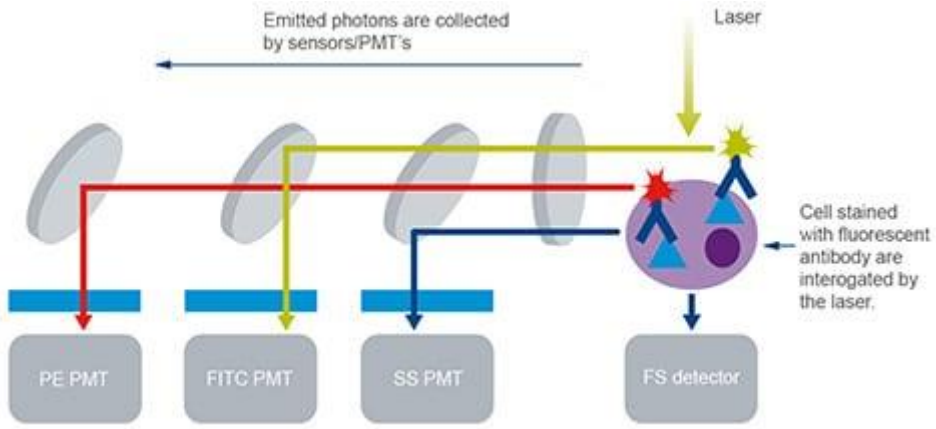

Figure 2.6. Fluorescent light emitted from fluorescently labelled cells was filtered so that each photomultiplying tube (PMT) detects a specific wavelength. The Phycoerythin (PE), Fluorescein isothiocyanate (FITC) and forward and side scatter (FSC and SSC) PMTs convert the energy of a photon emitted or scattered from the cell into an electronic signal – a voltage, which was used to generate a signal of an event on the flow cytometry computer software. Image taken from https://www.abcam.com/protocols/introduction-to-flow-cytometry.

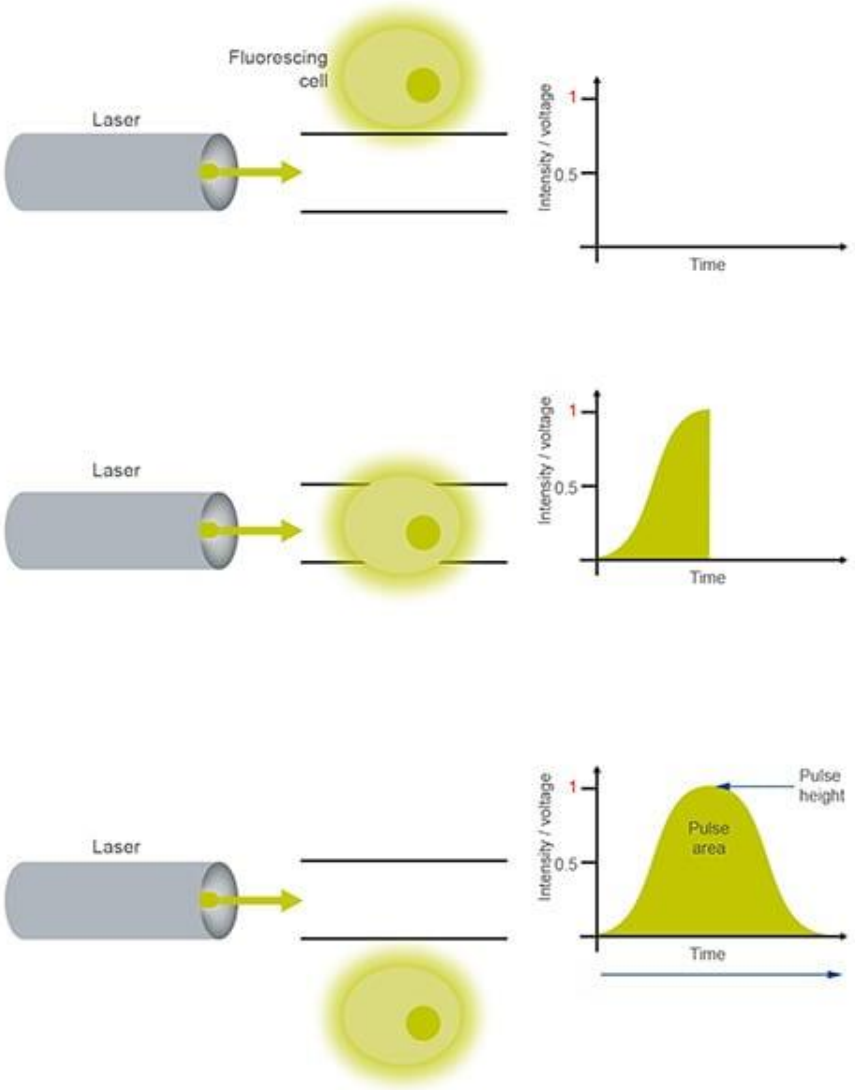

Figure 2.7. The photomultiplier tube (PMT) measured the pulse area of the electrical signal (voltage) generated each time a fluorescing cell released photons. In the absence of fluorescing cells, no photons are emitted. Once the fluorescently labelled cell passed through the laser path, photons were emitted and converted to electrical signals (voltages) by the flow cytometer, which created a pulse, which is increased to maximum when the cell is directly in the laser beam path and decreases as the cell passes through the laser beam, resulting in a plot of the pulse of voltage over time. Image taken from https://www.abcam.com/protocols/introduction-to-flow-cytometry.

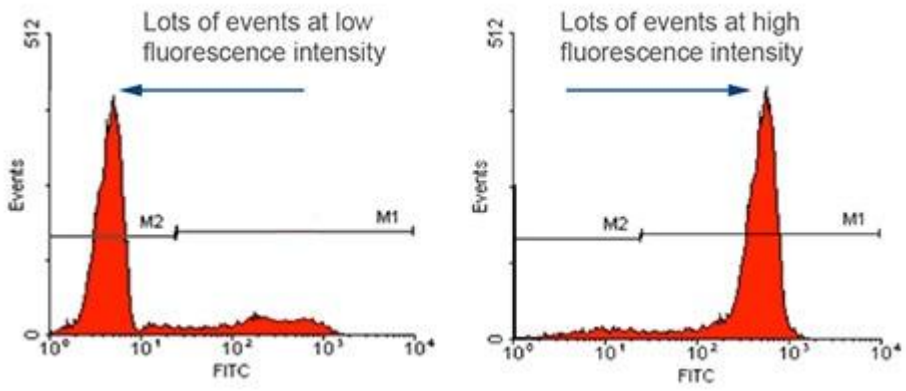

Figure 2.8. Fluorescence intensity measurements for an unstained and stained cell population. Unstained cells demonstrated fluorescence events at low fluorescence intensity of Fluorescein isothiocyanate (FITC), indicative of a negative result (left image). Stained cells were represented on the right image and demonstrated a large number of events at higher fluorescence intensity. M1 and M2 represent the positive and negative populations, respectively. Image taken from https://www.abcam.com/protocols/introduction-to-flow-cytometry.

2.4.3 Analysis and Gating:

For characterisation experiments, the overall median fluorescence intensity (MFI) of each antibody was calculated by subtracting the MFI obtained for the isotype control from the MFI obtained for the samples stained with specific antibodies, to determine positive populations based on specific antibody expression. These were represented as histograms (on a modal scale) in representative flow cytometry plots with the addition of the unstained and or isotype control for each characterisation antibody used, to demonstrate the distinction between each population. During experimental analysis, the MFI of treated cell samples were gated by first excluding dead cells from the population, then into the cell type of interest using FSC and SSC, and finally gated from the background fluorescence signal (left plot in Figure 2.6). BifurGate (M1 or M2 in Figure 2.6) and the rectangle gating tool, both provided

in FloJo software, allowed for generation of gates to analyse experimental data, then compared to the parent population, before being expressed as a percentage of the untreated or vehicle control treated cells. Due to use of multiple fluorescently conjugated antibodies and potential fluorescence spill-over, compensations were applied with the use of single stains and fluorescence minus one (FMO) controls. FMO controls were generated from samples stained with all fluorophores included in the sample analysis, however, omitted one of them, which provided a FMO control. This allowed for identification of the background signal by the samples and aided in gating positive populations during multicolour flow cytometry experiments, which was crucial as in some cases, positive populations were not clearly separated from the negatives, due to low or variable expression.

CHAPTER 3: HARMFUL COMPONENTS OF POLLUTANTS ARE ACTIVATORS AT THE CASR.

3.1 Introduction:

Exposure to ambient air pollution is a major problem worldwide, with 9 of every 10 people living in areas of poor air quality (World Heath Organisation 2018). Global excess mortality from ambient air pollution has been more recently estimated at around 8.8 million per year, a doubling on previous estimations, highlighting the importance of tackling the detrimental effects of exposure to ambient air pollution (Burnett *et al*. 2018; Lelieveld, Pozzer, Pöschl, *et al*. 2020).

Particulate matter (PM) is one of the major components of ambient air pollution and is generated from a variety of sources including combustion of fossil fuels such as diesel and petrol, and cigarette smoking (Braun *et al*. 2019; Vohra *et al*. 2021). PM is known to contain an array of heavy metals within the inorganic component, which are unable to be broken down and therefore persist and accumulate in the environment (Briffa *et al*. 2020). Continued inhalation of PM, results in acute exacerbations of lung diseases such as asthma and COPD and more recently IPF (Atkinson *et al*. 2012; Winterbottom *et al*. 2018; Wang *et al*. 2021). However, the direct molecular targets and potential mechanisms underlying PM-induced acute exacerbations of these lung diseases are yet to be elucidated.

The CaSR has been demonstrated to be involved in the pathogenesis of lung diseases and NAM reduces airway hyperresponsiveness, inflammation and some aspects of remodelling in animal models of asthma (Yarova *et al*. 2015; Yarova *et al*. 2021). Therefore, in this Chapter, I sought to elucidate whether 1)

PM generated from distinct sources exert its effects via the CaSR and 2) the NAM reduces PM-induced CaSR activation, measured as an increase in intracellular Ca^{2+} levels.

3.2 Methods:

3.2.1 Cells:

Human embryonic kidney cells (HEK293) stably transfected with the human CaSR (HEK-CaSR), or an empty vector (HEK-0) were previously generated and stored in liquid nitrogen until use (Maldonado-Pérez *et al.* 2003; Yarova *et al.* 2015).

3.2.2 HEK293 Cell Culture and Seeding for Experiments:

HEK293 cells were thawed and expanded complete DMEM (Merck, cat. # 5671), prepared by the addition of fetal bovine serum (FBS, 10%) (Gibco, cat. #A3160802) and Penicillin/Streptomycin (1%) (Gibco, cat. #15140122). Medium was replaced every other day during expansion and hygromycin B (Gibco, Thermofisher Scientific, cat. #10687010) was added (2 µl/ml) to positively select CaSR-transfected cells within the population. Cells were collected from liquid nitrogen stores, transported to the lab in liquid nitrogen and thawed rapidly at 37 °C and transferred to a T75 flask containing 15 ml warmed complete DMEM and left to adhere at 37 °C and 5% CO_2 overnight. On the following day, complete DMEM was removed and replaced with 15 ml fresh complete DMEM with the addition of 30 µl hygromycin B. Expansion was monitored using phase-contrast microscopy and once >60% confluent, medium was removed from the flask, 3 ml of 0.25% Trypsin-EDTA (Merck, cat. #T4049) was added and then incubated at 37 °C for a maximum of 5 minutes. Inactivation of trypsin was performed by adding 10 ml complete DMEM to the

flask. Detached cells were transferred into a 15ml Falcon tube and centrifuged at 500 g for 5 minutes. The supernatant was carefully poured from the tube and the cell pellet was resuspended in 1 ml complete DMEM, mixed well by gentle pipetting before 9 ml of complete DMEM was added. 60 µl of the cell suspension (~4,500 cells) was carefully pipetted to the centre of a poly-D-lysine (PDL)-coated glass coverslip (#1.5 thickness) in a 24-well plate or into a non-coated 96-well plate. Both types of plates were placed into an incubator to allow for cell attachment. Following 1 hr incubation, 500 µl complete DMEM was added to each well of the 24-well plate and 40 µl complete DMEM added to each well of the 96-well plate (100 µl total volume).

3.2.3 Intracellular Ca^{2+} Imaging:

General methodological principles of intracellular Ca^{2+} imaging is provided in Chapter 2, section 2.1.

3.2.3.1 Preparation of Extracellular Solutions:

First, a non-Ca^{2+} containing extracellular solution (0 Ca^{2+} ECS) was prepared by adding the following compounds to a 2 L beaker to result in final concentrations of: 135 mM NaCl (Atom Scientific, cat. #GPC8030), 5 mM KCl (Sigma, cat. #P3911), 5 mM HEPES (Sigma, cat. #PHG0001) and 10 mM D-glucose (Fisher Scientific, cat. #10373242) in 2 L MilliQ H_2O. Finally, a 1 M stock of $MgCl_2$ was prepared (Sigma, cat. #M9272) in 100 ml MilliQ water. Once fully dissolved, 2.4 ml of 1 M stock of $MgCl_2$ was added to the beaker containing the other components of the ECS. The pH of the solution was maintained at 7.4 and stored at 4 °C for up to one week. 98.8 ml was removed from the 0 Ca^{2+} ECS and placed into a separate container with lid. 120 µl $CaCl_2$ (from a 1 M $CaCl_2$ stock solution at a final concentration of 1.2 mM) and 0.2 g (0.2%) bovine serum albumin (BSA) was carefully added to this solution (loading

buffer). The container was inverted and placed at 4 °C overnight to fully dissolve. 0 Ca^{2+} ECS was also used to prepare baseline and treatment solutions containing different concentrations of Ca^{2+}. 1.2 mM and 2 mM Ca^{2+} ECS were prepared from a 1 M $CaCl_2$ (Sigma, cat. #21115) solution in 0 Ca^{2+} ECS, resulting in final concentrations of 1.2 and 2 mM, respectively. Aliquots of these solutions were used to prepare baseline and treatment solutions for use in imaging experiments immediately or stored at 4 °C for up to one week.

3.2.3.2 HEK Cell Loading:

On the day of experiments, solutions were warmed to RT before the pH of all solutions adjusted to 7.4 before use. HEK cells were loaded with Fura-2AM (3 µM, Invitrogen, ThermoFisher Scientific, cat. #F1221) in loading buffer for 1 hour at 37 °C and 5% CO_2. After loading, cells were incubated with loading buffer (without Fura-2AM) for 15 minutes at 37 °C and 5% CO_2. HEK293 cells were removed from the incubator and allowed to cool to RT before adding the baseline solution: DMSO (vehicle control, prepared by serial dilution of 100% DMSO to a final concentration of 0.01% DMSO in ECS) or NAM (NPS2143, prepared by serial dilution of 10 mM in 100% DMSO to a final concentration of 1 µM in ECS) for 10mins prior to mounting on the microscope stage.

3.2.3.3 Preparation of Stock Solutions for Treatment of HEK Cells:

Cigarette smoke extract (CSE) was prepared based on a modification of a previously developed method (Carp and Janoff 1978). For the equipment set up, A 50 ml syringe was connected to one arm of a 3-way stopcock and the other 2 arms of the stopcock was connected to a cigarette via a holder (1000

µl pipette tip) and connected to a length of Tygon tubing (Cole-Parmer, Cat. No. 06509–17) and placed through a hole in the lid of the beaker, sealed with parafilm and Blue Tack and submerged into the beaker containing 100 ml 0 Ca^{2+} ECS or RPMI (Gibco, cat. #11875093) (Figure 3.2.1). 5 full-strength Marlboro Red cigarettes (filters removed; Marlboro Red, Class A cigarette, Tar 10 mg, Nicotine 0.8 mg; Phillip Morris USA, Richmond, VA) were lit in a fume cupboard one by one and the cigarette smoke (CS) was drawn into the 50 ml syringe (to the 60 ml mark) over 10 seconds. Following this, CS was extracted into 0 Ca^{2+} ECS by turning the stopcock and gently pushing plunger of syringe to "bubble" the smoke through the ECS or RPMI. This process was repeated until the cigarette had been "smoked" to 5 cm from the butt. This solution represented "100%" CSE and was sterilised by passing through a 0.20 µm Minisart™ Plus Syringe Filter (Sartorius, cat. #10730792). 100% CSE was diluted to the required strength (2-10%) and used within 1 hour of preparation or stored at -80 °C for future use (Oltmanns *et al.* 2005; Walters *et al.* 2005).

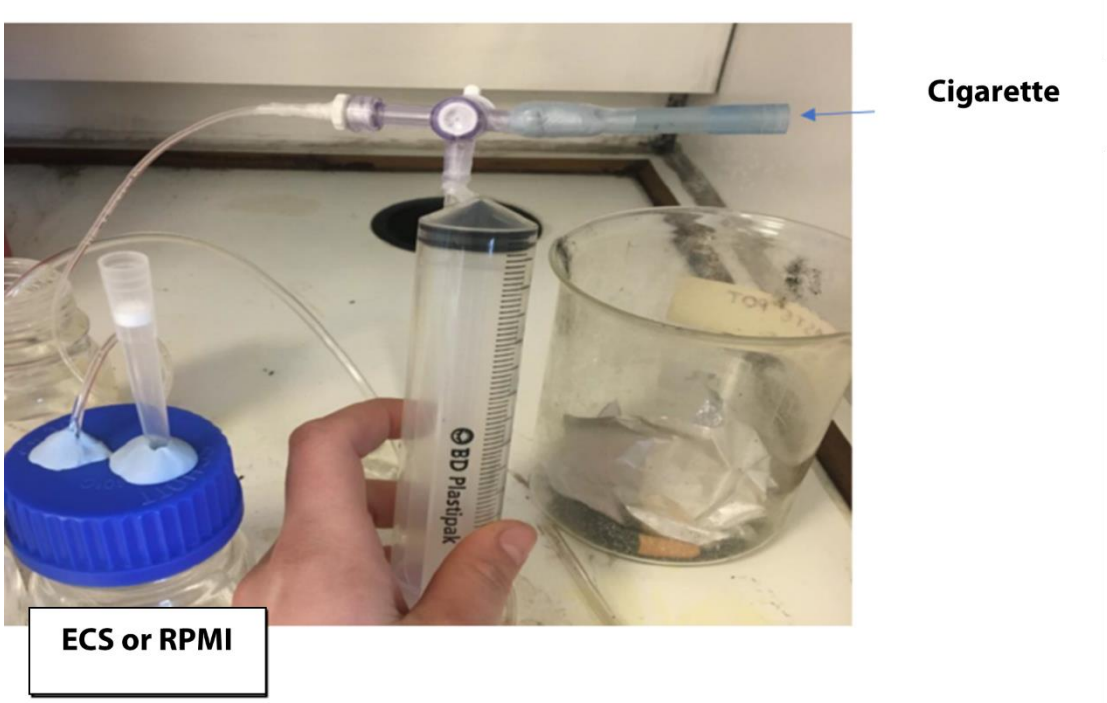

Figure 3.1: The generation of cigarette smoke extract (CSE) and equipment set up. The filter was removed from a Marlboro Red cigarette and placed into the holder. Each cigarette (5 total) was lit, and the smoke drawn into the syringe over 10 seconds and then "bubbled" through 100 ml of extracellular solution (ECS) or RPMI culture medium. The resulting solution (CS extract, CSE) was filtered through a 0.2 µm filter and analysed for the presence of nicotine and cotinine (nicotine metabolite) using solid phase micro extraction (SPME) followed by gas chromatography and mass spectrometry.

3.2.3.4 Analysis of Cigarette Smoke Extract Using Solid-Phase Micro Extraction Followed by Gas Chromatography and Mass Spectrometry:

Calibrators: (-)-Nicotine PESTANAL® was supplied in liquid form (1 g/ml) (Sigma-Aldrich cat. #36733). (-)-Cotinine (Sigma-Aldrich, cat. #C5923) was supplied in powdered form and dissolved into methanol (Sigma-Aldrich, cat. #32213) (1.35 g/ml). Working dilutions of 10 mg/ml, 1 mg/ml, 100 µg/ml, and

10 µg/ml were prepared in RPMI and stored at -20°C. Eight-point calibrations (5, 10, 20, 50, 100, 200, 500, 1000 ng/ml) were made from subsequent dilutions of the stock solutions of both nicotine and cotinine in RPMI. NaCl was added to each dilution to enhance solid phase micro extraction (SPME). SPME fibres were exposed to each dilution of nicotine/cotinine and the experimental CSE sample for a total of 30 mins at 37 °C. The SPME fibre was then placed into the Thermo Scientific™ TSQ™ 8000 gas chromatography/ mass spectrometry (GC/MS) machine (Thermofisher Scientific).

3.2.3.5 Experimental Analysis:

GC/MS analysis was performed using an Thermo Trace 1300 GC (ThermoFisher Scientific) interfaced with Thermo ISQLT (single quadrupole) mass-selective detector ran in selective ion mode (SIM) and selecting peaks at a mass/charge ratio (*m/z*) of 162, 161, 133 and 84 *m/z*. The parameters for the experimental set up were selected using the Chromeleon 7.2 software. The GC/MS was equipped with a TG5MS (ThermoFisher Scientific) column (39 m x 0.25 mm with phase thickness of 0.25 µm) with helium as the carrier gas at a septum purge flow rate of 30 ml/min. Samples were injected in the splitless mode as a standard mode for low concentration samples, with 2 minutes desorption. The oven temperature started at 65°C for 2 mins, followed by a temperature ramp up to 200 °C and then 300 °C. The temperature of the injection port was 260 °C, the transfer line was 280 °C and the ion source remained at 230 °C. Quantitative peak used for nicotine was 84 *m/z* and the confirming peak, 162 *m/z*. Peak area ratios of nicotine and internal standards were calculated for each concentration by the Chromeleon 7.2 software (Thermo Scientific, cat. #CHROMELEON7) and plotted to allow us to determine nicotine concentration in the in-house generated CSE. Standard curves were generated from known

concentrations of nicotine in RPMI plotted with a sigmoidal non-linear regression fit. Unknown values from CSE in RPMI were interpolated from the graph using the Chromeleon 7.2 software.

3.2.3.6 Preparation of Heavy Metal Solutions:

Cadmium chloride ($CdCl_2$, Sigma-Aldrich, cat. #202908) 100 mM stock solution was made by weighing 96.66 mg $CdCl_2$ in a glass vial with lid and adding 5 ml deionised H_2O. The mixture was vortexed well to fully dissolve before serial dilution in 2 mM Ca^{2+} ECS to a final concentration of 20 µM for use in imaging experiments. Nickel (II) chloride hexahydrate ($NiCl_2$, Sigma-Aldrich, cat. #654507) 100 mM stock solution was prepared by weighing 64.8 mg $NiCl_2$ in a glass vial with lid and adding 5 ml deionised H_2O. The mixture was vortexed well and heated slightly by submerging the tube in warm water to allow for $NiCl_2$ to fully dissolve. Serial dilutions were prepared from this in 2 mM Ca^{2+} ECS to the final concentration of 20 µM to be used to conduct measurements of intracellular Ca^{2+} levels in response to heavy metals.

3.2.3.7 Preparation of Particulate Matter:

PM powder (Sigma-Aldrich, cat. #NISTSRM1648a) was vortexed, then 25 mg was weighed directly into a 20 ml universal tube. PBS was added to this resulting in a final concentration of 1 mg/ml. This solution was vortexed and sonicated using a sonicating water bath (GT Sonic, cat. #Z0001) at 40 Hz for 15 minutes. Following this, the solution was vortexed and aliquoted before being stored at -80 °C for future use. Before preparation of final concentrations of PM, the 1 mg/ml stock aliquots were thawed and sonicated again as above

then serial diluted to 100 µg/ml then, 30 µg/ml then to 10 µg/ml in 2 mM Ca^{2+} ECS or RPMI.

3.2.3.9 Preparation of Treatment Conditions:

Treatment groups were as follows: DMSO (vehicle control, final concentration of 0.01% DMSO) NAM (NPS2143, final concentration of 1 µM), Ca^{2+} (final concentration 2.5 mM prepared by adding 125 µl of 1 M $CaCl_2$ and adding to 50 ml 0 Ca^{2+} ECS), CSE (10%), Cd^{2+} (20 µM), Ni^{2+} (20 µM) and PM (100 µg/ml) all prepared in 2 mM Ca^{2+} ECS. Additionally, 100 mM ATP stock solution was prepared by weighing 551.15 mg ATP (Sigma, cat. #2135791) in a glass vial with lid and adding 10 ml MilliQ H_2O. This solution was vortexed well and aliquoted into 1 ml and stored at -20 °C. On the day of experiments, ATP stock solution was thawed and serially diluted to 100 µM in 2 mM Ca^{2+} ECS. Each treatment was poured into the tubes of rapid perfusion system for use in the experiments to measure changes in intracellular Ca^{2+} levels. Imaging was conducted using the MetaMorph microscopy automation system (Cairn Research).

3.2.4 Lactate Dehydrogenase Cytotoxicity Assay:

The CyQUANT™ lactate dehydrogenase (LDH) assay (ThermoFisher, cat. #C20300) was used to determine the cytotoxicity of PM (10-300 µg/ml) at 4 and 24hr time points. HEK-CaSR cells were seeded at a density of 10,000 cells per well in a 96-well plate in complete DMEM and left to adhere overnight at 37 °C and 5% CO_2. A set of triplicate wells containing no cells were used to determine LDH activity in RPMI culture medium. Triplicate wells of cells with RPMI only were used to determine the spontaneous and maximum LDH release and acted as controls. PM (10-300 µg/ml) was prepared as in section

3.2.3.9 in 1% FBS-containing DMEM and were added to wells (with an equivalent PBS dilution) and placed in an incubator at 37 °C and 5% CO_2 for 4 or 24 hrs. At the end of each experiment, 10 µl of sterile H_2O was added to treatment, spontaneous control, and no cell-containing wells and LDH positive control, to monitor background and maximum LDH release. To the triplicate set of well which served as the maximum LDH control, 10 µl of lysis buffer was added and mixed by gentle tapping. The plates were then incubated at 37 °C and 5% CO_2 for 45 minutes. Following this, 50 µl of the suspension from each well was transferred to a separate sterile flat-bottomed 96-well plate and 50 µl of reaction mixture was added. Plates were incubated in the dark at RT for 30 minutes before 50 µl of stop solution was added to each well. Absorbance was measured at 490nm and 680nm using the CLARIOstar® Plus microplate reader and analysed using the MARS data analysis software (BMG LABTECH). The 680nm absorbance was subtracted from the 490nm absorbance to determine the LDH activity levels.

3.2.5 Statistical Analysis:

Prism 9 (Graphpad) was used to present and statistically analyse data. Data are presented as representative traces of Ca^{2+} imaging experiments, where each line represents a single cell within the experiment. These were repeated 3-10 times depending on the experimental set up. Collated data is represented as violin plots to demonstrate frequency distribution of the data. The solid line within the plot represents the median and the dotted lines above and below this represents the upper and lower quartiles, respectively. Normality tests were performed on data sets (Shapiro-Wilk or Kolmogorov-Smirnov) and both parametric and non-parametric One-way ANOVA was used for data interrogation with Tukey's, or Dunn's multiple comparisons tests used to reveal

statistical differences between groups. Differences were statistically significant when the probability value (p) for accepting the null hypothesis were $p<0.05$, and non-significant if $p>0.05$.

3.3 Results:

3.3.1 Cigarette Smoke Extract Exposure to HEK-CaSR Cells Does Not Potentiate Extracellular Ca^{2+}-Induced Activation of the CaSR

Tobacco smoke inhaled actively or passively from cigarettes is deemed to be one of the most toxic and harmful environmental stimuli and causes acute exacerbations of lung diseases. First, I generated CSE in house and tested the nicotine concentration as a marker of efficient generation. I demonstrated that using the method of CSE generation described above yields nicotine containing CSE (Appendix 1). Then, I went on to test whether CSE activates the CaSR using fluorescent intracellular Ca^{2+} imaging as one of the biological readouts for receptor activation. I considered the potential of CSE as an allosteric modulator at the CaSR and I demonstrated that Extracellular Ca^{2+} (2.5 mM) activates the CaSR by increasing intracellular Ca^{2+} levels, as expected, however, CSE (10%) was ineffective at potentiating activation of the CaSR. Therefore, CSE is not an allosteric modulator at the CaSR and does not significantly alter intracellular Ca^{2+} levels compared to Ca^{2+} treatment alone (Figure 3.1 A-C). Acute exposure of HEK cells to Ca^{2+} (2.5 mM) or CSE (10%) did not alter the function of GPCR machinery as demonstrated by ATP stimulation at the end of each experiment (Figure 3.1 A-C).

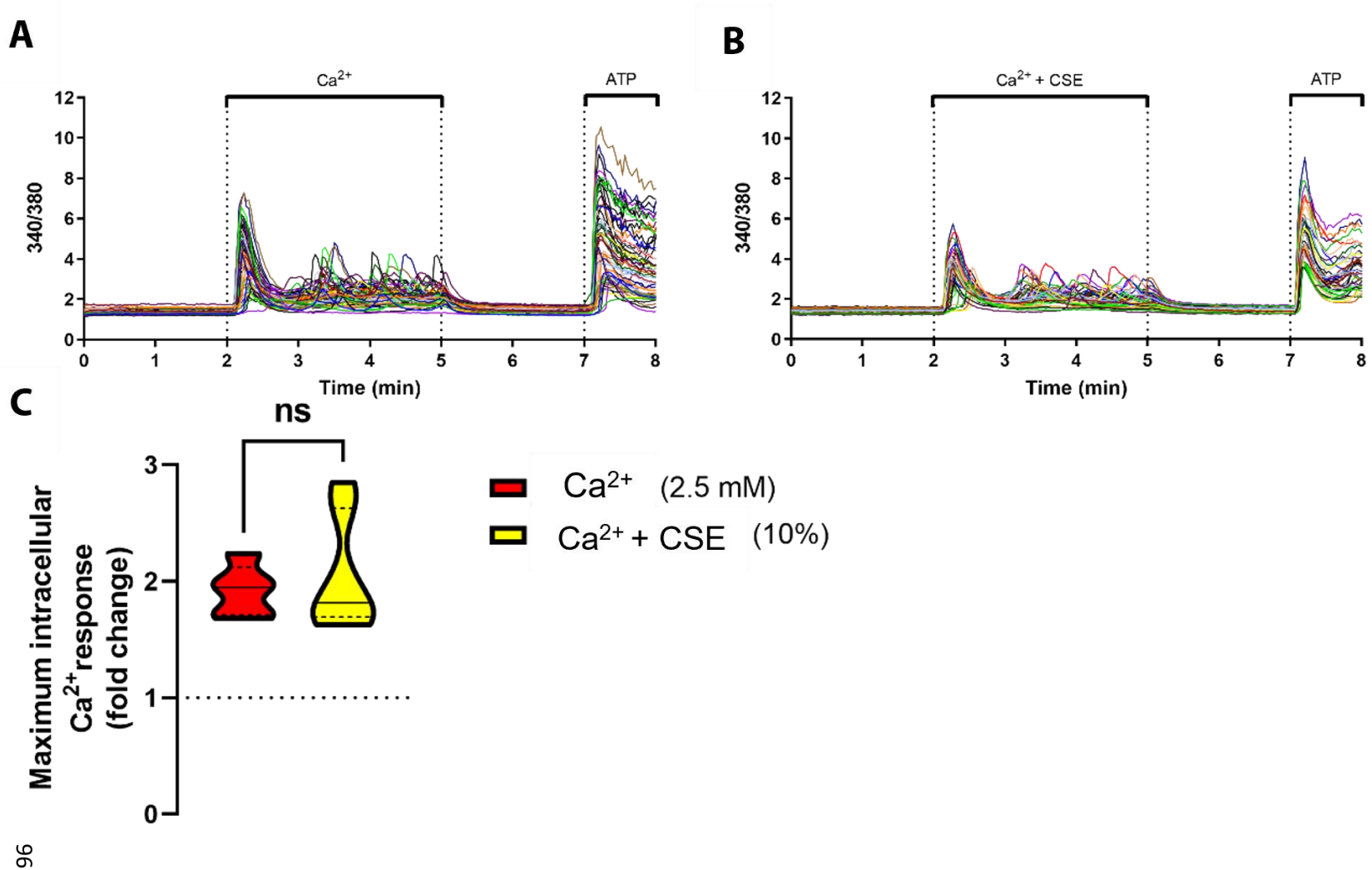
A
Ca2+
ATP
340/380
Time (min)
B
Ca2+ + CSE
ATP
340/380
Time (min)
C
ns
Maximum intracellular Ca2+ response (fold change)
Ca2+ (2.5 mM)
Ca2+ + CSE (10%)

Figure 3.2: Cigarette Smoke Extract (CSE) does not allosterically modulate the calcium-sensing receptor (CaSR). Representative traces of HEK293 cells stably transfected with the human CaSR (HEK-CaSR) loaded with the Ca^{2+} (Ca^{2+})-sensitive fluorescent dye, fura-2AM to measure changes in intracellular Ca^{2+} concentration as one of the biological readouts for CaSR activation. Cells were acutely exposed to a baseline solution (1.2 mM Ca^{2+}, 0-2 mins and 5-7 mins), then Ca^{2+} (2.5 mM, A) or Ca^{2+} (2.5 mM) in the presence of CSE (10%) to determine the allosteric properties (B). At the end of each experiment, cells were stimulated with ATP (100 μM, A & B) as a positive control for cell viability and integrity of G protein-coupled receptor machinery following exposure to CSE. Average maximal Ca^{2+} responses were calculated (fold from baseline) for Ca^{2+} (2.5 mM) ± CSE (10%) in HEK-CaSR cells, where the dotted line represents no change (C). Each data point was normalised to the baseline and within the violin plots, the solid line represents the median and the dotted lines within the violin plots represents the upper and lower quartiles, respectively. Data represent N=5 (Ca^{2+}, 2.5 mM, C) and N=7 (Ca^{2+}, 2.5 mM + CSE 10%, C) analysed using an unpaired, two-tailed T-test where p=0.1449 (not significant, ns).

3.3.2 Heavy Metals Cd^{2+} and Ni^{2+} Directly Activate the CaSR in HEK-CaSR Cells, an Effect Abolished by CaSR NAM:

The most abundant metal found within CS is the group one carcinogen cadmium (Cd^{2+}). Cd^{2+} (20 μM) activated the CaSR by increasing intracellular Ca^{2+} levels, an effect which was significantly reduced by co-treatment with NAM and was not observed in HEK-0 cells (Figure 3.2 A-D). In addition, acute exposure of HEK cells to Cd^{2+} did not alter the function of GPCR machinery as demonstrated by ATP stimulation at the end of each experiment (Figure 3.2 A-C).

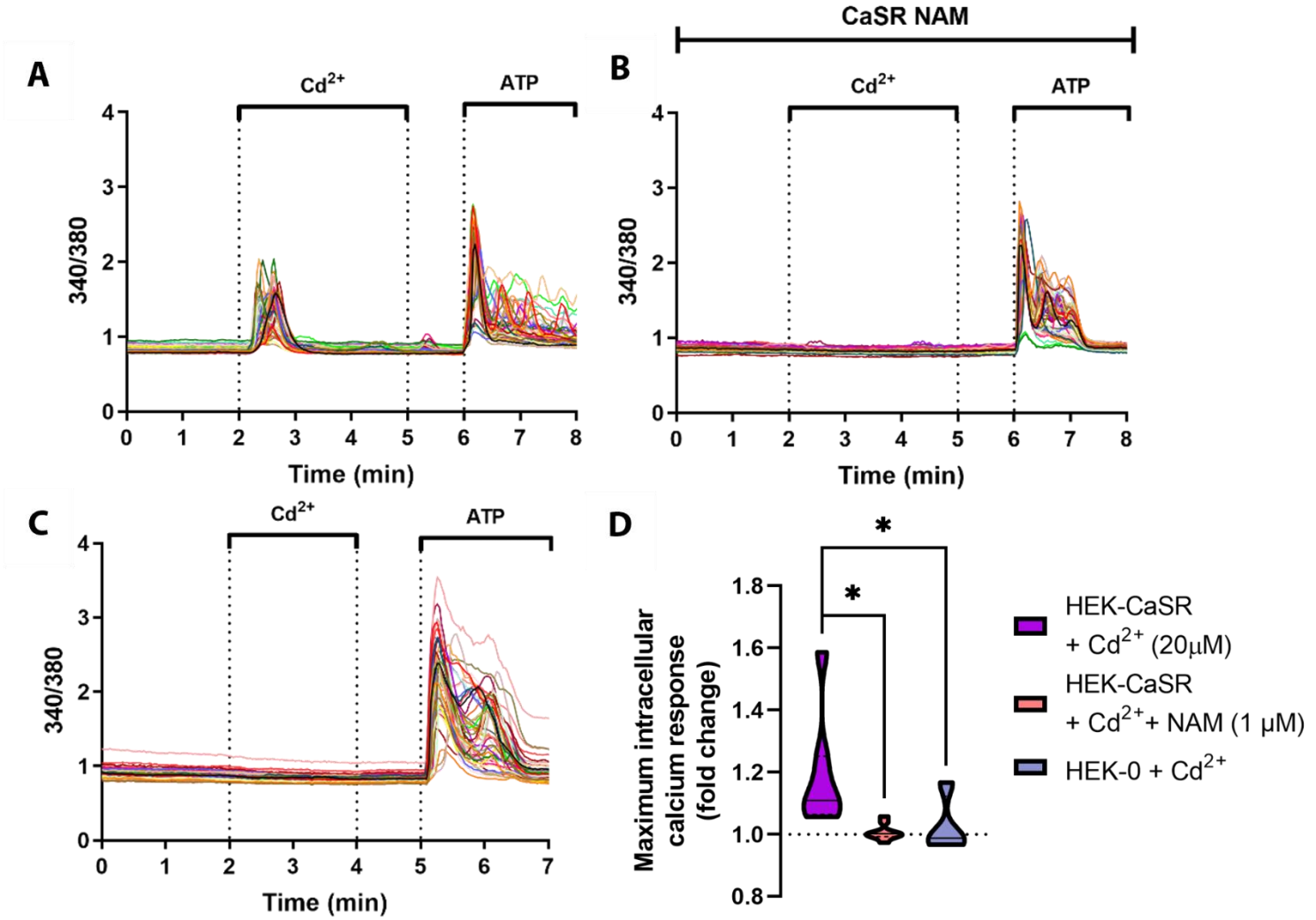
A
Cd2+
ATP
340/380
Time (min)
B
CaSR NAM
Cd2+
ATP
340/380
Time (min)
C
Cd2+
ATP
340/380
Time (min)
D
Maximum intracellular calcium response (fold change)
HEK-CaSR + Cd2+ (20µM)
HEK-CaSR + Cd2+ + NAM (1 µM)
HEK-0 + Cd2+

Figure 3.3: Cadmium (Cd^{2+}) directly activates the human calcium-sensing receptor (CaSR), and these responses are abolished by a negative allosteric modulator at the CaSR (NAM). Representative traces of HEK293 cells stably transfected with the human CaSR (HEK-CaSR, A, B) or transfected with an empty vector (HEK-0, negative control, C) loaded with the Ca^{2+}-sensitive fluorescent dye, fura-2AM (3 μM) to measure changes in intracellular Ca^{2+} concentration as a biological readout for CaSR activation. Cells were exposed to baseline (1.2 mM Ca^{2+}, 0-2 mins and 4-5 mins) Cd^{2+} (20 μM, A-C), in the presence of NAM (NPS2143, 1μM, B). At the end of each experiment, cells were stimulated with ATP (100μM, A-C) a positive control for cell viability. Average maximal Ca^{2+} responses (fold from baseline) to Ni^{2+} in the presence of NAM in HEK-CaSR cells and in HEK-0 cells, where the dotted line represents no change (D). Each data point was normalised to the baseline and within the violin plots, the solid line represents the median and the dotted lines within the violin plots represents the upper and lower quartiles, respectively. Data were analysed using a One-way ANOVA with Dunn's Multiple Comparisons test. Cd^{2+} in HEK-CaSR vs. Cd^{2+} + NAM in HEK-CaSR (*, P= 0.0130); Cd^{2+} in HEK-CaSR vs. Cd^{2+} in HEK-0 (*, P= 0.0249). N = 4-9; n = 45-50 cells per experiment.

Additionally, Ni^{2+} is found at trace levels in CS, however, is also generated from combustion of fossil fuels, diesel and incineration of waste and sewage, contributing to an increase in ambient air pollution (Genchi *et al.* 2020). Ni^{2+} (20 μM) also activated the CaSR by increasing intracellular Ca^{2+} levels and this was significantly reduced by co-treatment with NAM and was not observed in HEK-0 cells (Figure 3.3 A-D). In addition to this, acute exposure of HEK cells to Ni^{2+} did not alter the function of GPCR machinery as demonstrated by ATP stimulation at the end of each experiment (Figure 3.3 A-C).

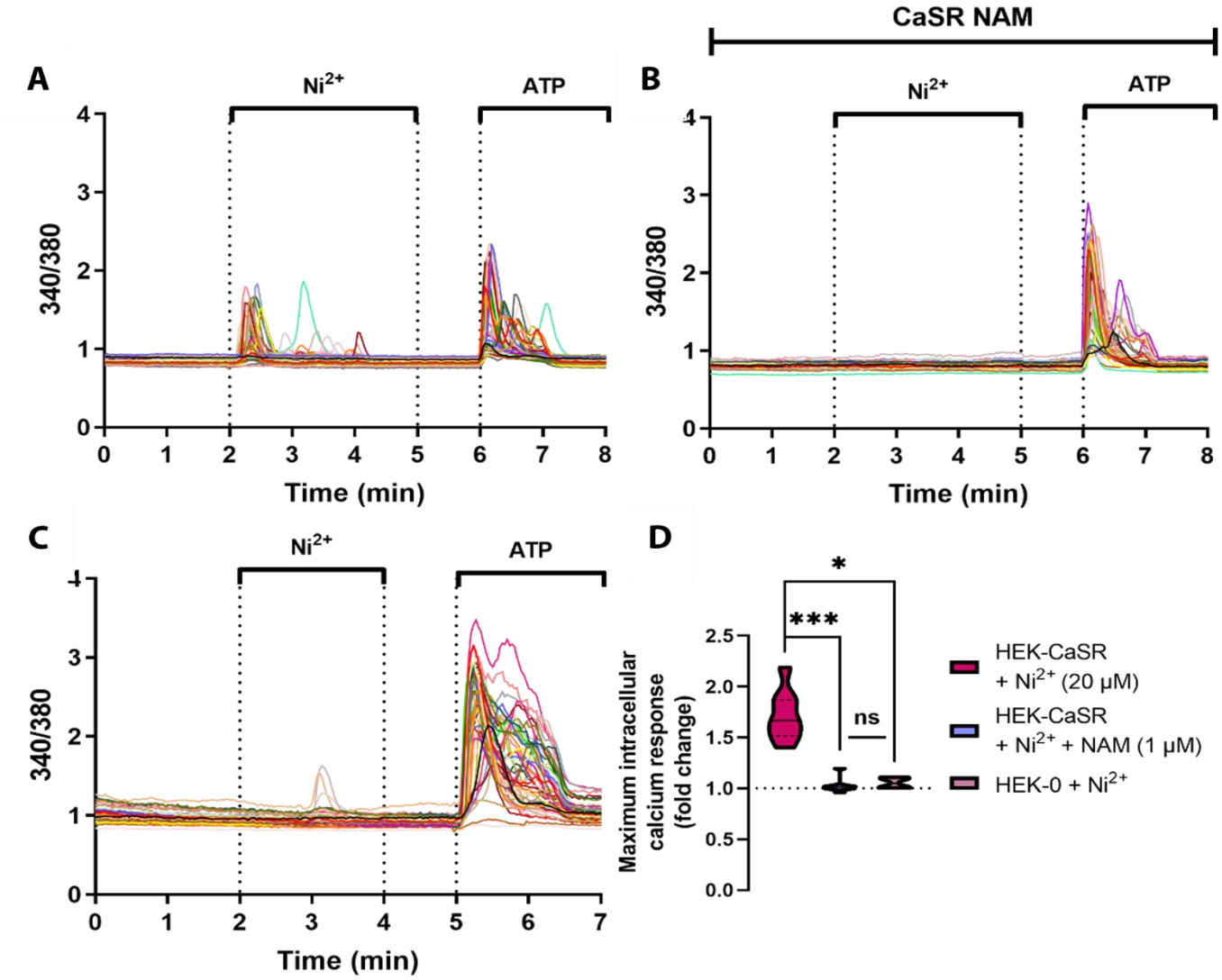
A
Ni2+
ATP
340/380
Time (min)
B
CaSR NAM
Ni2+
ATP
340/380
Time (min)
C
Ni2+
ATP
340/380
Time (min)
D
*
***
ns
Maximum intracellular calcium response (fold change)
HEK-CaSR + Ni2+ (20 µM)
HEK-CaSR + Ni2+ + NAM (1 µM)
HEK-0 + Ni2+

Figure 3.4: Nickel (Ni^{2+}) directly activates the human calcium-sensing receptor (CaSR), and these responses are abolished by a negative allosteric modulator at the CaSR (NAM). Representative traces of HEK293 cells stably transfected with the human CaSR (HEK-CaSR, A, B) or transfected with an empty vector (HEK-0, negative control, C) loaded with the Ca^{2+}-sensitive fluorescent dye, fura-2AM (3 μM) to measure changes in intracellular Ca^{2+} concentration as a biological readout for CaSR activation. Cells were exposed to baseline (1.2 mM Ca^{2+}, 0-2 mins and 4-5 mins) and Ni^{2+} (20 μM, A-C), in the presence of NAM (NPS2143, 1 μM, B). At the end of each experiment, cells were stimulated with ATP (100 μM, A-C) a positive control for cell viability. Average maximal Ca^{2+} responses (fold from baseline) to Ni^{2+} in the presence of NAM in HEK-CaSR cells and in HEK-0 cells, where the dotted line represents no change (D). Each data point was normalised to the baseline and within the violin plots, the solid line represents the median and the dotted lines within the violin plots represents the upper and lower quartiles, respectively. Data were analysed using a One-way ANOVA with Dunn's Multiple Comparisons test. Ni^{2+} in HEK-CaSR vs. Ni^{2+} + NAM in HEK-CaSR (***, P= 0.0004); Ni^{2+} in HEK-CaSR vs. Ni^{2+} in HEK-0 (*, P= 0.0357). N = 4-10; n = 45-50 cells per experiment.

3.3.3 Particulate Matter Directly Activates the CaSR in HEK-CaSR Cells, an Effect Abolished by CaSR NAM:

Heavy metals are rarely found in isolation in the environment and aggregate together to form a range of environmental pollutants which are generated from a variety of sources. Standard Reference Material PM (SRM1648a) contains an extensive list of metals, most of which are potential activators at the CaSR, including Ca^{2+} (most abundant), Cd^{2+} and Ni^{2+} (National Institute of Standards & Technology 2020). I demonstrated that PM, which contains a plethora of CaSR activators, drives CaSR activation and causes an increase in intracellular Ca^{2+} levels, where NAM abolished this effect, and the PM-induced increase in intracellular Ca^{2+} level was not observed in HEK-0 cells (Figure 3.4 A-D). In addition to this, acute exposure of HEK cells to PM did not alter the

function of GPCR machinery as demonstrated by ATP stimulation at the end of each experiment (Figure 3.4 A-C).

After determining that PM indeed activates the CaSR and does not seem to negatively affect HEK cell functioning during an acute exposure, it was important to determine whether PM altered viability of HEK-CaSR cells in a longer-term exposure to inform future experimental plans. Surprisingly, 4 & 24 hr exposure to PM (10-300 µg/ml) induced reductions in LDH absorbance in a concentration-dependent manner, indicating that more concentrated PM (100 & 300 µg/ml) promotes cell survival, rather than PM-induced cell death (Appendix 2).

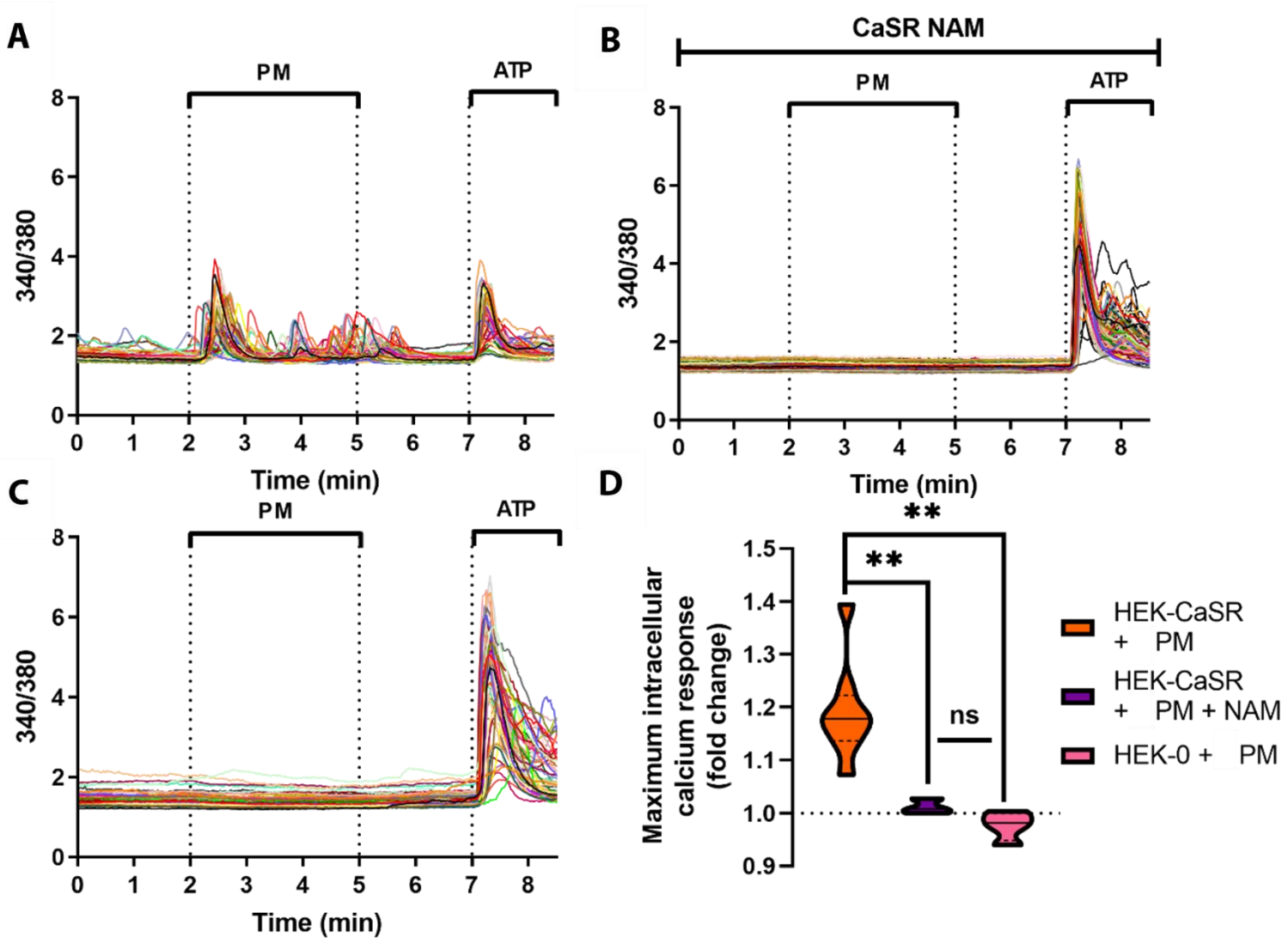
A
PM
ATP
340/380
Time (min)
B
CaSR NAM
PM
ATP
340/380
Time (min)
C
PM
ATP
340/380
Time (min)
D
**
**
ns
Maximum intracellular calcium response (fold change)
HEK-CaSR + PM
HEK-CaSR + PM + NAM
HEK-0 + PM

Figure 3.5: Urban particulate matter (PM) directly activates the human calcium-sensing receptor (CaSR), and these effects are abolished by a negative allosteric modulator at the CaSR (NAM). Representative traces of HEK293 cells stably transfected with the human CaSR (HEK-CaSR, A, B) or transfected with an empty vector (HEK-0, negative control, C) loaded with the Ca^{2+}-sensitive fluorescent dye, fura-2AM to measure changes in intracellular Ca^{2+} concentration as a biological readout for CaSR activation. Cells were exposed to baseline (2 mM Ca^{2+}, 0-2 mins and 5-7 mins), PM (SRM1648a, 100 µg/ml, A-C), in the presence of NAM (NPS2143, 1 µM, B). At the end of each experiment, cells were stimulated with ATP (100 µM, A-C) a positive control for cell viability. Average maximal Ca^{2+} responses (fold from baseline) to PM in the presence of NAM in HEK-CaSR cells and in HEK-0 cells, where the dotted line represents no change (D). Each data point was normalised to the baseline and within the violin plots, the solid line represents the median and the dotted lines within the violin plots represents the upper and lower quartiles. Data were analysed using a One-way ANOVA with Tukey post-hoc test. PM in HEK-CaSR vs. PM + NAM in HEK-CaSR (P=0.0096); PM in HEK-CaSR vs. PM in HEK-0 (P=0.0013). N = 3-7; n = 53-78 cells per experiment.

3.4 Discussion:

In this chapter, I have revealed, for the first time, that the heavy metals contained within ambient air pollution, alone or as a component of PM, directly activate the human CaSR by increasing intracellular Ca^{2+} levels in HEK-CaSR cells. Importantly, this activation can be abolished by co-treatment with NAM and is not observed in HEK-0 cells. Together, these results highlight the CaSR as one of the potential mechanisms behind PM sensing in the airways, where NAM provides a potential therapeutic to directly counteract the PM-induced pro-inflammatory cellular responses in the airways.

CS is a contributor to ambient air pollution and is a major driver of the pathogenesis and acute exacerbations of lung diseases. Tobacco smoking is the number one preventable cause of death, with around 7 million deaths per year, a figure still below that of the mortality caused by exposure to ambient air pollution (Lelieveld, Pozzer, Pö Schl, *et al.* 2020; Jafari *et al.* 2021). Therefore, better understanding of the mechanisms by which CS could drive progression and exacerbation of lung disease is imperative. Smoke obtained from Marlboro Red Cigarettes contain potential activators of the CaSR, including Cd^{2+}, Ni^{2+}, and lead (Pappas *et al.* 2014). However, the levels of these metals were not thought to be of a sufficient level to drive activation of the CaSR in an orthosteric manner, so we assessed the potential of CS as an allosteric modulator at the CaSR, using CSE as a model of airway CS exposure.

CSE is a complex mix of substances which differ between brands of cigarettes and preparations using different protocols. CSE is widely used in *in vitro* research to recapitulate the liquid environment in the airways following tobacco smoke inhalation. However, production of CSE results in the loss of many of the highly reactive and volatile substances in CS, and the filtration

step poses another mechanism by which some of the larger particles are lost (Shapiro 2004). Even so, this model is widely used to assess the effects of CSE *in vitro* and in HEK-CaSR cells, CSE does not potentiate extracellular Ca^{2+}-induced activation of the CaSR and is therefore not an allosteric modulator at the CaSR. During my experiments, I considered CSE as an allosteric modulator at the CaSR rather than an orthosteric activator as minor trace levels of metals are present in CSE, compared to being one of the major components of PM. CSE has been demonstrated to contain <0.049 µg of Cd^{2+} from 20 Marlboro Red Cigarettes (Pappas et al 2014), however, during my studies, this would have been in the nm range. This contrasts with the PM used in my studies, where 73.7 mg/kg of Cd^{2+} is contained (NIST), which prompted me to test the potential of orthosteric activation of the CaSR by PM during my studies. However, during my studies, I only focused on one of the biological readouts for CaSR activation and therefore we cannot rule out activation of alternative CaSR-mediated intracellular signalling pathways by CSE and PM.

Previous studies have suggested that one of the mechanisms in which CSE induces harmful effects in the airways is through generation of reactive oxygen species (ROS) and activation of Phosphoinositide 3-kinase (PI3K) and Akt signalling pathways in primary nasal fibroblasts (Park *et al.* 2020). In addition to these pathways, activation of NF-κB intracellular signalling pathways was observed in these cells and was shown to be RhoA dependent in the 16HBE airway epithelial cell line (Zhang *et al.* 2016). Finally, the ERK/MAPK intracellular signalling pathway has been shown to be activated by CSE in human small airway epithelial cells (Mercer *et al.* 2004). Although not tested directly in the aforementioned studies, activation of PI3K/Akt (F. Zhang *et al.* 2020), mTOR (Rybchyn *et al.* 2019), ERK/MAPK (Ward 2004; Zhao *et al.* 2020) and RhoA (Min

et al. 2002; Ward 2004; Davies *et al*. 2006a; Zhang *et al*. 2017) intracellular signalling are downstream of CaSR activation (Ward 2004; Chakravarti *et al*. 2012; Brennan, Thiem, Roth, Aggarwal, Irfete Sh Fetahu, *et al*. 2013) (Figure 3.5). Therefore, future studies would be required to test whether NAMs abrogate these CSE-induced effects, to improve our understanding of the potential mechanistic link between the CaSR and CSE-induced airway damage.

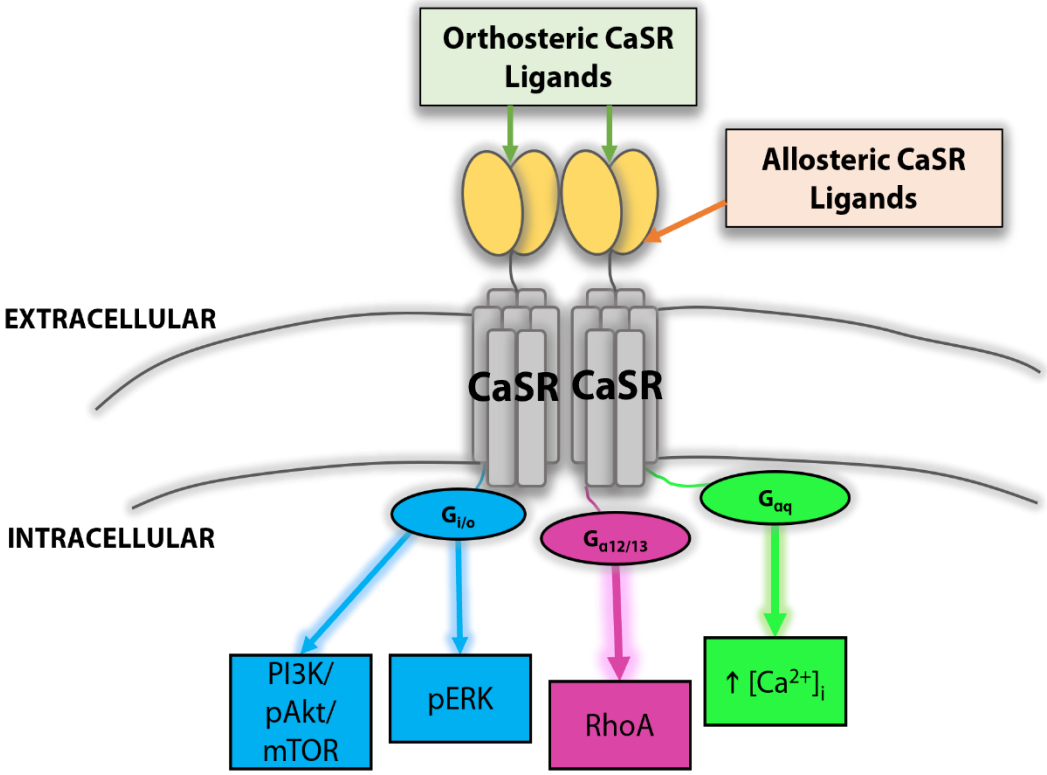

Figure 3.6: Simplified representation of Ca^{2+}-sensing receptor (CaSR)-mediated intracellular signalling pathways. The CaSR is activated by several orthosteric and allosteric ligands. The CaSR signals through downstream intracellular signalling pathways via three main groups of heterotrimeric G-proteins, $G_{i/o}$, $G_{\alpha 12/13}$, $G_{q/11}$. Activation of these G proteins by orthosteric or allosteric ligands at the CaSR result in activation of Phosphoinositide 3-kinase (PI3K) which phosphorylates Akt (pAkt) and activates mTOR, phosphorylation of extracellular signal-regulated kinase (pERK), activation of ras homolog gene family, member A (RhoA) and increases in intracellular Ca^{2+} concentration ($[Ca^{2+}]_i$). In addition, recent evidence has suggested that these signals all go via $G_{q/11}$ as inhibition of $G_{q/11}$ reduces activation of downstream signalling molecules associated with other G proteins, such as PI3K, Akt, mTOR, ERK, and RhoA (Leach et al 2020). Figure adapted from Smith et al 2016; Leach et al 2020).

Cd^{2+} is one of the most abundant heavy metals within most brands of cigarettes, including Marlboro Red used in this study; additionally, Ni^{2+} is also present in trace amounts (Pappas *et al.* 2014). Like CSE, both Cd^{2+} and Ni^{2+} have been previously demonstrated to activate the downstream effectors linked to CaSR signalling such as phospholipase A_2 (PLA_2) and MAPK (Handlogten *et al.* 2000b). In this chapter, we reveal that Cd^{2+} and Ni^{2+} both activate the CaSR in an orthosteric manner and result in an increase in intracellular Ca^{2+} levels, in line with previous studies conducted in the immortalised human alveolar epithelial cell line (A549) (Cortijo, Milara, Mata, Donet, Gavara, Peel, Hall and E. J. Morcillo 2010a; Gu *et al.* 2018). In the Cortijo and Gu studies, the NAM NPS2390 blocked Cd^{2+} and Ni^{2+} -induced increases in intracellular Ca^{2+} which suggests that this effect might be mediated by CaSR activation. However, NPS2390 also acts as a non-competitive antagonist of another class C GPCR, the metabotropic glutamate receptor 1 (Carroll *et al.* 2001; Lavreysen *et al.* 2003), therefore, my studies contribute to these findings where specific NAM NPS2143 abolishes Cd^{2+} and Ni^{2+}-induced intracellular Ca^{2+} responses, indicating that the CaSR could comprise a key mechanism of the cellular responses induced by inhalation of heavy metals present in CSE and PM.

In my studies I used HEK cells overexpressing the CaSR and the receptor-specific NAM, NPS2143 to clarify whether these intracellular Ca^{2+} responses are directly linked to the CaSR. In concordance with the studies mentioned above, I concluded that these effects are indeed CaSR-dependent as the metal-induced increase in intracellular Ca2+ was abolished by co-treatment with the NAM, NPS2143 in HEK-CaSR cells. This intracellular Ca2+ response was not observed in HEK-0 cells which do not express the CaSR. Therefore, this work

suggests that heavy metal components of CSE could directly activate the CaSR to drive disease progression and acute exacerbations, which could be ameliorated with NAM treatment. The experimental concentrations of Cd^{2+} and Ni^{2+} were both in the millimolar range which is orders of magnitude greater than the amount typically found in cigarettes (Pappas *et al.* 2014). Therefore, I suggest that CaSR activation by these heavy metals and others found in CSE, and PM may potentially act in combination to induce increases in intracellular Ca^{2+}, in a manner similar to CaSR activation by individual amino acids and amino-acid mixtures reminiscent of the composition of fasting human plasma (Conigrave *et al.* 2000).

Although there is a decline in the number of people who smoke tobacco, a harmful level of ambient air pollution persists worldwide due to continued combustion of fossil fuels such as diesel and petrol, incineration of waste and sewage products and more recently the devastating wildfires witnessed across the globe (Perera 2018). In combination, these result in the generation of PM, one of the major components of ambient air pollution. Additionally, although levels of total air pollution have been declining since the 1990s, ambient PM has remained at a stable level from 1990-2019 and a steady increase of deaths can be attributed to exposure to ambient air pollution over this time period (Dhimal *et al.* 2021). This highlights the importance of gaining better understanding of the mechanisms underlying PM-induced effects in the airways and possible mechanisms for counteracting these effects.

PM is made up of a plethora of inorganic and organic molecules, including an extensive list of potential CaSR activators, including Ca^{2+}, Cd^{2+}, and Ni^{2+} as demonstrated in the characterisation information provided by The National Institute of Standards & Technology (2020). Each of the metals in isolation are

below the concentrations required to elicit orthosteric CaSR activation, however, in combination, PM provides a surfeit of potential drivers of CaSR activation and therefore proposes the CaSR as a potential mechanism by which airway cells sense the presence of PM.

Similar to CS, PM has been demonstrated to drive ROS production and the release of inflammatory cytokines which are thought to result in imbalances of intracellular Ca^{2+} homeostasis in a range of cells involved in asthma pathogenesis (Deweirdt *et al.* 2017; Pfeffer, Lu, *et al.* 2018a; Dong *et al.* 2019; Valacchi *et al.* 2020). However, it is still unclear exactly which mechanisms underpin the harmful effects brought about by PM exposure and therefore, there has been little research into developing treatments to directly counteract the effects of PM-induced effects in the airways and at present, many rely on reducing personal exposure by staying indoors (Laumbach *et al.* 2015). In this chapter, we reveal that PM directly activates the CaSR and causes an increase in intracellular Ca^{2+} level, an effect which was abolished by NAM and not observed in HEK-0 cells. These findings provide clear evidence of the CaSR comprising one of the potential mechanisms of PM-sensing and responding in the airways. Additionally, NAM-induced abolishment of PM-induced effects in HEK-CaSR cells provides proof of concept to go on to further test NAM as an effective therapeutic for asthma sufferers, especially those exacerbated by exposure to PM.

Interestingly, an increasing PM dose induced a concentration-dependent decrease in LDH activity levels as an indicator of cell viability, which was unexpected. Previous studies suggest conflicting effects on cell viability in response to PM used in this study in a range of cell types and cell viability assays (Mitkus *et al.* 2013; Choi *et al.* 2021). However these observations could

be due to nanoparticle interference with assay reagents which would explain the current conflicting evidence based around cell viability measurements in cells exposed to PM (Holder *et al.* 2012).

3.5 Future Studies:

The CaSR signals in a promiscuous manner with activation leading to amplification of distinct intracellular GPCR-mediated signalling pathways. To complement the studies above, in future studies, it would be important to assess the alternative CaSR-mediated intracellular signalling pathways activated upon exposure to harmful components of air pollution such as CSE or PM, in addition to other, more recent sources of PM such as bushfire smoke. Additionally, it would be important to use an alternative method to determine PM-induced alterations by using specific assays targeting apoptotic or necrotic potential of PM and comparing to a suitable control. Together, this data would provide better understanding of the CaSR-mediated sensing of harmful components of ambient air pollution and further assess the potential of NAM for pollution-induced or exacerbated lung disease.

3.6 Conclusion:

These findings provide a rationale for investigating the potential of the CaSR expression in the structural and immune cells of the airways, where the CaSR could act as a mediator of the pathogenesis and acute exacerbations of asthma, and NAM could provide an effective therapy for PM-induced exacerbations of lung diseases.

CHAPTER 4: ESTABLISHING CASR EXPRESSION IN AIRWAY EPITHELIAL AND TISSUE- AND BLOOD-DERIVED IMMUNE CELLS INVOLVED IN PM-SENSING AND ACUTE EXACERBATIONS OF LUNG DISEASES

4.1 Introduction

The structural and immune cells comprising the airways are the first line of defence against inhaled stimuli, such as PM. Direct, T2 and non-T2 inflammatory responses are initiated in airway epithelial cells and tissue-resident AMs and DCs upon exposure to PM. These cells work synergistically to mediate the recruitment and differentiation of blood-derived immune cells via indirect PM-induced mechanisms, to assist in the pro-inflammatory response (Barlow *et al.* 2007; Sokol and Luster 2015; Leikauf *et al.* 2020). Continued activation of these structural and tissue-resident and blood-derived immune cells are also known to drive the pathogenesis of asthma, however, the underlying, upstream mechanisms of activation of these inflammation-associated pathways by PM in airways cells is unclear.

The CaSR has previously been shown to be expressed in some of the cells which mediate inflammation (Yamaguchi, Olozak, *et al.* 1998; Yamaguchi, Kifor, *et al.* 1998; Yarova *et al.* 2015). Furthermore, we have previously demonstrated that the CaSR plays a key role during asthma-associated features in murine models of T2 and non-T2 asthma (Yarova *et al.* 2015; Yarova *et al.* 2016; Huang *et al.* 2019; Yarova *et al.* 2021). Together, this proposes the CaSR as a critical mediator of the immune responses in the lungs and potentially comprises one of the drivers of chronic inflammation associated with the pathogenesis and acute exacerbations lung diseases, such as asthma. During Chapter 3 of my thesis, I demonstrated that the CaSR is directly activated by PM in HEK-CaSR cells, therefore during this Chapter, I sought to determine whether airways

structural and immune cells involved in sensing and responding to inhaled PM, expressed the CaSR at the protein level, using immunohistochemical (IHC) staining.

4.2 Methods:

4.2.1 Basal Human Bronchial Epithelial Cell Thawing and Culture:

4.2.1.1 Basal Human Bronchial Epithelial Cells:

Ethically consented and cryopreserved NHBECs were purchased from Lonza (cat. #CC-2450) from N=3 donors, with no history of alcohol abuse or smoking. Information related to NHBEC characteristics of each donor are provided in Table 4.1.

Table 4.1: Normal human bronchial epithelial cell (NHBECs) donor characteristics. Characteristics of N=3 donor NHBECs, obtained from Lonza, demonstrating each donors' Age, Sex (Female, F, or Male, M), Race, seeding efficiency, viability and population doubling time. Seeding efficiency was calculated by determining the level of cells which seed to the flask during the initial stages of expansion, following isolation. Both viability and population doubling time was determined by Trypan Blue exclusion of dead cells and cell counts. Each of the characteristics were determined at Lonza during the initial isolation and expansion of cells from each NHBEC donor. Table adapted using information provided on donor lists from Lonza.

Age	Sex	Race	Seeding Efficiency (%)	Viability (%)	Population Doubling time (hrs)
24	F	Caucasian	78	82	29
36	M	Caucasian	100	92	22
56	M	Black	79	80	21

4.2.1.2 Basal Human Bronchial Epithelial Cell Culture:

4.2.1.2.1 Initial Seeding and Culture to Confluence:

Before thawing basal NHBECs, 500ml of complete PneumaCult™-Ex Plus Medium (Stem Cell Technologies, cat. #05040) was prepared, which comprised of 10ml of 50x supplement (provided with medium), 5ml of 100µg/ml Penicillin/Streptomycin and 2.5ug/ml Amphotericin B mix (Gibco, ThermoFisher Scientific, cat. #15290018), 0.5ml of 200µM hydrocortisone solution (Stem Cell Technologies, cat. #07926). The cryovial of cells was rapidly thawed (2-3 minutes at 37°C) and immediately seeded into a T75 containing 25ml complete PneumaCult™-Ex Plus medium. Cells were left to adhere overnight at 37°C and 5% CO_2. The following day the complete PneumaCult™-Ex Plus medium was replaced with 25ml of fresh complete PneumaCult™-Ex Plus medium. Culture medium was replaced every other day during expansion and basal NHBECs were monitored under phase-contrast microscopy to determine expansion rates and when splitting of cells was required (>60% confluent).

4.2.1.2.2 Seeding of Basal Human Bronchial Epithelial Cells for Experiments:

Once >60% confluent, medium was removed from the cells and flasks were briefly washed twice with PBS (Thermofisher Scientific, cat. #14190136). Then, 3ml of 0.25% Trypsin-EDTA (Merck, cat. #T4049) was added to the flask and incubated at 37°C for a maximum of 5 minutes. Trypsin was inactivated by adding 10ml of RMPI-1640 (Gibco cat. #31870) supplemented with 10% FBS to the flask. The detached cells in supplemented RPMI were then transferred into a 15ml Falcon tube. These tubes were centrifuged at 500g for 5 minutes and the supernatant was carefully removed. Basal NHBECs were re-suspended

in 1ml complete PneumaCult™-Ex Plus medium and counted with the LUNA automated cell counter (Logos Biosystems) using trypan blue for exclusion of dead cells from the cell count. 10 µl of the cell suspension (containing up to 500 cells) was added to a 0.2 ml PCR tube under the hood before adding 10 µl 0.4% Trypan Blue stain (Labtech, cat. #T13000), before mixing by pipetting up and down, resulting in a 1:1 cell suspension (of ~ 250 cells). The tube was then transferred to the LUNA™ automated cell counter and 10 µl of the cell suspension with trypan blue was added to the LUNA™ Cell Counting Slide (provided with kit). Then the slide was inserted into the slide port of the instrument and focus was adjusted using the knob on the side of the machine, to ensure an appropriate cell image. Cells were counted and the parameters provided by the LUNA™ automated counter were the number of live and dead cells/ml, number of total cells/ml, viability % (% live vs. dead cells), cell images (where live and dead cells were highlighted with green and red circles, respectively) and a histogram to demonstrate cell size distribution. The values obtained for the live cells within the suspension were used to calculate volumes of medium required for cell seeding. Basal NHBECs were then plated at densities of 2,000 cells per well in an EZ slide (Merck, cat. #C86024) for IHC. Cells were placed in the incubator at 37°C and 5% CO_2 overnight to allow for attachment and left for 48 hrs to reach ~60% confluency. Once ~60% confluent, Cell culture medium was removed from the wells containing basal NHBECs and washed once with warmed 1 X PBS, prior to fixation.

4.2.2 Isolation and Purification of Primary Alveolar Macrophages:

The work outlined during this section of this chapter of my thesis regarding the isolation and purification of AMs, and subsequent analysis of CaSR expression in AMs was carried out in the laboratory of Professor David Thickett

in The University of Birmingham with methodological and experimental assistance from Dr Sebastian Lugg and Dr Aaron Scott.

4.2.2.1 Research Ethics:

Patients were recruited at the pre-operative thoracic surgical clinic typically 1 week before surgery for suspected lung cancer (REC 17/WM/0272) and asked to self-report smoking status and perform an exhaled carbon monoxide (eCO) measurement (CareFusion). A smoker was defined as self-reported or have an eCO >10 parts per million (ppm), whereas a never smoker was defined as having smoked <100 cigarettes in a lifetime. Finally, an ex-smoker was defined as having quit smoking cigarettes, with an eCO of <10 ppm.

4.2.2.2 Alveolar Macrophage Isolation

A sample of the lung resection distant from the tumour site, without any evidence of macroscopic malignancy was placed in a sterile sealed container with 0.9% saline and stored at 4 ^{o}C. Within 24 hours of surgery AM isolation was performed from the lung resection samples using 0.9% (0.15 M) sodium chloride solution (Sigma, cat. #7647145) lavage via pressure bag by inserting a 21-gauge needle into visible bronchioles. The tissue was gently massaged to facilitate emptying lavage from the tissue and the process was repeated until the perfusate contained less than $1x10^4$ monocytes/ml, which was assessed by the increasing transparency of the lavage solution, indicating collection of all cells within the airways of the sample. Cells were then pelleted from the perfusate by centrifugation at 500 g for 5 minutes, before supernatant was removed and 2 ml PBS was added to the first cell pellet, resuspended, and transferred to the next cell pellet and mixed, until all the cell pellets were combined. This cell suspension was made up to 18 ml and then 12 ml density

gradient medium, Lymphoprep™, was added to a separate tube. The 18 ml volume of pooled cell pellets in PBS were carefully overlaid onto the Lymphoprep™. This was centrifugation at 800 g and 4°C for 30 minutes, with no brake, which resulted in separation of plasma and mononuclear cells, such as AMs, from the cell suspension which sediment on top of the Lymphoprep™ layer. Granulocytes and erythrocytes have higher density than mononuclear cells and sediment through the Lymphoprep™ layer and to the bottom of the centrifugation tube (Figure 4.1). Mononuclear cells were gently aspirated using a disposable 2.5 ml Pasteur Pipette and transferred to a new 50 ml tube. 40 ml PBS was added to this and then centrifuged at 500 g for 10 minutes at 4 °C, to remove most of the platelet population. The supernatant was removed, and cells were re-suspended in 2 ml RPMI medium supplemented with 10% FBS and 5% penicillin streptomycin (Gibco, cat. #15070063) and 2 mM L-glutamine (Gibco, cat. #25030149) (complete medium) and the cells were counted using a haemocytometer, as described below.

10 µl aliquot of the cells were mixed gently with 10 µl 0.4% Trypan Blue Solution in a 0.2 ml PCR tube, resulting in a 1:1 dilution of cells with trypan blue (ThermoFisher, cat. #15250061). Then, the haemocytometer was cleaned with 70% EtOH, before a glass coverslip dampened and affixed to the haemocytometer. Following preparation of the haemocytometer, 10 µl of the 1:1 cell and Trypan Blue suspension was applied carefully, under the coverslip attached to the haemocytometer. The haemocytometer was placed under phase-contrast microscopy with a 10X magnification to reveal large, bright (viable) AMs which were counted in each of the 4 quadrants, made up of 16 squares each, using a hand tally (Figure 4.2). AMs were identified as large granular cells under the microscope and other smaller cells were not included in the cell count. To calculate AM yield following isolation, the number of cells

counted in each quadrant were averaged and multiplied by 10,000 to determine cells/ml. This value was finally multiplied by 2 to account for the 1:1 Trypan Blue dilution of the cell suspension. 1 x 10^6 cells were prepared for phenotyping, to assess purity and a further 1 x 10^6 cells/ ml was removed and placed into a cytospin device (as described in section 4.2.7. below), to affix the isolated cells to slides for fixation and subsequent immunohistochemical staining of the CaSR.

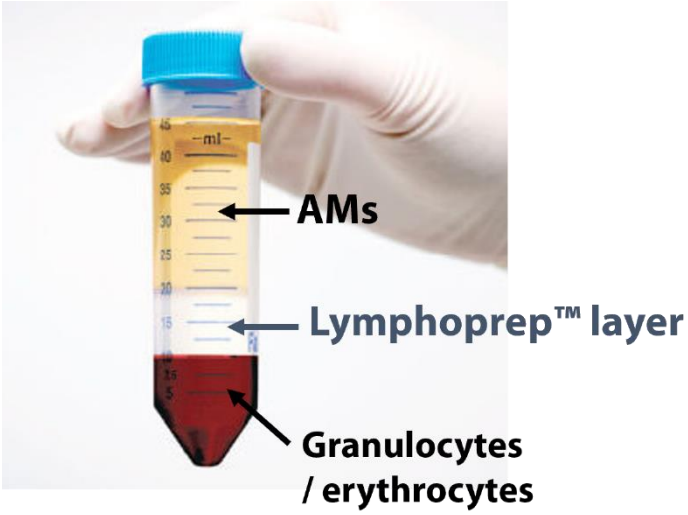

Figure 4.1: Representative image to demonstrate Lymphoprep ™ gradient centrifugation separating cell types from a heterogenous immune cell population. After centrifugation at 800 g, 4 °C for 30 minutes, erythrocytes and granulocytes sediment through the Lymphoprep™ layer. Mononuclear cells, such as alveolar macrophages (AMs) are present in the upper layer, as depicted and separated by the Lymphoprep™ layer which displaces upwards during centrifugation. Image adapted from https://www.stemcell.com/products/lymphoprep.html.

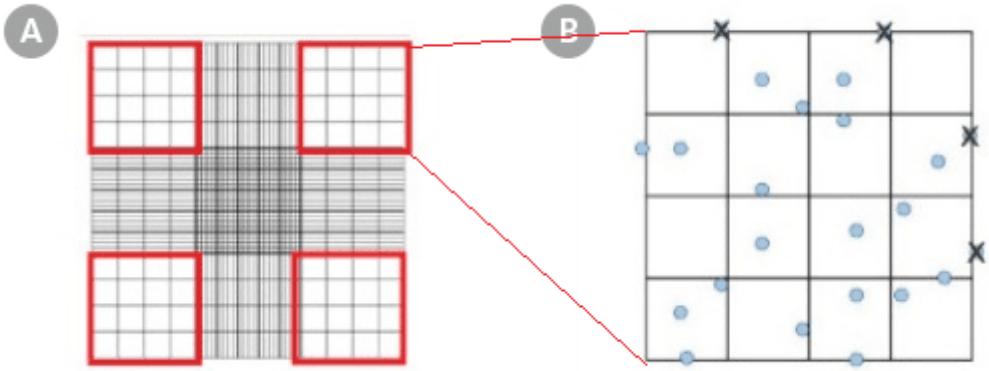

Figure 4.2: Determining cell counts, using a haemocytometer. A suspension of cells (~500 cells) was loaded onto the haemocytometer and placed under phase-contrast microscopy set at 10X magnification. In A, cells were counted within each quadrant, highlighted in red using a hand tally. In B, more detail is demonstrated for the inclusion and exclusion of cells during counting of each quadrant. The value of each quadrant was averaged and used to determine the cell count. Image taken from https://www.stemcell.com/how-to-count-cells-with-a-hemocytometer.html.

4.2.2.3 Alveolar Macrophage Phenotyping and Purity Analysis:

Before proceeding with staining of AMs with classical surface markers (phenotyping), using flow assisted cell sorting (FACS) and cytometry, a 1% bovine serum albumin (BSA) in 1X PBS was made by adding 5 g of BSA (Sigma, cat. A9418) to 500 ml 1X PBS. The BSA solution was left to dissolve at 4 °C without shaking to avoid breakdown of BSA. The 1% BSA in 1X PBS solution (FACS buffer) was stored at 4 °C and used for up to 2 weeks.

The AMs phenotype was analysed, by flow cytometry. General methodological principles of flow cytometry is provided in Chapter2, section 2.3. First, 100,000 cells in 100 µl complete media were added to 8 separate FACS tubes (Fisher Scientific, cat. #10186360) containing 2 ml of FACS buffer, then centrifuged at 500 g for 5 mins, at 4 ^{o}C. To avoid non-specific staining of antibodies to Fc receptors present on AMs, the supernatant was removed from each tube following centrifugation and then 1 µl of Fc block solution (BD, cat. #564219) was added to 2 ml of FACS buffer. This mixture was incubated for 10 minutes at room temperature (RT) before antibodies and isotype controls, at a 1:20 dilution, were added and incubated for 30 minutes in the dark at RT (Table 4.2), with unlabelled control cells subjected to the same incubation periods, with FACS buffer only. The cells were then washed with 2 ml FACS buffer, gently mixed and centrifuged at 500 g for 3 minutes and this process was repeated twice. Supernatants were carefully poured off the cell pellet and 300 µl of FACS buffer added, before samples were placed on ice and run on the Accuri C6 Plus flow cytometer, to assess AM phenotype following isolation.

Table 4.2: Surface Marker Antibodies Used to Assess Purity and Phenotype of Alveolar Macrophages (AMs). Primary human AMs were isolated from human lung tissue without macroscopic malignancy by lavage and Lymphoprep™ separation. Each antigen of interest is provided along with conjugated fluorochrome Allophycocyanin (APC) and represent mouse monoclonal antibodies to the human epitope of the antigen of interest. Each antibody was applied to cells at a 1:20 dilution in a buffer consisting of 1% bovine serum albumin (BSA) and 1X PBS. Details of clone and supplier are also provided.

Antigen	Fluorochrome	Clone	Catalogue No.	Supplier
CD14	APC	61D3	17-0149-42	Invitrogen
hMer (MerTK)		FA38912a	FAB8912A	RD Systems
CD80		2D10	305219	Biolegend
HLA-DR		LN3	17-956-42	Invitrogen
CD33		WM-53	17-0338-42	Invitrogen
CD45		H130	17-0459-42	eBioscience
CD163		eBioGH/6I	17-1639-42	Invitrogen
CD206		19.2	550889	BD
IgG1k		P3.6.2.8.1	17-4714-42	eBioscience
IgG12bk		eBM2b	17-4732-42	eBioscience

4.2.2.4 Flow Cytometric Analysis Protocol and Gating Strategy used for Alveolar Macrophages:

Using the Accuri C6 Plus flow cytometer the unlabelled/unstained samples were first mixed gently and then run on the machine. Cells were gated for forward scatter area (FSC-A) against FSC-height (FSC-H) to eliminate doublets, and then AMs were gated based on high FSC, side scatter (SSC) and autofluorescence, and counted at 5,000 gated events (Figure 4.3). AMs were gated based on high forward scatter (FSC) and side scatter (SSC) due to their large size and by autofluorescence particularly in the yellow-green spectrum, which is a common characteristic of AMs analysed via fluorescence techniques (Havenith *et al.* 1993). AMs were gated out of the singlet cell population by

high granularity and autofluorescence, and a propidium iodide (PI) (ThermoFisher, cat. #P1304MP) stain was used to measure baseline viability of AMs. Isotype controls were also used to factor in non-specific binding and cell autofluorescence in the gating and subsequent analysis of these cells. Cells were counted at 5,000 events within the gated alveolar macrophages and assessed for autofluorescence using median fluorescence intensity (MFI). Expression of characteristic markers for AMs were used to phenotype the isolated cells and predict % purity.

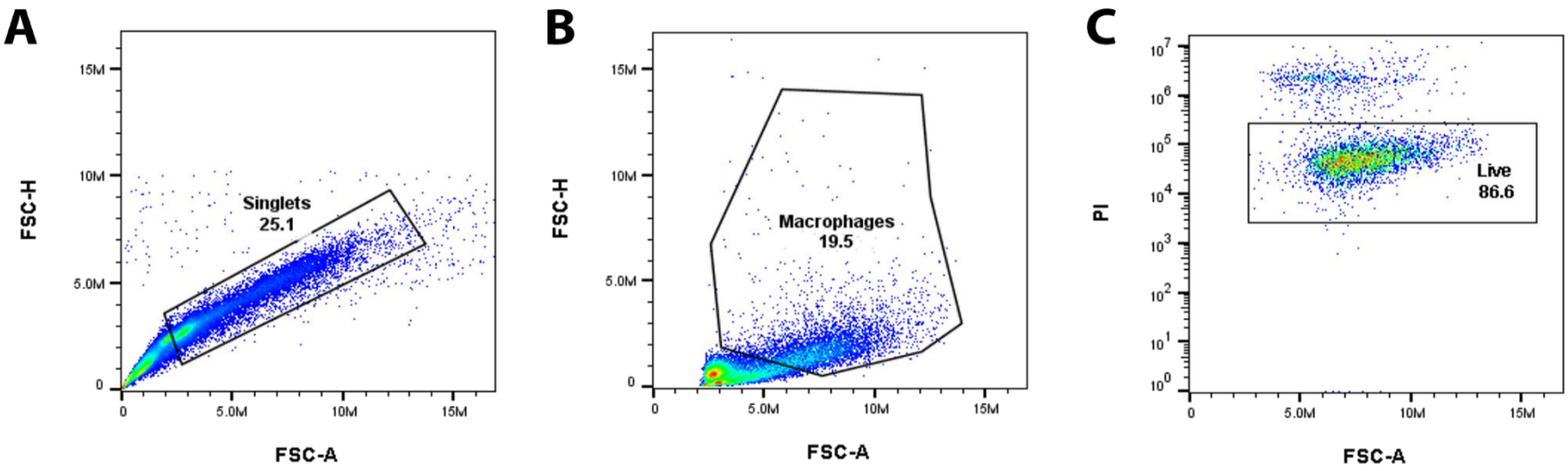

Figure 4.3: Gating strategy used to determine purity and viability of primary alveolar macrophages (AMs) isolated from human lung tissue. Representative flow cytometry plots of AMs isolated from human lung tissue without macroscopic malignancy, obtained from resection surgery and ran on the BD Accuri C6 Plus flow cytometer. AMs were isolated using the Lymphoprep™ method which resulted in a heterogenous mononuclear cell population with presence of AMs and smaller monocytes, dead cells, and debris, which were gated using FloJo. First, single large cells within the population were gated using forward scatter height (FSC-H, Y axis) against forward scatter area (FSC-A, X axis) (Singlets, A), which included 25.1% of the cell population. Of those singlets, AMs were gated (Macrophages, B), according to their FSC-H and FSC-A, where 19.5% of the singlet cell population fell within the AM gate. Finally, one sample of isolated AMs was exposed to propidium iodide (PI) which selectively stains dead cells in the sample. AMs isolated during my studies were viable, as represented by 2 clear populations of live (86.6%) and dead cells represented in C, where PI is represented on the Y axis, and FSC-A on the X axis.

To determine the purity of my samples, I assessed the expression of known AM surface markers following isolation. First, cluster of differentiation, (CD)163 and CD206, were used as AM markers, which stain M2-like AMs within the cell population (Kaku *et al.* 2014; Nouno *et al.* 2019). Human Leukocyte Antigen (HLA-DR) was also used as an established marker of antigen-presenting cells, such as AMs (Lipscomb *et al.* 1986), whilst CD45 expression allowed for measurement of general haematopoietic cells within the cell population (Bharat *et al.* 2016). Finally, CD33 staining was used to measure myeloid cells within the cell population (Wasserman *et al.* 1994). To rule out contamination from non-AM cells within isolated samples, I also stained for non-AM specific markers which included CD14, a known monocyte marker (Kapellos *et al.* 2019), CD80 a known bone-marrow derived macrophage and mature dendritic cell marker (antigen presenting cells) (Lim *et al.* 2012; Jiménez-Uribe *et al.* 2019). Finally, I also stained for MER proto-oncogene tyrosine kinase (MerTK) in each sample which is highly expressed in all macrophages, but not specific to AMs (Mohning *et al.* 2018). This panel of AM markers has been well established in the laboratory of Prof. David Thickett at the University of Birmingham (Mahida *et al.* 2021). Representative figures of marker profiles are shown in Figure 4.4. Within the figure, due to the high autofluorescence of AMs, the unstained panel was displayed and showed a similar staining pattern to the isotype control stain, highlighting the level of autofluorescence in these cells.

Count (Unit Area)
CD14
CD163
HLA-DR
CD80
MerTK
CD45
CD206
CD33

Figure 4.4: Representative histograms of phenotype of alveolar macrophages (AMs) isolated from human lung tissue from a long-term ex-smoker. AMs were stained with antibodies targeting antigens of interest, isotype controls, or were unstained for 1 hr at RT. Representative plots of antibody stained (purple), isotype control stained (light blue), and unstained controls (red) cells are presented from AMs isolated from lung tissue following resection surgery. AMs yielded expressed key AM markers, such as cluster of differentiation (CD)-163 and 206, typical antigen-presenting marker Human Leukocyte Antigen (HLA-DR), haematopoietic cell marker CD45 and myeloid cell marker CD33. To determine purity of AMs isolated, AMs did not express markers used to determine monocytes, monocyte-derived macrophages, or dendritic cells, by CD14, CD80 and MER proto-oncogene tyrosine kinase. The unstained peak within each panel represents the characteristic high autofluorescence of AMs. Each plot demonstrates the antigen of interest on the X axis and the Y axis represents the % cell count at a given level of cells expressing the antigen of interest, which was normalised to the area under each curve (Count Unit Area). Representative plots from N=4 isolations of AMs.

4.2.3 Isolation, Purification, and Generation of Monocyte-Derived Dendritic Cells and Myeloid Dendritic Cells:

The work outlined during this section of Chapter 4 of my thesis regarding isolation and purification of blood-derived monocytes and generation of both immature and mature dendritic cells, and subsequent analysis of CaSR expression these cells, was performed in the laboratory of Professor Catherine Hawrylowicz at King's College London. Methodological and experimental assistance was obtained from Dr Tzer-Ren Ho and Mr Drew Glencross during my time as a visiting scientist to their laboratories.

4.2.3.1 Research Ethics:

Human peripheral blood was obtained from healthy (non-asthmatic) consenting healthy adult volunteers under full Research Ethics Committee (REC) approval (REC 14/LO/1688).

4.2.3.2 Peripheral Blood Mononuclear Cell Isolation:

120 ml of citrated peripheral venous blood (5 ml:5 ml citrate: blood) was collected from healthy volunteers and gently inverted to mix. Citrated blood was diluted 1:1 with Hanks' Balanced Salt Solution (HBSS) (Gibco, cat. #24020117) and gently inverted to mix. Meanwhile, 15 ml LymphoPrep™ (Stemcell Technologies, cat. #07851) was added to eight 50 ml Falcon tubes. 30 ml of diluted citrated blood was layered onto the LymphoPrep™ before tubes were centrifuged at 800 g for 20 minutes at 4 °C. After the centrifugation, peripheral blood mononuclear cells (PBMC) rich fluid was removed from above the interface and was transferred to a new 50 ml Falcon tube. The tubes containing PBMC-rich fluid were then centrifuged at 600 g for 10 minutes and supernatant was discarded. If no red blood cells (RBC) were present, the cell pellets were re-suspended in 1 ml of 2% foetal bovine serum (FBS) in HBSS (FBS-HBSS) per pellet, combined into one 50 ml falcon tube then made up to 50 ml with FBS-HBSS. If RBC were present, pellets were combined into one 50 ml Falcon tube and 1 ml of 1x RBC lysis buffer solution (Miltenyi Biotec, cat. #130-094-183) was added, mixed by gently pipetting up and down and then vortexed for 5 seconds before being incubated at RT for 10 mins. Once this incubation period had finished, this solution was made up to 50 ml with FBS-HBSS to dilute and wash out the lysis buffer. Tubes were centrifuged again at 300 g for 10 minutes. Supernatant was discarded and cell pellet was re-suspended in 1 ml FBS-HBSS per pellet. After gentle mixing by pipetting up and down, this solution was made up to 50 ml with FBS-HBSS. Cell counting was performed as described in section 4.2.2.2.

4.2.3.3 $CD14^+$ Monocyte Isolation:

Cells remaining from the previous step were centrifuged again at 300 g for 10 minutes and supernatant was completely aspirated from the cells. The cell pellet was re-suspended in 80 µl cold (from the fridge) 2% FBS in 1X PBS with

8 µM EDTA (MACs buffer) per 10^7 total cells. The suspension was mixed well by pipetting with $CD14^+$ MicroBeads human (Miltenyi Biotec, cat. #130-050-201) and incubated at 2-8 °C for 15 minutes. Cells were washed using 1-2 ml of MACs buffer per 10^7 cells and tubes were centrifuged at 300 g for 10 minutes. Up to 10^8 of this cell suspension was re-suspended in 500 µl of MACs buffer for magnetic separation of $CD14^+$ monocytes using LS columns (Miltenyi Biotec, cat. #130-122-729). An aliquot of these cells underwent cytospin, as described in section 4.2.7.1 below.

4.2.3.4 Magnetic Separation of $CD14^+$ Monocytes and Preparation for Phenotype and Purity Analysis:

To perform magnetic separation of $CD14^+$, first, LS columns (Miltenyi Biotec, cat. #130-122-729) were assembled and rinsed with 3 ml MACs buffer. The cell suspension was applied to the column and was washed 3 times with 3 ml of MACs buffer (collected in one tube). The column was removed from the magnet and a new tube was placed below the column to collect the $CD14^+$ monocytes. 5 ml MACs buffer was added to the column and cells were flushed out immediately using the plunger provided. 10 µl of this cell suspension was counted as described in section 4.2.2.2. Then, cells were washed again using 20 ml FBS-HBSS and centrifuged at 300 g for 10 minutes and this process was repeated twice. The $CD14^+$ monocyte pellet was resuspended in in RPMI (Gibco, Thermofisher Scientific, cat. #11875101) supplemented with 10% FBS (Thermofisher Scientific, cat. #10500-064), L-glutamine (Thermofisher Scientific, cat. #25030081) and gentamicin (Gibco, Thermofisher Scientific, cat. #15750060) (full medium).

An aliquot of the magnetically separated cells was used for analysis of purity of monocytes obtained using the isolation method described above. These cells were stained with phycoerythrin (PE) conjugated $CD14^+$ antibody (1:20 dilution) (Miltenyi Biotec, cat. #170-078-013) for 20 minutes at 4 °C to be

assessed via flow cytometry analysis, as described in section 4.2.3.11 below. A wash with FACS flow solution (Fisher Scientific, cat. #12756528) was performed before the samples were ran on Invitrogen™ Attune™ NxT flow cytometer.

4.2.3.5 Granulocyte-Macrophage Colony Stimulating Factor (GM-CSF) and Interleukin (IL)-4 Exposure to Monocytes:

The remaining $CD14^+$ monocytes were seeded at a concentration of 5 million cells per 3 ml (cell density: $1.67x10^6$ cells/ml) full medium supplemented with 100 ng/ml of granulocyte-macrophage colony stimulating factor (GM-CSF) (R&D systems, cat. #215-GM-050) and 50 ng/ml interleukin-4 (IL-4) (R&D systems, cat. #204-IL-010) in each well of a 6 well plate and incubated at 37 °C and 5% CO_2 for 4 days to generate immature monocyte derived dendritic cells (iDCs). After 4 days of culture, 2 ml of the full medium supplemented with GM-CSF (100 ng/ml) and IL-4 (50 ng/ml) was added to each well. On day 6, supernatant containing non-adherent iDCs, was aspirated and washed with 45 ml of FBS-HBSS before centrifugation at 300 g for 10 minutes at RT. The cell pellet was re-suspended in FBS-HBSS and counted as described in section 4.2.2.2. After counting, cells were centrifuged at 300 g for 10 minutes before being resuspended with full medium at a cell density of $1x10^5$ cells/ml. An aliquot of these cells was transferred to FACS tubes (100 µl per FACS tube) for characterization and remaining cells were plated at a density of 20,000 cells/well in 200 µl full medium in a u-bottom 96-well plate (Thermofisher, cat. #10344311), to proceed with generation of mature monocyte-derived DC (mDC). An aliquot of these cells (~100,000 cells) underwent cytospin, as described in section 4.2.7.1 below.

4.2.3.6 Preparation of Particulate Matter:

To assess whether the CaSR was expressed in mDCs, I used exposure to PM as a stimulant of DC maturation, as reported previously (Matthews et al 2016). Urban PM powder (Sigma-Aldrich, cat. #NISTSRM1648a) was vortexed, then

20 mg was weighed directly into a 20 ml universal tube. 20 ml PBS was added to this, resulting in a final concentration of 1 mg/ml. This solution was vortexed and then sonicated using a sonicating water bath (GT Sonic, cat. #Z0001) at 40 Hz for 15 minutes. Following this, the solution was vortexed again before aliquoting into 1 ml and then stored at -80 °C for future use. On the day of exposure of iDCs to mDCs, 1 mg/ml stock aliquots were thawed and sonicated again as above and then diluted to 10 µg/ml in full medium for treatment of iDCs.

4.2.3.7 Particulate Matter Exposure to Immature Dendritic Cells:

To generate mDCs, iDCs were treated with 10 µg/ml urban PM (SRM1648a, Sigma, cat. #NIST1648a) in full medium for 24hrs, as an established method to generate mDCs. An aliquot of these cells underwent cytospin, as described in section 4.2.7.1 The non-adherent iDCs and mDCs were removed from the wells of the plate using cold MAC's buffer and transferred to FACS tubes

4.2.3.8 Preparation of Immature and Mature Dendritic Cells for Phenotype and Purity Analysis:

To determine purity of iDCs and mDCs, an aliquot of each was used to ensure full differentiation of monocytes to iDC and to determine maturity status of PM-induced mDC. Cells were stained with antibodies, at a 1:20 dilution, which targeted antigens such as those expressed on antigen presenting cells, HLA-DR (Lipscomb *et al.* 1986), a known dendritic cell marker CD11c (Ganguly *et al.* 2013). In addition, I assessed expression of CD14, as a monocyte marker (Kapellos *et al.* 2019), CD11b, as a leukocyte activation marker (Yu *et al.* 2016), CD1a, a marker for monocyte-derived DCs (Cernadas *et al.* 2009), CD40, a marker for activated DCs (Ma and Clark 2009), CD83, a marker for mDCs (Bender *et al.* 1996), and CD86, a marker expressed on a range of immune cells, such as mDCs and macrophages (Sousa and Caetano 2006; Bertani *et al.* 2017).

Each antibody, conjugated fluorochrome, clone and supplier details are listed in Table 4.3.

For analysis of maturation, mDCs were stained with allophycocyanin (APC) anti-CD83 (BD Bioscience, cat. #551073) and the viability dye eBioscience™ fixable viability dye eFluor 780 (eBioscience™, cat. #65-0865-14) for 30 minutes at 4 °C to determine maturity status (Bender et al 1996). In addition, a fluorescence minus one (FMO) APC was included, as a control for multicolour fluorescence staining, by omission of the APC antibody from the staining panel, to assist in gating for percentage APC $CD83^+$ in PM stimulated cells. A wash with FACS flow solution was performed before the samples were ran on Invitrogen™ Attune™ NxT flow cytometer, as described in section 4.2.3.11. Each antibody, conjugated fluorochrome, clone and supplier details are listed in Table 4.3, To generate an estimation of non-specific binding of each antibody of interest, isotype control antibodies, which were relevant to the antigens of interest, were also prepared to a 1:20 dilution in FACs buffer, where specific details are provided in Table 4.4.

Table 4.3: Surface marker antibodies used to assess purity and phenotype of monocytes and monocyte-derived dendritic cells (DCs). $CD14^+$ monocytes were isolated from whole human blood obtained from healthy volunteers (N=7) and DC were generated from these. Each antigen of interest is provided along with conjugated fluorochromes: Peridinin-Chlorophyll-protein (PerCP), Allophycocyanin (APC), Phycoerythrin (PE) and Fluorescein (FITC) and represent mouse monoclonal antibodies to the human epitope of the antigen of interest. Each antibody was applied to cells at a 1:20 dilution in a buffer consisting of 1% bovine serum albumin (BSA) and 1X PBS. Clone and supplier details are also shown.

Antigen	Fluorochrome	Clone	Catalogue Number	Supplier
HLA-DR (MHC Class II)	PerCP	L243	307628	Biolegend
CD11C	APC	BU15	21487111	ImmunoTools
CD14	PE	TÜK4	130-080-701	Miltenyi Biotec
CD11b	PE	ICRF44	557321	BD Biosciences
CD1a	PE	H149	555807	
CD40	PE	5C3	555589	
CD83	FITC	HB15e	556910	
CD86	APC	2331	555660	

Table 4.4: Isotype control antibodies used to assess non-specific background signal during phenotyping of monocytes and monocyte-derived dendritic cells (DCs). $CD14^+$ monocytes were isolated from whole human blood obtained from healthy volunteers (N=7) and DC were generated from these. Each isotype control, with conjugated antibody is provided: Fluorescein (FITC), Phycoerythrin (PE), Peridinin-Chlorophyll-protein (PerCP), and Allophycocyanin (APC). Isotype controls represent mouse monoclonal antibodies to the human epitope of the isotype which corresponds to antibodies used for phenotyping of monocytes and DCs. Each isotype control antibody was applied to cells at a 1:20 dilution in a buffer consisting of 1% bovine serum albumin (BSA) and 1X PBS. Supplier details are also shown.

Fluorochrome	Isotype	Company	Catalogue Number
FITC	IgG1K1	Biolegend	400108
PE	IgG2aK	BD	G155-178
PE	IgG1K1	BD	555749
PerCP	IgG2K	Biolegend	400250
APC	IgG1K1	eBioscience	17-4714-42

In total, 4 FACS tubes were prepared with an aliquot of monocytes and iDCs, making a total of 8 FACS tubes. Each antibody and isotype control were prepared to a 1:20 dilution. To Tube 1, HLA-DR, CD11c, and CD11b antibodies were added to each tube monocytes and iDCs. To Tube 2, the CD14 antibody was added and to Tube 3, CD1a antibody was added to the tubes containing monocytes and DCs. Finally, CD40, CD83 and CD86 antibodies were added to Tube 4 of monocytes and iDCs (details provided in Table 4.5) A wash with FACS flow solution was then performed before the samples were ran on Invitrogen™ Attune™ NxT flow cytometer.

Table 4.5: Tube setup for assessment of monocytes and monocyte-derived dendritic cell (DC) phenotype. $CD14^+$ monocytes were isolated from whole human blood obtained from healthy volunteers (N=7) and DC were generated from these. The antibody of interest and relevant isotype controls were added to the corresponding tubes. Fluorescent conjugated antibody is provided: Peridinin-Chlorophyll-protein (PerCP), Allophycocyanin (APC), Phycoerythrin (PE), and Fluorescein (FITC). Antibodies and isotype controls represent mouse monoclonal antibodies to the human epitope of the antigen or isotype corresponding to the antibodies used for phenotyping of monocytes and DCs. Each antibody was applied to cells at a 1:20 dilution in a buffer consisting of 1% bovine serum albumin (BSA) and 1X PBS.

Tube	Antigen	Fluorochrome	Isotype
Tube 1	HLA-DR	PerCP	IgG2ak
Tube 1	CD11c	APC	IgG1K1
Tube 1	CD11b	PE	IgG1K1
Tube 2	CD14	PE	IgG2aK
Tube 3	CD1a	PE	IgG1K1
Tube 4	CD40	PE	IgG1K1
Tube 4	CD83	FITC	IgG1K1
Tube 4	CD86	APC	IgG1K1

4.2.3.9 $CD1c^+$ Myeloid Dendritic Cell Isolation:

Expression of the CaSR in myeloid DCs has not been previously investigated, therefore, I used cells remaining from section 4.3.2 and centrifuged again for 300 g for 10 minutes and carefully discarded the supernatant. The cell pellet was re-suspended in 200 µl cold MACs buffer per 10^8 total cells and then the suspension was mixed well with reagents from the human CD1c (BDCA-1)$^+$ DC isolation kit (Miltenyi Biotec, cat. #130-119-475). These reagents included 100 µl of FcR Blocking Reagent (Miltenyi Biotec, cat. #130-0590901) per 10^8 total cells, 100 µl of CD19 MicroBeads per 10^8 total cells and 100 µl of CD1c (BDCA-1) biotin per 10^8 total cells. The mixed suspension was then incubated at 2-8 °C for 15 minutes. Cells were washed using 1-2 ml of MACs buffer per 10^7 cells and tubes were centrifuged at 300 g for 10 minutes. Up to 10^8 of this cell suspension was re-suspended in 500 µl of MACs buffer.

Meanwhile, LD columns (Miltenyi Biotec, cat. #130-042-901) were assembled and rinsed with 2 ml of MACs buffer. The cell suspension was applied to the column and was washed with twice with 1 ml of MACs buffer. The unlabelled cells contained within the effluent that passed through was collected into a sterile falcon tube and were then centrifuged at 300 g for 10 minutes and supernatant carefully removed, then re-suspended with 400 µl of MACs buffer per 10^8 total cells. The suspension was mixed well by gentle pipetting with 100 µl of anti-biotin microbeads per 10^8 total cells of the $CD1c^+$ DC isolation kit and incubated for 15 minutes at 2-8 °C. Cells were washed using 1-2 ml of MACs buffer per 10^7 cells and tubes were centrifuged at 300 g for 10 minutes. Up to 10^8 of this cell suspension was re-suspended in 500 µl of MACs buffer. Meanwhile, MS columns (Miltenyi Biotec, cat. #130-042-201) were assembled and rinsed with 500 µl of MACS buffer and the cell suspension was applied to the column and washed 3 times with 500 µl of MACs buffer.

The column was removed from the magnet and a new sterile tube was placed below the column to collect magnetically separated $CD1c^+$ DC, by adding 1 ml of MACs buffer to the column and flushing cells out with the plunger provided. 10 µl of this cell suspension was counted as described in section 4.2.2.2. Following counting, cells were washed twice using 20 ml FBS-HBSS and centrifuged at 300 g for 10 minutes. The $CD1c^+$ DC pellet was resuspended in 10% FBS in RPMI (Gibco, Thermofisher Scientific, cat. #11875101) at a cell density of $1x10^5$ cells/ml for to carry out a cytospin for IHC staining, as described in section 4.2.7.1 below and an aliquot was taken for phenotyping and purity analysis.

4.2.3.10 Preparation of $CD1c^+$ Myeloid Dendritic Cell for Phenotype and Purity Analysis:

Magnetically separated $CD1c^+$ myeloid DCs were stained with PE anti-CD11c antibody (1:20 dilution) (BD Bioscience, cat. #555392) and PerCP anti-HLA-DR

(Biolegend, cat. #307628) for 20 minutes at 4°C. A wash with FACS flow solution was performed before the samples were ran on Invitrogen™ Attune™ NxT flow cytometer, as described below.

4.2.3.11 Flow Cytometric Analysis Protocol and Gating Strategy used for Immature and Mature Dendritic Cells:

The general methodological principles of flow cytometry are provided in Chapter 2, section 2.4. Using the Invitrogen™ Attune™ NxT flow cytometer, monocytes and iDCs were first gated by forward scatter area (FSC-A) and FS height (FSC-H) to remove the inclusion of debris and doublets in the analysis, as reported previously in Faith et al (2005). From this, cells were gated based on granularity and size, by plotting side scatter area (SSC-A) and FSC-A within the single cell population, respectively (Figure 4.5). Flow cytometry was used to assess the phenotype of day 0 purified $CD14^+$ monocytes and their subsequent phenotype following differentiation into iDCs by Day 6.

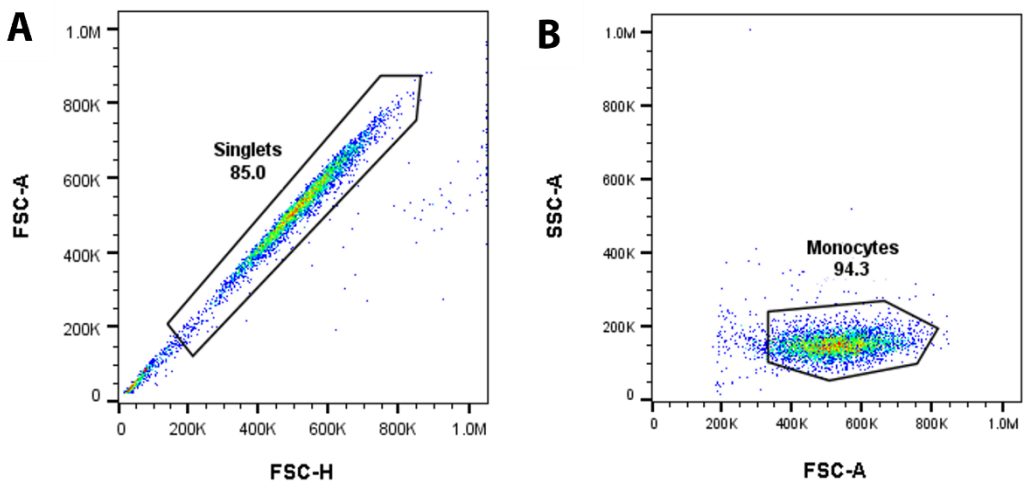

Figure 4.5: Gating strategy used to determine phenotype of day 0 monocytes and day 6 monocyte-derived dendritic cells. Representative images of gating strategy used to determine single cells (singlets, A) and Monocytes (B) within the cell population. Singlets were determined by plotting forward scatter area (FSC-A, Y axis) against the forward scatter height (FSC-H, X axis), and resulted in 85% of the cells run falling within the singlet gate (A). Side scatter area (SSC-A, Y axis) and FSC-A (B) was used to gate the monocytes within the singlet population, where 94.3% of cells fell within this gate (B).

Monocytes express the key surface markers CD14, CD11b, CD11c, HLA-DR, and CD86 but lack expression of CD1a, CD40 or CD83 (Figure 4.2.5) (Kapellos *et al.* 2019). Following 6-day stimulation with GM-CSF (100 ng/ml) and IL-4 (50 ng/ml), monocytes differentiate into immature monocyte-derived dendritic cells (iDCs) which express distinct surface markers with a clear shift in expression profile (Figure 4.6) (Hiasa *et al.* 2009). In contrast to monocytes, iDCs express CD1a, CD11b, CD11c and HLA-DR but exhibit reduced expression of CD14 and CD86 when compared to monocytes (Collin *et al.* 2013). In all experiments, isotype control staining was carried out to determine non-specific binding and cell autofluorescence. Compensations were applied with the use of single stains and gating was performed with either fluorescence minus one (FMO controls) or against unstained samples. All flow cytometric analysis was performed using FlowJo software (BD Life Sciences).

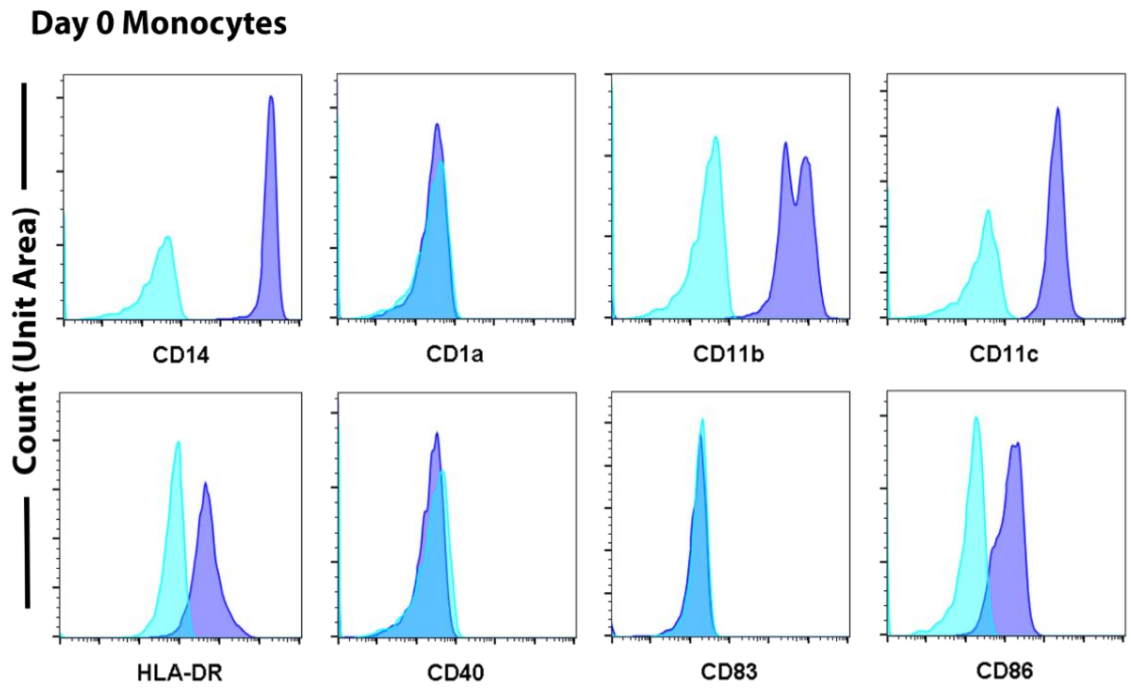
Day 0 Monocytes
Count (Unit Area)
CD14
CD1a
CD11b
CD11c
HLA-DR
CD40
CD83
CD86

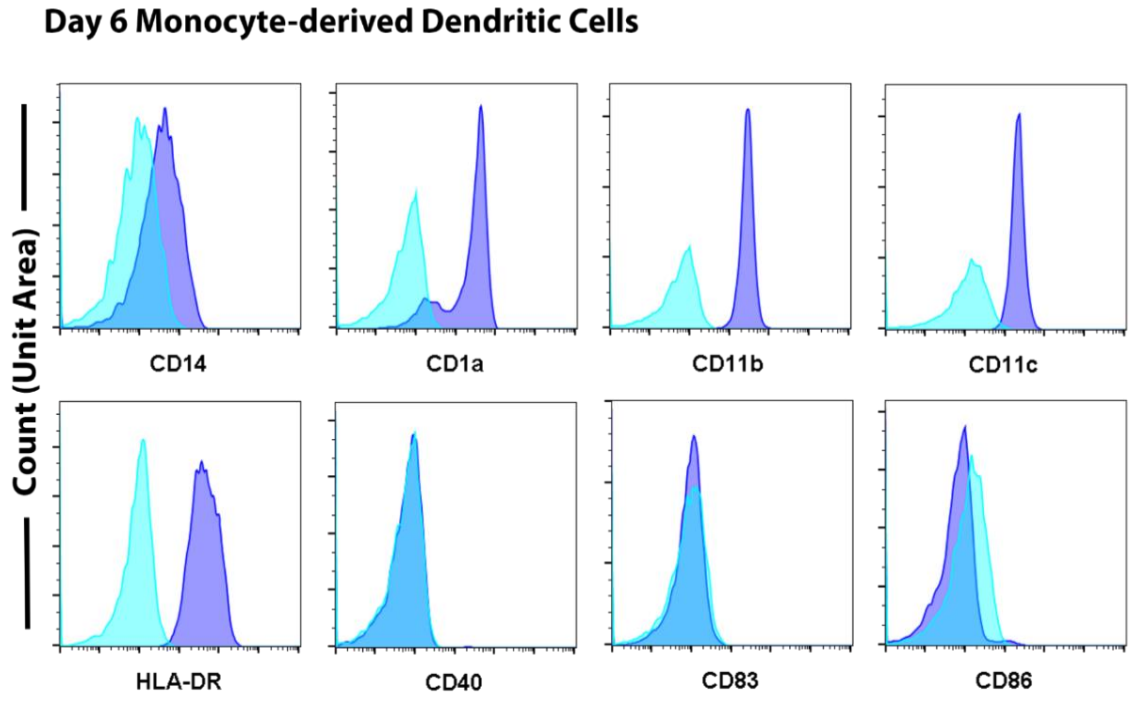
Day 6 Monocyte-derived Dendritic Cells
Count (Unit Area)
CD14
CD1a
CD11b
CD11c
HLA-DR
CD40
CD83
CD86

Figure 4.6: Representative histograms of the phenotype of monocytes and monocyte-derived dendritic cells (DCs) isolated from healthy human volunteer whole blood. Day 0 Monocytes underwent differentiation into DC following 6-day exposure to Granulocyte-macrophage colony stimulating factor (GM-CSF, 100 ng/ml) and interleukin (IL)-4 (50 ng/ml). Monocytes and DCs were stained with antibodies targeting antigens of interest: cluster of differentiation (CD)-14, CD1a, CD11b, CD11c, CD40, CD83, CD86, and Human Leukocyte Antigen (HLA-DR) (shown in purple) and relevant isotype controls (shown in pale blue). Data are represented as histograms with the purple peak within each panel representing the antibody of interest and the light blue peak within each panel representing the isotype control. Unstained cells are not shown within the plots due to order of magnitude difference between stained and unstained cells, representing low levels of cell autofluorescence. Each plot demonstrates the antigen of interest on the X axis and the Y axis represents the % cell count at a given level of cells expressing the antigen of interest, which was normalised to the area under the curve (Unit Area).

4.2.3.12 Flow Cytometric Analysis Protocol and Gating Strategy of $CD1c^{+}$Myeloid Dendritic Cells:

The general methodological principles of flow cytometry are provided in Chapter 2, section 2.4. The purity of myeloid ($CD1c^{+}$) DC was also analysed and similarly to monocytes, iDCs lack expression of CD40 and CD83, with no distinction from isotype control staining. Myeloid DCs were solely gated on characteristic expression markers and compared to the unstained control, as these cells do not have a round shape. Myeloid DCs exhibit clear expression of key myeloid DC markers CD11b and HLA-DR compared to the unstained sample (Figure 4.7). In all experiments, isotype control staining with relevant isotype control antibodies were carried out to determine non-specific binding and cell autofluorescence. Compensations were applied with the use of single stains and gating was performed with either fluorescence minus one (FMO controls) or against unstained samples. All flow cytometric analysis was performed using FlowJo software (BD Life Sciences).

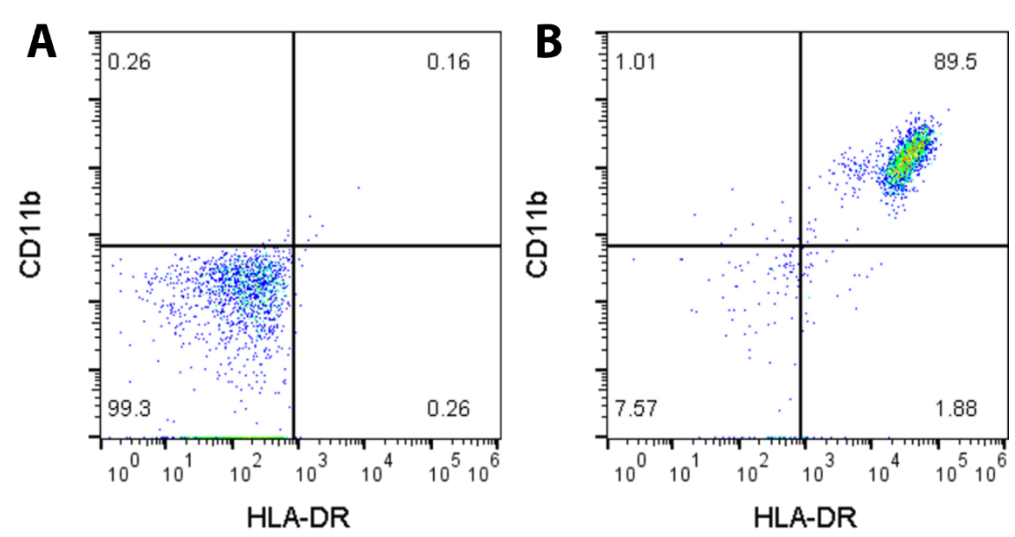

Figure 4.7: Representative image to demonstrate gating strategy used to assess purity of isolated myeloid (CD1c$^+$) dendritic cells (DC), from healthy whole human blood. CD1c$^+$ DC were isolated from whole human blood from healthy volunteers (N=3). Representative flow cytometry plots of Myeloid DC isolated from whole human blood. Quadrant gating was used to assess purity markers cluster of differentiation (CD)11b and human leukocyte antigen (HLA)-DR of unstained cells, where 99.3% of cells fell into the gate with low CD11b and HLA-DR expression (A). However, stained cells show 89.5% of cells fall into the gate representing high CD11b and HLA-DR expression (B), which is characteristic of CD1c$^+$ DCs.

4.2.4 Type 2 Innate Lymphoid Cell Isolation, Purification, and Flow Cytometric Analyses:

To analyse CaSR expression in ILC2, I forged a collaboration with Professor Luzheng Xue and Dr Jian Luo, to generate, analyse the phenotype, and fix ILC2 obtained in their laboratory from healthy human blood. The fixed cells were then sent to Cardiff for me to analyse CaSR expression in these cells, by IHC staining.

4.2.4.1 Research Ethics:

Human peripheral blood was obtained from healthy volunteers after they provided written consent, and with full approval from the Leicestershire, Northamptonshire, and Rutland Ethics Committee (REC 08/H0406/189)

4.2.4.2 Type 2 Innate Lymphoid Cell (ILC2) Preparation:

Human ILC2s were prepared from peripheral blood from healthy donors. Peripheral blood mononuclear cells (PBMCs) were isolated from leukocyte reduction system cones (National Blood Service, Bristol, United Kingdom) using Lymphoprep™ gradient. PBMC samples were depleted of T cells, B cells, natural killer (NK) cells and monocytes by labelling with FITC-conjugated anti-CD3, anti-CD14, anti-CD16 and anti-CD19 plus anti-FITC microbeads (Miltenyi) or the corresponding EasySep antibodies plus beads (StemCell Technologies). Lineage negative (Lin^-) (CD4/8/14/16/19/56/123 and FcεRI) $CD45^{high}CD127^+CRTH2^+$ ILC2 cells were sorted from human PBMCs by the FACSAria III (BD), and cultured in RPMI (Sigma, cat. #R0883) with the supplement of 10% human serum (Sigma, cat. #H3667) 1× L-glutamine (Sigma, cat. #G7513), 1× penicillin/streptomycin (Sigma, cat. #P4333), 1× sodium pyruvate (Sigma, cat. #P8574), 1× nonessential amino acids (Sigma, cat. #M7145), 50mmol/L 2-mercaptoethanol (Sigma, cat. #63689), and 250 U/mL IL-2 (Sigma, cat. #SRP3085). Full antibody details can be found in Table 4.6. An aliquot of ILC2 underwent cytospin for subsequent fixation and IHC staining of the CaSR, as described in section 4.2.7.1 below.

Table 4.6: Surface marker antibodies used to assess purity and determine phenotype of type 2 innate lymphoid cells (ILC2). Each antigen of interest is provided along with conjugated fluorochromes: Fluorescein (FITC), Peridinin-Chlorophyll-protein (PerCP), Phycoerythrin-Cyanine 7 (PE-Cy7), and Brilliant Violet (BV650). The antibodies represent mouse monoclonal antibodies to the human epitope of the antigen of interest. Each antibody was applied to cells at a 1:20 dilution in a buffer consisting of 1% bovine serum albumin (BSA) and 1X PBS, for 1 hr at room temperature. Clone and supplier details are also shown.

Antigen	Fluorochrome	Clone	Catalogue No.	Supplier
CD3	FITC	OKT3	317306	BioLegend
CD4	PerCP	OKT4	317432	BioLegend
CD8	PerCP	RPA-T8	301030	BioLegend
CD14	PerCP	MΨP-9	345786	BD
CD16	PerCP	3G8	302030	BioLegend
CD19	PerCP	HIB19	302228	BioLegend
CD56	PerCP	HCD56	318342	BioLegend
CD123	PerCP	32703	FAB301C	R&D Systems
FcεRI	PerCP	AER-37(CRA-1)	334616	BioLegend
CD45	PE-Cy7	H130	304016	BioLegend
CD127	BV650	A019D5	351326	BioLegend

4.2.4.3 Flow Cytometric Analysis Protocol and Gating Strategy:

The general methodological principles of flow cytometry are provided in Chapter 2, section 2.4. To sort ILC2 from PBMCs, the FACSAria III (BD) was used to first gate single cells from the PBMC sample by plotting FSC-A against FSC-H to avoid inclusion of doublets and debris in the gate. From this population, live cells lacking expression of CD3 were gated ($DAPI^-$ $CD3^-$) by plotting FSC-A against $DAPI^-$ $CD3^-$ (Figure 4.8).

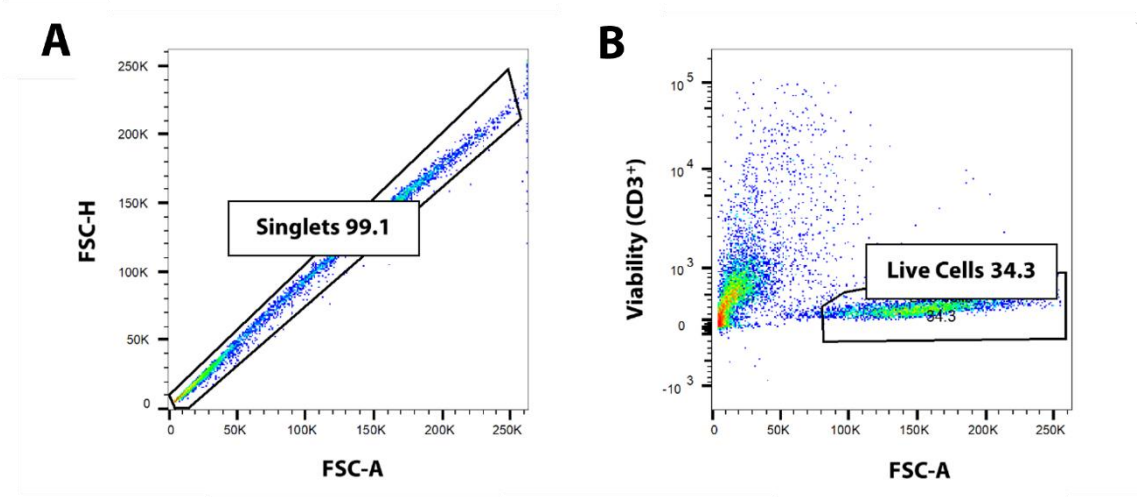

Figure 4.8: Representative image to demonstrate the gating strategy for selection of human type 2 innate lymphoid cells (ILC2). First, single cells within the population were gated using forward scatter height (FSC-H, Y axis) against forward scatter area (FSC-A, X axis) (A), which represented 99.1% of cells within the sample. Then using a viability dye (DAPI) and CD3 antibody staining, live cells were gated out which express low levels of CD3 ($CD3^-$, B), resulting in a clear population of 34.3% live cells within the single cell population.

Following selection of single and live cells, $CD3^-$ and $DAPI^-$ ILC2 cells were plotted alongside a $CD3^+$ $DAPI^-$ positive control cell type, $CRTH2^+$ T cells, to enable specific gating of ILC2 cells (Figure 4.9, A). ILC2 cells do not express Lineage (Lin^-) markers (CD4, CD8, CD14, CD16, CD19, CD56, CD123 and FCεRI) markers compared to the positive control cells, however, both express similar levels of leucocyte common antigen, CD45 (Figure 4.9, B). As the final step of

characterisation of these cells, ILC2 cells show a larger spread of CRTH2 expressing cells than the positive control cells (Figure 4.9, C). All flow cytometric analysis was performed using FlowJo software (Treestar).

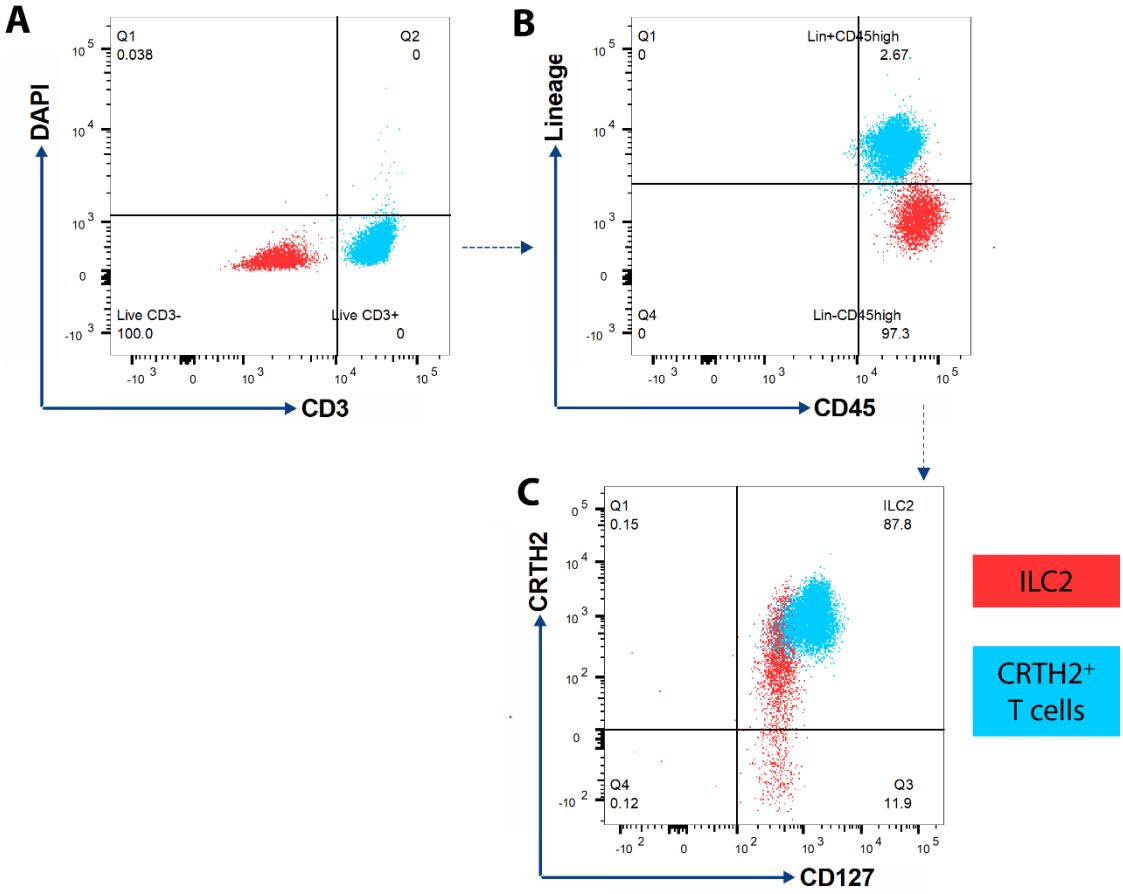

Figure 4.9: Demonstration of gating strategy used to sort type 2 innate lymphoid cells (ILC2) from peripheral blood mononuclear cells (PBMCs). ILC2 were obtained from human healthy volunteer blood (N=3). PBMCs were stained with Lineage (Lin^-) markers (CD4, CD8, CD14, CD16, CD19, CD56, CD123 and FCεRI) antibodies to assist with sorting ILC2 cells from PBMCs. A positive control cell type of T cells positive for CRTH2 ($CRTH2^+$, blue) was included in the analysis to gate ILC2 (red) from. First, cluster of differentiation (CD)-3^- and $DAPI^-$ cells within the cell population were identified via quadrant gating and show a clear separation from $CD3^+$ $CRTH2^+$ T cells (A). ILC2 cells do not express Lin^- markers compared to the positive control $CRTH2^+$ cells, however, both express similar levels of leukocyte common antigen, CD45 (B). Finally, ILC2 cells are distinct from the CRTH2 positive control cells (C). Each plot was analysed by quadrant gating where quadrant labels and numbers represent the % of cells within the ILC2 population which are $CD3^-$ (100%), Lin-CD45high (97.3%) and finally the cells which represent the ILC2 cells within the population (87.8%).

4.2.5 Monocyte-Derived Macrophage Cell Line (THP-1) Culture, Differentiation, and Preparation:

To validate expression of the CaSR in MDMs I used the established THP-1 cell line. These cells were generated in the laboratory of Professor Dipak Ramji at Cardiff University, with methodological assistance from Miss Jing Chen.

4.2.5.1 THP-1 Cell Culture and Seeding:

The THP-1 cell line is an established monocytic cell line commonly used as an in vitro model of human inflammation (Schwende *et al.* 1996). THP-1 cells were cultured and maintained in suspension in RPMI-1640 medium (containing L-glutamine and sodium bicarbonate, Gibco, cat. #21875034), supplemented with 10% heat-inactivated foetal bovine serum (HI-FBS; heated at 56 °C for 30 minutes, Thermofisher, cat. #10082147), 100 U/ml penicillin and 100 µg/ml streptomycin (Thermofisher, cat. #15140122) (complete medium). To obtain cells from the flask, the contents of the flask were transferred to a 50 ml Falcon tube and centrifuged at 110 g for 5 minutes at RT. The supernatant was carefully poured off and the cell pellet was resuspended in 2 ml of fresh complete medium. For experimental use, cells were counted as described in section 4.2.2.2 and 20,000 cells per well in 200 µl were seeded into EZ slides for use in IHC. THP-1 cells become adherent upon differentiation into macrophages by treatment with 0.16 µM phorbol 12-myristate 13-acetate (PMA) solution (Merck, cat. #P8139) (made with complete medium) before being placed back into the humidified 37 °C incubator with 5% CO_2 for 24 hours to allow differentiation. The following day, PMA-containing medium was removed from the adherent MDMs and replaced with fresh complete medium. Full medium was removed from the wells containing THP-1 cells and washed once with warmed 1 X PBS, before fixation and subsequent IHC, as described in section 4.2.7.2 and 4.2.7.3 below.

4.2.6 Cell fixation and Immunohistochemical Staining:

The general methodological principles of IHC are provided within Chapter 2, section 2.2.

4.2.6.1 Cytospin of Immune Cells:

Once cells had been isolated, an aliquot of the cell suspension was used to perform a cytospin (Shandon, ThermoFisher Scientific) to fix and stain the different cell types to determine CaSR expression. First, the cytospin apparatus was assembled according to manufacturer's instructions, then, ~50,000 AMs, ~50,000 $CD14^+$ monocytes, ~75,000 iDCs, ~75,000 mDCs, ~2000 Myeloid DCs, and ~1000 ILC2 in 100-200 µl culture medium were pipetted into the funnel of the cytospin apparatus and spun at 1000 g for 5 minutes. The slides were removed from the cytospin apparatus and air dried for ~1 minute, in a flow hood.

4.2.6.2 Cell Fixation:

First, a 4% paraformaldehyde (PFA, stock solution) (Sigma, cat. #158127) was made by measuring 800 ml of 1X PBS and weighing and adding 40 g PFA powder to this. The mixture was stirred in a ventilation hood and heated to 60 °C to start the dissolving process. The pH of the solution was adjusted to aid dissolving of PFA by adding 5 M NaOH dropwise to the solution until it cleared. The solution was cooled, and filtered using a 0.4 µm filter (Sartorius, cat. #4AJ9049865). The volume was then adjusted to 1L with 1X PBS, aliquoted into 15 ml falcons and stored at -20 °C for future use.

On the day of staining, an aliquot of 4% PFA was thawed and diluted to 2% with 1X PBS. All cells were fixed with 2% PFA in PBS for 20 minutes at RT. Following this, cells were washed with three changes of 1X PBS for 5 minutes each time. After this, fresh 1X PBS was added and the container was sealed

with parafilm and stored at 4 °C until staining commenced. Cells were left for a maximum of 72 hrs in 1X PBS at 4 °C before staining.

4.2.6.3 CaSR Staining in Basal Human Bronchial Epithelial Cells, Monocytes, Immature, Mature, and Myeloid Dendritic Cells, Type 2 Innate Lymphoid Cells, and Monocyte-Derived Macrophages:

On the day before staining, blocking buffer was prepared by first adding 48 ml of 1X PBS to a 50 ml Falcon tube. 0.05 ml Triton™X-100 (Sigma, cat. #X100) was slowly collected from the bottle using a wide bore pipette tip (VWR, cat. #7322341), before being slowly added to the 1X PBS. Finally, 1.5 ml Seablock (Thermofisher, cat. #37527) was added and the solution was made up to 50 ml with 1X PBS, resulting in the antibody dilution fluid (ABDF). 0.5 g of BSA was weighed and gently placed in the tube containing the ABDF, gently inverted and left to dissolve at 4 °C overnight.

On the day of staining, cell culture medium or PBS was removed from cell and then endogenous peroxidase activity was quenched using 0.3% H_2O_2 (Atom Scientific, cat. #GPC8054-D) in PBS for 30 mins at RT. Slides were washed 3x for 5 mins with 1X PBS and then blocking buffer was applied for 1hr at RT. Following this, mouse monoclonal antibody against the human epitope of the CaSR was prepared as the primary antibody (Abcam, cat. #ab19347) at a 1:200 dilution. This was added to cells and left to incubate over night at 4°C.

The next day, slides were washed 3x for 5 mins with 1X PBS and cells were incubated with goat-anti mouse IgG Biotinylated secondary antibody (Abcam, cat. #ab97263) (1:250 dilution) for 1hr at RT. During the final 1X PBS wash, ABC detection reagent (Vector Laboratories, cat. #PK6-100) was prepared by measuring 5 ml 1X PBS and adding 2 drops of reagent A, vortexing and then adding 2 drops of reagent B, from the kit. ABC reagent was then applied to cells and incubated at RT for 30mins. Slides were washed 3x for 5 mins with 1X PBS. During the final wash, DAB (Vector Laboratories, cat. #SK-4100) solution

was prepared by measuring 5 ml deionised H_2O and adding to a clean universal tube. Then, 2 drops of reagent 1, 4 drops of reagent 2 and 2 drops of reagent 3 were added to the tube and protected from light. The slide with CaSR antibody stain was placed under phase-contrast microscopy (10x objective) and DAB solution was applied to cells until brown colour developed (~30 seconds) and the reaction was terminated in ddH_2O. H_2O was removed from cells and then counterstained with Harris haematoxylin (Atom Scientific, cat. #RRSP67-C) for 8 mins at RT and then washed under running tap water for 5 minutes. For differentiation, a 1% acid alcohol solution was prepared by adding 1% concentrated HCl to 70% EtOH, at the desired volume for 30 seconds and then washed under running tap water for 1 minute. Then, slides underwent "bluing" in 0.2% concentrated ammonium hydroxide in distilled water (0.2% ammonia water) for 45 seconds then washed under running tap water for 5 minutes. Slides were dehydrated with a series of ethanol (70, 90 & 100% for 2 minutes each) and xylene (2 changes for 2 minutes each) and then mounted with DPX, containing anti-fade medium (Atom Scientific, cat. #RRSP29-B).

4.2.7.4 IHC staining of the CaSR in Alveolar Macrophages:

AMs were fixed and stained for the CaSR as in section 4.2.9.3, however, the haematoxylin counterstain differed from the one used above. Following termination of DAB, AMs were counterstained with Weigert's haematoxylin by preparing a 1:1 solution using the A & B components of the kit (Weigert's A and B solution 1:1, Atom Scientific, cat. #25088B1-1 and 25088B2-1) for 5 mins and then washed under running tap water for 5 minutes. Slides were dehydrated with a series of ethanol (70, 90, 100%, 2 minutes each) and xylene (2 changes for 2minutes each) and then mounted with DPX as described in section 4.2.9.4.

4.2.7.5 Imaging of IHC Stains:

>24 hrs after mounting, slides were taken to the Bioimaging facility within the School of Biosciences at Cardiff University and imaged using an Olympus BX41 brightfield microscope equipped with 5x, 10x, 20x and 40x objectives, a QImaging QICAM Fast 1394 colour digital camera (with associated PC) and an OASIS motorised XYZ stage that can be controlled by a joystick or directly via the Surveyor software (Slide scanner). Images were obtained and cropped using IrfanView graphic viewer freeware available at: https://www.irfanview.com/, to generate images for use in my results section of this Chapter.

4.3 Results:

4.3.1 Basal Human Bronchial Epithelial Cells Express the CaSR at the Protein Level:

As the first hit for inhaled stimuli, such as PM, the airway epithelium comprises a major orchestrator of PM-induced pro-inflammatory cellular responses in the airways. Here I used a 2D *in vitro* model of basal NHBECs to determine whether these express the CaSR at the protein level, for potential identification of an *in vitro* model to assess the role of the CaSR in mediating PM-induced cellular responses in the airway epithelium.

Basal NHBECs express the CaSR, at the protein level, as revealed by IHC staining, and validated using a primary antibody omitted and isotype negative controls (Figure 4.10). My data provides evidence to further assess the role of the CaSR in these cells, to determine whether the airway epithelial CaSR could comprise one of the mechanisms behind PM-sensing and induced exacerbations of lung diseases. Therefore, NAM could provide an effective therapeutic to directly block PM-induced cellular responses, and subsequent exacerbations of lung diseases.

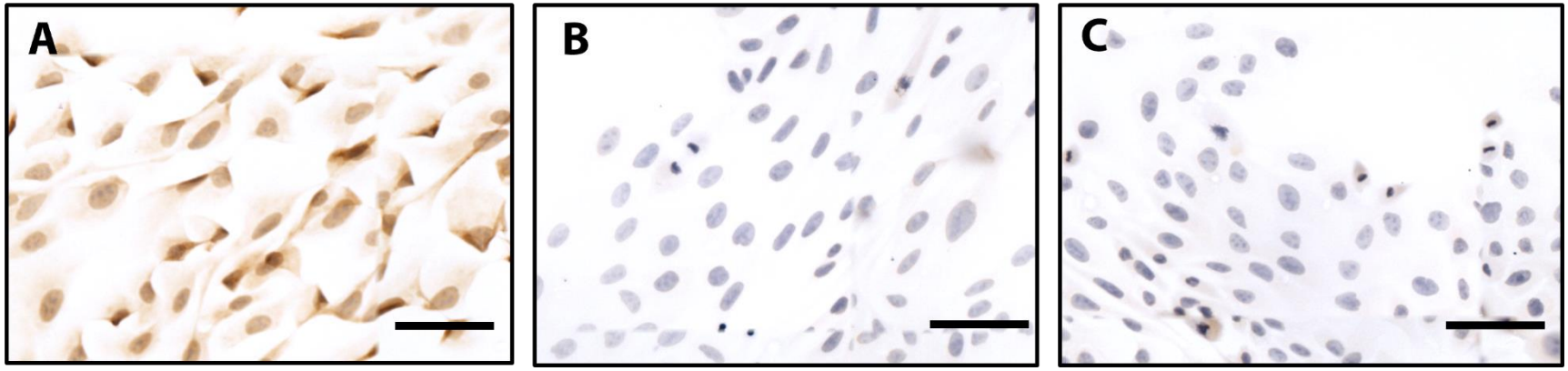

Figure 4.10: The calcium-sensing receptor (CaSR) is expressed at the protein level in primary basal human bronchial epithelial cells (NHBECs). Immunohistochemistry (IHC) images (40x objective, Olympus BX-40) of NHBECs. NHBECs were stained with mouse monoclonal antibody against the human epitope of the CaSR or an IgG2a isotype control at a 1:200 dilution in a buffer consisting of 1% bovine serum albumin (BSA) in 1X PBS. A primary antibody omitted negative control was included by adding buffer only during the primary antibody staining period. Visualisation of CaSR staining was performed using the 3,3'-Diaminobenzidine (DAB) method as a chromogenic substrate of horseradish peroxidase. Basal NHBECs demonstrate positive staining for the CaSR shown in brown (A). There was no positive staining in primary antibody omitted (B) or isotype (C) negative controls. In all images, cells were counterstained with haematoxylin, representing nuclei (blue). The scale bar within each panel represents 50 µm.

4.3.2 Alveolar Macrophages Express the CaSR at the Protein Level:

In addition to airway epithelial cells, tissue-resident AMs also play a key role in sensing and responding to pro-inflammatory cellular responses induced by environmental cues, such as PM (Mitsi *et al.* 2018). To provide an *in vitro* model to assess whether the CaSR plays a role in PM-induced cellular responses in AMs, I isolated primary AMs from lung tissue following resection surgery and determined CaSR expression, at the protein level.

In AMs isolated from lung tissue from a long-term ex-smoker, the CaSR was demonstrated to be expressed on the protein level, using IHC (Figure 4.11). Unfortunately, due to COVID-19-related restrictions during my studies, I was unable to carry out an isotype control stain with these cells. However, this novel finding provided a basis for further assessment of the role of the CaSR in mediating PM-induced cellular responses using this *in vitro* model of AMs.

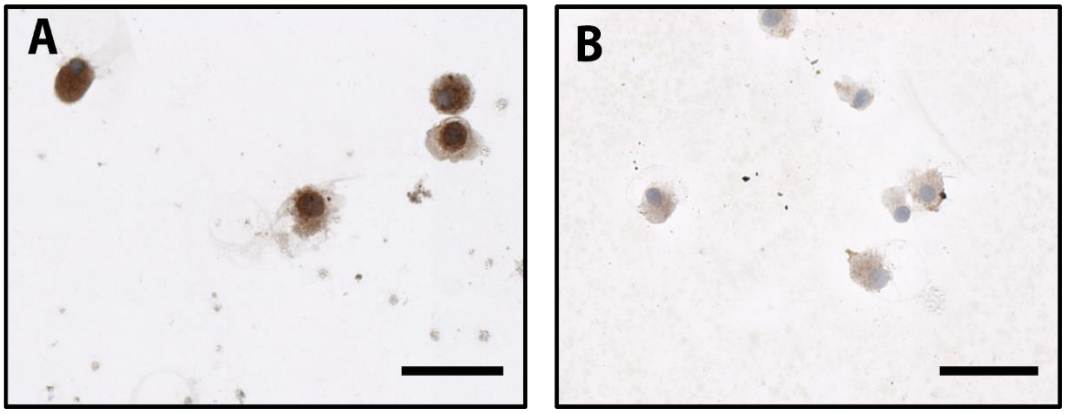

Figure 4.11: The calcium-sensing receptor (CaSR) is expressed at the protein level in primary human alveolar macrophages (AMs). Immunohistochemistry (IHC) images (40x objective, Olympus BX-40) of primary AMs isolated from lung tissue without macroscopic malignancy which were resected from a long-term ex-smoker undergoing assessment for lung carcinoma, with ~95% representing AMs. AMs were stained with mouse monoclonal antibody against the human epitope of the CaSR at a 1:200 dilution in a buffer consisting of 1% bovine serum albumin (BSA) in 1X PBS. A primary antibody omitted negative control was included by adding buffer only during the primary antibody staining period. Visualisation of CaSR staining was performed using the 3,3'-Diaminobenzidine (DAB) method as a chromogenic substrate of horseradish peroxidase. AMs demonstrate brown (positive) staining for the CaSR (A). There was reduced brown (positive) staining in primary antibody omitted negative control (B). In both images, cells were counterstained with haematoxylin, representing nuclei (blue). The scale bar within each panel represents 50 μm.

4.3.3 Dendritic Cells Express the CaSR at the Protein Level:

DCs are another key cell involved in the sensing, uptake, and processing of inhaled stimuli such as PM, and plays a sentinel role in bridging the innate and adaptive immune systems in their mature state (Matthews *et al.* 2016; Hilligan and Ronchese 2020). In addition, during inflammation, blood-derived monocyte-derived DCs are recruited to perpetuate the airways response induced by exposure to pro-inflammatory stimuli, such as PM. To provide an *in vitro* model to assess the role of the CaSR in key PM-induced functions, such as maturation and cytokine secretion, in this section, sought to understand whether cells of the monocyte lineage; monocytes and immature and mature

monocyte-derived DC, expressed the CaSR at the protein level, using IHC staining.

Cells of the monocyte lineage: monocytes (Figure 4.12) obtained from whole human blood and *in vitro* generated monocyte-derived iDC and mDC express the CaSR at the protein level (Figure 4.13). In addition, myeloid DC isolated from whole human blood also express the CaSR at the protein level (Figure 4.14). Unfortunately, due to COVID restrictions at King's College London (Guy's Hospital, where the research laboratory is based), I was unable to carry out an isotype control stain in myeloid DC. Together, these data provide evidence of each cell type as suitable *in vitro* models for further assessment of the role of the CaSR in mediating PM-induced cellular responses.

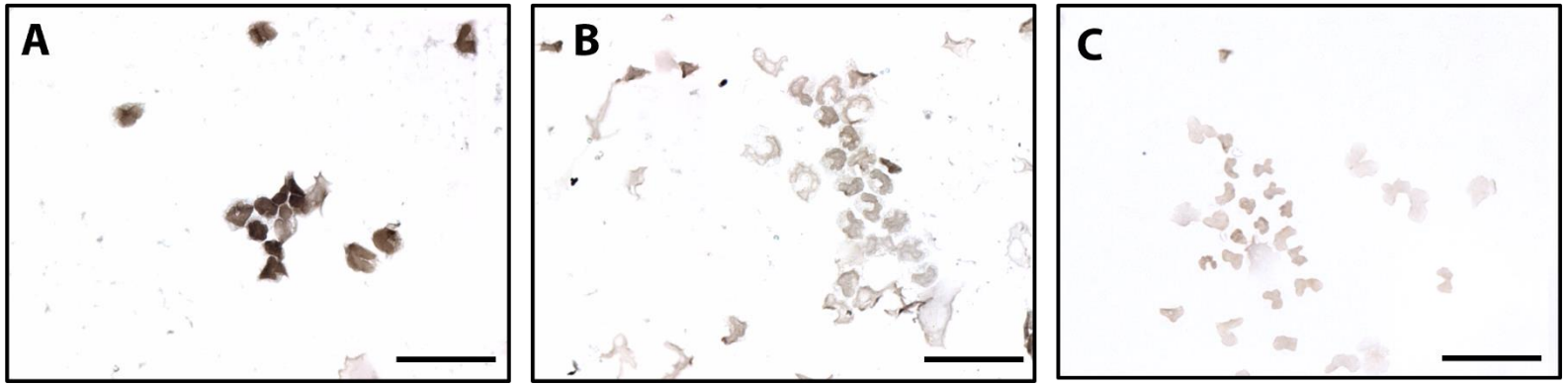

Figure 4.12: The calcium-sensing receptor (CaSR) is expressed at the protein level in human monocytes. Immunohistochemistry (IHC) images (40x objective, Olympus BX-40) of human $CD14^{+}$ monocytes, isolated and purified from whole human blood from a healthy volunteer. Monocytes were stained with mouse monoclonal antibody against the human epitope of the CaSR or an IgG2a isotype control at a 1:200 dilution in a buffer consisting of 1% bovine serum albumin (BSA) in 1X PBS. A primary antibody omitted negative control was included by adding buffer only during the primary antibody staining period. Visualisation of CaSR staining was performed using the 3,3'-Diaminobenzidine (DAB) method as a chromogenic substrate of horseradish peroxidase. Monocytes demonstrate brown (positive) staining for the CaSR (A). There was reduced brown (positive) staining in primary antibody omitted negative control (B) and relevant isotype control (C). In both images, cells were counterstained with haematoxylin, representing nuclei (blue). The scale bar within each panel represents 50 μm.

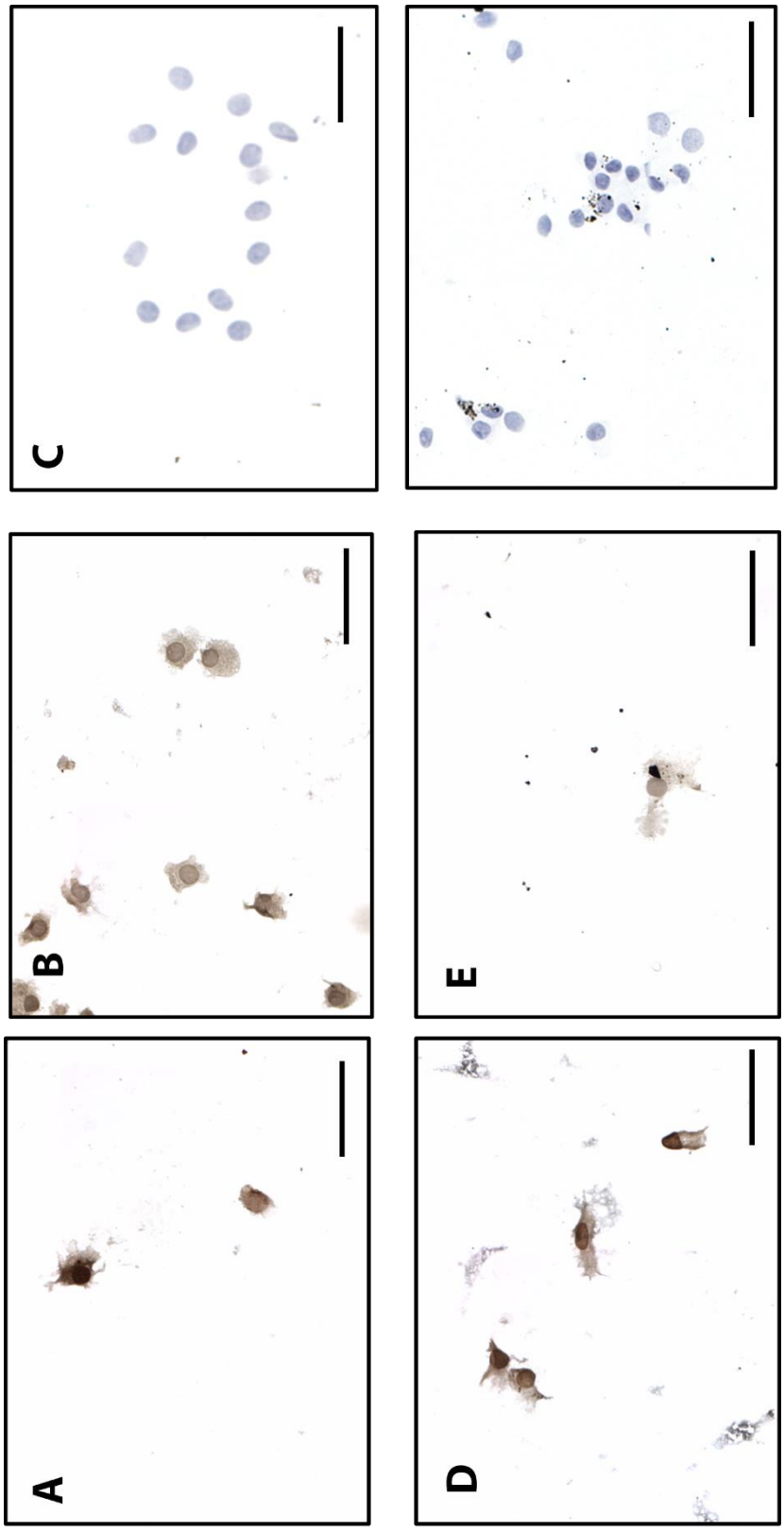
C
E
B
D
A

Figure 4.13: The calcium-sensing receptor (CaSR) is expressed at the protein level in immature and mature monocyte-derived dendritic cells (iDC and mDC, respectively). Immunohistochemistry images (40x objective, Olympus BX-40) of iDC and mDC generated from differentiation of $CD14^{+}$ monocytes obtained from whole human blood from a healthy volunteer. Cells were stained with mouse monoclonal antibody against the human epitope of the CaSR or an IgG2a isotype control at a 1:200 dilution in a buffer consisting of 1% bovine serum albumin (BSA) in 1X PBS. A primary antibody omitted negative control was included by adding buffer only during the primary antibody staining period. Visualisation of CaSR staining was performed using the 3,3'-Diaminobenzidine (DAB) method as a chromogenic substrate of horseradish peroxidase. A & D represent the CaSR receptor (brown) in iDC and mDC, respectively. B & E represent the negative control stains (primary antibody omitted but all other steps remained the same) and C and F represent the isotype (IgG2a) negative control antibody. Scale bar = 50μm.

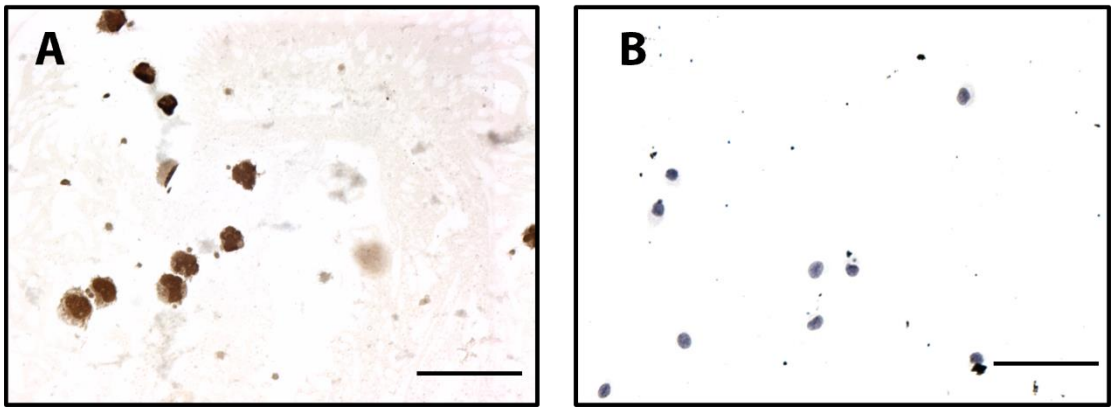

Figure 4.14: The calcium-sensing receptor (CaSR) is expressed at the protein level in myeloid dendritic cells (CD1c$^+$ DCs). Immunohistochemistry images (40x objective, Olympus BX-40) of CD1c$^+$ DCs isolated from whole human blood from a healthy volunteer. CD1c$^+$ DCs were stained with mouse monoclonal antibody against the human epitope of the CaSR at 1:200 dilution, in a buffer consisting of 1% bovine serum albumin (BSA) in 1X PBS. A primary antibody omitted negative control was included by adding buffer only during the primary antibody staining period. Visualisation of CaSR staining was performed using the 3,3'-Diaminobenzidine (DAB) method as a chromogenic substrate of horseradish peroxidase. CD1c$^+$ DCs demonstrate brown (positive) staining for the CaSR (A). There was very little brown (positive) staining in primary antibody omitted negative control (B). In both images, cells were counterstained with haematoxylin, representing nuclei (blue). The scale bar within each panel represents 50 µm.

4.3.4 Other Blood- and Airway-Derived Inflammatory Cells Express the CaSR at the Protein Level:

4.3.4.1 Type 2 Innate Lymphoid Cells Express the CaSR at the Protein Level:

Downstream of direct responses to PM in airways structural and immune cells which come into direct contact with PM, there is indirect activation of other immune cells by PM, such as ILC2. Activation occurs in response to epithelial cell-derived cytokines, where crosstalk between the epithelium and ILC2 has been shown to be crucial in initiating both T2 and non-T2 immune responses in the lungs (Martinez-Gonzalez *et al.* 2016). To determine whether the CaSR was expressed in ILC2, these cells were isolated from PBMCs from healthy

volunteers and cultured, before being affixed to slides and sent to Cardiff, for me to perform IHC staining.

In this section, I demonstrate that ILC2 cells also express the CaSR at the protein level (Figure 4.15). This provides novel evidence of a potential role for the CaSR in mediating crosstalk between ILC2, the airway epithelium, and other immune cells, thereby contributing to the propagation and maintenance of pro-inflammatory responses induced by exposure to inhaled stimuli, such as PM.

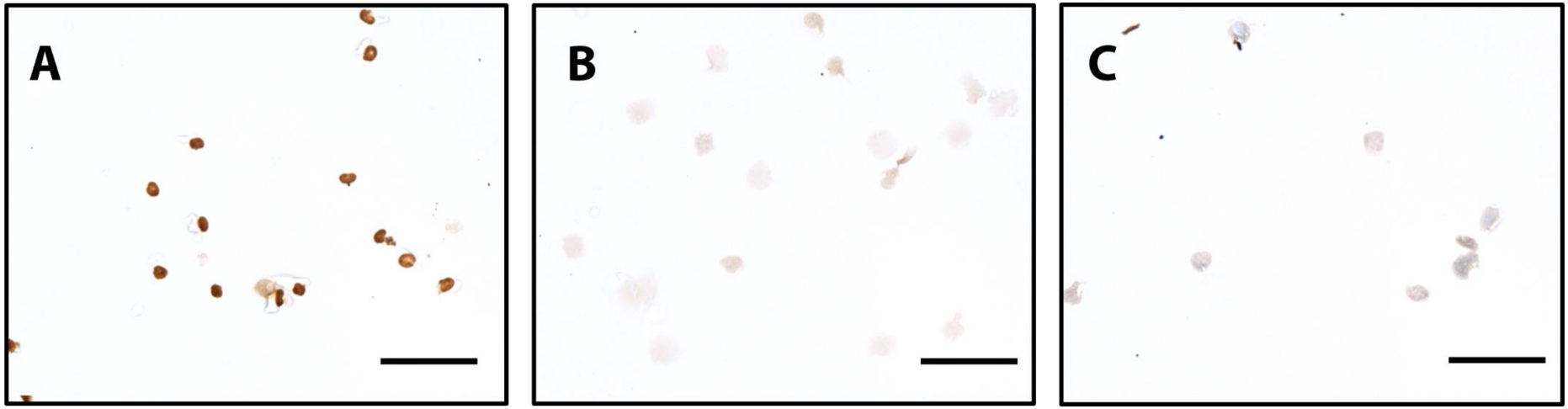

Figure 4.15: The calcium-sensing receptor (CaSR) is expressed at the protein level in type 2 innate lymphoid cells (ILC2). Immunohistochemistry images (40x objective, Olympus BX-40) of ILC2 isolated from peripheral human blood from a healthy volunteer. ILC2 were stained with mouse monoclonal antibody against the human epitope of the CaSR or an IgG2a isotype control at a 1:200 dilution in a buffer consisting of 1% bovine serum albumin (BSA) in 1X PBS. A primary antibody omitted negative control was included by adding buffer only during the primary antibody staining period. Visualisation of CaSR staining was performed using the 3,3′-Diaminobenzidine (DAB) method as a chromogenic substrate of horseradish peroxidase. ILC2 demonstrate brown (positive) staining for the CaSR (A). There was very little brown (positive) staining in primary antibody omitted negative control (B) or isotype control (C). In all images, cells were counterstained with haematoxylin, representing nuclei (blue). The scale bar within each panel represents 50 μm.

4.3.4.2 Monocyte-Derived Macrophages Express the CaSR at the Protein Level:

Circulating monocytes also respond rapidly to chemotactic agents released by PM-exposed airway structural and immune cell types. These infiltrate areas of inflammation, where they differentiate into MDMs to contribute to the innate inflammatory response (Italiani and Boraschi 2014). To enable further analysis of the role of the CaSR in immune cells such as PM, this cell line was used to develop a model to test PM-induced and CaSR-mediated effects in MDMs.

MDMs express the CaSR at the protein level (Figure 4.16) and this provides validation of MDM derived from THP-1 cells as a suitable model to further assess the role of the CaSR in mediating PM-induced effects in MDM.

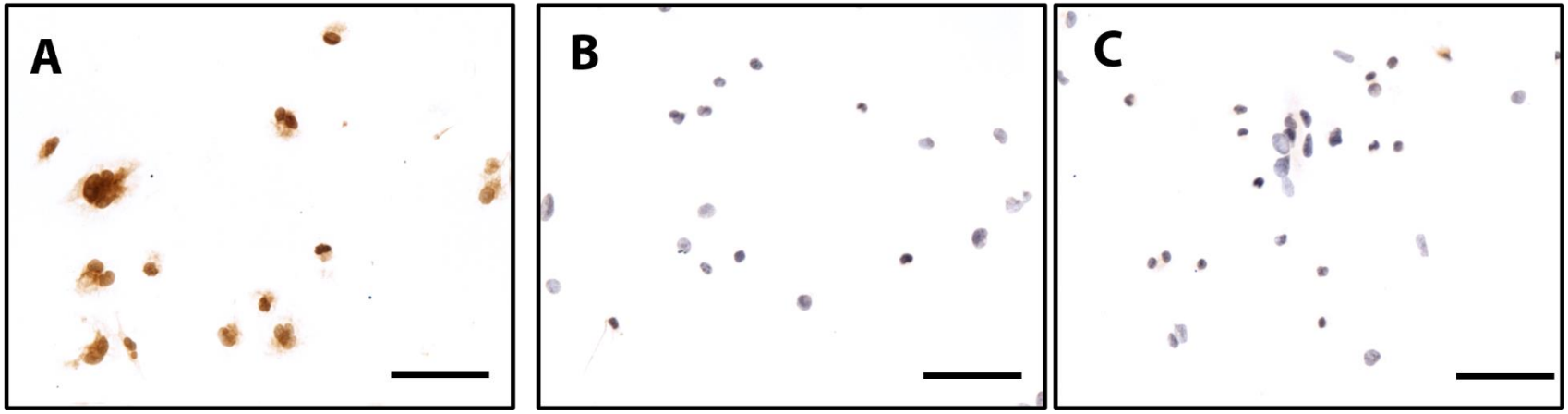

Figure 4.16: The calcium-sensing receptor (CaSR) is expressed at the protein level in monocyte-derived macrophages (MDMs) generated from differentiation of THP-1 monocyte cell line. Immunohistochemistry images (40x objective, Olympus BX-40) of THP-1 MDMs generated by exposure of THP-1 monocytes to 0.16 μM phorbol 12-myristate 13-acetate (PMA) solution for 24 hrs. MDMs were stained with mouse monoclonal antibody against the human epitope of the CaSR or an IgG2a isotype control at a 1:200 dilution in a buffer consisting of 1% bovine serum albumin (BSA) in 1X PBS. A primary antibody omitted negative control was included by adding buffer only during the primary antibody staining period. Visualisation of CaSR staining was performed using the 3,3′-Diaminobenzidine (DAB) method as a chromogenic substrate of horseradish peroxidase. MDMs demonstrate brown (positive) staining for the CaSR (A). There was very little brown (positive) staining in primary antibody omitted negative control (B) or isotype control (C). In all images, cells were counterstained with haematoxylin, representing nuclei (blue). The scale bar within each panel represents 50 μm.

4.4 Discussion:

In this chapter, I have demonstrated that CaSR protein is expressed in key cells involved in mediating pro-inflammatory response to inhaled stimuli such as PM and associated with the pathogenesis of lung disease. Together with my findings from Chapter 3, these data suggest the CaSR could comprise a key multimodal environmental chemosensor, expressed throughout the lungs, which responds directly and indirectly to exposure of inhaled stimuli, such as PM. Therefore, airways epithelial and immune cells, expressing the CaSR, could work synergistically to perpetuate a pro-inflammatory environment in response to PM exposure, contributing to lung disease pathogenesis and acute exacerbations. This lays the basis for better understanding the role of the CaSR in these cell types, by establishment of suitable CaSR-expressing *in vitro* models to assess the efficacy of NAM as a therapeutic for PM-exacerbated lung disease, such as asthma.

4.4.1 The CaSR is Expressed at the Protein Level in Airway Epithelial Cells:

First, I confirmed protein level expression of the CaSR in submerged basal NHBECs to determine whether this could provide a 2D model to assess PM-induced and CaSR-mediated effects in airway epithelial cells. Previous studies have demonstrated functional expression of the CaSR in basal NHBECs and NHBECs grown at the air-liquid interface (ALI) (Cortijo et al. 2010; Milara et al. 2010). These revealed that components of PM, such as calcium and nickel directly activate the CaSR in a human lung adenocarcinoma cell line (A549) and in basal NHBECs, an effect which can be blocked by NAM (Cortijo et al. 2010)). However, this study based their findings on the non-specific NAM, NPS 2390 and therefore, whether the model used in this chapter is suitable for assessing PM-induced effects in the airways, and the efficacy of NAM as a potential therapeutic for PM-exacerbated lung disease, remains unclear.

Expression of the *CASR* gene is of low abundance in tissues not involved in extracellular Ca^{2+} homeostasis (non-calciotropic tissues), therefore it was important to determine which airway cells express the CaSR to provide models to use in assessing PM-induced effects in the airways. The Human Protein Atlas is an online repository of single cell RNA sequencing (scRNA-seq) datasets, where the lung-specific consensus of *CASR* mRNA expression was generated from data obtained by Vieira Braga et al. (2019). This study included 26,154 cells sequenced from 17 individuals, to reveal a cellular map of the human lung and reveals that respiratory ciliated epithelial cells such as those found in the nasal passage or the peripheral bronchi, express the *CASR* gene most abundantly (Figure 4.17) (Vieira Braga *et al.* 2019). The previous chapter revealed the potential for the CaSR as a PM-sensor in the airways and as respiratory ciliated cells are one of the first hits for inhaled substances, the data obtained by The Human Protein Atlas further promotes a role for the CaSR in sensing and responding to PM. CaSR protein expression has also been confirmed in peripheral bronchial ciliated epithelial cells by my laboratory and PhD colleague, Mrs Kasope Wolffs, using an established IHC method for detection of the CaSR in non-calciotropic tissues developed by Dirk Adriaenssen (Wolffs *et al.* 2020) (Figure 4.18).

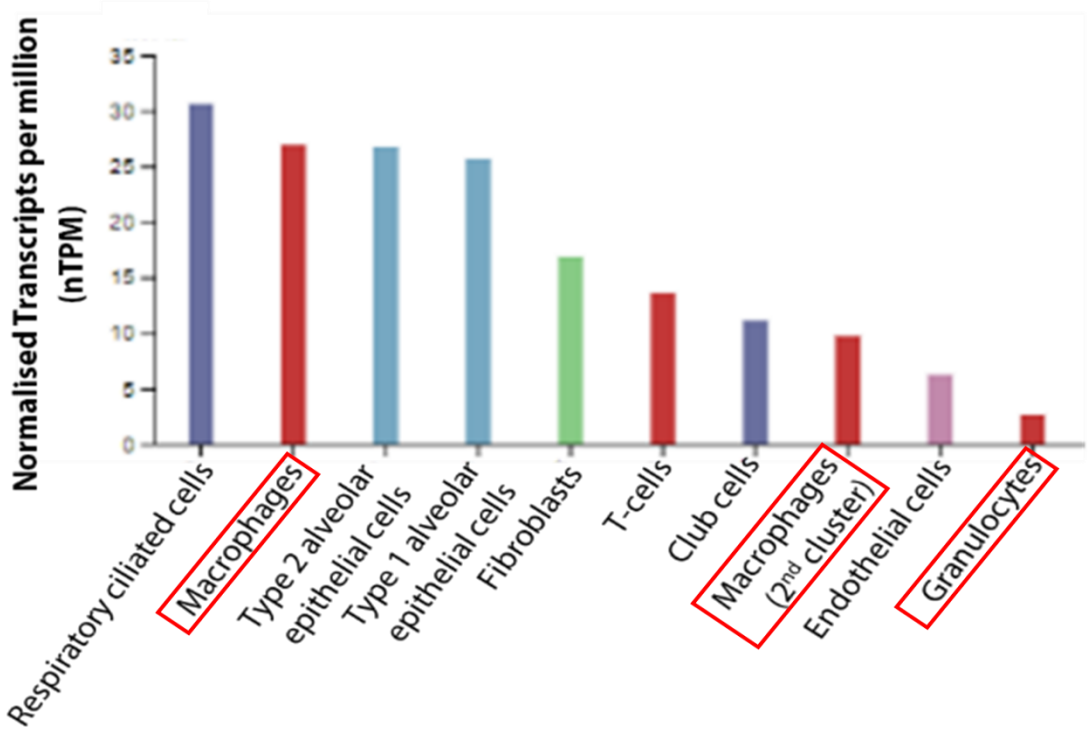

Figure 4.17: Respiratory ciliated cells are the most abundant expressors of the calcium-sensing receptor (CaSR) on the mRNA level. Dataset was obtained from The Human Protein Atlas to demonstrate mRNA expression of the CaSR in a range of lung cells, with those used in this chapter highlighted in red. The lung sc-RNA seq dataset was obtained from Vieira Braga et al (2019). Values obtained from the databases were normalised using Transcript per million (TPM), to estimate gene expression level and gain consensus transcript expression, all TPM values were scaled to a sum of 1 million TPM (pTPM) to compensate for non-coding transcripts, previously removed from the analysis. Finally, normalised TPM (nTPM) was calculated using Trimmed mean of M values (TMM). Figure adapted from The Human Protein Atlas, available at: https://www.proteinatlas.org/ENSG00000036828-CASR/single+cell+type/lung

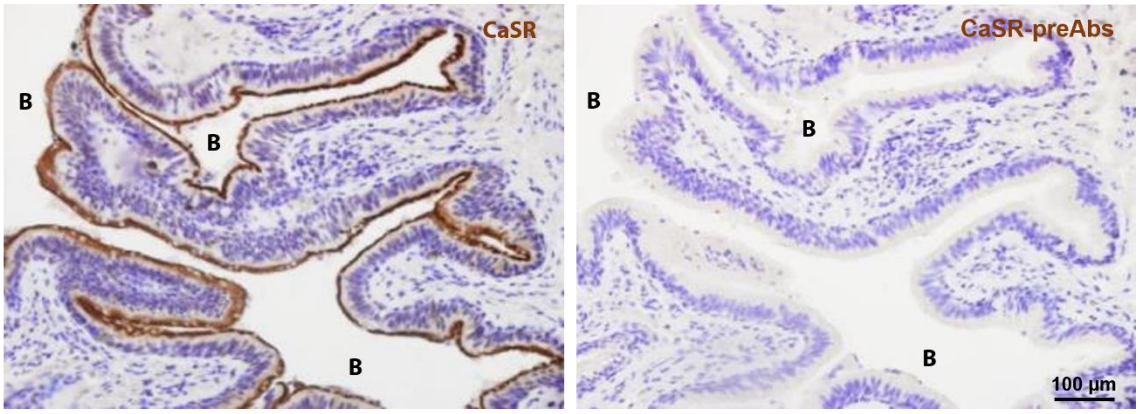

Figure 4.18: The ciliated cells of the bronchial epithelium express the calcium-sensing receptor (CaSR) most abundantly. Images of consecutive paraffin sections of control human lungs (healthy tissue distant from tumour site) which were used to determine CaSR expression. Epithelial cells of peripheral bronchioles appear to express CaSR; especially the apical membrane of ciliated cells, where CaSR immunostaining in the airway epithelium was fully abolished after pre-absorption of the CaSR (CaSR-preAbs) antibody with CaSR peptide. B: lumen of bronchiole, scale bar represents 100 µm. Figure adapted from Wolffs et al (2020).

4.4.2 The CaSR is Expressed at the Protein Level in Airway and Blood-Derived Immune Cells:

In addition, during this Chapter, I sought to establish CaSR expression in the key airways and blood-derived immune cells involved in sensing and responding to inhaled stimuli, such as PM and involved in the pathogenesis and acute exacerbations of lung diseases (Falcon-Rodriguez *et al.* 2016; Larsen *et al.* 2020). During this Chapter I demonstrated novel findings of CaSR expression, at the protein level, in primary AMs, myeloid DCs and ILC2. In addition, I corroborated previous findings of protein level expression of the CaSR in MDDCs, and MDMs (Canton *et al.* 2016a). These findings highlight the potential of the lung CaSR as both a sensor of and responder to inhaled stimuli, such as PM, however, the downstream intracellular signalling mechanisms induced by exposure to PM in these cells, and whether these involve the CaSR, remains unclear.

CaSR expression determined during my studies were corroborated on the mRNA level in human macrophages and granulocytes in data obtained by Vieira Braga et al (2019) and presented on The Human Protein Atlas (Figure 4.19). In addition, CaSR mRNA level expression has also been reported by the Monaco dataset on the Human Protein Atlas (Monaco *et al.* 2019) of blood-derived immune cells from 4 healthy donors such as DCs, monocytes and neutrophils (Figure 4.19), however, it was not corroborated with the Schmiedel et al. (2018) dataset of blood from 91 healthy donors. Furthermore, the scRNA-seq data generated within the Krasnow laboratory from the healthy tissue distant from the tumour site of 3 patients undergoing lung resection and the map of the ageing lung, generated by the Schiller laboratory from 15 ageing mice. To understand whether the CaSR was expressed on the mRNA level in these datasets, for further corroboration of my findings, I interrogated these datasets for *CASR* gene expression; however, both report no *CASR* gene expression in any human or mouse lung cell types. During scRNA-seq analysis, low abundance transcripts such as the CaSR provide a low signal and are not easily detected during scRNA-seq which is thought to be due to different scRNA-seq data normalisation methods between each of the databases studied (Angelidis *et al.* 2019; Travaglini *et al.* 2020; M. J. Zhang *et al.* 2020). Despite the differences in findings of online scRNA-seq databases, I have confirmed protein level expression in each cell type in this chapter, which provides us with the premise to establish *in vitro* models to test the functional expression of the CaSR and uncover the role of the CaSR in mediating direct and indirect PM-induced cellular responses.

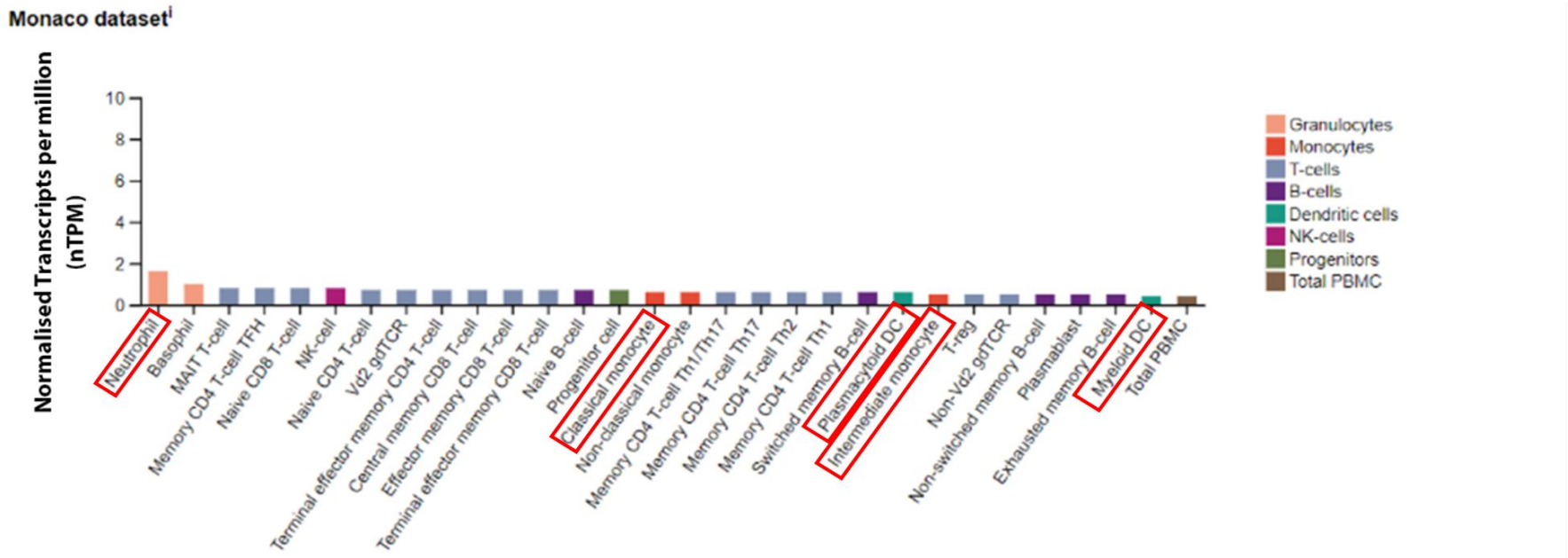

Figure 4.19: Immune cells express the calcium-sensing receptor (CaSR) on the mRNA level. The Monaco dataset demonstrates low-level mRNA expression of the CaSR in a range of blood-derived human immune cell types, with cells used in this study highlighted in red. The immune cell sc-RNA seq dataset was obtained from the Monaco et al (2019) dataset from four healthy donor blood samples. Values obtained from the databases were normalised using Transcript per million (TPM), to estimate gene expression level. To allow for consensus transcript expression, all TPM values were scaled to a sum of 1 million TPM (pTPM)to compensate for non-coding transcripts, previously removed from the analysis. Finally, all samples were then normalised using Trimmed mean of M values (TMM) (nTPM). Figure

4.4.3 Known Functional Roles of the CaSR During Inflammation:

Pro-inflammatory cytokines released from the airway epithelium and inflammatory cells following PM-exposure such as IL-1ß, IL-6 and TNF-α are upregulated in lung diseases such as asthma (Manzano-León *et al.* 2016; Pfeffer, Ho, *et al.* 2018; Kim *et al.* 2019; Almaraz-De-Santiago *et al.* 2021). Importantly, upregulation of these pro-inflammatory cytokines has been shown to drive upregulation of *CASR* gene expression via defined response elements on the *CASR* gene (Canaff and Hendy 2005; Canaff *et al.* 2008; Fetahu *et al.* 2014; Yarova *et al.* 2015). However, whether the CaSR mediates PM-induced upregulation of these cytokines remains unclear.

Previous studies have hinted at a link between the CaSR and activation of inflammatory processes. AMs and DCs sample the inhaled environment and perform functions such as actin-driven extension of plasma membrane ruffles to uptake large portions of extracellular fluid (macropinocytosis) (Canton *et al.* 2016a). Constitutive macropinocytosis has been demonstrated to be CaSR-dependent in MDM and monocyte-derived DC *in vitro* models, highlighting a role for the CaSR in regulating lung homeostasis, however, whether the CaSR drives this key inflammatory process in AMs and DCs is yet to be determined (Canton *et al.* 2016a).

The CaSR has also been demonstrated to drive chemotaxis of human and mouse monocytes, highlighting a role for the CaSR in mediating inflammatory cell infiltration to areas of inflammation, following exposure to extracellular Ca^{2+} and PAMs (Olszak *et al.* 2000). In addition, activation of the NOD-, LRR- and pyrin domain-containing protein 3 (NLRP3) inflammasome is CaSR-mediated in MDM and neutrophils (Lee *et al.* 2012a; Ren *et al.* 2020), an important inflammatory response to inhaled stimuli, such as PM and cigarette smoke (Zheng *et al.* 2018; Wang *et al.* 2019). Furthermore, airway epithelial cells and AMs demonstrate activation of the NLRP3 inflammasome upon PM

exposure, however, whether this is CaSR-mediated is yet to be uncovered (Hirota *et al.* 2012; Tang *et al.* 2019a). Together, these findings propose the CaSR as a critical mediator of key functions of immune cells and as a putative therapeutic target for PM-exacerbated lung diseases.

4.5 Future Directions:

To complement the results obtained in this chapter, it would be important to assess the roles of the CaSR in the cells directly exposed to inhaled PM: airway epithelial cells, AMs, and DCs, and determine functional expression of the CaSR in basal NHBECs, due to disparities between the mRNA and protein level expression. Future experiments in each cell type would be focussed on determining whether the CaSR mediates potential PM-induced cellular responses, such as secretion of pro-inflammatory cytokines, macropinocytosis, chemotaxis, and NLRP3 inflammasome activation, which are associated with the pathogenesis and acute exacerbations of asthma.

4.6 Conclusion:

This chapter reveals that the CaSR is expressed on the protein level in airway epithelial and tissue-resident and blood-derived immune cells, providing premise to further assess the role of the CaSR in some of these cell types. Better understanding of the role of the CaSR in these cells and during inflammation would continue our proposal of NAM as a potential therapeutic for PM-induced cellular responses associated with exacerbations of lung diseases.

CHAPTER 5: ESTABLISHING SUITABLE *IN VITRO* MODELS OF AIRWAY STRUCTURAL AND INFLAMMATORY CELLS TO INVESTIGATE THE POTENTIAL FOR CASR-MEDIATION OF PARTICULATE MATTER-INDUCED RESPONSES IN AIRWAYS CELLS.

5.1 Introduction

PM drives acute exacerbations of the symptoms of lung diseases, such as asthma (asthma attacks) and COPD, which can prove fatal, through activation of inflammatory pathways in already inflamed airways of asthma or COPD patients (WHO 2018; Liu *et al.* 2019). However, the cellular mechanisms behind how PM induces airway cell dysfunction and drives acute exacerbations of lung diseases remains unclear. Better understanding of how PM exposure drives inflammatory responses in key airway cells would allow for development of more effective therapeutics for lung diseases, such as asthma and COPD. Therefore, I decided to investigate the CaSR as a potential underlying mechanism for how PM exposure drives airway cell dysfunction and consider NAM as a potential therapeutic to counteract harmful PM-induced effects in the airways.

Following inhalation, PM primarily deposits on airway structural and immune cells, such as epithelial cells, AMs and DCs, which work synergistically, upon stimulation by inhaled innocuous stimuli, to orchestrate innate and adaptive inflammatory responses through a range of downstream signalling effectors (Hamanaka and Mutlu 2020) (Figure 5.1). The precise mechanisms underpinning PM-induced inflammation in these cell types are poorly understood, however, during my PhD, I have revealed that the airway CaSR could be a common underlying mechanism for PM-induced effects in a range of CaSR-expressing airway cells.

Previous studies have demonstrated that the CaSR mediates inflammatory responses to a range of pro-inflammatory stimuli in animal models of asthma or COPD. Furthermore, CaSR NAMs are effective against inflammation, remodelling and AHR in these models. These observations propose the CaSR as a key coordinator of an inflammatory response through activation of a range of airway structural and immune cells (Yarova *et al.* 2015; Yarova *et al.* 2016). Whether the CaSR underpins aspects of PM-induced responses in airway cells is unclear, therefore in this chapter, I sought to: 1) establish suitable *in vitro* models to assess the role of the CaSR in key, pro-inflammatory processes in airway epithelial cells, AMs and DCs, and; 2) assess the efficacy of NAM against harmful PM-induced effects using fluorescent intracellular Ca^{2+} imaging, RT-qPCR, and flow cytometry analysis of primary and monocyte-derived airway structural and immune cells. Therefore, determining whether the CaSR mediates PM-induced effects in the airways could implicate CaSR NAM as an effective treatment for asthma and COPD patients, who suffer sometimes fatal exacerbations of their symptoms upon exposure to ambient PM.

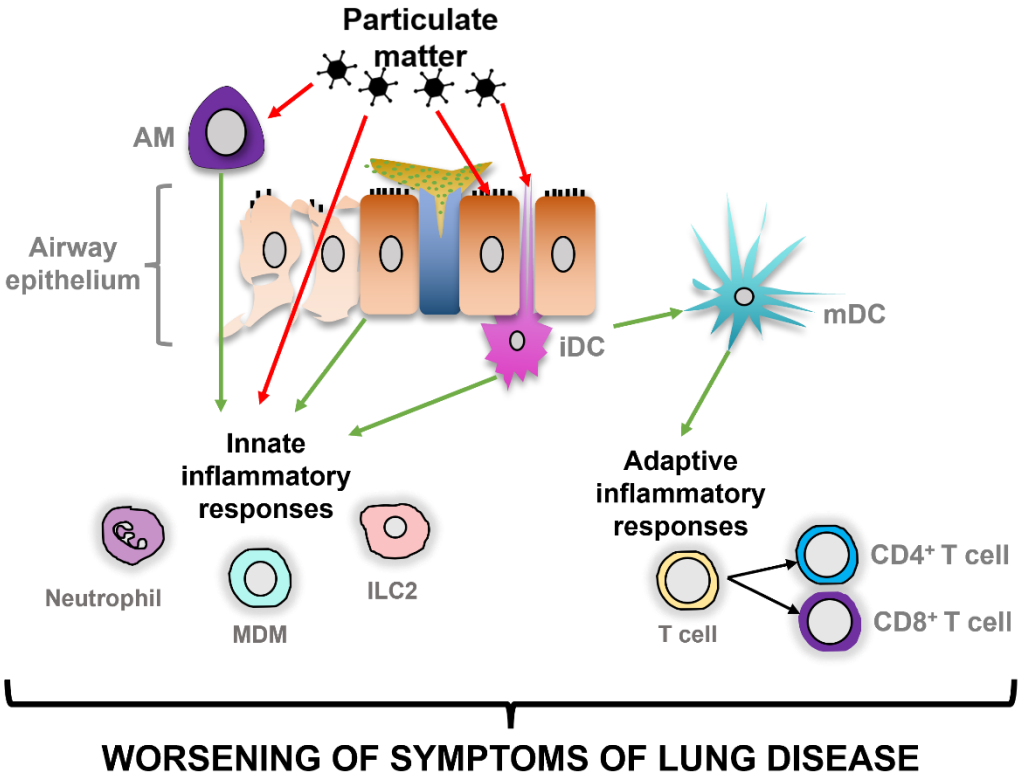

Figure 5.1: Exposure to particulate matter (PM), drives innate and adaptive immune responses, through activation of a range of downstream effector cells. PM, one of the major components of air pollution, is generated from a variety of sources and causes direct (red arrows) effects to alveolar macrophages (AM), airway epithelial cells and immature dendritic cells (iDC). PM can also cross the airway epithelium, in spaces which have been damaged by continued exposure to PM, where the PM-induced effects (green arrows) in each cell type leads to initiation of innate immunity through activation of AM, airway epithelial cells, and iDC and also recruitment of blood- and tissue-derived immune cells such as neutrophils, monocyte-derived macrophages (MDM) and type 2 innate lymphoid cells (ILC2), which contribute to the rapid response to inhaled PM, and it's associated pro-inflammatory effects in the airways. Exposure of iDC to PM results in maturation of DC (mDC) and activation of adaptive immune responses through activation of T (lymphocyte) cells, into $CD4^+$ or $CD8^+$ T cell populations, to enhance the adaptive immune response to inhaled innocuous stimuli, such as PM. Together, these contribute to the worsening of the symptoms of lung diseases, such as asthma and COPD. However, the mechanisms underpinning the plethora of PM-induced effects in the airways, remains poorly understood.

5.2 Methods

5.2.1 Investigating the Effect of Particulate Matter in the Presence and Absence of CaSR NAM on Basal Human Bronchial Epithelial Cell Alarmin mRNA Expression and Intracellular Ca^{2+} Mobilisation:

5.2.1.1 Culture and Seeding for Experimental Analysis:

Ethically consented and cryopreserved NHBECs were purchased from Lonza (cat. #CC-2450) from N=3 donors, with information related to NHBEC characteristics of each donor are provided in Table 4.1.

NHBECs were thawed, cultured, and expanded as in Chapter 4, section 4.2.1.2. Following expansion, NHBECs were counted as described in Chapter 4, section 4.2.1.2.2. For fluorescent intracellular Ca^{2+} imaging, cells were plated at a density of 2,000 cells in 80 µl complete PneumaCult™-Ex Plus medium, in the center of coverslips, in each well of a 24-well plate (see Chapter 3, section 3.2.2). Cells were placed in the incubator at 37 °C and 5% CO_2 and left to adhere for 1 hr, before cells were removed from the incubator and 500 µl complete PneumaCult™-Ex Plus medium was added to each well containing a coverslip of NHBECs. For mRNA expression analysis cells were seeded at a density of 100,000 cells in 2 ml complete PneumaCult™-Ex Plus medium in each well of a 6-well plate. For analysis of ATP levels, as an indicator of cell viability, cells were seeded at a density of 2,000 cells in 100 µl complete PneumaCult™-Ex Plus medium in each well of a 96-well plate. In all cases, cells were placed in the incubator at 37°C and 5% CO_2 overnight for 24 to 48 hrs, depending on expansion rate of donor, and then expanded to around 60% confluency, before proceeding with splitting of cells and induction of experiments.

5.2.2 Intracellular Ca^{2+} Imaging of Basal Human Bronchial Epithelial Cells:

The general methodological principles of intracellular Ca^{2+} imaging is provided within Chapter 2, section 2.1.

5.2.2.1 Preparation of Extracellular and Loading Solutions:

Preparation of 0 Ca^{2+} ECS, loading buffer, fura-2AM, and stocks of orthosteric and allosteric CaSR ligands used during the intracellular calcium imaging experiments were initially carried out as in Chapter 3, section 3.2.3.1. However, due to limited responses to CaSR ligands and visible "pre-activation" (Figure 5.2) of NHBECs after loading as in Chapter 3, section 3.2.3.1, I modified the loading buffer components for later experiments with NHBECs. The modified loading buffer was prepared by first adding 100 ml of RPMI, which contains 0.42 mM Ca^{2+} (Zimmermann *et al.* 2015), to a container with a lid and then supplementing this with 0.1% BSA, as in Chapter 3.2.3.1, before storage at 4 °C.

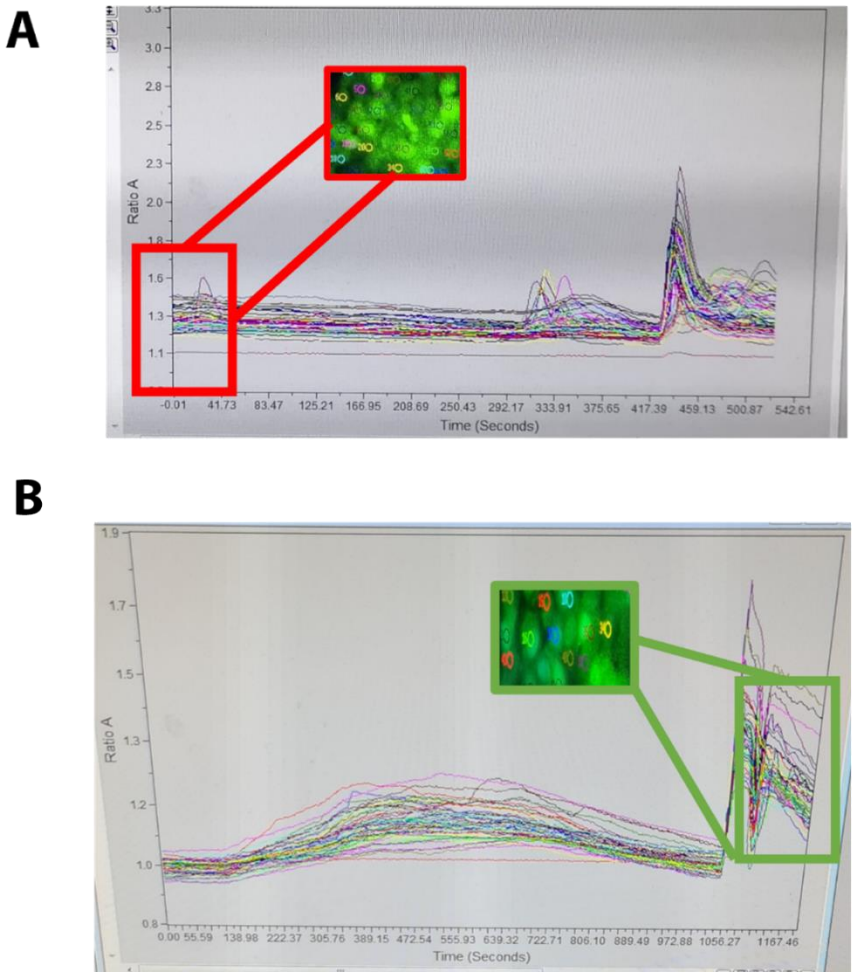

Figure 5.2: Exemplar figure to demonstrate "pre-activation" of normal human bronchial epithelial cells (NHBECs) during initial fluorescent intracellular Ca^{2+} imaging experiments, compared to under the modified loading and exposure protocol. NHBECs were loaded with fura-2AM (3μM) for 1 hr at 37 °C and 5% CO_2 in a loading buffer containing Ca^{2+} (1.2 mM) and bovine serum albumin (BSA, 0.2%) (A) or loading buffer containing RPMI (with a Ca^{2+} concentration of 0.42 mM), to reduce "pre-activation", BSA and sulphobromophtalein (SBP, 100 μM), to reduce Fura-2 extrusion from NHBECs (B). Following loading, NHBECs were pre-incubated with baseline pre-treatment solution containing 2 mM Ca^{2+} solution and 0.01% DMSO (vehicle control, A) or with baseline solution consisting of 0.5 mM Ca^{2+} and Vehicle Control (B), before being placed in a perfusion chamber, mounted on an inverted microscope (Olympus IX71). At baseline, cells should be blue-ish, which represents a low ratio (~1.0 or below), however, as demonstrated, NHBECs had an initial 340:380 ratio of >1 and were bright green (A, red box and inset), which was comparable to the NHBECs activated by ATP (100 μM) in B. Due to the pre-activation of NHBECs, there were no intracellular Ca^{2+} responses to high extracellular Ca^{2+} (A), however, in B, NHBECs had initial 340:380 ratios of ≤1, which allowed for measurements of alterations of intracellular Ca^{2+}, in response to exposure to high extracellular Ca^{2+}.

5.2.2.2 Loading of Basal Human Bronchial Epithelial Cells with Fura-2AM:

During initial experiments, the NHBEC loading solution was prepared and applied as in Chapter 3, section 3.2.3.2. However, as mentioned above, the loading protocol was modified following initial pilot experiments. On the day of experiments, solutions were removed from the fridge and warmed to RT before the pH of all solutions were adjusted to 7.4. During this time, a sulphobromophtalein (SBP) 10 mM stock solution was prepared by weighing 83.8 mg of SBP (Sigma, cat. #S0252) and adding 10 ml of 0 Ca^{2+} containing ECS, mixing well by vortexing and then the solution was aliquoted in volumes of 100 µl to be used during experiments that day or stored at -20 °C for future experimental use. The loading buffer was warmed to 37 °C using a water bath and just before cells were removed from the incubator, 500 µl of warmed loading buffer was added to 4 wells of a 24-well plate. NHBECs were removed from the incubator and 4 coverslips were transferred to the loading buffer-containing wells within the 24-well plate and briefly washed. Loading buffer was removed and then 495 µl fresh loading buffer was added to each well containing coverslips, followed by adding 5 µl SBP (final concentration of 100 µM) and 1.5 µl fura-2AM (final concentration of 3 µM) to each well, before being placed in the incubator at 37 °C and 5% CO_2 for 45 minutes. Following this, cells were removed from the incubator and loading buffer containing SBP and fura-2AM was removed and then replaced with loading buffer with the addition of SBP (minus fura-2AM) and placed back in the incubator at 37 °C and 5% CO_2 for 15 minutes for de-esterification. This loading process using the initial protocol and the modified protocol is demonstrated in Figure 5.3.

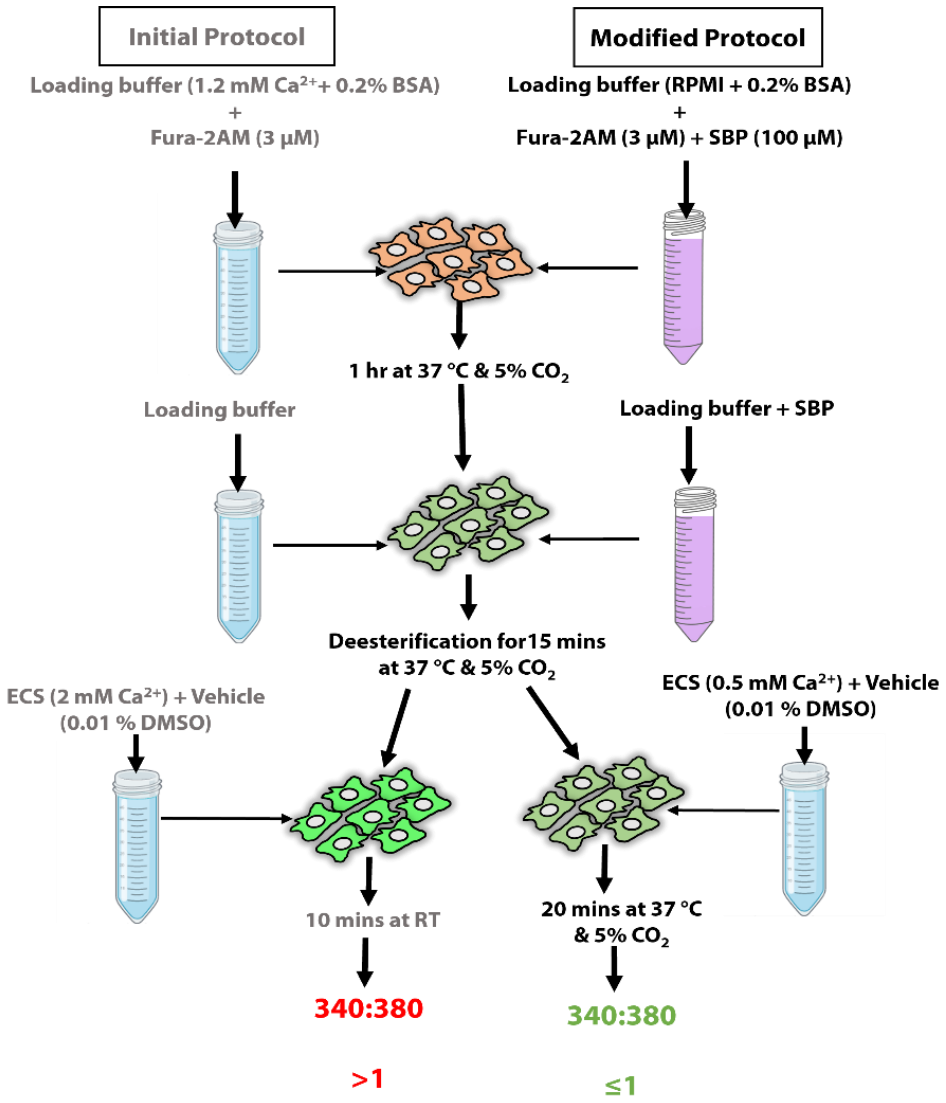

Figure 5.3: Process of initial and modified loading protocols for normal human bronchial epithelial cells (NHBECs) with Fura-2AM, and exposure to pre-treatment conditions, for fluorescent intracellular Ca^{2+} imaging experiments. First, NHBECs were loaded with fura-2AM (Ca^{2+} indicator, 3 µM) in loading buffer consisting of 1.2 mM Ca^{2+} + 0.2% bovine serum albumin (BSA) in the initial protocol and RPMI + 0.2% BSA + sulphobromophtalein (SBP, 100 µM) in the modified protocol. In the initial protocol an extracellular solution (ECS) was prepared with a final concentration of 2 mM Ca^{2+} and Vehicle (0.01% DMSO), for 10 mins at room temperature (RT). In the modified protocol, NHBECs were pre-treated with a baseline solution of reduced Ca^{2+} ECS (0.5 mM) and Vehicle, for 20 mins at 37 °C and 5% CO_2. A ratio between 340 and 380 (340:380) was generated from the values obtained for the emission (at 510 nm), at both excitation wavelengths. NHBECs appeared to be "pre-activated" following the initial protocol of loading and exposure to the pre-treatment ECS, which was evidenced by bright green NHBECs under the microscope and a 340:380 ratio of >1, calculated using the MetaMorph™ computer software. In contrast, the modified protocol resulted in duller NHBECs under the microscope and 340:380 ratios of ≤1, allowing for measurements of discreet alterations to intracellular Ca^{2+} levels.

5.2.2.3 Preparation of Baseline Treatment Solutions:

The "0 Ca^{2+}"-containing solution was used to prepare a 0.5 mM Ca^{2+} ECS (baseline), which was used on that day or stored at 4 °C for up to one week. Vehicle Control (VC)- or NPS3143 (NAM)- containing baseline ECS were prepared by serial dilution of 100% DMSO to final concentrations of 0.01%, 0.03% and 0.1% DMSO in baseline ECS (VC) and by serial dilution of 10 mM NPS2143 stock to a final concentration of 1, 3 or 10 µM (NAM) in baseline ECS. Exposure of NHBECs to baseline solutions are also outlined in Figure 5.3, representing the difference between the initial and modified protocols for loading and exposure to baseline pre-treatment conditions.

5.2.2.4 Preparation of Treatment Solutions for use During Initial Fluorescent Intracellular Ca^{2+} Imaging Experiments:

For initial experiments using the same protocol as used in Chapter 3, a 100 mM spermine stock solution was prepared (Sigma, cat. #S3256), before vortexing and aliquoting into 1 ml to be used on the day or stored at -20 °C for future use. This was used to prepare spermine to a final concentration of 1 mM in 0.5 mM Ca^{2+} ECS. Finally, a 100 µg/ml PM solution was prepared as in Chapter 3, section 3.2.3.7, in baseline ECS.

5.2.2.5 Pharmacochaperoning the CaSR:

Due to limited responses of NHBECs to CaSR ligands during the initial fluorescent intracellular Ca^{2+} imaging experiments, I attempted to increase expression of the CaSR at the plasma membrane of NHBECs, using CaSR ligands spermine and R-568 (CaSR PAM), in an established process termed pharmacochaperoning. Exposing cells to CaSR ligands, drives agonist driven insertional signalling (ADIS) to increase CaSR expression at the plasma membrane, and to provide a tool to enhance CaSR-mediated intracellular Ca^{2+} mobilisation, in response to CaSR ligands (Brennan *et al.* 2016).

To pharmacochaperone the CaSR to the plasma membrane in NHBECs, I performed overnight exposures of NHBECs to 100 μM spermine or 100 nM R-568 (CaSR PAM) in PneumaCult™-Ex Plus medium. Aliquots of 1 ml of each were stored into Eppendorf tubes at 4 °C short-term and -20 °C longer-term. A serial dilution of 10 mM R-568 was then made on the day of the experiment by adding 10 μl R-568 to 9.9 ml complete PneumaCult™-Ex Plus medium, resulting in a 100 μM R-568 solution. Unloaded NHBECs on coverslips were removed from the incubator and medium was removed. For the cells exposed to spermine, 495 μl warmed complete PneumaCult™-Ex Plus medium was added to each well and 5 μl of 10 mM spermine was added, resulting in a final concentration of 100 μM. For the cells exposed to R-568, medium was removed from wells and 499.5 μl warmed complete PneumaCult™-Ex Plus medium was added, before making up to 500 μl with 0.5 μl of 10 mM R-568, resulting in a final concentration of 100 nM.

5.2.2.6 Preparation of Treatment Solutions for use During Fluorescent Intracellular Ca^{2+} Imaging Experiments - Modified Protocol:

For the experiments using the modified protocol, a 10 mM Ca^{2+} treatment was first prepared by removing 148.5 ml of 0 Ca^{2+} containing ECS and adding to a bottle with a lid, before 1.5 ml of $CaCl_2$ was added to this. In addition, 50 ml was removed from this and added to a separate bottle with lid and then 50 ml 0 Ca^{2+} containing ECS was added, resulting in a 5 mM Ca^{2+} containing solution.

During the final 15 minutes of incubation at 37 °C and 5% CO_2 with loading buffer, where NHBECs underwent deesterification of Fura-2, the VC- or NAM-containing baseline solutions were transferred to the relevant tubes in the rapid perfusion system and then treatment solutions containing spermine, PM, 5 and 10 mM Ca^{2+} ± VC (0.01%, 0.03% and 0.1%) or NAM (1, 3 or 10 μM). Following de-esterification, pre-treatment of NHBECs was performed by first

adding 2 ml of VC- or NAM-containing baseline solution was added to a 10 mm cell culture dish (Thermofisher, cat. #150318) and then NHBECs were removed from the incubator. One coverslip was removed from the 24-well plate and placed in the VC/NAM baseline solution and placed back in the incubator at 37 °C and 5% CO_2 for 20 mins. During this time, the rapid perfusion system was then checked for correct valve functioning and consistent flow rates of solutions, before proceeding with fluorescent intracellular Ca^{2+} imaging experiments, utilising the MetaMorph® Microscopy Automation & Image Analysis Software (Cairn Research), as in Chapter 3.2.3.1.

5.2.3 mRNA Expression Analysis of Genes Associated with Particulate Matter Exposure and the Pathogenesis of Lung Diseases:

The general principles of mRNA expression analysis by RT-qPCR are provided within Chapter 2, section 2.3.

5.2.3.1 Primer Design and Validation:

To gain expression profiles for key genes of interest, thymic stromal lymphopoietin *(TSLP)* and interleukin-33 *(IL-33)*, and housekeeping gene Glyceraldehyde-3-Phosphate Dehydrogenase *(GAPDH)*, primer sequences were selected and designed using the coding region of the genomic sequences for each gene, obtained from GenBank (National Center for Biotechnology Information, NCBI). Intron-spanning primers for genes of interest were designed with use of PrimerBLAST software available online (NCBI) and the selected primers were subjected to BLAST (NCBI) searches to eradicate the possibility for potential homology to sequences other than the selected target. Primer sequences and associated information is provided in Table 5.1. Assessment of *CASR* mRNA expression was carried out at the Medical University of Vienna, and details associated to this are provided in section 5.2.3.10.

Table 5.1: Primer pairs designed for use in quantitative real-time polymerase chain reaction (qPCR) experiments, to assess mRNA expression of key inflammatory cytokines thymic stromal lymphopoietin (TSLP) and interleukin (IL)-33. Primer pairs were designed with the aid of PrimerBLAST (NCBI), using the coding sequence of the genes *IL-33*, *TSLP*, and *GAPDH*. Sequences, melting temperature (Tm), molecular weight (MW), guanine and cytosine (GC) content and PCR expected molecular weight of products are demonstrated.

Oligo name	Sequence (5′ -> 3′)	Tm (°C)	MW (g/mol)	GC Content (%)	PCR product size (bp)
IL-33 Forward	ATCAGGTGACGGTGTTGATGG	59.8	6557.3	52.4	128
IL-33 Reverse	GGTCTGGCAGTGGTTTTTCAC	59.8	6459.2	52.4	
TSLP Forward	TATCTGGTGCCCAGGCTATTC	59.8	6388.1	52.4	128
TSLP Reverse	TTGTGACACTTGTTCCAGACA	59.5	6396.2	42.9	
GAPDH Forward	GGTCACCAGGGCTGCTTTTA	60.25	6124.0	55.0	243
GAPDH Reverse	GACTCCACGACGTACTCAGC	60.18	6046.9	60.0	

5.2.3.2 Primer Validation Step 2 - PCR Amplification of Genes of Interest:

To assess whether primers I designed were specific to the genes of interest (*TSLP and IL-33,*) and the reference gene (*GAPDH*), I carried out amplification of these genes, using PCR, to generate a product of specific size to the gene of interest or housekeeping gene. *GAPDH* was used as a reference gene during my experiments as this has been shown to be one of the most stable reference genes available for lung research (Liu *et al.* 2005; Ali *et al.* 2015). However, previous research focused on using lung cancer cells during these experiments, which may not fully recapitulate the distribution of *GAPDH* expression in healthy lung tissue. Based on data available on the Human Protein Atlas, protein expression of GAPDH is stable between distinct lung tissues, however, does alter slightly between distinct lung tissues at the RNA level. Additionally, more recent research has indicated that *GAPDH* may not be the most suitable

reference gene for lung research due to differences between expression levels of *GAPDH* in a mouse model of acute lung injury (Giri and Sundar 2022). However, there are clear anatomical differences between mouse and human lungs and thus far no consensus has been reached on the most suitable reference gene for lung research.

First, human total lung RNA (ThermoFisher Scientific, cat. #AM7968) was retrotranscribed into cDNA (1000 ng) using the SuperScript™ VILO Retro Transcriptase Kit (ThermoFisher Scientific, cat. #11754050). First, a master mix of the 5X VILO reaction mix (containing random primers, $MgCl_2$, and dNTPs),10x SuperScript™ Enzyme and nuclease free H_2O was prepared. 19 µl of the master mix was added to an Eppendorf tube and 1 µl of total human lung RNA was added to each tube before mixing gently by pipetting and incubating at RT for 10 minutes. Following this, samples were incubated at 42 °C for 1 hour and reactions were terminated by incubating at 85 °C for 5 minutes. This cDNA was stored at -20 °C and was used as a template for validating all primer pairs designed for key genes of interest.

Then, two 0.2 ml PCR tubes (Thermofisher, cat. #AB0620) were allocated to each primer set and then a master mix of 12.5 µl Standard *Taq* Reaction Buffer (New England BioLabs, cat. #M0273L), 2.5 µl of 10 mM dNTPs (Thermofisher, cat. #R0191), 2.5 µl 10 µM forward primer and 2.5 µl 10 µM reverse primer, 0.625 µl *Taq* DNA polymerase and 101.88 µl Nuclease Free H_2O (Qiagen, cat. #129114) was prepared per primer set on ice. 49 µl of the master mix for each primer pair was transferred into each 0.2 ml PCR tube before 1 µl of 1000 ng/µl cDNA obtained from total lung RNA (Invitrogen, cat. #AM7968) was added to one of the tubes and 1 µl nuclease free H_2O was added to the other tube, to serve as a no template control (NTC). Tubes were briefly spun by spin centrifugation to collect the contents at the bottom of the tubes, then the tubes were transferred to the PCR machine. The thermocycling conditions were

as follows: initial denaturation at 95 °C for 30 seconds, then 40 cycles of 95 °C for 30 seconds, 60 °C for 1 minute and 72 ° C for 1 minute, then the final extension was performed at 72 °C for 10 minutes, before products were held at 4 °C until subsequent gel electrophoresis.

5.2.3.3 Primer Validation Step 3 – Gel Electrophoresis for Visualisation of PCR Products:

First a 50 X Tris-Acetate EDTA (TAE) buffer was prepared by weighing 242 g of Tris Base (Sigma, cat. #TRIS-RO) and dissolving in 700 ml MilliQ H_2O by adding a magnetic stir bar and mixing using a magnetic lab stirrer. Once dissolved, 100 ml of 0.5 M ethylenediaminetetraacetic acid (EDTA, Sigma, cat. #03690) and 57.1 ml glacial acetic acid (Alfa Aesar, cat. #39745) was added and the solution was mixed again using the magnetic lab stirrer. The pH of the solution was adjusted to 8.4 before the volume was made up to 1 L with MilliQ H_2O and the final solution was stored at RT. An aliquot of this 50 X buffer was taken to make a 1 X working buffer of TAE for use in gel electrophoresis. For validation of PCR products using designed primers, a 2% agarose gel was prepared by weighing 2 g molecular grade agarose (Invitrogen, cat. #16500500) and placing into a 250 ml conical flask. 100 ml of 1 X TAE buffer was added to this and mixed briefly by swirling the flask. The flask was placed in the microwave for 2 minutes to dissolve and was carefully observed during the dissolving process to avoid boiling the solution. Once dissolved, the solution was cooled to less than 50°C and 5 µl SafeView Nucleic Acid Stain (NBS Biologicals, cat. #NBS-SV1) was added and mixed by swirling the flask. The solution was poured into a gel casting chamber and left at RT to set for ~ 20 minutes. Once set, the gel was placed into the gel electrophoresis chamber and 1 X TAE buffer was added to the chamber to submerge the gel. To prepare the samples for loading in the gel, 10 µl of the PCR products were transferred into a new 0.2 ml PCR tube and 3.3 µl of 6 X purple loading dye (Promega, cat. #G190A) was added and mixed by pipetting up and down. The entire contents of each tube

were loaded into the wells of the gel and 5 µl molecular weight ladder (PCRBIO Ladder 3, PCR biosystems, cat. #PB40.13-05) was added to the first and last wells of the gel, to aid in assessing molecular weights of PCR products. Following 60 minutes of gel electrophoresis at 80-100 V, PCR products were visualised using a Gel Doc XR+ machine (Biorad), to determine product sizes and therefore assess specificity of primers designed (Figure 5.4).

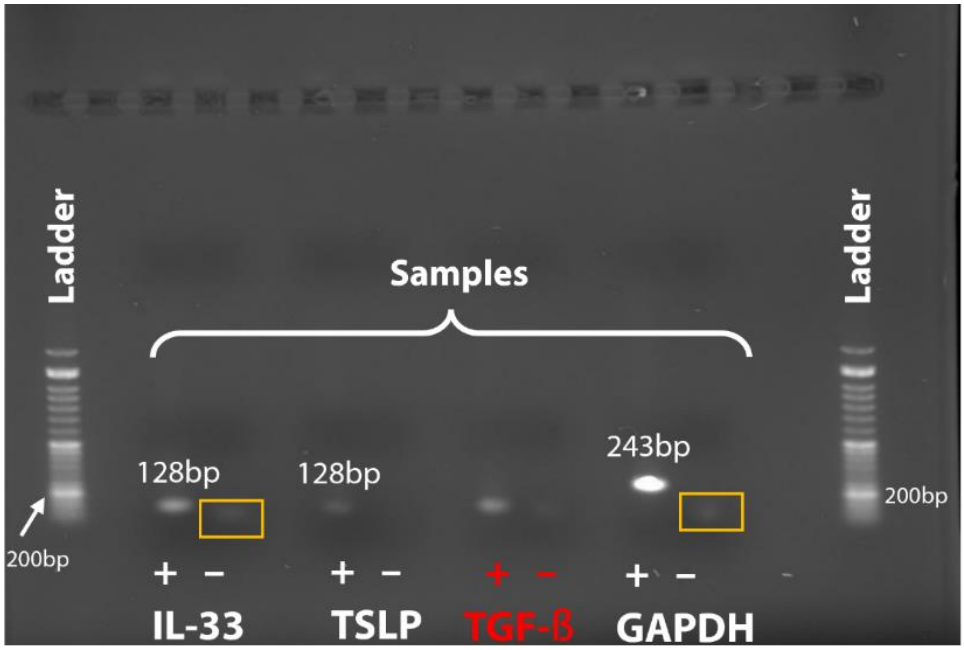

Figure 5.4: Exemplar gel of interleukin-33 (*IL-33*), thymic stromal lymphopoietin (*TSLP*), transforming growth factor beta (*TGF-ß)* and *GAPDH* PCR products. PCR products were generated following PCR reaction using cDNA (1000 ng) which was retrotranscribed from total lung RNA (ThermoFisher Scientific, cat. #AM7968) and primers which were designed to target *IL-33*, *TSLP, TGF-ß* (not used in studies, shown in red) and *GAPDH*. Primer sequences for IL-33 were 5'-ATCAGGTGACGGTGTTGATGG-3' (forward) and 5'-GGTCTGGCAGTGGTTTTTCAC-3' (reverse), for TSLP 5'- TATCTGGTGCCCAGGCTATTC-3' (forward) and 5'-TTGTGACACTTGTTCCAGACA-3' (reverse) and for GAPDH 5'-GGTCACCAGGGCTGCTTTTA-3' (forward) and 5'- GACTCCACGACGTACTCAGC-3' (reverse). PCR was carried out using the following thermocycling conditions: The thermocycling conditions were as follows: initial denaturation at 95 °C for 30 seconds, then 40 cycles of 95 °C for 30 seconds, 60 °C for 1 minute and 72 ° C for 1 minute, then the final extension was performed at 72 °C for 10 minutes, before products were held at 4 °C until subsequent gel electrophoresis. Product were run on a 2% agarose gel with addition of loading dye (Promega, cat. #G190A) and following 60 minutes of gel electrophoresis at 80 V, PCR products were visualised using a Gel Doc XR+ machine (Biorad) and compared to a molecular weight ladder (PCRBIO Ladder 3, PCR biosystems, cat. #PB40.13-05), where the lowest bright band of the ladder represents 200 bp (labelled within figure). The PCR generated products of 128 bp, 128 bp and 243 bp, for the IL-33, TSLP and GAPDH primers, respectively and a no-template control was also used (nuclease free H_2O, rather than cDNA) for each primer pair, to determine whether contamination was present and to determine level of primer dimer formation, where primer dimers are highlighted in yellow boxes within the figure.

5.2.3.4 Primer Validation Step 4 – PCR Product Clean Up and Preparation for Sequencing:

Once PCR products of the correct size were produced for each primer pair, the PCR products were purified using a PCR clean up kit (Biobasic, cat. #BT5100). First, a master mix of the stock components in a 1.5 ml Eppendorf tube was made for 4 samples, which consisted of: 1.04 µl MIXS, 0.52 µl MIXE, 2 µl 10X Reaction Buffer and Nuclease Free H_2O and was mixed gently by pipetting. Meanwhile, 6 µl of each PCR product was added to separate Eppendorf tubes before 5 µl of the master mix was added and the contents were mixed briefly by spin centrifugation. Following this, samples were incubated at 37 °C for 45 minutes and the reaction was terminated by incubation at 85 °C for 15 minutes. Samples were prepared for sequencing by transferring 8 µl purified PCR products to a separate 1.5 ml Eppendorf tube. Then 4 µl of 10 µM forward primer was added, before applying the sequencing label and sending to Eurofins Genomics for sequencing. All primers returned sequencing data were consistent with the gene of interest and validated by BLAST analysis of the sequenced products.

5.2.3.5 Preparation of Pre-treatment and Treatment Conditions:

As in Chapter 3, section 3.2.3.9, pre-treatment conditions were prepared following the same protocol, however, these were prepared in complete PneumaCult™-Ex Plus medium. First, tissue culture (TC) grade 100% DMSO and 10 mM NPS2143 (NAM) were thawed from 4 °C and then serially diluted to 10% DMSO or 1 mM CaSR NAM in sterile H_2O and then to 1% DMSO or 100 µM CaSR NAM in complete PneumaCult™-Ex Plus medium which was used to prepare appropriate volumes of to 0.01% DMSO (VC) or 1 µM NAM for the pre-treatment exposure period.

For the exposure treatment, PM was thawed from -80 °C and prepared as in Chapter 3, section 3.2.3.7 before being serially diluted to 100 or 200 µg/ml in

complete PneumaCult™-Ex Plus medium with the addition of VC or NAM, using stock prepared as described above, to final concentrations of 0.02 and 0.2% VC and 2 and 20 mM NAM.

5.2.3.6 Exposure of Basal Human Bronchial Epithelial Cells to Pre-treatment and Treatment Conditions:

After preparation of the pre-treatments of VC and NAM, 6-well plates of NHBECs were removed from the incubator and existing medium was removed from all wells. NHBECs were pre-treated with 1 ml of VC or NAM in complete PneumaCult™-Ex Plus medium, for 1 hour, in the incubator at 37 °C and 5% CO_2.

Following pre-treatment, NHBECs were removed from the incubator and each treatment was mixed thoroughly by pipetting before adding 1 ml of each treatment group to the appropriate wells, resulting in final concentrations of 0.01 and 0.1% VC, 1 and 10 µM NAM, 50 and 100 µg/ml PM + 0.01 and 0.1% VC, and 50 and 100 µg/ml PM + 1 and 10 µM NAM. Each plate was then placed in the incubator at 37 °C and 5% CO_2 for 4 or 24 hours, depending on the experimental endpoint.

5.2.3.7 RNA Extraction from Basal Human Bronchial Epithelial Cells:

Total RNA from NHBECs was extracted using the TRIzol method according to the manufacturer's instructions. Following 4 or 24-hr exposure to treatment conditions, medium was removed from wells and stored in labelled 1.5 ml Eppendorf tubes at -80 °C for downstream analysis of secreted cytokines or metabolites. Then, cells were washed once with warmed 1X PBS to remove cell debris before cells were harvested by the addition of 1ml of TRIzol Reagent (ThermoFisher Scientific, cat. #15596026) by pipetting up and down and washing the well to increase yield. NHBECs in TRIzol were collected and

transferred into labelled 1.5 ml Eppendorf tubes and placed on ice, then stored at -80 °C until RNA extraction.

To proceed with the RNA extraction, NHBECs were thawed from -80 °C on ice and then 200 µl of molecular grade chloroform (Alfa Aesar, cat. #J67241.AP) was added to each tube and mixed by inverting and reverting the tubes for a total period of 15 seconds. Tubes were then centrifuged at 11400 rpm (13,512 rcf) for 15 minutes at 4 °C. During this time, fresh Eppendorf tubes were labelled and prepared by adding 1 µl of molecular grade glycogen (Thermofisher, cat. #R0561) to the bottom of the tube. Following this, the visible transparent phase, containing RNA, was collected, and transferred to the labelled Eppendorf tube containing glycogen, taking care to not disturb the opaque layer containing DNA, to avoid DNA contamination of RNA. To this Eppendorf tube, 500 µl of molecular grade 2-Propanol (Sigma-Aldrich, cat. #I9516) was added. The tubes were mixed again by inverting and reverting as above and then stored at RT for 10 minutes. Following this, tubes were centrifuged again at 11,400 rpm (13,512 rcf) for 10 minutes at 4 °C. Following centrifugation, the supernatant was removed, and an RNA pellet was visible at the base of the tube. The pellet was washed by adding 1 ml of 75% freezing cold 100% ethanol (prepared with molecular grade ethanol, Merck, cat. #1.08543.0250 and stored at -20 °C before use). The pellet was washed by inverting and gentle flicking of the tube to lift the pellet from the bottom of the tube and ensure the pellet was washed thoroughly. Following this, tubes were centrifuged for 5 minutes at 9,000 rpm (8422 rcf) at 4 °C. The ethanol wash step was repeated, and all liquid was aspirated from the tube before the tube was laid on its side with the lid open to air-dry the pellet. Just before the pellet became invisible, 25 µl of nuclease free H_2O was added to the RNA pellet and mixed by gently pipetting up and down. To remove contaminating DNA, the TURBO DNA-*free* kit (Invitrogen, cat. #AM1907) was used. 0.5 µl DNAse

provided in the kit was added to each RNA sample, mixed by pipetting up and down, and stored at RT for 10 minutes, then incubated at 37 °C for 30 minutes. Following this, inactivation reagent supplied in the kit was vortexed well before adding 2.5 µl to each sample. Then, samples were stored on ice with gentle mixing by flicking the tube every minute for a total of 5 minutes. Samples were centrifuged at 10,000 rpm (10397 rcf) and the supernatant (containing RNA) was transferred to a new labelled Eppendorf tube, before storage on ice to immediately carry out RNA quality analysis or at - 80°C longer-term.

5.2.3.8 RNA Purity and Integrity analysis:

The concentration and purity (260/280 nm Absorbance ratio) of total RNA was carried out using a Nanodrop 1000 spectrophotometer (ThermoFisher Scientific) prior to downstream analysis. All samples returned an A260/A280 of 1.8-2.1 confirming RNA of sufficient quality to proceed with cDNA synthesis and subsequent real-time quantitative PCR (RT-qPCR). RNA integrity was analysed in all samples using the 2200 TapeStation system (Aligent). Reagents from the Broad Range (BR) RNA ScreenTape Assay were removed from 4 °C and -20 °C to equilibrate to RT for 30 minutes. Following this, 5 µl RNA sample buffer was added to each tube in Optical tube strips (Agilent, cat. #401428) on ice before adding 1 µl RNA ladder to the first tube and then 1 µl extracted RNA from each well of the treatment groups was added to the other tubes, and the order was recorded. The Optical caps (Agilent, cat. #401425) were then applied to the tubes and spun down by brief spin centrifugation. Tubes were vortexed using the MS 3 IKA vortexer (IKA, cat. #0003617000) at 2000 rpm for 1 minute. Tubes were spun down again by brief spin centrifugation to position the sample at the bottom of the tube. Sample and ladder denaturation was performed by placing the tubes in a heat block at 72 °C for 3 minutes before being placed on ice for 2 minutes. The tubes were then inserted into the Aligent 2200 Tapestation, caps removed and then the BR RNA screen tape was

placed into the machine. The samples were run, and RNA integrity number (RIN^e) was determined, with all samples returning a RIN^e of >9.0, confirming sufficient RNA integrity to proceed with cDNA synthesis and RT-qPCR. An example of the data obtained from the Tapestation, including the RIN^e values is supplied in Figure 5.5.

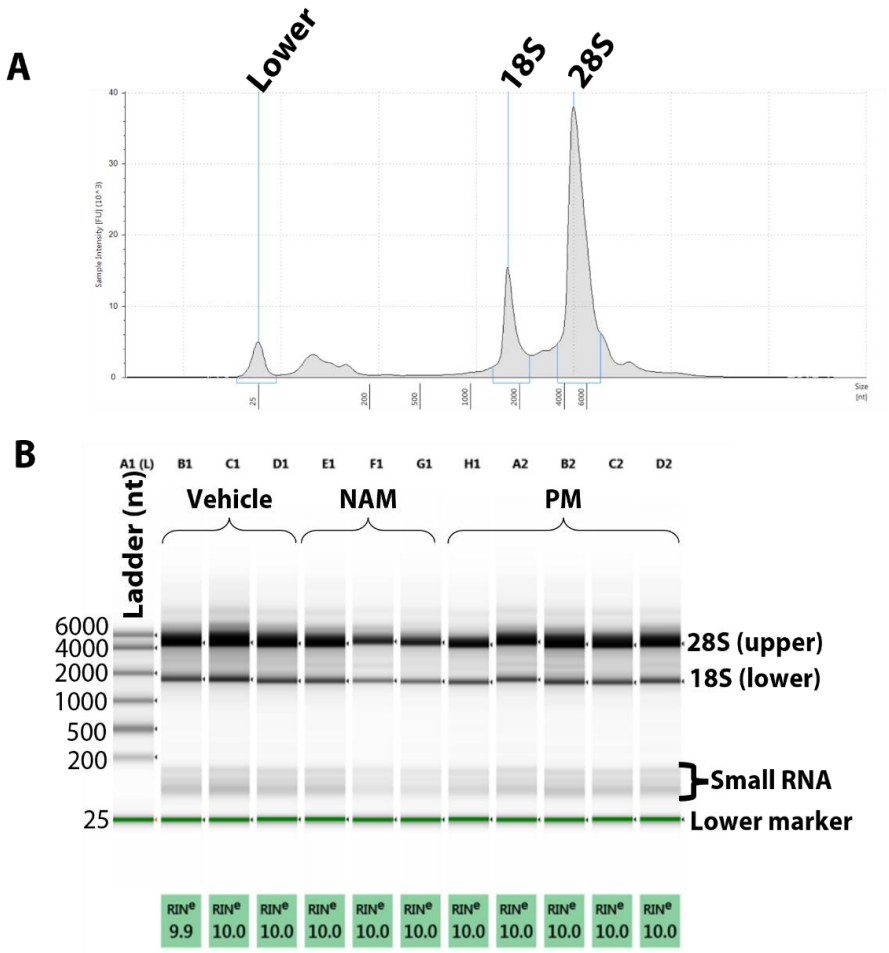

Figure 5.5: Representative trace and gel image of RNA integrity for generation of RNA integrity scores (RIN^e) obtained from RNA extractions from submerged normal human bronchial epithelial cells (NHBECs) exposed to Vehicle, a negative allosteric modulator at the calcium-sensing receptor (NAM) and particulate matter (PM). Representative trace of RNA integrity of NHBEC RNA extracted using the TRIzol® method (A). A represents a trace of an RNA sample, analysed by the Agilent Tapestation 2200, which provides a peak for 18S (1715 nucleotides, nt) and 28S (4680 nt) ribosomal RNA (rRNA), which correspond to the lower and upper bands depicted on the gel image, respectively (B). Within the gel (B), the RNA ladder is represented in lane A1 and then lanes B1-D1, E1-G1, and H1-D2 represent RNA samples extracted from Vehicle (0.01% DMSO), NAM (1 μM NPS2143) and PM (100 μg/ml) exposed NHBECs, respectively. The bands present at between 25 and 200 nt contain smaller RNA species, and the band at 25 nt represents the lower marker. RNA is considered of high quality when the 28S peak is ≥ twice the size of the 18S peak, as clearly demonstrated in A which corresponds to the intensity of the bands demonstrated in B. RIN^e scores (shown in green boxes in B) demonstrate the integrity of RNA samples, which is assessed on a scale of 1-10 and calculated using an algorithm which uses factors including total RNA ratio between 28S and 18S peaks. A score of 10 represents high quality RNA, with very little degradation, validating the RNA extraction method used during these experiments.

5.2.3.9 cDNA synthesis:

Purified RNA was retro-transcribed into cDNA using the SuperScript™ VILO Retro Transcriptase Kit (ThermoFisher Scientific, cat. #11754050), as in section 5.2.3.2 of this Chapter, however, was scaled up to account for number of samples. Following cDNA synthesis, samples were diluted by addition of 400 µl nuclease free H_2O, for subsequent use in RT-qPCR.

5.2.3.10 RT-qPCR:

First, 100 µM forward and reverse primer stocks validated to target *TSLP*, *IL-33* and *GAPDH* were thawed from -20 °C. During this process, 1.5 ml Eppendorf tubes were prepared per primer pair and then 975 µl nuclease free H_2O was added. Primer stocks were vortexed and 12.5 µl of forward and reverse primer were transferred to the tube containing nuclease free H_2O, resulting in a 2.5 µM primer stock mix which was used on the day or stored at -20 °C.

On the days of qPCR experiments, primers, cDNA, and qPCRBIO SyGreen Mix Lo-ROX (PCR Biosystems, cat. #PB20.11-05) were thawed from -20 °C and stored on ice. A master mix of 5 µl qPCRBIO SyGreen Mix Lo-ROX and 2.5 µl of 2.5 µM primer mix was prepared per gene, for a maximum of 6 samples, each run in triplicate. Then, 2 lots of 0.1 ml tubes (Qiagen, cat. #981103) were placed in a loading block for analysis of *TSLP* or *IL-33* and *GAPDH*, in triplicate per sample, then 7.5 µl of this master mix was added to each tube, resulting in a final primer concentration of 300 nM. 2.5 µl of diluted cDNA samples was added to one set of triplicate tubes and 2.5 µl nuclease free H_2O was added to one tube per gene of interest as a no-template (NT) control.

RT-qPCR was performed by placing tubes into the RotorGene 6000 or Q (Qiagen) machines. The thermal cycling profile included: uracil DNA glycosylase (UDG) and dUTP pre-incubation stage at 95 °C for 2 minutes, to remove DNA contaminants, then denaturation for 40-45 cycles at 95 °C for 5

seconds each, followed by annealing and extension at 60 °C for 30 seconds. A dissociation cycle verified the amplification of one product by ramping temperature from 50 °C to 95 °C (1 degree every 5 seconds), to generate melt curves. In all cases, the expression level (copy-number) of the transcripts were compared to the reference gene *GAPDH* mRNA expression using the "ΔΔCT method" as described in Chapter 2, section 2.3.2.

RT-qPCR was also performed on N=1 NHBEC for analysis of *CASR* mRNA expression due to disparity between protein level expression determined during Chapter 4 of my thesis and datasets of scRNA-seq data available online via the Human Protein Atlas. Validation of the mRNA expression of the CaSR in these cells was important during the validation of this *in vitro* model for my studies. Established and well published primers for assessing *CASR* mRNA expression were used, along with the reference gene *RPLP0* in RT-qPCR experiments conducted by Dr Martin Schepelmann at the Medical University of Vienna (Iamartino *et al*. 2020). Following expansion and seeding into 6-well plates, supernatant was collected and EXTRAzol (Blirt, cat #EM30-200), a reagent similar to TRIzol™, was added each well of NHBECs for cell collection. RNA was isolated as in section 5.3.2.7 of this Chapter before being retro transcribed to cDNA using the High Capacity RT kit (Applied Biosystems, cat. #10704217) and qPCR was carried out using Power SYBR green Master Mix (Applied Biosystems, cat. #4368577) and established primers for *CASR:* Forward 5'-GCCAAGAAGGGAGAAAAGAC-3' and reverse 5'-CACACTCAAAGCAGCAGG-3' and reference gene *RPLP0:* Forward 5'-TGGTCATCCAGCAGGTGTTCGA-3' and reverse 5'-GCAGCAGCTGGCACCTTATTG-3' with the same cycling profile as described above during my experiments, however, was carried out on the QuantStudio 12K Flex RT PCR system (ThermoFisher) (Ianmartino et al 2020).

These experiments revealed that there was specific amplification of a single product in the reference *RPLP0* samples, as expected, which was verified by no amplification in the no template negative control sample shown in blue during the melt curve analysis (Figure 5.6 A). However, very low mRNA expression of *CASR* was demonstrated by very poor amplification of *CASR* which was represented by multiple, unspecific products forming upon assessment of melt curves (Figure 5.6 B). To verify the PCR conditions were suitable, I demonstrated that there was no amplification in the no template negative control sample shown in blue and the calibrator RT-qPCR melt curve is provided within the inset of Figure 5.5 B. This calibrator experiment used cDNA obtained from total human RNA in the laboratory of Dr Martin Schepelmann and produced a melt curve which represented the amplification of one specific product. This calibrator experiment was also important to ensure that the PCR conditions used were suitable to detect *CASR* expression at the mRNA level.

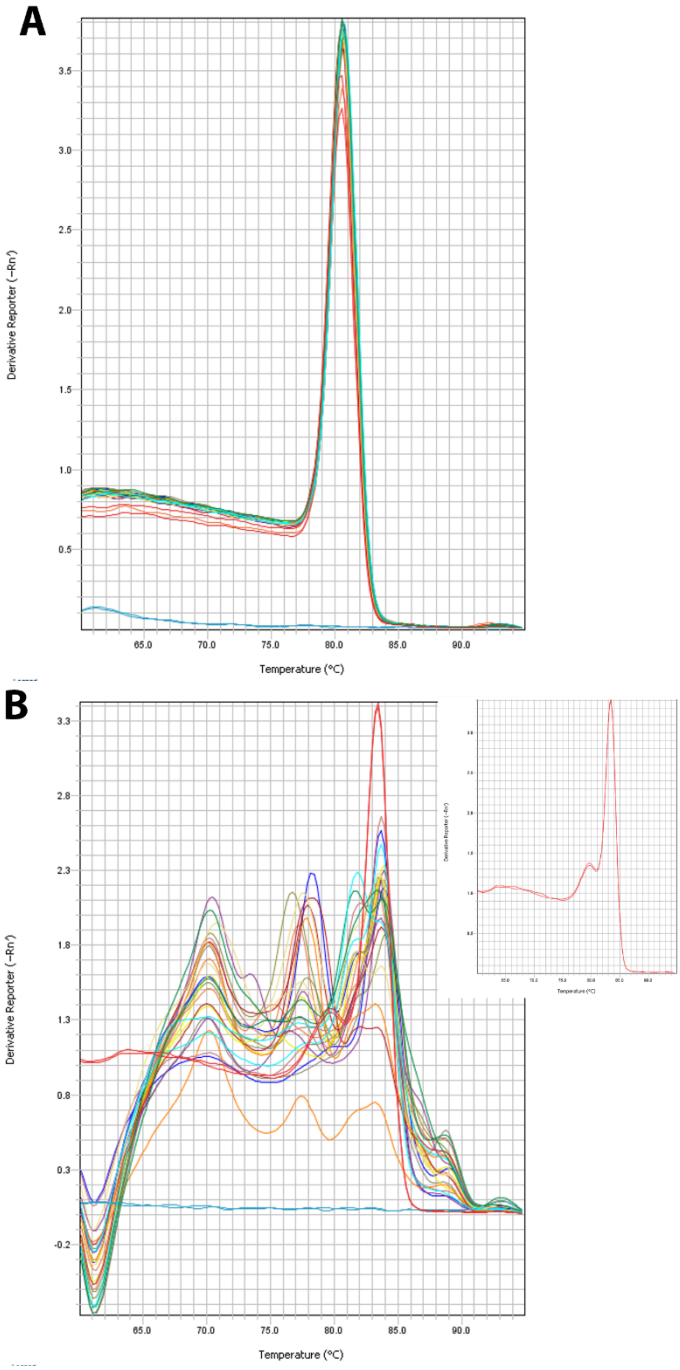

Figure 5.6: Validation of expression of the calcium-sensing receptor (*CASR*) at the mRNA level in normal basal human bronchial epithelial cells (NHBECs). Representative melt curves following qPCR of NHBECs, exposed to vehicle control conditions for 24 hours revealed that the reference gene (RPLP0) demonstrated stable amplification of one product, with no amplification in the no template (negative control) sample shown in blue (A). However, *CASR* mRNA expression in NHBECs was determined to be extremely low as demonstrated by poor amplification of the *CASR* gene and many unspecific products formed during these experiments (B). There was no amplification in the negative control (shown in blue) and the PCR protocol was verified for these primers by including a calibrator sample for assessing *CASR* expression using total human RNA. This sample is included in the main figure and is shown in the inset of B to ensure PCR conditions were suitable for analysing *CASR* expression in these cells.

5.2.3 Determination of ATP levels as an Indicator of Cell Viability:

ATP levels in NHBECs were determined using the Vialight ® Plus Cell Proliferation and Cytotoxicity Kit (Lonza, cat. #LT07-221), as an indicator for cell viability. First, ATP Monitoring Reagent (AMR) was prepared by reconstituting AMR Plus with 50ml of the Assay Buffer (all reagents supplied with kit). AMR Plus was equilibrated at RT for 15 minutes and the cell lysis solution (supplied with kit) was brought to RT before use, aliquoted and stored at -20 °C. Following culture, expansion and seeding of NHBECs (as in section 5.1.2 of this Chapter) and subsequent treatment preparation and 24 hr exposure to the treatment conditions listed in sections 5.2.3.5 and 5.2.3.6 of this Chapter, the cells (in 96-well plates) were removed from the incubator and left to equilibrate to RT for a minimum of 5 minutes. Then, 100 µl of cell lysis reagent was added to each of the treatment wells and to triplicate wells containing complete PneumaCult™-Ex Plus medium only (no cells), to provide a background reading before being incubated at RT for 10-15 minutes. 100 µl of this cell lysate was collected and transferred to a white walled, white bottom 96-well plate (Thermofisher, cat. #165306) and then 100 µl AMR plus was added to the each well (total volume 200 µl), before the plate was incubated in the dark for 2 minutes, at RT. Luminescence was read at 1 second integrated readings of each well using the CLARIOstar® *Plus* microplate reader (BMG Labtech) and analysed using the MARS data analysis software (BMG Labtech). Background luminescence was subtracted from the sample luminescence using the values obtained from the complete PneumaCult™-Ex Plus medium containing wells (no cells), then each value was normalised to the un-stimulated cells (set at 100%).

5.2.4 Investigating the Effect of Particulate Matter in the Presence and Absence of NAM on the Ability of AMs to Efferocytose Apoptotic Neutrophils:

This work was carried out in the laboratory of Professor David Thickett as detailed in Chapter 4, section 4.2.2. The methodological approaches described below used established protocols of determining resolving functions of AMs, such as efferocytosis, which is the engulfment of apoptotic cells, such as neutrophils.

5.2.4 Alveolar Macrophage Isolation and Seeding:

Primary human AMs were isolated from ethically approved samples of lung tissue resection, without the evidence of macroscopic malignancy, counted as in Chapter 4 section 4.2.2.2 and seeded at a density of 250,000 AMs per well in 500 µl complete medium in 24-well plates for efferocytosis analysis and 50,000 AMs per well in 100 µl complete medium in 96-well plates for viability analysis. Then plates were placed in an incubator at 37 °C and 5% CO_2 overnight for adherence of AMs.

5.2.5 Alveolar Macrophage Efferocytosis of Apoptotic Neutrophils:

5.2.5.1 Human Primary Neutrophil Isolation and Labelling:

On the same day as the AM isolation, neutrophils were isolated as in Chapter 4 section 4.2.8.1 and were counted as in Chapter 4, section 4.2.2.2 before being resuspended at 4 million neutrophils per ml in complete medium. CellTracker™ red CMTPX dye (Invitrogen, Thermofisher Scientific, cat. #C34552), was prepared by adding 20 µl of sterile DMSO to the vial and mixing by pipetting up and down, before adding to the neutrophils at a concentration of 5 µl per ml and being incubated at 37 °C, 5% CO_2 for 45 minutes. Following this, cells were centrifuged at 1500 g for 5 minutes, then supernatant was carefully removed and the neutrophil pellet was suspended in serum-free RPMI medium at a concentration of 2 million cells per ml in a 15 ml Falcon tube. Then, labelled

neutrophils were placed in the incubator at 37 °C and 5% CO_2 for 24 hrs to undergo apoptosis.

5.2.5.2 Pre-treatment and Treatment Conditions:

As in Chapter 3 Section 3.2.3.9 and briefly described in Chapter 5, section 5.2.3.5, pre-treatment conditions were prepared in complete medium (described in Chapter 4, section 4.2.2.2). 250 µl of 0.05% DMSO (VC) or 5 µM NAM was added to relevant wells before the plates were placed back in the incubator at 37 °C and 5% CO_2 for 1 hr pre-treatment. Then, PM stock (1 mg/ml) was thawed from -80 °C.

During the pre-treatments, 1X PBS was warmed and PM stock was prepared as in Chapter 3, section 3.2.3.7. 250 µl of each treatment was added to the relevant wells, resulting treatment groups of: 0.05% DMSO (VC), 5 µM NAM, 30 µg/ml PM and PM + NAM. Then, AMs were returned to the incubator at 37 °C and 5% CO_2 for 4 hours.

5.2.5.3 Efferocytosis of Apoptotic Neutrophils by Alveolar Macrophages:

Following treatmet, AMs were removed from the incubator one plate at a time and supernatants were removed and collected into 1.5 ml Eppendorf tubes and stored at -80 °C. Medium was then replaced with fresh complete medium and to the untreated wells, cytochalasin D (cyt-D) (Invitrogen, Thermofisher Scientific, cat. # PHZ1063), a negative control for efferocytosis, was added at a concentration of 5 µg/ml and placed in the incubator for 30 minutes. Other untreated wells were not treated with cyt-D, as controls. After 30 minute treatment with cyt-D, AMs were removed from the incubator and medium was removed from all wells before adding 1,000,000 (4-fold excess) of labelled apoptotic neutrophils to the wells being investigated for efferocytosis. In one of the remaining untreated wells, neutrophils were not added (AM only) and

neutrophils alone were added to an empty well (neutrophil only), as controls for flow cytometric gating and subsequent analysis. Then, plates were returned to the incubator at 37 °C and 5% CO_2, for 2 hours. During the final 45 minutes, sterile 1X PBS was placed on ice. Following the 2 hrs incubation, supernatant was removed and 1 ml of ice-cold PBS was added to each well to wash away excess neutrophils and this process was repeated twice. Following this, 500 µl of TrypLE Express (ThermoFisher Scientific, cat# 12605036) was added to each well and incubated for 8 minutes at 37°C and 5% CO_2. Once cells had detatched, trypsin was neutralised by adding 1 ml complete RPMI and well contents were collected into labelled FACS tubes. To these FACS tubes, 1 ml of FACS buffer (prepared as in Chapter 4, section 4.2.2.3) was added and centrifuged at 500 g for 5 minutes. Supernantant was carefully poured from the tubes and cell pellets were resuspended in 300 µl FACS buffer and placed on ice for subsequent flow cytometry analysis.

5.2.5.4 Flow Cytometric Gating Strategy:

General methodological principles of flow cytometry are provided within Chapter 2, section 2.4. During experiments investigating AM Efferocytosis, the Accuri C6 Plus flow cytometer was used. First, the labelled neutrophils in complete medium were run and first gated for forward scatter area (FSC-A) against FSC-height (FSC-H) to eliminate doublets, and then labelled neutrophils were gated so that >98% of cells fell within the Allophycocyanin (APC) gate. Then, the AM only in complete medium control cells were run and the singlet gate determined by neutrophils only was applied to these cells. AMs were gated out of the singlet cell population by high granularity and autofluorescence, then the untreated AM + neutrophils were run, where gating described above was applied and allowed for determination of efferocytosed neutrophils by gating APC^+ cells, above that of the auto fluorescent AM population (APC^+ above macrophages) (Figure 5.7). The cyt-D treated cells

were used as a negative control and aided in gating of efferocytosed neutrophils. Finally, all stimulated cells were run in duplicate, and gating described above was applied, to determine efferocytosis index. The efferocytosis index was calculated using the median fluorescence intensity (MFI) obtained in the APC^+ above macrophage gate in treated cells minus the MFI obtained in the APC^+ above macrophage cyt-D control. Initial analysis was performed on the BD Accuri machine during experiments, then final analysis and figure preparation was performed using FlowJo software (Treestar).

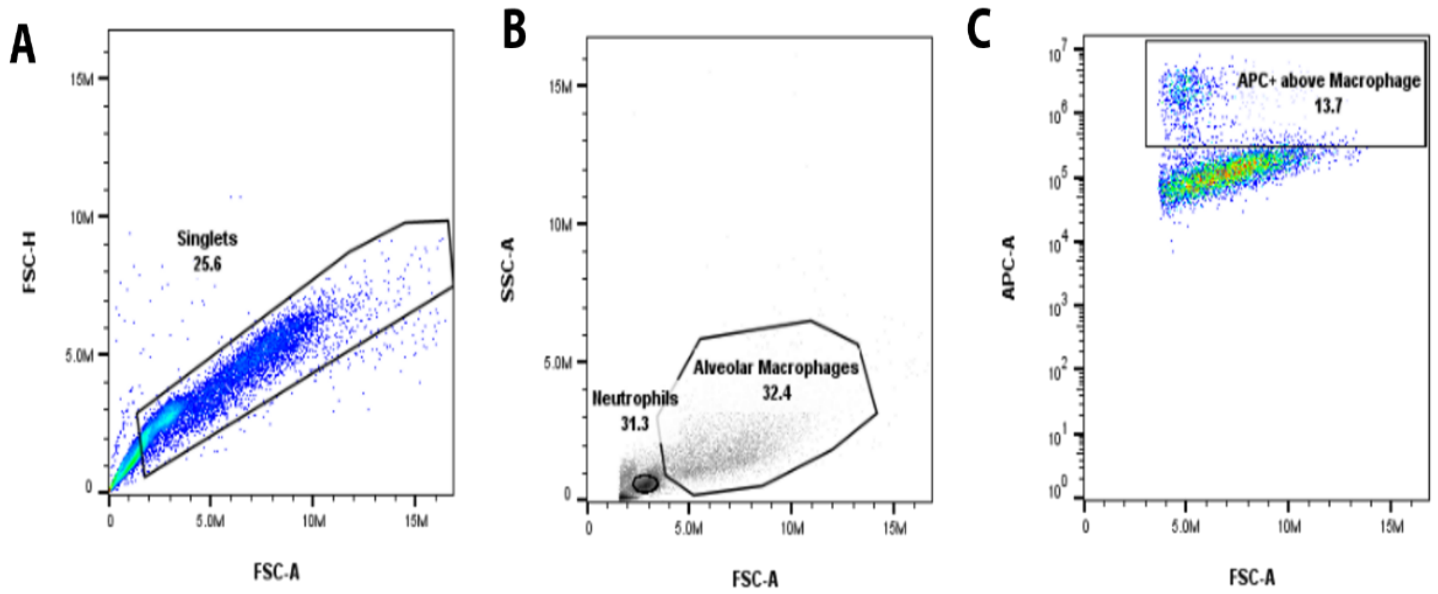

Figure 5.7: Representative flow cytometry plots of gating strategy to determine efferocytosis index of human primary alveolar macrophages (AMs). First, AMs were exposed to fluorescently labelled apoptotic human primary neutrophils in the presence or absence of cytochalasin D, as a negative control. In both cases, singlets were gated out of the cell population using forward scatter height (FSC-H, y axis) and FSC-area (A) which excluded doublets in the analysis and is represented by 25.6% of the cells within the population falling into this gate. Density plotting was then used to exclusively gate AMs and neutrophils, using side scatter-A (y axis) and FSC-A (x axis) (B) which determined that 32.4% of the singlet cells within the population are AMs and neutrophils, respectively. Then fluorescent cells in the allophycocyanin (APC) channel (far red) which were above that of the AM population were gated (with FSC-A on the X axis, which acts as a determinant of size of AMs) and represented the AMs which had efferocytosed neutrophils (13.7% of the population). The efferocytosis index was calculated by subtracting the value obtained in the cytochalasin D-treated cells, from the value obtained in non-cytochalasin D-treated cells, or any other treatment condition. In all panels, data is presented on a log scale.

5.2.6 Determination of ATP Levels as an Indicator of Cell Viability in Response to Particulate Matter Exposure:

5.2.6.1 Pre-treatment and Treatment Conditions:

As in Chapter 3 Section 3.2.3.9 and briefly described in Chapter 5, section 5.2.3.5, pre-treatment and treatment conditions were prepared and applied in complete medium (described in Chapter 4, section 4.2.2.2). During the pre-treatments, 1X PBS was warmed and PM stock was sonicated as in Chapter 3, section 3.2.3.7, before preparation and application of treatment conditions as described in Chapter 5, section 5.2.3.5.

5.2.6.2 Determination of ATP levels:

Following this, ATP levels in AMs were determined using the Vialight ® Plus Cell Proliferation and Cytotoxicity Kit (Lonza, cat. #LT07-221) following the protocol described in section 5.2.3 However, AMs were exposed to treatment groups in complete medium for a 6-hr period, rather than a 24-hr period (as in NHBECs).

5.2.7 Investigating the Effect of Particulate Matter in the Presence and Absence of CaSR NAM on Dendritic Cell Maturation and Cytokine Release:

This work was carried out in the laboratory of Dr Catherine Hawrylowicz at King's College London, as described in Chapter 4, section 4.2.3. The methodological approaches described below used an established model of monocyte-derived DCs, as an *in vitro* model of DCs, to assess the role of the CaSR in PM-induced DC maturation and specific cytokine release patterns.

5.2.7.1 Dendritic Cell Isolation and Seeding:

Monocyte-derived iDCs were isolated from purified $CD14^+$ monocytes as in Chapter 4 section 4.2.3. For maturation and activation studies, iDC were seeded at a density of 20,000 cells per well in 100 µl full medium in a 96-well plate.

5.2.7.2 Pre-treatment and Treatment Conditions:

Pre-treatment conditions were prepared in complete medium as described in Chapter 3 Section 3.2.3.9. Pre-treatment were prepared and applied as in section 5.2.5.2 of this chapter, however, in final volumes of 100 µl of full medium.

Then, PM stock (1 mg/ml) was thawed from -80 °C. 1X PBS was warmed and PM stock was sonicated, and dilutions prepared as in Chapter 3, section 3.2.3.7 in full medium. Each treatment was prepared and applied as in section 5.2.3.5 of this chapter, however, in final volumes of 100 µl per well and in full medium. Finally, TNFα (R&D Systems, cat. #210-TA) and IL-1ß (R&D Systems, cat. #201-LB) stocks were prepared to final concentrations of 100 µg/ml in full medium. Briefly, following pre-treatment, each treatment solution was mixed by gentle pipetting before DCs were removed from the incubator and 50 µl of each treatment was added to the relevant wells, resulting treatment groups of: untreated, 0.1% DMSO (VC), 0.5, 1, 5, and 10 µM NAM, 10 µg/ml PM, PM + NAM and 50 ng/ml of both TNF-α and IL-1ß. Then, DCs were returned to the incubator at 37 °C and 5% CO_2 for 24 hours.

5.2.8 Analysis of Maturation and Activation of Dendritic Cells by Particulate Matter in the Presence and Absence of CaSR NAM:

The general methodological principles of flow cytometry are provided in Chapter 2, section 2.4.

5.2.8.1 Staining and Preparation of Samples for Flow Cytometric Analyses of Dendritic Cell Maturation:

Following 24 hr stimulation of maturation by PM or TNF-α and IL-1ß (positive control), the non-adherent iDCs and mDCs were removed from the wells of the plate using cold MAC's buffer (described in section 4.2.3.7 of Chapter 4) and transferred to FACS tubes for flow cytometric analyses. The collected cells were stained with allophycocyanin (APC) anti-CD83 (BD Bioscience, cat. #551073, information relating to this antibody is supplied in Table 5.2) as an established marker of DC maturation (Li *et al.* 2019). The viability dye eBioscience™ fixable viability dye eFluor 780 (eBioscience™, cat. #65-0865-14) was also added to each sample and samples were incubated for 30 minutes at 4 °C. In addition, a fluorescence minus one (FMO) APC was included to assist in gating for percentage APC $CD83^+$ in PM stimulated cells, which omitted the APC fluorophore during staining, to provide a "background" signal to assist with gating strategy. A wash with FACS flow solution was performed before the samples were ran on Invitrogen™ Attune™ NxT flow cytometer.

Table 5.2: CD83 surface marker antibody used to assess maturation of dendritic cells (DCs). CD83 antigen information provided along with conjugated fluorochrome Allophycocyanin (APC), clone and supplier details.

Antigen	Fluorochrome	Clone	Catalogue No.	Supplier
CD83	APC	HB15e	551073	BD Biosciences

5.2.8.2 Flow Cytometric Analysis Protocol and Gating Strategy for Determination of Maturation Status of Dendritic Cells:

The maturation status of DC was estimated using the Invitrogen™ Attune™ NxT flow cytometer, live DCs were first gated by using the viability dye (AlexaFluor 780) against forward scatter area. These data allowed me to estimate initial % viable DCs in response to VC, NAM, PM + VC and PM + NAM treatment groups. From this, agranular cells were gated based on granularity and size, by plotting side scatter area (SSC-A) and FSC-A within the single cell population, respectively. Then, flow analysis was also used to evaluate the CD83 expression after 24 hr exposure to PM or TNF-α/IL-1ß and compared to the FMO control, which assisted in setting gates to determine % CD83 expressing mDCs (Figure 5.8). All flow cytometric analysis was performed using FlowJo software (Treestar).

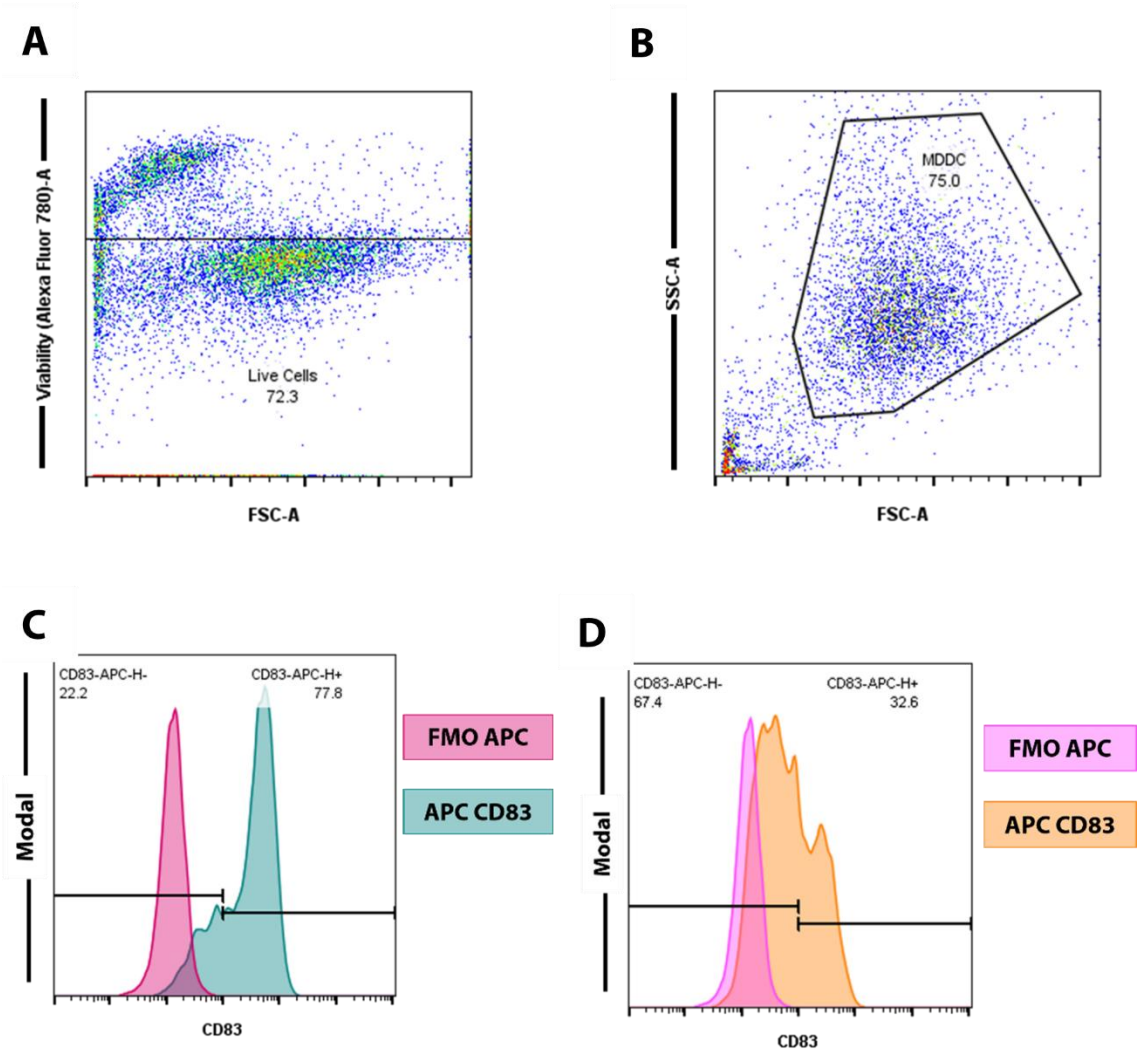

Figure 5.8: Representative gating strategy used to determine maturation status of dendritic cells (DCs). First, monocyte-derived DCs (DCs) were gated using a fixable viability dye (Alexafluor 780) and these values were used to determine baseline viability following treatment with urban particulate matter (PM, 10 µg/ml) ± a negative allosteric modulator at the calcium-sensing receptor (NAM, NPS2143, 10 µm) (A), where 72.3% of cells within the population are viable/live. Then, DCs (MDDC) were gated based on granularity using side scatter area (SSC-A, y axis) and size, using forward SC-A (x axis) (B), where 75% of cells within the live population were gated as MDDCs. MDDCs were exposed for 24 hrs to PM (C) or TNF-α and interleukin (IL)-1ß (50 ng/ml each) as a positive control for DC maturation (D). Gating was applied using the allophycocyanin (APC) conjugated CD83 and the fluorescence minus one (FMO) APC to demonstrate background and CD83 expressing signal (determined by FMO control). This allowed for determination of CD83 expressing MDDCs, represented by CD83-APC-H+ (77.8% in C and 32.6% in D) in the MDDCs, and FMO control staining is represented by CD83-APC-H- (22.2% in C and 67.4% in D). The viability and MDDC gating was performed using the data on a log scale (A, quadrant gating & B, free draw gating tool, both available within the FloJo software). CD83 expression gating was performed using the Bifur gate (FloJo) and the x axis represents scaled APC as a percentage of the maximum count (Modal in A & B).

5.2.8.3 Cytokine Release from Mature Dendritic Cells in Response to Particulate Matter Exposure:

To investigate the cytokine release patterns from PM ± NAM exposed DCs, the supernatants from PM-stimulated DCs were collected, spun at 0.5 g for 5 minutes to sediment cell debris and then transferred to labelled 0.2 ml Eppendorf tubes, and stored at -20°C. The cytometric bead array (CBA, BD), a multiplex assay was used to measure cytokines secreted by DC. BD™ CBA Flex Sets (BD Bioscience) were employed to allow greater flexibility in cytokines selection. The kits selected are listed Table 5.3. In the CBA, each group of beads is labelled with a small amount of fluorescent dye so it can be distinguished by its MFI, during flow cytometric analyses. Each bead population was given an alphanumeric position designation indicating its position relative to other beads in the CBA. Beads were covalently coupled with the antibodies interleukin (IL)-6, IL-10, and IL-12/23p40, to capture these analytes in the supernatant of DCs treated with PM ± NAM. Detection was carried out by addition of a phycoerythrin (PE) (~ 585nm) coupled detection antibody, to each sample, as the wavelengths emitted by this were distinguishable from the fluorescent signal emitted from the CBA beads. Finally, the levels of these cytokines (proportional to the bound detection antibody MFI signals) captured by the different bead groups (distinguished by their MFI signals) were measured and compared to the standards for each cytokine to determine secretion of each cytokine in response to PM ± NAM.

CBA was performed according to the manufacturer instructions, with the following in-house modifications. First, instead of using the prescribed CBA buffer, an in-house CBA buffer was made consisting of 200 ml FacsFlow (Fisher Scientific, cat. #BD342003), 1ml FBS, 500 µl Tween-20 (Sigma, cat. #9005-64-5) and 100 µl EDTA (from stock concentration of 0.5 M EDTA, Sigma, cat. #30-158). The volume of the Phycoerythrin (PE)-conjugated detection antibody and capture beads was diluted 1:5 with in-house buffer. The incubation time of the

supernatants with the diluted capture beads and detection antibody was prolonged to 3 hrs to increase binding. In addition, the standards were diluted in 2 ml of full medium instead of 4 ml of full medium to increase the detection range of the kit from 2500 pg/ml to 5000 pg/ml. IL-12p70 and IL-12/23p40 consist of the same bead position, hence IL-12/23p40 was analysed on a separate plate of supernatant.

50 µl of each diluted supernatant or standard were thawed and incubated at room temperature for 3 hrs on a plate shaker in the presence of antibody coated capture beads. After incubation, plates were washed three times with FACS Flow, before adding the PE-conjugated detection antibody. The plates were then incubated for a further 2 hrs on the plate shaker at room temperature. The plates were then washed twice with FACS Flow and suspended in 150 µl of Attune Focusing Fluid (Thermofisher, cat. #A24904) before being analysed on an Attune NxT flow cytometer (Thermofisher). Flow Jo was used to gate the individual beads based on their bead position for each cytokine. Subsequently, the median fluorescence intensity (MFI) of PE was analysed to allow for comparison with the standards and therefore determine the concentration of each cytokine secreted by PM-stimulated DCs.

Table 5.3: Details of cytokines and associated information for interleukin (IL)-6, IL-10, and IL-12/23p40, used in the cytometric bead array (CBA) experiments. In the CBA, each group of beads is labelled with a small amount of fluorescent dye so it can be distinguished by its MFI, during flow cytometric analyses. Each *bead* population was given an alphanumeric *position* designation indicating its *position* relative to other *beads* in the *CBA (A7, B7 & E5)*. Beads were covalently coupled with the antibodies interleukin (IL)-6, IL-10, and IL-12/23p40, to capture these analytes in the supernatant of monocyte-derived dendritic cells (DCs) treated with particulate matter (PM) ± a negative allosteric modulator at the calcium-sensing receptor (NAM). Detection was carried out by addition of a phycoerythrin (PE) (~ 585nm) coupled detection antibody, to each sample, as the wavelengths emitted by this were distinguishable from the fluorescent signal emitted from the CBA beads. Finally, the levels of these cytokines (proportional to the bound detection antibody MFI signals) captured by the different bead groups (distinguished by their MFI signals) were measured and compared to the standards for each cytokine to determine secretion of each cytokine in response to PM ± NAM, using flow cytometry.

Cytokine	Bead Position	Detection range (pg/mL)
IL-6	A7	10-5000
IL-10	B7	10-5000
IL-12/23p40	E5	40-20,000

5.2.10 Analysis of Soluble Fractions of Particulate Matter:

Analysis of soluble fractions of PM was carried out by the London Metallomics Facility at King's College London, with results analysed and presented by Dr Tzer-Ren Ho.

Since PM was obtained from a commercial source, full characterisation of this was available from the supplier (National Institute of Standards & Technology 2020). However, to better understand the distribution of soluble and insoluble metals contained within supernatants of PM exposed DCs, we carried out component analysis using inductively coupled plasma mass spectrometry (ICP/MS). First, tubes were washed with 3-5% nitric acid prepared in Chelex®-treated water using 60% Ultrapur® Nitric Acid (Sigma, cat. #1.01518). 900 µl of Aqua Regia (1:3 dilution of 60% Ultrapur® Nitric Acid and 30% Ultrapur® H_2O) containing Yttrium standard (20 µl of Yttrium standard stock added to 1.98 ml of Aqua Regia) was added to each tube containing 100 µl of PM sample and controls. Subsequently, the tubes were placed inside a water bath that had been heated to 85 °C for 90 minutes. After 90 minutes of incubation, the tubes were cooled for 1hr before the addition of 6 ml of Chelex®-treated water. The final concentration of PM and acid achieved in each tube was 1.9% v/v HNO_3, 5.8% v/v HCl, 2.14 µg/ml PM and 20 parts per billion (ppb) Yttrium. Sample metal and metalloid concentrations were analysed within London Metallomics Facility at King's College London using a PerkinElmer ICP-MS 'NexION 350DD' system with a dynamic reaction cell, a CETAC 'ASX 520' autosampler and Perkin Elmer's 'Syngistix v1.0' software. It has also been fitted with a Meinhard concentric nebuliser and cyclonic spray chamber. The concentration of elements was determined from a 3-point standard curve for the examined elements, prepared from an ICP Multi Element Standard Solution VI CertiPUR® (Sigma, cat. #1.10580). The elements measured were ^{27}Al, ^{75}As, ^{137}Ba, ^{9}Be, ^{55}Mn,

^{51}V, ^{122}Sb, ^{40}Cd, ^{52}Cr, ^{64}Cu, ^{96}Mo, ^{59}Ni, ^{207}Pb, ^{65}Zn, ^{88}Sr, ^{40}Ca, ^{56}Fe, ^{11}B, ^{59}Co, ^{197}Au, ^{89}Y.

5.2.11 Data Presentation and Statistical Analysis:

Prism 9 (Graphpad) was used to present and statistically analyse data. Data are presented as representative traces of calcium imaging experiments, where each line represents a single cell within the experiment. These were repeated 3-10 times, using 22 to 61 NHBECs, defined by the MetaMorph™ software, per experiment, depending on the experimental set up. Collated data from NHBECs, AMs, and DCs are represented as violin plots to demonstrate frequency distribution of the data. The solid line within each plot represents the median and the dotted lines above and below this represents the upper and lower quartiles, respectively. Normality tests were performed on data sets (Shapiro-Wilk or Kolmogorov-Smirnov) to determine whether parametric or non-parametric analyses was required of the data obtained. Two-way ANOVA was conducted as the method of statistical interrogation of most of the data obtained. All data were grouped and analysed using two-way repeated measure ANOVA due to there being 2 categorical variables or factors in each experimental set up, the PM exposure and the effect of NAM. Two-way ANOVA results were subjected to Tukey's, Sidak's, or Dunn's multiple comparisons tests to correct for the multiple hypotheses testing within each analysis. One-way ANOVA with Tukey's multiple comparisons test was used to interrogate data with 1 categorical variable or factor included. Differences were deemed to be statistically significant when the probability value (p) for accepting the null hypothesis was $p<0.05$, and not significant if $p>0.05$.

5.3 Results:

5.3.1 Basal Human Bronchial Epithelial Cells Are Responsive to Exposure to Extracellular Ca^{2+}, An Effect Which was Partially Reduced by CaSR NAM:

Epithelial cells lining the airways are among the first sites of PM exposure and deposition. In the previous chapter, I confirmed the most abundant CaSR mRNA and protein expression in ciliated cells of the airway epithelium, however, although I determined protein level expression of the CaSR in NHBECs, there are no reports of CaSR mRNA expression in NHBECs on the mRNA level. Due to the discrepancy between mRNA and protein expression in these cells, I sought to confirm functional expression of the CaSR in NHBECs by fluorescent intracellular Ca^{2+} imaging by exposing NHBECs to CaSR agonists, such as Ca^{2+}, PM and spermine, to determine whether 1) the CaSR is functionally active in NHBECs and 2) whether potential PM-induced effects, such as alterations to alarmin mRNA expression, were mediated via the CaSR. Therefore, these data would provide evidence of using these cells as a suitable *in vitro* model to assess the role of the CaSR in mediating PM-induced effects in airway epithelial cells.

Due to disparity between protein and mRNA expression of the CaSR reported in this thesis and by online repositories of sc-RNAseq data, I sought to determine whether the CaSR was functionally active in NHBECs, using fluorescent intracellular Ca^{2+} as one of the biological readouts for CaSR activation and therefore functional expression, to assess whether this *in vitro* model of NHBECs was suitable to test the potential of PM-induced and CaSR-mediated effects in these cells. To assess the functional expression of the CaSR using this biological readout, I first followed the protocol for loading and exposure as in Chapter 3, section 3.2.3.2. However, exposure of NHBECs to 5 mM Ca^{2+} and 100 µg/ml PM, resulted in no change to intracellular calcium levels (Appendix 3), suggesting that the CaSR was not functionally active in these cells, using this biological readout. Previous studies have hinted at

functional CaSR expression in airway epithelial cells, therefore, I carried out pharmacochaperoning to enhance CaSR expression at the plasma membrane of NHBECs, to further assess the functional expression of the CaSR in these cells (Cortijo, Milara, Mata, Donet, Gavara, Peel, Hall and E. J. Morcillo 2010b; Brennan *et al*. 2016). I performed a pharmacochaperoning experiment with overnight exposure to 100 μM spermine or 100 nM R-568 (CaSR PAM) to promote CaSR expression at the plasma membrane. Following overnight exposure to spermine or R-568, NHBECs remained unresponsive to 5 mM Ca^{2+} or 1 mM spermine, used an alternative agonist at the CaSR (Appendix 4), however, I confirmed that non-responsiveness of NHBECs to CaSR agonists using this protocol was not due to deleterious effects on GPCR machinery as a robust ATP response was observed in all experiments (Appendix 3 and 4). Therefore, whether the CaSR is functionally active in NHBECs, using this biological readout, remained elusive.

However, during these experiments, I noticed NHBECs appeared to be "pre-activated" by the loading and baseline solutions and during the running of the experiments, there was clear fura-2 extrusion from these cells. Therefore, I modified the experimental protocol by reducing Ca^{2+} concentration in the loading buffer (by loading in RPMI, with 0.42 mM Ca^{2+}, compared to 1.2 mM Ca^{2+} in the initial loading buffer) and addition of SBP (100 μM) during the loading periods to avoid "pre-activation" and fura-2 extrusion, to make accurate measurements of changes to intracellular calcium levels. Using the modified protocol, exposure of NHBECs to 5 or 10 mM Ca^{2+} induced small but significant increases of intracellular calcium levels (Figure 5.9). These Ca^{2+}-induced alterations to intracellular calcium levels were significantly reduced by co-treatment with 3 μM NAM, however, co-treatment with 1 or 10 μM NAM was comparable to the VC (Figure 5.10).

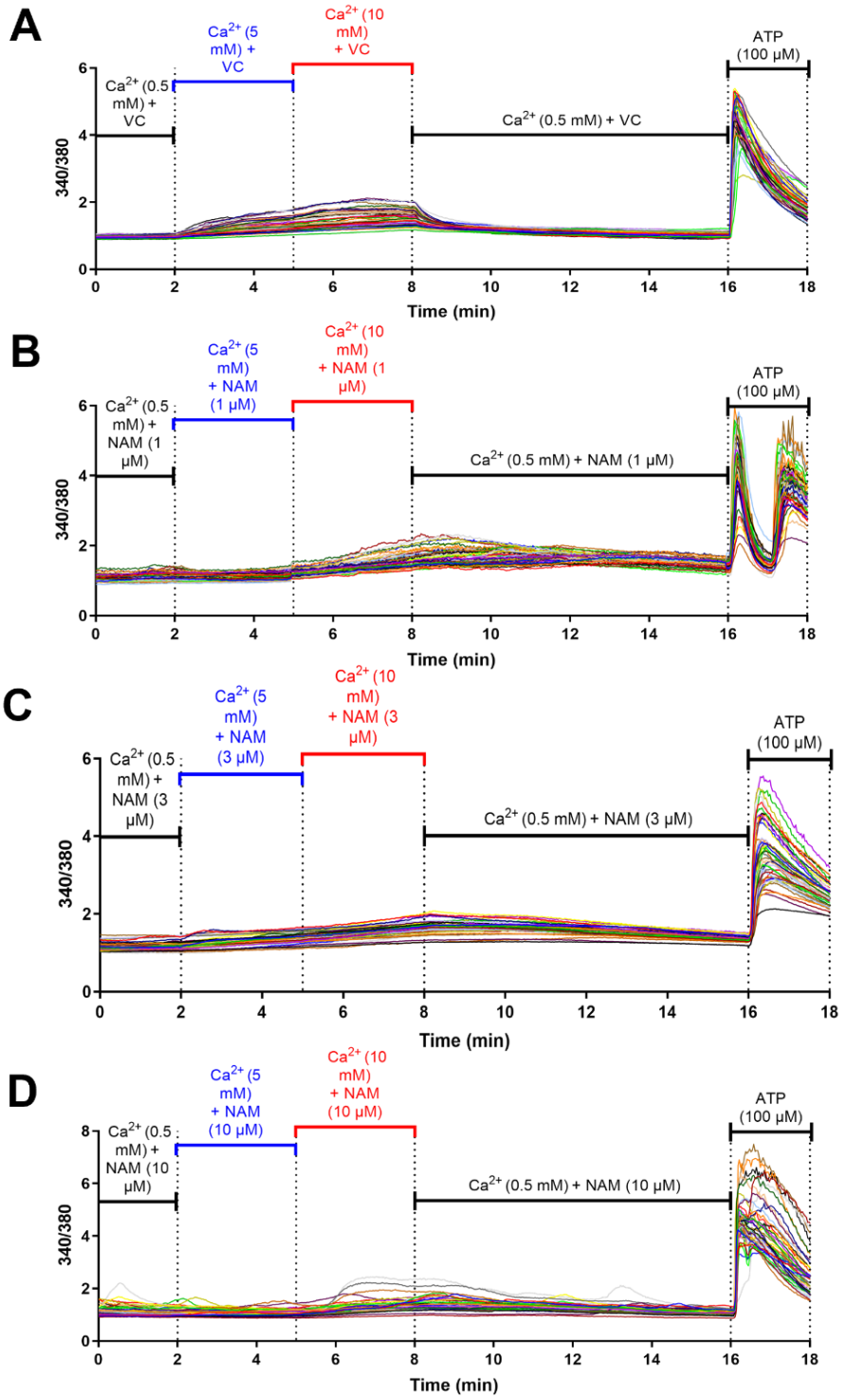
A
Ca2+ (5 mM) + VC
Ca2+ (10 mM) + VC
ATP (100 μM)
Ca2+ (0.5 mM) + VC
Ca2+ (0.5 mM) + VC
340/380
Time (min)
B
Ca2+ (5 mM) + NAM (1 μM)
Ca2+ (10 mM) + NAM (1 μM)
ATP (100 μM)
Ca2+ (0.5 mM) + NAM (1 μM)
Ca2+ (0.5 mM) + NAM (1 μM)
340/380
Time (min)
C
Ca2+ (5 mM) + NAM (3 μM)
Ca2+ (10 mM) + NAM (3 μM)
ATP (100 μM)
Ca2+ (0.5 mM) + NAM (3 μM)
Ca2+ (0.5 mM) + NAM (3 μM)
340/380
Time (min)
D
Ca2+ (5 mM) + NAM (10 μM)
Ca2+ (10 mM) + NAM (10 μM)
ATP (100 μM)
Ca2+ (0.5 mM) + NAM (10 μM)
Ca2+ (0.5 mM) + NAM (10 μM)
340/380
Time (min)

Figure 5.9: Intracellular Ca^{2+} mobilisation is partially blocked by a negative allosteric modulator (NAM) at the calcium-sensing receptor (CaSR) in primary human bronchial epithelial cells (NHBECs) exposed to extracellular Ca^{2+}. Representative traces of NHBECs loaded with the Ca^{2+}-sensitive fluorescent dye, Fura-2AM (3 μM), to measure changes in intracellular Ca^{2+} concentration as one of the biological readouts for CaSR activation. Cells were loaded in low Ca^{2+}-containing RPMI medium (0.42 mM Ca^{2+}) with the addition of sulphobromophtalein (SBP, 100 μM), to reduce "pre-activation" of NHBECs and Fura-2 extrusion from NHBECs during the fluorescent intracellular Ca^{2+} imaging experiments. After loading, NHBECs were pre-treated with Vehicle Control (VC, 0.01% DMSO) or a negative allosteric modulator at the CaSR (NAM, NPS2143, 1, 3 & 10 μM) for 20 minutes in 0.5 mM Ca^{2+} extracellular solution, prior to initiation of experiments. Then NHBECs on coverslips were transferred to a perfusion chamber, mounted on an inverted microscope (Olympus IX71) and continuously perfused with a slow flow of baseline solutions using a rapid perfusion system. In all experiments, NHBECs were acutely exposed to extracellular Ca^{2+} (5 and 10 mM) in vehicle control (0.01% DMSO) or 1, 3 or 10 μM NAM (NPS2143) and at the end of each experiment, HBECs were stimulated with 100μM ATP, a positive control for cell viability and proper functioning of the G protein-coupled receptor machinery. Intracellular Ca^{2+} mobilisation is reduced by NAM (NPS2143, B, C & D). N=3-6 per trace and n=37-57 cells per condition.

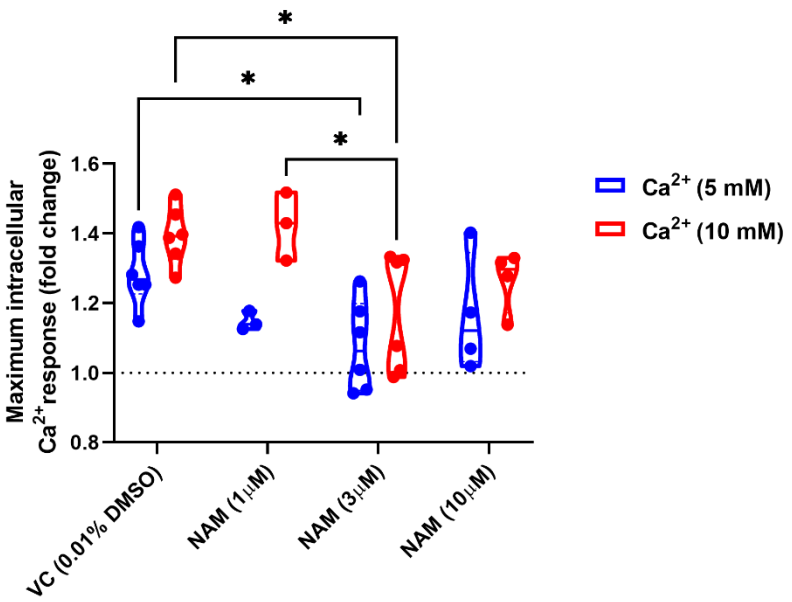

Figure 5.10: A negative allosteric modulator (NAM) at the calcium-sensing receptor (CaSR) significantly reduces maximum intracellular calcium responses in primary human bronchial epithelial cells (NHBECs) exposed to extracellular Ca^{2+}. Collated data from of NHBECs loaded with the Ca^{2+}-sensitive fluorescent dye, Fura-2AM (3 μM) to measure changes to intracellular Ca^{2+} concentration as one of the biological readouts for CaSR activation. After loading, NHBECs were pre-treated with Vehicle Control (VC, 0.01% DMSO) or a NAM (NPS2143, 1, 3 & 10 μM) for 20 minutes in 0.5 mM Ca^{2+} extracellular solution, prior to initiation of experiments. Then NHBECs on coverslips were transferred to a perfusion chamber, mounted on an inverted microscope (Olympus IX71) and continuously perfused with a slow flow of baseline solutions using a rapid perfusion system. In all experiments, NHBECs were acutely exposed to extracellular Ca^{2+} (5 and 10 mM) in vehicle control (0.01% DMSO) or 1, 3 or 10 μM NAM (NPS2143). Maximum intracellular Ca^{2+} responses were calculated from fluorescence intensities of single NHBECs following excitation at 340 (Fura-2 bound to Ca^{2+}) and 380 nm (unbound Fura-2), and emission at 510 nm to generate 340:380 ratios of fluorescence intensity (representing intracellular Ca^{2+} levels). Comparisons between the baseline responses and the response to extracellular Ca^{2+} (5 and 10 mM) are expressed as a fold change to the baseline. Data are represented as violin plots (displaying the data from each experiment within each plot). The solid line represents the median and the dotted lines within the plot represent the upper and lower quartiles, respectively. The dotted line at a fold change of 1, represents no change. Data analysed by 2-way ANOVA with Tukey's multiple comparisons test. Vehicle control (VC) vs NAM (3 μM) p=0.0249 (5 mM Ca^{2+}), p=0.0177 (10mM Ca^{2+}) and NAM (1 μM) vs NAM (3 μM) p=0.0315 (10 mM Ca^{2+}), N=3-6 per treatment group.

5.3.2 Particulate Matter Exposure to Basal Human Bronchial Epithelial Cells Does Not Alter mRNA Expression of Alarmins:

Although findings in Chapter 4 and the section above do not fully confirm functional expression of the CaSR in NHBECs, this model is widely used as an *in vitro* tool to assess the damaging effects of PM on airway epithelial cells. Exposure to PM has been linked to induction of damage associated molecular patterns (DAMPs or alarmins) such as TSLP and IL-33, which promote inflammation in the airways, however, the precise molecular mechanisms behind this remains unclear (Shadie *et al.* 2014; Brandt *et al.* 2020). First, I used PM-exposed NHBECs as an *in vitro* model to assess PM-induced alterations to alarmin mRNA expression and determined that exposure of NHBECs to 50 µg/ml PM in the presence or absence of 1 or 10 µM NAM, induced no significant changes to *TSLP* mRNA expression at 4 or 24 hr time-points (Appendix 5 and 6). Additionally, whilst NHBEC exposure to 50 µg/ml PM did not induce alterations to IL-33 mRNA expression at 4 or 24 hr time-points, 10 µM NAM alone induced a significant reduction in IL-33 mRNA expression at the 4 hr time-point (Appendix 7 and 8). Finally, 24 hr exposure of NHBECs to 100 µg/ml PM resulted in an increase (ns) in *TSLP* mRNA expression, and in contrast, a decrease (ns) in *IL-33* mRNA expression (Appendix 9). However, exposure of NHBECs to 100 µg/ml PM resulted in a significant reduction of ATP levels of NHBECs, which is used as an indicator of cell viability (Appendix 10), suggesting PM-induced effects may have been due to mechanical damage or injury of NHBECs in response to this dose of PM.

5.3.3 Exposure of Alveolar Macrophages to Particulate Matter in the Presence and Absence of CaSR NAM Does Not Significantly Affect Efferocytosis of Apoptotic Neutrophils:

AMs are professional phagocytes and are considered the gatekeepers of the lungs, playing a key role in the uptake and processing of inhaled innocuous stimuli such as PM (Hiraiwa and Van Eeden 2013a). However, AMs also respond

rapidly to pro-inflammatory cytokines, such as alarmins, released from the airway epithelium, whilst also releasing factors to promote an inflammatory response in other airway structural and inflammatory cells and blood-derived inflammatory cells. Neutrophils are recruited from the bloodstream in response to chemotactic agents released from PM-exposed airway epithelial cells and AMs. They are rapidly activated and short lived compared to AMs and undergo apoptosis (programmed cell death) to avoid releasing their often-toxic internal contents by non-programmed cell death or necrosis and further propagating a pro-inflammatory environment in the airways (Fox *et al.* 2010). Therefore, AMs play a key role in resolving innate inflammatory responses to inhaled innocuous stimuli, such as PM, by clearing the airways of apoptotic cells, such as neutrophils, by a process termed efferocytosis.

To assess the effects of PM and potential of uncovering a role for the CaSR in resolving functions of AMs, I exposed AMs to 30 μg/ml PM ± 5 μM NAM for 6 hours and then exposed them to apoptotic neutrophils for 2 hours. NAM alone induced no alterations in efferocytosis index and although there is a clear reduction in efferocytosis with PM ± NAM stimulation, these data were not deemed to be statistically significant (Figure 5.11). Additionally, I ruled out potential effects of each treatment group on AM viability by demonstrating that the ATP levels of AMs, as an indicator of cell viability, in response to each treatment group, was unaffected (Appendix 11).

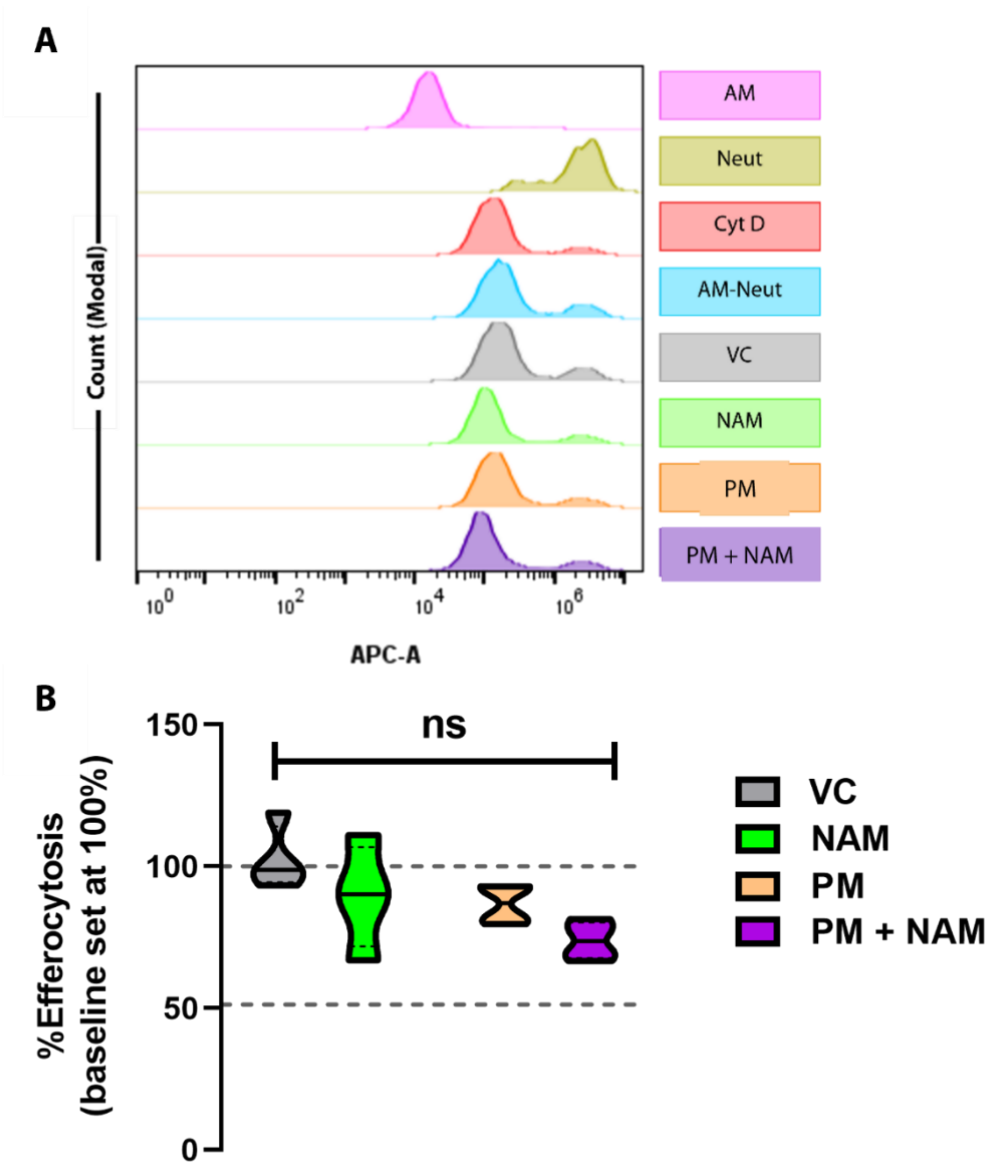
A
Count (Modal)
AM
Neut
Cyt D
AM-Neut
VC
NAM
PM
PM + NAM
10^0
10^2
10^4
10^6
APC-A
B
%Efferocytosis
(baseline set at 100%)
150
100
50
0
ns
VC
NAM
PM
PM + NAM

Figure 5.11: Exposure of primary alveolar macrophages (AM) to urban particulate matter (PM) ± a negative allosteric modulator at the calcium-sensing receptor (NAM) has no effect on AM efferocytosis of apoptotic neutrophils. Primary AMs were isolated from the healthy lung tissue (without macroscopic malignancy) of samples obtained following resection surgery. AMs were exposed for 6 hrs to vehicle control (0.05% DMSO), NAM (5 μM), PM (30 μg/ml) and PM + NAM. Then, the ability of AMs to uptake fluorescently labelled apoptotic neutrophils, in a function termed efferocytosis, was measured by exposing AMs: complete medium alone (AM), cytochalasin-D + apoptotic neutrophils (Cyt-D, 5 μg/ml, a negative control for efferocytosis) and apoptotic neutrophils alone (AM-Neut) and apoptotic neutrophils were also applied to treated AMs, for 2 hrs, to assess the effect of each treatment on efferocytosis. Each exposure condition is demonstrated in the representative flow cytometry plot, which is demonstrated on a modal scale, which scales all channels are a percentage of the maximum count, which also ensures each peak demonstrated are of the same height and the level of fluorescence in the Allophycocyanin (APC) channel, is represented on a log scale (x axis) (A). Treatment of AMs with PM + NAM resulted in a significant decrease in % efferocytosis of fluorescently labelled apoptotic neutrophils, however, there was no significant difference between the other treatment groups (B). Data are represented as % efferocytosis in violin plots with the solid line representing the median and the dotted lines within the plot representing the upper and lower quartiles, respectively. Data calculated using median fluorescence intensity (MFI) of the APC channel per treatment condition, where the baseline (culture medium only) is set at 100% (represented by the dotted line at 100%) and the average of the negative control for efferocytosis, Cyt-D, is represented by the lower dotted line at (51.306%). Data represents N=4 independent experiments with 250,000 AMs, per well exposed to 1 million neutrophils, run in triplicate per biological replicate, and were analysed using a Two-Way ANOVA with Sidak's multiple comparisons test, where ns = not significant.

5.3.4 Particulate Matter Exposure to Dendritic Cells Drives Maturation and Activation, an Effect Reduced by CaSR NAM:

Along with AMs, DCs are also professional phagocytes in the airways and play a key role in the uptake and processing of inhaled innocuous stimuli such as PM (Matthews *et al.* 2016). DCs respond to PM exposure by maturing and releasing pro-inflammatory cytokines to aid in the innate inflammatory response and as a result form a key link between the innate and adaptive arms of the immune system (Steinman and Hemmi 2006). As material abundance of myeloid DCs is low, here, I used an established model of monocyte derived DCs (referred to as DC from here), to assess the role of the CaSR in the

maturation and activation of DCs, in response to PM exposure. 24 hr exposure of DCs to 10 µg/ml PM or TNF-α and IL-1ß (positive control) results in a significant increase in the level of DCs expressing the maturation marker, CD83. Moreover, this effect was significantly reduced by co-treatment with NAM, in a concentration-dependent manner, however, most importantly, the level of CD83 expressing cells were reduced to a level not significantly different from the VC with 10 µM, suggesting a maximal effect with this concentration, without completely abolishing the PM or TNF-α and IL-1ß-induced responses (Figures 5.12 and 5.13).

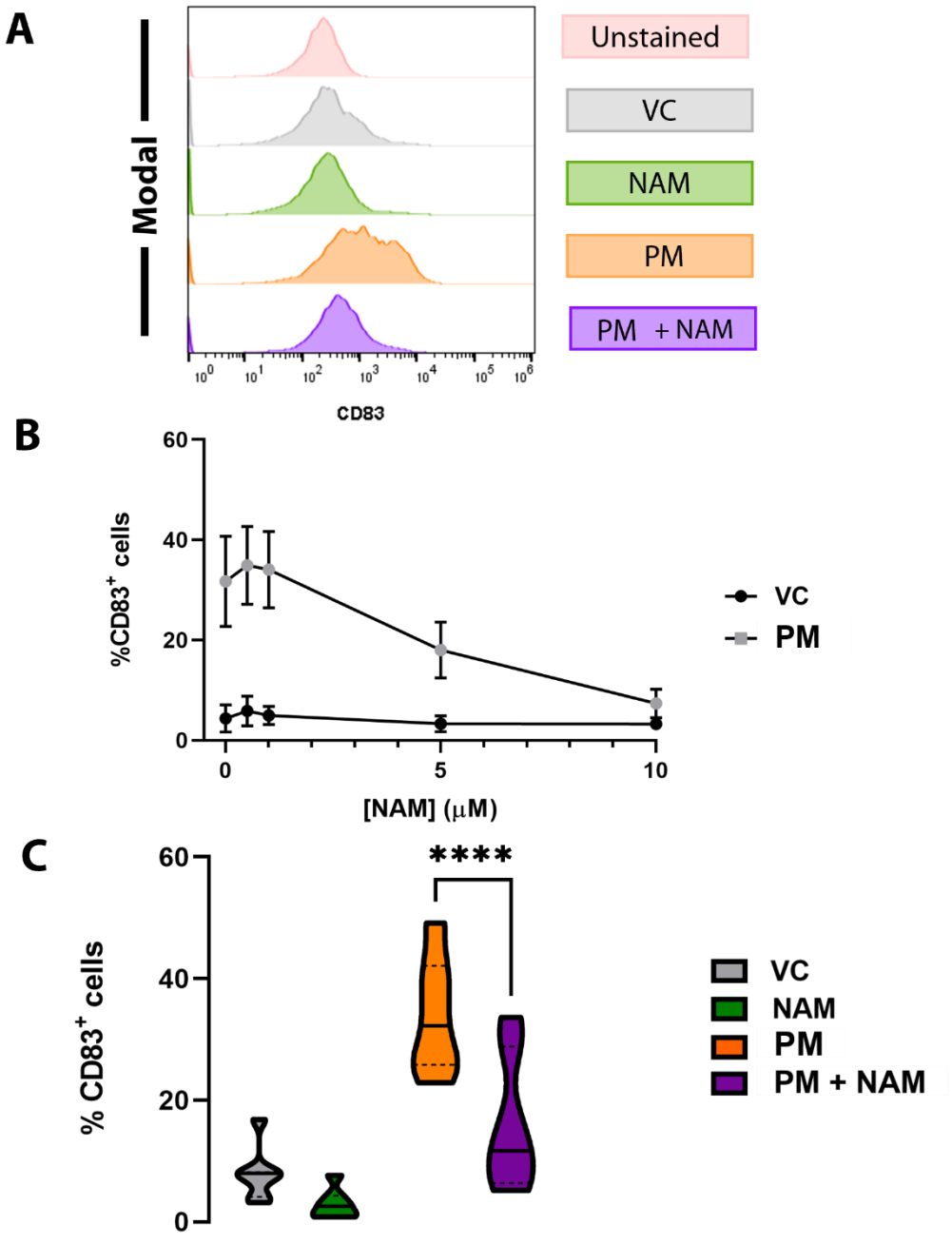
A
Modal
Unstained
VC
NAM
PM
PM + NAM
CD83
B
%CD83+ cells
60
40
20
0
0
5
10
[NAM] (μM)
VC
PM
C
% CD83+ cells
60
40
20
0
****
VC
NAM
PM
PM + NAM

Figure 5.12: Urban particulate matter (PM) induced maturation (%CD83) of monocyte-derived dendritic cells (DCs) which was significantly reduced by co-treatment with a negative allosteric modulator at the calcium-sensing receptor (NAM). An established, in vitro model of DCs, differentiated from monocytes obtained from ethically consenting healthy whole blood samples, were exposed to PM (10 µg/ml) ± NAM (NPS2143, 1, 2, 3, 5 & 10 µM) for 24 hrs and level of CD83 expression was determined, as an indicator of DC maturation, in response to each treatment group. Representative plot of flow cytometry data, where the level of CD83 expression (log scale, x axis) in unstained cells, vehicle control (VC, 0.01% DMSO), NAM and PM ± NAM treated DCs are demonstrated on a modal scale, which scales all channels are a percentage of the maximum count, which also ensures each peak demonstrated are of the same height (A). 3 biological repeats of these experiments were used to determine the dose-response of NAM against PM-induced maturation (increased CD83 expression) and revealed that NAM reduced PM-induced increases to CD83 expression and therefore maturation, in a concentration-dependent manner (B). Finally, the CD83 expression in response to DC treatment with PM ± NAM was collated from 7 biological repeats where NAM (10 µM) induced a significant reduction in percentage CD83 expression, where data are represented in violin plots with the solid line representing the median and the dotted lines representing the upper and lower quartiles, respectively (C). Data was analysed using 2-way ANOVA with Sidak's multiple comparisons test, where **** p = <0.0001.

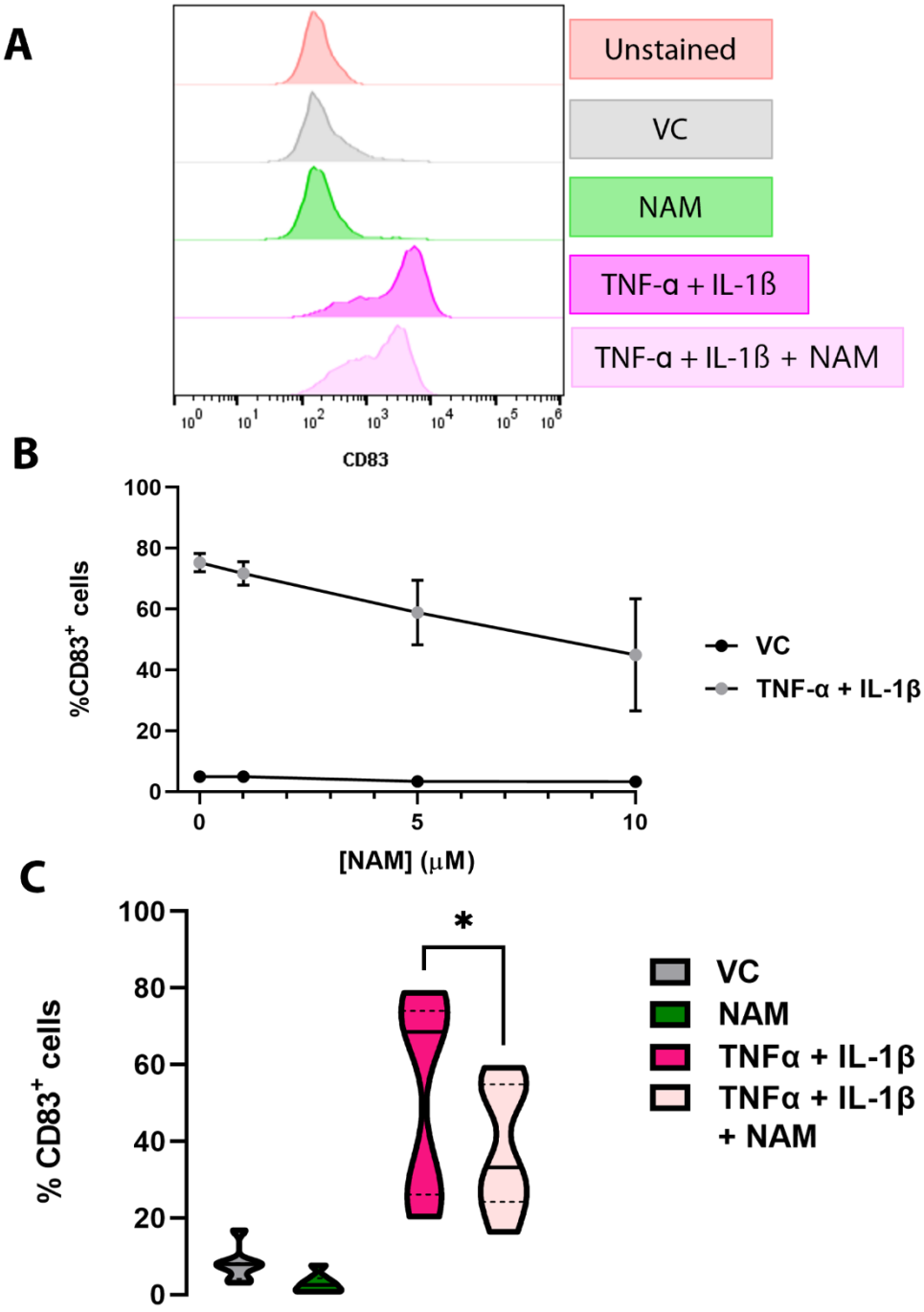
A
Unstained
VC
NAM
TNF-α + IL-1ß
TNF-α + IL-1ß + NAM
CD83
B
%CD83+ cells
[NAM] (μM)
VC
TNF-α + IL-1β
C
% CD83+ cells
VC
NAM
TNFα + IL-1β
TNFα + IL-1β + NAM

Figure 5.13: Tumour necrosis factor-alpha (TNF-α) and interleukin (IL)-1ß induced maturation (%CD83) of monocyte-derived dendritic cells (DCs) which was significantly reduced by co-treatment with a negative allosteric modulator at the calcium-sensing receptor (NAM). An established, in vitro model of DCs, differentiated from monocytes obtained from ethically consenting healthy whole blood samples, were exposed to TNF-α and IL-1ß (50 ng/ml each) ± NAM (NPS2143, 1, 5 & 10 μM) for 24 hrs and level of CD83 expression was determined, as an indicator of DC maturation, in response to each treatment group. Representative plot of flow cytometry data, where the level of CD83 expression (log scale, x axis) in unstained cells, vehicle control (VC, 0.01% DMSO), NAM and TNF-α and IL-1ß ± NAM treated DCs are demonstrated on a modal scale, which scales all channels are a percentage of the maximum count, which also ensures each peak demonstrated are of the same height (A). 3 biological repeats of these experiments were used to determine the dose-response of NAM against TNF-α and IL-1ß -induced maturation (increased CD83 expression) and revealed that NAM reduced TNF-α and IL-1ß -induced increases to CD83 expression and therefore maturation, in a concentration-dependent manner (B). Finally, the CD83 expression in response to DC treatment with TNF-α and IL-1ß ± NAM was collated from 7 biological repeats where NAM (10 μM) induced a significant reduction in percentage CD83 expression, where data are represented in violin plots with the solid line representing the median and the dotted lines representing the upper and lower quartiles, respectively (C). Data was analysed using 2-way ANOVA with Sidak's multiple comparisons test, where * p= 0.0134.

In addition, PM exposure resulted in DC activation and subsequent release of cytokines IL-6, IL-10 and IL-23p40. NAM induced a significant reduction in the release of IL-10 (Figure 5.14), however, once the dataset underwent baseline correction, to reduce patient-patient variability, NAM also significantly reduced IL-23p40 release from DCs (Figure 5.15). PM or NAM induced effects in DCs were deemed not to be due to alterations in DC viability as was evidenced by no significant differences in the viable cells used in the analysis (Appendix 12).

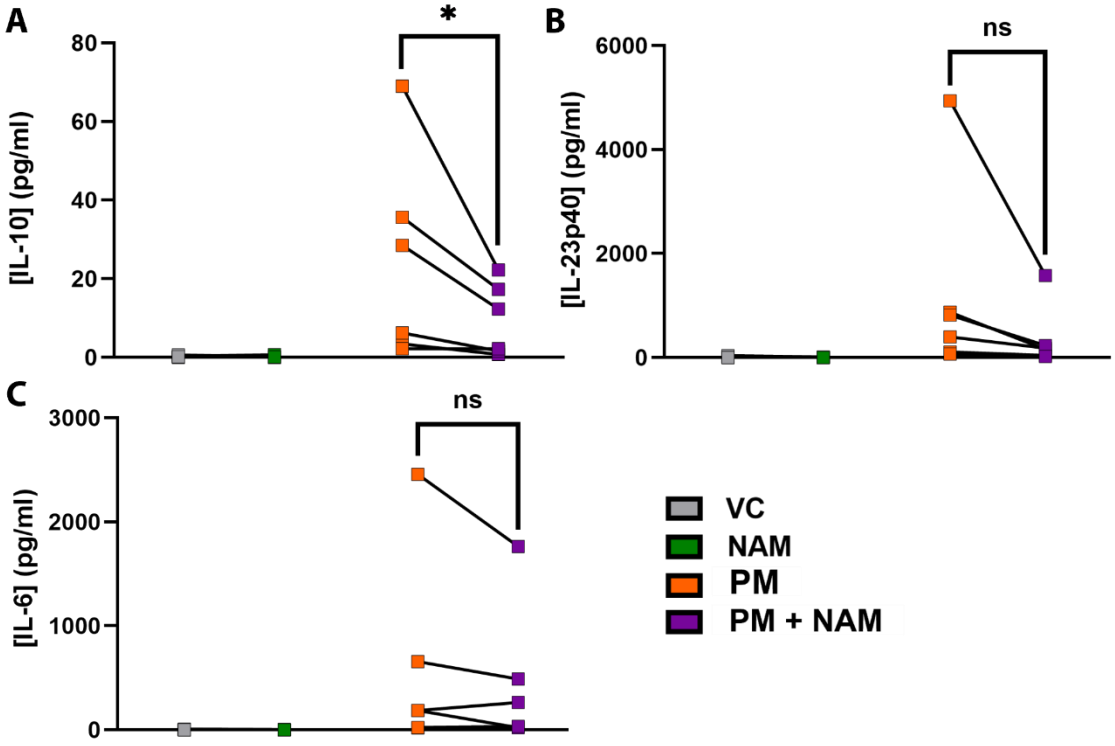

Figure 5.14: A negative allosteric modulator at the calcium-sensing receptor (NAM) partially reduced urban particulate matter (PM)-induced cytokine release from dendritic cells (DCs). An established, in vitro model of DCs, differentiated from monocytes obtained from ethically consenting healthy whole blood samples, were exposed to PM (10 µg/ml) ± NAM (NPS2143, 10 µM) for 24 hrs and level of interleukin (IL)-10, IL-23p40 and IL-6 release was measured using the cytometric bead array kits (BD) and appropriate standards for each cytokine analysed (provided in the kit). 24 hr exposure of DCs to PM drives interleukin (IL)-10, IL-23p40, and IL-6 cytokine release (A, B and C, respectively), which was reduced (significantly in A) by co-treatment with NAM. Data are expressed as individual data points per donor with the line between treatment groups representing the "before & after" treatment of each donor. No difference was observed in the vehicle control (VC, 0.01% DMSO) or NAM alone groups. Data were analysed by 2-way ANOVA and Sidak's Multiple Comparisons Test, where ** p=0.0052. N=6 donors per treatment group.

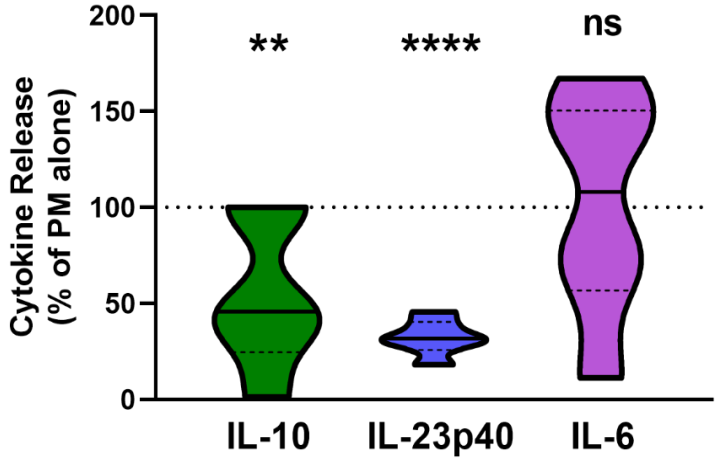

Figure 5.15: A negative allosteric modulator at the calcium-sensing receptor (NAM) significantly reduced urban particulate matter (PM)-induced interleukin (IL)-10 and IL-23p40, but not IL-6 release from dendritic cells (DCs). An established, in vitro model of DCs, differentiated from monocytes obtained from ethically consenting healthy whole blood samples, were exposed to PM (10 µg/ml) ± NAM (NPS2143, 10 µM) for 24 hrs and level of interleukin (IL)-10, IL-23p40 and IL-6 release was measured using the cytometric bead array kits (BD) and appropriate standards for each cytokine analysed (provided in the kit). 24 hr exposure of DCs to PM drives interleukin (IL)-10, IL-23p40, and IL-6 cytokine release (A, B and C, respectively), which was reduced (significantly in A) by co-treatment with NAM. No difference was observed in the vehicle control (VC, 0.01% DMSO) or NAM alone groups. Data are expressed as violin plots, with the solid line within each plot representing the median and the dotted lines above and below this are the upper and lower quartiles, respectively. Data were analysed by 2-way ANOVA and Sidak's Multiple Comparisons Test, where ** p=0.0052. N=6 donors per treatment group. Data represents baseline corrected values, and each plot is displayed as a percentage of the PM-alone treated DCs, which is demonstrated by the dotted line at 100%. N=6 donors per treatment group, where data were compared to PM-only treated samples (set at 100%) and analysed by 2-way ANOVA with Sidak's Multiple Comparisons Test, where IL-10 p=0.0052, IL-23p40 p=<0.0001 and IL-6 not significant (ns).

5.3.5 Supernatant of Particulate Matter-Exposed Dendritic Cells contains an array of CaSR agonists:

PM used in this study has been extensively characterised and contains many potential activators at the CaSR. Supernatant collected from PM-exposed DCs contains an extensive list of metals, most of which potential activators at the CaSR, including Ca^{2+} (most abundant), Cd^{2+} and Ni^{2+} and are also partially soluble in culture medium (Table 5.4).

Table 5.4: Soluble Heavy metals present in urban particulate matter (PM) are potential activators at the calcium-sensing receptor (CaSR). Data represents mean mass ± standard deviation (SD) (ng/µg) determined by inductively coupled plasma mass spectrometry (ICP-MS) analysis and % solubility of the metals contained in the supernatant of PM-exposed dendritic cells. Insoluble PM was removed from supernatants by centrifugation. *Beryllium (Be) represents mean mass (pg/ µg).

Metalloid	Mean Mass ± SD (ng/µg)			% Solubility
Calcium (Ca)	45.0055	±	0.731687	41%
Iron (Fe)	16.74861	±	0.106151	ND
Aluminium (Al)	6.5334	±	0.156287	ND
Lead (Pb)	4.604121	±	0.025611	0%
Zinc (Zn)	2.258299	±	0.017595	2%
Arsenic (As)	0.921756	±	0.014159	ND
Manganese (Mn)	0.497894	±	0.003982	13%
Barium (Ba)	0.418516	±	0.003883	ND
Strontium (Sr)	0.344928	±	0.003817	38%
Copper (Cu)	0.320447	±	0.004841	9%
Boron (B)	0.192746	±	0.005109	ND
Chromium (Cr)	0.090054	±	0.002898	ND
Nickel (Ni)	0.069903	±	0.001464	4%
Vanadium (V)	0.06485	±	0.001394	16%
Cadmium (Cd)	0.054869	±	0.000362	27%
Antimony (Sb)	0.02551	±	7.76E-05	17%
Molybdenum (Mo)	0.012493	±	0.000372	33%
Cobalt (Co)	0.0101	±	0.000112	17%
Beryllium (Be*)	1.216174	±	0.031846	0%

5.4 Discussion:

9 out of every 10 people worldwide live in areas in which the air quality is so poor, it exceeds the limits set by the WHO, and exposure to PM, which is a major component of ambient air pollution, is a huge issue worldwide, and contributes to acute exacerbations of lung diseases, such as asthma, COPD, and more recently, IPF (Atkinson *et al.* 2012; Gan *et al.* 2013; Winterbottom *et al.* 2018). These exacerbations can prove fatal for some patients, and it is estimated that around 4.2 million deaths each year can be attributed to exposure to ambient air pollution, through induction and exacerbation of diverse diseases, such as lung disease, heart disease and stroke (World Heath Organisation 2018). The diverse nature of the diseases associated with exposure to ambient air pollution may suggest that there is a common underlying mechanism for PM-induced effects in the distinct body tissues. So far, the precise cellular mechanisms which underpin harmful PM-induced effects in the airways remains unclear, so during this thesis, I sought to better understand the role of the CaSR in mediating PM-induced effects in the airways, to potentially provide an underpinning mechanism for sensing and responding to inhaled innocuous stimuli, such as PM.

In this chapter, I reveal that the CaSR plays potential roles in mediating PM-induced effects in the airways and that NAM comprise a potential novel therapeutic to directly counteract some of the pro-inflammatory effects brought about by PM exposure. The previous chapters revealed that the CaSR can be directly activated by PM and that the CaSR is expressed on the protein level in key cells involved in initiating an innate inflammatory response to PM and thereby directly responding to PM. In this Chapter, I sought to establish suitable *in vitro* models to assess the roles of the CaSR in mediating PM-induced effects in basal NHBECs DCs, AMs. Here, I validated these models and revealed that although basal NHBECs may not be the most suitable model for

assessing CaSR-mediated effects, primary AMs and monocyte-derived DCs comprise suitable *in vitro* models which demonstrate roles for the CaSR in key inflammatory processes, in response to PM exposure. Therefore, this current chapter begins to lay the basis for unravelling the complexity of PM-induced pro-inflammatory effects and highlights the potential multifaceted roles of the CaSR in sensing and responding to PM in key structural and inflammatory airway cells. Finally, these data corroborate the potential role for the CaSR NAM as a novel therapeutic for lung diseases such as asthma and COPD exacerbated by PM and could directly counteract PM-induced activation of CaSR-mediated pro-inflammatory effects in a range of airway cells.

5.4.1 Potential Roles for the CaSR in Airway Epithelial Cells:

In the previous chapter, I revealed protein level expression of the CaSR in basal NHBECs by IHC, however, this was not corroborated on the mRNA level using data obtained from The Human Protein Atlas, an online repository of sc-RNAseq data. Therefore, it was imperative to determine whether functional expression of the CaSR exists in basal NHBECs using fluorescent intracellular calcium imaging as one of the biological readouts for measuring CaSR activation. In this chapter, I sought to determine whether this 2D *in vitro* model of basal NHBECs is a suitable model for investigating PM-induced and CaSR-mediated effects in airway epithelial cells, to better our knowledge of the potential involvement of the CaSR in PM-sensing in the airways. I initiated these experiments following the protocol developed in Chapter 3, using the HEK-CaSR or HEK-0 cells, however, during these initial experiments, there were no inductions of intracellular calcium responses by CaSR ligands: Ca^{2+}, spermine and urban PM. The CaSR is functionally active at the plasma membrane, where it exists as a homodimer, however, CaSR monomers are also found in the cytoplasm, where agonist-driven insertional signalling (ADIS) plays an important role in the trafficking of CaSR monomers to the plasma

membrane, therefore contributing to regulation of CaSR trafficking and therefore CaSR-mediated intracellular signalling (Breitwieser 2012).

From the data obtained in the previous chapter, there was no detectable CaSR expression at the plasma membrane and the expression of CaSR appeared to be diffused throughout the cytoplasm of basal NHBECs. Therefore, to bring the CaSR to the plasma membrane, I performed a pharmacochaperoning experiment, to enhance AIDS, by overnight exposure of basal NHBECs to the CaSR agonist spermine or the PAM R-568 and repeated the fluorescent intracellular calcium imaging experiments. Using an identical exposure protocol as the initial experiments, I was again unable to induce alterations to intracellular calcium levels suggesting that the CaSR was not activated in these cells, using this biological readout. Finally, to validate that the non-responsiveness of basal NHBECs to CaSR ligands was not due to decreases in cell viability or dysfunction in GPCR machinery, I performed an ATP exposure at the end of each experiment, which was robust and reproducible in all experiments. This evidence suggests that basal NHBECs were viable and functioning following the loading and exposure protocols, but factors observed during the running of these experiments led me to modify the components of the loading and exposure solutions, to better suit to basal NHBECs and provide a suitable *in vitro* model to assess CaSR-mediated alterations to intracellular calcium levels in these cells and therefore confirm functional expression of the CaSR.

These factors included the appearance of "pre-activated" basal NHBECs following the exposure to loading and baseline solutions and mounting on the microscope stage. This was represented by a large 340/380 ratio (between 1 and 2), which was validated by eye, as the basal NHBECs in the ratio image panel of the Optoflour software were greener/brighter and comparable to activated HEKs in previous experiments, suggesting "pre-activation" of these

cells. This observation was important as it suggested that minor alterations to intracellular calcium levels would not be measurable using the identical protocol to that used in HEK cell experiments of Chapter 3, where HEK-CaSR are genetically engineered to express the CaSR abundantly. In addition to "pre-activated" basal NHBECs, I observed fura-2 extrusion from the cells during running of the experiments described above. These were visible as bright specs on the images obtained during the initial experiments and were deemed to be extrusion of fura-2 from loaded basal NHBECs. These specs appeared and disappeared in the images in the same manner as the fluid movement over the coverslip, applied via the rapid perfusion system and removed via the suction pump on the microscope stage. As these factors had the potential to negatively influence the measurements of alterations to intracellular calcium, in cells which had low CaSR expression, I went on to modify the components and timings of exposure to loading and baseline solutions, to ensure minimal "pre-activation" and fura-2 extrusion from loaded basal NHBECs during these experiments.

First, to overcome "pre-activation" during the fura-2 loading process, I modified the components of the loading solution and instead of using a 1.2 mM Ca^{2+} containing ECS, as used in the HEK experiments, I opted for using RPMI, which contains 0.42 mM Ca^{2+}, a concentration much below the threshold for potential CaSR activation. Then, to reduce fura-2 extrusion from basal NHBECs following loading and exposure to baseline solutions, I added SBP to the loading solutions, to reduce dye extrusion through anion exchangers and has been shown to aid in in Ca^{2+} indicator retention in lung slices (Perez and Sanderson 2005). In addition, to further reduce potential of "pre-activation", pre-treatment of basal NHBECs with VC or NAM, was performed in RPMI, and at 37 °C and 5% CO_2, in contrast with the HEK cell experiments in Chapter 3. Finally, all baseline solutions were maintained in a 0.5 mM Ca^{2+} containing ECS,

to minimise "pre-activation" of basal NHBECs before exposure to 5 or 10 mM Ca^{2+}. As confirmations of the modifications, basal NHBECs appeared to be quiescent at the start of experiments, as visualised by lower initial 340/380 ratios (~ 1), compared to without protocol modification, and bluer/duller basal NHBECs in the ratio image panel of the Optoflour software. Modification of the protocol revealed that increases of intracellular calcium levels in these cells were able to be detected in response to treatment with 5 or 10 mM Ca^{2+}, and this can be partially blocked by co-treatment with NAM (1, 3 or 10 μM), however this was only significant with 3 μM NAM co-treatment. These data suggest that, although CaSR expression is low in these cells, what is there seems to be functionally active, however, an *in vitro* model with more abundant CaSR expression, would be a more suitable model to assess CaSR-mediated effects in basal NHBECs.

However, whether alterations to intracellular Ca^{2+} are truly mediated by the CaSR remains unclear, as alternative CaSR ligands, such as spermine induced no alteration to intracellular Ca^{2+}, suggesting that responses to 5 or 10 mM Ca^{2+} are not entirely mediated through the CaSR. This finding was also validated by no clear concentration-dependent inhibition of alterations to intracellular Ca^{2+} with 1, 3 and 10 μM NAM. Finally, intracellular Ca^{2+} mobilisation is just one of the biological readouts for CaSR activation and as mentioned in the Discussion of Chapter 3, activation of the CaSR leads to stimulation of distinct intracellular signalling pathways which are stimulated in response to CaSR activation and are determined by the ligand which binds the receptor in a concept termed ligand-biased signalling (Brennan, Thiem, Roth, Aggarwal, Irfete Sh. Fetahu, *et al.* 2013; Leach *et al.* 2014). Based on the results obtained in the previous chapter and further investigated in this chapter, the expression of CaSR appears to be low in these cells and therefore, this 2D *in vitro* model may not be the most suitable for assessing CaSR-mediated effects

in airway epithelial cells. However, this model is widely used for assessing PM-induced effects in airway cells and therefore, I continued to investigate other PM-induced and potentially CaSR-mediated effects using this *in vitro* basal NHBEC cell model.

To better understand how PM drives innate inflammatory responses in airway epithelial cells, I used this *in vitro* model of basal NHBECs to determine mRNA expression of key mediators of a PM-induced, pro-inflammatory response in these cells. The bronchial epithelium plays an important role in orchestrating innate inflammatory responses in the airways and releases important mediators to activate innate inflammatory cells, to form a link between the innate and adaptive arms of the immune system (Gras *et al.* 2017; MacKay *et al.* 2017; Rider *et al.* 2017). Bronchial epithelial cells form a major source of some of these mediators, such as damage-associated molecular patterns (DAMPs) or alarmins such as TSLP and IL-33 which are thought to be upregulated in response to exposure to PM and have been shown to be increased in the asthmatic epithelium (Ying *et al.* 2005; Bleck *et al.* 2008; Ying *et al.* 2008; Bleck *et al.* 2010; Nguyen *et al.* 2010; Shikotra *et al.* 2012; Brandt *et al.* 2020). However, due to disparity between PM samples and experimental set ups used in previous studies, there has not yet been a mechanism revealed for PM-induced expression of alarmins in the airway epithelium.

To this end, I used the *in vitro* model of basal NHBECs to assess the potential of the CaSR in mediating PM-induced effects in these cells. However, due to difficulties in measuring secreted alarmins from airway cells *in vitro*, I measured mRNA expression levels of *TSLP* and *IL-33* during this study. In this chapter, I reveal that 24 hr exposure of basal NHBECs to 100 µg/ml PM induces a significant increase in TSLP mRNA expression. Moreover, NAM brought about a non-significant decrease in *TSLP* mRNA expression, when compared to the PM-alone treated cells, however, the expression was not significantly different

from NAM alone, suggesting that the CaSR may be mediating some of the effects of PM. Conversely, *IL-33* mRNA expression was significantly reduced in response to this dose and exposure time of PM and although NAM co-treatment led to a less significant reduction in *IL-33* mRNA expression compared to the VC, this was not significantly different from the PM alone treated basal NHBECs. Upon further analysis, I revealed that a 24 hr exposure of 100 µg/ml PM to basal NHBECs induced a significant reduction in ATP levels of these cells which is used as an indicator of cell viability, therefore suggesting that increases in *TSLP* mRNA expression, and decreases in *IL-33* expression could have been partly due to PM-induced cell death/damage. My data were corroborated by studies by Pfeffer et al. (2018), where no alterations to *TSLP* or *IL-33* mRNA expression were observed upon exposure to the same PM as used in my studies. However, in studies using a 3D HBEC ALI model, Gras et al. (2017) demonstrated that PM exposure drove alterations to TSLP and IL-33 secretion in HBECs derived from severe asthmatic patients, but not in healthy controls.

It has been demonstrated that damaged or necrotic cells release full-length IL-33, which upon exposure to proteases, such as neutrophil elastase, released from neutrophils, is cleaved into active IL-33, which has been shown to be 30 x more biologically active than full-length IL-33 (Lefrançais *et al.* 2012; Lefrançais *et al.* 2014; Drake and Kita 2017). Other proteases, which are activated upon cellular apoptosis, such as Caspase-3 and 7 cleave IL-33 in alternative regions, rendering the cleaved IL-33 protein as biologically inactive, due to the inability to bind its receptor on target cells (Lüthi *et al.* 2009). These considerations highlight the complexity in measuring IL-33 *in vitro* and validates that measuring mRNA expression of alarmins such as IL-33, is important, due to the complexities related to the multiple biological forms of the IL-33 protein, however, measuring mRNA expression does not necessarily

indicate which form of IL-33 would be secreted in response to exposure to PM. In studies by my laboratory colleague, Miss Ping Huang, the CaSR was shown to be a key mediator of T2 (ovalbumin, OVA) and non-T2 (IL-33) induced asthma-like features, which were returned to baseline following co-treatment with NAM, in *in vivo* models of OVA and IL-33 induced asthma (Huang *et al*. 2019; Mansfield *et al*. 2020). However, there are clear species differences between mice and humans in terms of the biological activity of IL-33, which need to be taken into account when attempting to translate the *in vivo* findings of our laboratory, to an *in vitro* human model. For example, mice airways exposure to allergens or cigarette smoke has been demonstrated to drive IL-33 expression whereas increased IL-33 expression in human lungs is associated with lung diseases such as asthma or COPD (Préfontaine *et al*. 2010; Byers *et al*. 2013; Iijima *et al*. 2014; Kearley *et al*. 2015). Therefore, utilising an *in vitro* model of diseased or damaged airway cells would prove beneficial in furthering our understanding of the potential role of the CaSR in mediating alarmin expression and release.

As mentioned in the Discussion of Chapter 3, I attempted to validate these findings using a different measure of cell viability – the Lactate Dehydrogenase (LDH) release assay, where release of LDH is indicative of cell membrane damage and rupture, however, this assay brought about conflicting results to that found with the ATP assay. The LDH assay appeared to suggest that increasing doses of PM promoted cell viability, however, these observations could have been due to nanoparticle interference with the assay reagents, potentially going some way in explaining the conflicting evidence of the effect of PM on cell viability (Holder *et al*. 2012). As a result of these combined findings, I repeated the experiments using a reduced dose of PM (50 µg/ml) which has been previously published in studies from our collaborators at King's

College London and to identify time-sensitive effects of PM on alarmin mRNA expression, I performed analysis at 4 or 24-hr timepoints (Pfeffer et al. 2018).

The reduced dose of PM in the presence and absence of the NAM induced no significant alterations in *TSLP* mRNA expression at 4 or 24 hr timepoints. In a similar manner, *IL-33* mRNA expression was also unaltered in response to PM exposure at 4 or 24 hr timepoints, however, NAM alone (10 μM) induced a significant reduction in *IL-33* mRNA expression at 4 hrs, suggesting potential off-target effects of NAM with this dose. Across these mRNA expression data, there were significant degrees of variation between distinct samples of basal NHBECs, making it difficult to make concrete conclusions from the N=3 samples used during these experiments. The disparity in these findings emphasized that expression of alarmins is notoriously difficult to measure *in vitro* due to instability and rapid metabolization (Nagarkar *et al.* 2013; Salter *et al.* 2015). Despite the findings described above, the mechanisms for PM-induced effects on alarmin expression and potential involvement of the CaSR in these processes remains unclear.

Together, these data suggest that cellular damage or stress induced by PM is required to drive alterations to alarmin mRNA expression in basal NHBECs, which corroborates previous findings (Rider *et al.* 2017; Calvén *et al.* 2020). Additionally, the CaSR does not appear to play a role in alarmin mRNA expression in this 2D model of basal NHBECs, which could be explained by low abundance of the receptor in these cells. Therefore, to better understand the role of the CaSR in these cells, we require a more suitable *in vitro* model with sufficient levels of CaSR expression to enable us to draw concrete conclusions of the potential PM-induced and CaSR-mediated effects in the airway epithelium. However, we have shown that *in vivo* exposure to IL-33 drives pro-inflammatory, asthma-related responses in the airways, which are significantly reduced by co-treatment with NAM (Huang, Unpublished). This reveals a role

for the CaSR in mediating alarmin-induced inflammation, however, the underlying CaSR-mediated mechanisms behind this, remain somewhat unclear.

The adenocarcinomic human alveolar basal epithelial cells (A549) cell line has been reported to express the CaSR, and therefore could provide a suitable model to assess the role of the CaSR in the airway epithelium (Cortijo, Milara, Mata, Donet, Gavara, Peel, Hall and E. J. Morcillo 2010b; Li *et al.* 2020). However, the role of the CaSR has been investigated previously in numerous cancers, where it appears to have conflicting roles in regulating proliferation, migration, differentiation, apoptosis, and angiogenesis depending on the location or origin of the cancer, where the CaSR appears to function in a "ying-yang" fashion as a tumour suppressor or oncogene (Tennakoon *et al.* 2016). Therefore, although the A549 cell line express the CaSR, using these to assess PM-induced and CaSR-mediated effects may skew the findings to the cancerous phenotype, which could be distinct from "normal" airway epithelial cells or even those from patients of lung diseases such as asthma. Additionally, A549 cells are alveolar epithelial cells, so therefore do not provide a model which recapitulates the *in vivo* exposure to PM, as bronchial epithelial cells are the first to encounter inhaled innocuous stimuli, such as PM. Therefore, we are yet to determine a suitable *in vitro* 2D model for better understanding of the effects of PM-exposure to airway epithelial cells.

Disparities between the 2D *in vitro* models available for use in assessing PM-induced effects in the airways highlights the necessity for more suitable *in vitro* models, which better recapitulate the human airway epithelium, and which express the CaSR, to enable us to further our understanding of the role of the CaSR in PM-induced effects in the airways. One way in which this could be addressed is by differentiation of the basal NHBECs at the air-liquid interface, resulting in a 3D *in vitro* model which recapitulates the pseudostratified human

bronchial epithelium *in vivo* and is now considered one of the gold standards for respiratory research. Additionally, as discussed in Chapter 3, my colleague Mrs Kasope Wolffs has confirmed most abundant expression of the CaSR in the ciliated cells of the bronchial epithelium, suggesting that this model would be suitable to assess the role of the CaSR in the airway epithelium. However, this *in vitro* model poses its own issues as application of PM to the apical surface of the 3D cell culture is difficult without a specialised exposure system, such as the SciReq's inExpose system.

As we did not have the tools available to perform these experiments in our laboratory at Cardiff University, during the final year of my PhD, I applied for a European Respiratory Society Long-Term Research Fellowship (aimed at all levels of early-career respiratory research) to visit the laboratory of Professor Philip Hansbro based in the University of Technology, Sydney, to perform these experiments. Although I was successful in gaining an interview and received positive feedback of my project proposal, lay summary, and interview, I did not receive the fellowship. However, I set up a collaboration with Prof. Hansbro for their laboratory to conduct experiments using the 3D *in vitro* model and their specialised SciReq's inExpose system, due to their experience and standing on the world stage regarding respiratory research. These experiments are planned for 2022 and will contribute to our investigation of the potential of CaSR-mediation of PM-induced effects in the airways, leading to a long-lasting collaboration and publication in high-impact journals.

5.4.2 The Potential Roles for The CaSR in Alveolar Macrophages:

In the previous chapter, I revealed that AMs express the CaSR on the protein level, by IHC, and on the mRNA level in lung macrophages from data obtained from The Human Protein Atlas online repository of scRNA-seq data. Currently, there is conflicting evidence of the effect of PM on phagocytotic functions, such as efferocytosis, partly due to our lack of understanding of the

mechanisms by which PM induces its harmful effects in airway cells. Therefore, in this chapter, I sought to investigate whether any alterations to PM-induced AM ability to efferocytosed apoptotic neutrophils was in any way mediated via the CaSR, thereby providing a potential underlying mechanism to better understand harmful PM-induced effects in AMs and provide a suitable *in vitro* model to assess the role of the CaSR in AMs. I reveal that 24-hr exposure of AMs to PM ± NAM induced reductions in AM efferocytosis, however, these findings were deemed to not be statistically significant. The reductions were never reduced to levels of the potent cytoskeletal rearrangement inhibitor, Cyt-D, therefore suggesting that PM ± NAM produced minor alterations to the ability of "healthy" AM to perform efferocytosis. There seems to be a lack of understanding of potential effects of PM on AM functions such as efferocytosis, however, conflicting evidence thus far could be partially explained the variations in PM and experimental setup used during these studies and the increased demand of phagocytotic functions of AMs during inflammation in response to PM exposure (Hiraiwa and Van Eeden 2013a; Moreira *et al.* 2020). Therefore, this highlights the need to generate suitable *in vitro* models to test the harmful effects induced by PM exposure, and uncover underlying mechanisms, such as CaSR activation, to produce a therapeutic, such as NAM, which has the potential to directly counteract PM-induced effects in airway cells, such as AMs.

Professional phagocytes such as AMs and DCs perform efferocytosis to remove apoptotic cells, such as neutrophils, from the airways to prevent necrotic cell build up, and release of pro-inflammatory cell contents, at sites of inflammation (Boada-Romero *et al.* 2020). Dysfunctional efferocytotic ability of AMs has been demonstrated in asthma and COPD patients, where apoptotic cells are significantly increased in the BALF from patients, compared to healthy controls, however, these findings do not describe a mechanism underpinning

AM dysfunction in asthma or COPD (Kasahara *et al*. 2001; Huynh *et al*. 2005; Bewley *et al*. 2016). In addition to dysfunctional efferocytosis, extracellular calcium levels at sites of inflammation are ~2 mM, a level sufficient to partially activate the CaSR and to result in perpetuation of a pro-inflammatory environment (Kaslick *et al*. 1970; Robertson *et al*. 1981; Brancaccio *et al*. 2002; Rossol *et al*. 2012a; Yarova *et al*. 2015; Geoffrey N Hendy and Canaff 2016; Centeno *et al*. 2019; Shridhar *et al*. 2019). However, during the current study, AMs were cultured in RPMI medium, with a Ca^{2+} concentration of 0.42 mM, much below that found at sites of inflammation, such as the airways of asthma or COPD patients, or for partial activation of the CaSR (Centeno et al 2019; Moon et al 2020). In addition, recognition of phosphatidylserine-binding proteins on apoptotic cells, an "eat me" signal, and uptake via efferocytosis has been demonstrated to be dependent on extracellular and intracellular Ca^{2+}, however, the mechanism behind the signalling pathways which induce calcium flux during functions such as efferocytosis is incompletely understood (Wang *et al*. 2017; Moon *et al*. 2020).

In Chapter 3, I revealed that the CaSR mediates PM-induced increases to intracellular calcium in HEK-CaSR cells, however, these effects were observed in the presence of 2 mM extracellular Ca^{2+} and therefore could go some way in explaining why there were only minor alterations to AM efferocytosis of these "healthy" AMs. These findings suggest that the low Ca^{2+} concentration contained within RPMI medium (0.42 mM), in combination with PM (30 µg/ml), would not have been sufficient to promote CaSR activation and CaSR-mediated functions in these cells. Therefore, increased serum Ca^{2+} or polyamine levels in asthma or COPD patients, in combination with exposure to PM, could contribute to dysfunctional AM efferocytosis, via the CaSR, where these findings also highlight the need for an experimental set up which better recapitulates the environment in which AMs are exposed to *in vivo*. Finally, as

the CaSR is abundantly expressed in these cells, modification of the experimental set up in this *in vitro* model could provide a vital tool in assessing potential PM-induced and CaSR-mediated effects in AMs.

Cell membrane ruffling and cytoskeletal rearrangements are crucial features of phagocytotic processes such as efferocytosis, which are important functions of professional phagocytes such as AMs (Canton *et al.* 2016a). These cytoskeletal rearrangements are driven via activation of Rho kinase-mediated intracellular signalling, which has been demonstrated to be downstream of CaSR activation and underpins morphological changes to macrophages and iDCs, HEK-CaSR cells, and oesophageal epithelial cells (Davies *et al.* 2006a; Abdulnour-Nakhoul *et al.* 2015; Canton *et al.* 2016a). Furthermore, members of the Rac subfamily of Rho family of GTPases have been previously uncovered to be key regulators of apoptotic cell engulfment, however, whether activation or inhibition of these mediators leads to enhanced phagocytotic functions, is unclear, however, this pathway provides a potential therapeutic target in professional phagocytes implicated in lung diseases such as asthma and COPD (Luo *et al.* 2011; Hallgren *et al.* 2012; Htwe *et al.* 2017; Majolée *et al.* 2019; Wang *et al.* 2020; Wu *et al.* 2021). Finally, exposure to PM has been demonstrated to induce Rho-mediated intracellular signalling pathway activation *in vitro* in PM-exposed airway epithelial cells, CSE-exposed murine cell lines of macrophages, and in an *in vivo* rat model of PM exposure (Chirino *et al.* 2017; Yan *et al.* 2017; Ito *et al.* 2020; Jheng *et al.* 2021). However, whether PM-induced activation of Rho-mediated intracellular signalling and potential effects on efferocytosis by professional phagocytes are mediated via the CaSR is yet to be determined.

Inhibition of the Rho kinase pathway (by the pan Rho kinase inhibitor PF4950834) has been demonstrated to significantly enhance COPD AM efferocytosis, however, the Rho kinase inhibitor induced no changes to efferocytotic ability in healthy ex-smoker control AMs (Bewley *et al.* 2016).

These findings suggest that first, Rho kinase inhibition, potential via treatment with NAM, could be a target for enhancing dysfunctional efferocytosis in AMs and secondly, may also add to the explanation of minor effects of PM ± NAM in these "healthy" AMs, due to limited effects of Rho kinase inhibition on healthy AMs. Together, this evidence suggests that the CaSR may play role in AM phagocytic functions such as efferocytosis, where CaSR-mediated membrane ruffling, and cytoskeletal changes are crucial for effective uptake and removal of apoptotic cells and debris such as PM. Moreover, NAM could provide an effective therapeutic, acting as a Rho/Rac inhibitor, to enhance dysfunctional efferocytotic ability of AMs in lung diseases such as asthma and COPD, however, further research is required to determine the roles of the CaSR in AMs.

5.4.3 Potential Roles for The CaSR in Dendritic Cells:

In the previous chapter, I revealed that immature and mature monocyte-derived DCs and myeloid DCs express the CaSR on the protein level, an observation which was corroborated on the mRNA level by the scRNA-seq data available on The Human Protein Atlas. Therefore, the data obtained provided suitable premise to investigate the potential of the CaSR in mediating PM-induced effects in DCs. Due to low abundance of myeloid DCs in the circulation, I used an established *in vitro* model of monocyte derived DCs to determine the potential of the CaSR in mediating PM-induced maturation and activation of DCs. In this chapter, I demonstrate that 24-hr exposure of DCs to PM drives increases in maturation levels, measured by increases in % CD83 expressing DCs, and activation, measured by secretion of IL-10, IL-23p40 and IL-6, which corroborates previous studies (Matthews et al. 2014; Mann et al. 2017; Pfeffer et al. 2018). Furthermore, I reveal that maturation and IL-10 and IL-23p40 (once baseline corrected) secretion is significantly reduced by co-treatment with NAM, suggesting that the CaSR plays a role in DC maturation

and some aspects of activation and thereby contributes to the pro-inflammatory response induced by inhaled innocuous stimuli, such as PM. Therefore, NAM could provide an effective therapeutic to counteract PM-induced pro-inflammatory responses in the airways of asthma and COPD patients, by both reducing chronic airway inflammation and exacerbations induced by PM exposure and is a common feature of lung diseases such as asthma and COPD.

During this chapter, I used an established model of monocyte-derived DCs, to study the potential involvement of the CaSR in PM-induced maturation and activation of DCs. This model has been previously established at our collaborator's laboratory at King's College London, due to limited material abundance of myeloid DCs, and therefore provides a suitable *in vitro* model to assess effects of PM ± NAM, with comparable functional outputs to myeloid DCs and are not limited by abundance (Ho et al, Unpublished). To investigate maturation levels of DCs, in response to PM ± NAM, I used CD83 as an established marker for mature DCs, as this is a key regulator of maturation, activation, and homeostasis of mature DCs (Prechtel and Steinkasserer 2007; Li *et al.* 2019). In addition, CD83 has been previously targeted as a potential therapeutic avenue for inflammatory diseases such as asthma and COPD, however, no currently available treatments directly and effectively target CD83 expression in DCs, which highlights the complexity of targeting specific molecules to regulate immune responses and proposes the CaSR as a more suitable, upstream therapeutic target for inflammatory lung diseases (Gómez *et al.* 2004; Prazma and Tedder 2008; Li *et al.* 2019). In addition, DC exposure to asthma-associated cytokines TNF-α and IL-1ß and PM has been previously linked to increased CD83 expression and therefore increased maturation of DCs, and leads to pro-inflammatory responses *in vivo* (Pfeffer et al. 2018; Wu et al. 2018). Therefore, during this study, I sought to determine the potential

of CaSR-mediation of DC maturation in response to PM. First, I used the potent drivers of DC maturation, TNF-α and IL-1ß, as a positive control, which allowed me to clearly gate CD83 expressing DC from the FMO CD83 control (no CD83 conjugated to APC fluorochrome). Then, I applied the gating strategy to the PM-exposed DC data, where I observed less clear separation between the CD83 expressing DCs and FMO CD83 control, which was indicative of a less pronounced effect of PM on DC maturation, compared to TNF-α and IL-1ß, confirmed in subsequent analysis by a reduced percentage of CD83 expressing DCs after PM-exposure, compared to those treated with TNF-α and IL-1ß. Once I had confirmed maturation in response to these drivers, I then determined that NAM significantly reduces both PM and TNF-α and IL-1ß-induced maturation of DCs. This demonstrates that the CaSR plays a key role in DC maturation, in response to distinct drivers of inflammation, however, the precise CaSR-mediated intracellular signalling pathways underpinning DC maturation in response to these stimuli, are yet to be determined.

During Chapter 3, I demonstrated that the CaSR is directly activated by PM, suggesting that in DCs, PM-induced activation of the CaSR could be one of the mechanisms behind DC maturation, however, TNF-α and IL-1ß have not been shown to directly activate the CaSR, which suggests that these potentially drives DC maturation through indirect activation of the CaSR. During this study, DCs were cultured and exposed to treatments made up in RPMI medium, which as discussed in Section 5.4.2 of this Chapter, has a Ca^{2+} concentration of 0.42 mM, much below that found at sites of inflammation, such as the airways of asthma or COPD patients, or for partial activation of the CaSR (Centeno *et al.* 2019; Moon *et al.* 2020). Even so, I revealed that the CaSR plays a role in DC maturation and activation, however, further establishment of this model is required to better recapitulate the *in vivo* environment of DCs during key inflammatory functions, to better understand the role of the CaSR

of DCs during inflammation, in response to a variety of stimuli. During inflammation *in vivo*, there are increased levels of circulating cytokines such as TNF-α and IL-1ß and sites of inflammation are well known to have increased extracellular Ca^{2+} levels, which contribute to the perpetuation of the viscous cycle of inflammation, which is a key feature of the pathogenesis of lung diseases, such as asthma and COPD (Kaslick *et al.* 1970; Robertson *et al.* 1981; Brancaccio *et al.* 2002; Rossol *et al.* 2012a; Geoffrey N Hendy and Canaff 2016; Lambrecht *et al.* 2019; Shridhar *et al.* 2019). In previous studies, TNF-α and IL-1ß exposure to colonocyte cell lines, healthy human ASM cells, and an LPS-induced murine macrophage cell line, results in increases in CaSR expression on both the mRNA and protein level, suggesting that the CaSR is a key player during inflammation, in response to a variety of stimuli, in a range of cell types (Kelly *et al.* 2011; Fetahu *et al.* 2014; Yarova *et al.* 2015). Furthermore, the CaSR is a critical regulator of IL-1ß release, through CaSR-dependent activation of the NLR Family Pyrin Domain Containing 3 (NLRP3) inflammasome, an important mechanism during the pathogenesis of asthma, which further proposes the CaSR as a key player during inflammation (Lee *et al.* 2012a; Lee *et al.* 2017). Together, increased levels of circulating cytokines and increased extracellular Ca^{2+}, provoke alterations to the expression of the lung CaSR, which in turn potentially increases CaSR sensitivity to exogenous and endogenous stimuli. Therefore, the CaSR could be a key contributor to the perpetuation of the pathogenesis of lung diseases, such as asthma and COPD, however, the precise CaSR-mediated intracellular mechanisms underpinning this, remains unclear.

Along with AMs, many DC functions, such as maturation, are dependent on actin cytoskeletal rearrangements, for the development of characteristic dendrites and the immunological synapse between DCs and T cells, linking innate and adaptive immunity (Matthews et al. 2014; Liu and Roche 2015;

Mann et al. 2017; Pfeffer et al. 2018). Cytoskeletal rearrangements occur via alterations to the f-actin network and is important in features of immune cells, such as the lamellipodia extension/retraction cycle and stress fibre formation, in response to exposure to a variety of pro-inflammatory stimuli, such as LPS and high extracellular Ca^{2+}, in DCs and HEK-CaSR cells. These occur through several effectors, such as Rho kinases (RhoA), and intracellular Ca^{2+} signalling, which are downstream of CaSR activation, suggesting the CaSR could play a role in mediating cytoskeletal rearrangements associated with key functions of DCs (Al-Alwan *et al.* 2001; Bagley *et al.* 2004; Giannone *et al.* 2004; Verdijk *et al.* 2004; Davies *et al.* 2006a; Vaeth *et al.* 2015). Furthermore, CaSR-mediated activation of RhoA leads to stress actin fibre assembly and can be inhibited (to control levels) by NAM, in HEK-CaSR cells, with no activation of RhoA in HEK-0 cells, suggesting a key role for the CaSR during this key function (Davies *et al.* 2006a). Together, these results suggest cytoskeletal rearrangements, a mechanism which underpins many functions of immune cells, could be mediated via the CaSR, in response to a variety of pro-inflammatory stimuli.

It has been reported that RhoA expression is upregulated in human asthmatic lungs and is increased in response to asthma-associated cytokines, in a range of *in vitro* and *in vivo* models (Chiba *et al.* 2009; Wang *et al.* 2020). However, the studies focused on RhoA expression in the structural lung cells which are associated with bronchial smooth muscle contraction and AHR, rather than the role of RhoA in immune cell functions, such as maturation of DCs. Nevertheless, other studies have described a role for RhoA during inflammatory responses, to a variety of pro-inflammatory, asthma-associated stimuli, driven by DC maturation, migration to lymph nodes, and antigen presentation to naïve T cells. These functions of DCs drive innate and adaptive immune responses such as, inflammatory cell airways infiltration, cytokine release, and Th17 cell differentiation, forming the immunological synapse

between innate and adaptive immunity (Henry *et al.* 2005). These studies have also demonstrated that genetic ablation or pharmacological inhibition of RhoA reduces airways inflammation, and migration of DCs, suggesting that inhibition of RhoA signalling could be an effective therapeutic target for a multitude of asthma features, mediated via DC activation (Nitschké *et al.* 2012). As activation of RhoA is downstream of CaSR signalling, this suggests the CaSR may play a role in Rho-mediated features of both structural and immune cells present in asthmatic airways, however, further work is required to identify potential additional CaSR-mediated functions in DCs which would allow for further assessment of the effectiveness of NAM as a potential therapeutic for lung diseases such as asthma and COPD. Cytokine release patterns from DCs also alter following exposure to a range of pro-inflammatory stimuli, such as PM, in a process that has been demonstrated to be specific to the pro-inflammatory driver that DCs are exposed to, to induce an appropriate inflammatory response.

PM-exposure has been demonstrated to induce activation of DCs, culminating in release of specific cytokines, such as IL-10, IL-6 and IL-23p40, which assist in driving innate and adaptive immune responses, through the development of the immunological synapse (Matthews *et al.* 2016; Mann *et al.* 2017; Glencross *et al.* 2020). However, the precise mechanisms underpinning DC release of specific cytokines in response to PM-exposure are poorly understood. During this chapter, I demonstrate that PM-induced IL-10 release from DCs is partially mediated via the CaSR, as NAM co-treatment significantly reduces PM-induced IL-10 release, in an established *in vitro* model of monocyte-derived DCs. In contrast, PM-induced IL-6 or IL-23p40 release was not affected by co-treatment with NAM, suggesting the CaSR does not play a role in PM-induced secretion of IL-6 or IL-23p40 from DCs. However, there was large patient-patient variability in values obtained for each cytokine and so to correct for the

large variability within these data, I performed a baseline correction (set all values as a percentage of the PM-only treated DCs, set at 100%). I reveal that PM-induced IL-23p40 secretion is also significantly reduced by co-treatment with NAM, however, there was no effect of NAM on PM-induced IL-6 release. These data suggest that the CaSR plays a partial role in cytokine release from PM-exposed DCs, however, the mechanisms underpinning PM-induced and CaSR-mediated secretion of a range of pro- and anti-inflammatory cytokines, from a variety of airway immune and structural cells, are yet to be determined.

Upon stimulation by innocuous stimuli, such as PM, DCs trigger a Th1 or Th2 immune response through antigen presentation to T cells, however, they also release IL-10, as an "anti-inflammatory" cytokine, which acts in a paracrine and autocrine fashion to block the process of DC maturation, and skews the Th1/Th2 balance, leading to subsequent Th2-type inflammatory responses *in vivo* (De Smedt *et al*. 1997; Corinti *et al*. 2001; Fukao *et al*. 2001). Upon maturation, DCs become unresponsive to IL-10, and therefore can go on to activate adaptive arms of the immune system and promote a pro-inflammatory response in the airways (Steinbrink *et al*. 2002). Moreover, not only is IL-10 a major player in regulating functions of DCs, such as maturation, IL-10 release by a range of immune cells signals inhibition of Th1 cells, NK cells monocytes and macrophages and therefore a dampening of immune responses, and other inflammatory cytokines, such as IL-6, leading to its classification as an anti-inflammatory cytokine (Couper *et al*. 2008). However, cells which are effectively "switched off" by IL-10 also play an important role in pathogen clearance and therefore, although IL-10 is thought to be anti-inflammatory, sustained release of IL-10 from immune cells can lead to impaired pathogen control and subsequent immunopathology, leading to perpetuation of pro-inflammatory responses in already inflamed airways, such as those in asthma or COPD patients (Couper *et al*. 2008).

During the pathogenesis of asthma, IL-10 levels appear diminished, however, in novel diseases such as COVID-19, there are elevated levels of IL-10. This suggests that both diminished and elevated IL-10 levels during the pathogenesis of these diseases can be responsible for potentiation of pro-inflammatory responses, proposing a potential dual role for IL-10 during the pathogenesis of distinct lung diseases (Raeiszadeh Jahromi *et al.* 2014; Islam *et al.* 2021). The mechanisms underpinning the role of IL-10 during inflammatory diseases, remains unclear, however, the CaSR has been previously linked to IL-10 release in neutrophils, in response to potent neutrophil stimulator, N-formyl-Met-Leu-Phe (fMLP), which promotes neutrophil stimulation by formation of transient intracellular Ca^{2+} oscillations, which are partially driven through the CaSR (Rey et al 2006; Zhai et al 2017). Interestingly, PAM induced a significant reduction in IL-10 release, in response to fMLP treatment, however, NAM significantly enhanced IL-10 release from fMLP-exposed neutrophils, further adding to the complexity of the potential duality of IL-10, in response to a variety of pro-inflammatory stimuli, in a range of cell types (Zhai *et al.* 2017). Therefore, this evidence proposes the CaSR as a potential modulator of IL-10 release during the pathogenesis of lung diseases, such as asthma and COPD, however, the intracellular mechanisms underpinning potential CaSR-mediated IL-10 release requires further work. Modulation of IL-10 levels has been proposed as a potential treatment for inflammatory diseases, such as asthma and COPD, as IL-10 imbalance is thought to partially underpin disease pathogenesis. However, the biological form of IL-10 is an unstable homodimer, with a short half-life and easily degradable *in vivo*, highlighting the difficulties in using IL-10 as a treatment for inflammatory lung diseases, such as asthma or COPD (Minshawi *et al.* 2020). The complexity which underlies the roles of IL-10 during inflammation highlights the necessity for better understanding of the influence of the cytokine environment on key functions of DCs, such as maturation and the

potential involvement of the CaSR in these functions. This suggests that NAM could provide a potential effective upstream therapeutic to ameliorate PM-induced IL-10 release and propagation of pro-inflammatory responses.

During the analysis of these experiments, I also measured changes in IL-23p40 and IL-6 release in response to PM ± NAM, demonstrating that although PM drives an increase in release of these cytokines, following baseline correction, NAM significantly reduces PM-induced IL-23p40 but not IL-6 release from DCs. IL-23p40 is a heterodimeric cytokine which contains disulphide-lined p35 and p40 subunits with IL-12, therefore, the beads used for detection of this cytokine during these experiments allowed us to measure release of both cytokines in response to PM-exposure to DCs (Lupardus and Garcia 2008). However, PM exposure to DCs has been previously shown to induce IL-23p40 release specifically and therefore measures of IL-23p40 cytokine could be accurately made using the beads targeted to this heterodimeric cytokine (Mann *et al.* 2017). DCs secrete IL-23p40 to promote the development of a mostly neutrophilic immune response by driving migration of mature DCs to lymph nodes, to initiate differentiation of both Th1 and Th17 cells which highlights IL-23p40 as a both a trigger and maintenance pro-inflammatory response to stimuli, such as PM during the pathogenesis of lung diseases, such as asthma and COPD (Oppmann *et al.* 2000; Cua *et al.* 2003; Langrish *et al.* 2005; Reinhardt *et al.* 2006; Teng *et al.* 2015). Since DCs and macrophages are the major cellular sources of IL-23p40, it would be important to undertake further analysis of these cell types to better understand the potential role of the CaSR in release of PM-associated cytokines and the potential synergy between cytokines in initiating and maintaining inflammatory responses to PM-exposure (Tato and Cua 2008).

IL-6 functions to block the DC maturation process, *in vivo*, and therefore maintains DCs in an immature, antigen capturing and processing state, to drive

influx of blood-derived inflammatory cells and perpetuate inflammation, highlighting IL-6 as a key regulator of maturation in DCs (Park *et al.* 2004; Peng *et al.* 2010; Matthews *et al.* 2016; Mann *et al.* 2017). Moreover, IL-6 has also been demonstrated to drive upregulation of CaSR expression, which could potentially sensitise DCs to PM-induced and CaSR-mediated maturation and activation, and therefore contribute to the vicious cycle of inflammation and acute exacerbations observed in patients with lung diseases, such as asthma (Rossol et al. 2012; Yarova et al. 2015; Hendy and Canaff 2016). Although during the current study, I reveal that the CaSR does not play a role in IL-6 secretion from PM-exposed DCs, there are other sources of IL-6 secretion in the airways of asthma patients, such as the airway epithelium, where cationic CaSR activators, such as poly-L-arginine, drive secretion of IL-6 from epithelial cells *in vitro*, suggesting a role for the CaSR in IL-6 release from alternative airway cells (Marini *et al.* 1992). Moreover, NAM has been shown to be effective against IL-6 release in response to a variety of pro-inflammatory stimuli and in a range of cell types, however, this has not been previously investigated in the lung (Chiarini *et al.* 2020).

5.3.4 CaSR Activators are Present in Particulate Matter:

In this chapter, I also reveal that PM contains an array of CaSR agonists, such as calcium, cadmium, and nickel, which are partially soluble in culture medium, as confirmed by ICP/MS. Although efforts have been made to reduce calcium emissions specifically, the levels remain at a steady rate from 2009 to today, especially from sources such as quarrying, where 53% of calcium emissions in the UK were attributed to this sector in 2019 (Department for Environment 2020). This supports our hypothesis of the potential of the CaSR as an airway sensor for inhaled innocuous stimuli, such as PM, and in response to soluble components of PM which persist in the circulation, when go on to cause harmful effects in other organs or tissues, some of which express the CaSR.

Therefore, the CaSR could be a common underlying mechanism which drives key pro-inflammatory processes, in a range of cell or tissue types and thereby directly contributes to the pathogenesis of inflammatory diseases. Therefore, NAM provides an upstream mechanism which could potentially counteract the harmful, pro-inflammatory effects brought about by exposure to PM. However, further work is required to better establish these CaSR-expressing *in vitro* models for testing our hypothesis, to contribute to our understanding of the role of the airway CaSR during physiology and pathophysiology.

Unfortunately, due to COVID-19-related restrictions, I did not investigate other functions which potentially rely on CaSR-mediated cytoskeletal rearrangements during this study, such as those involved in uptake of PM by AMs and DCs. However, as mentioned above, downstream effectors of CaSR signalling have been demonstrated to be involved in cytoskeletal rearrangements, one of the key features of uptake functions such as macropinocytosis. The CaSR has been demonstrated to mediate the constitutive form of macropinocytosis in human monocyte derived DCs and macrophages, where this form is dependent on extracellular Ca^{2+}, and is significantly reduced by NAM, without a detrimental effect on other endocytic processes, such as phagocytosis (Canton et al. 2016). Furthermore, cells which exclusively undergo growth factor driven macropinocytosis, such as HEK293 cells, can be rendered constitutively macropinocytotic by expressing the CaSR in these cells, suggesting that expression of the CaSR establishes a growth factor-independent mechanism for macropinocytosis in cells which would not usually perform constitutive macropinocytosis (Bouschet et al. 2007; Canton et al. 2016). These data suggest that activation of the CaSR in AMs or DCs, by PM, could drive uptake of PM via functions such as macropinocytosis, and contribute to PM-induced effects in AMs and DCs.

5.4.4 General Discussion Points:

Together, these data suggest that the CaSR plays roles in driving PM-induced effects in NHBECs, AMs and DCs, leading to initiation and maintenance of both innate and adaptive immune responses during the pathogenesis of lung diseases, such as asthma and COPD. Through direct and indirect activation of the CaSR by inhaled innocuous stimuli, such as PM, NAM could provide an "off-switch" to these responses, to control levels, without completely diminishing responses to pro-inflammatory stimuli, such as PM. The precise mechanisms underpinning PM-induced and CaSR-mediated functions in these cells, have not yet been fully elucidated, however, our laboratory has previously demonstrated that NAM is effective against OVA, IL-33, and LPS-induced aspects of remodelling, tissue and BALF inflammation and AHR in animal models of asthma and COPD (Yarova *et al.* 2015; Yarova *et al.* 2016; Huang *et al.* 2019; Yarova *et al.* 2021). This highlights a multi-faceted role for the CaSR in a range of airway cells, where it mediates features of human asthmatic airways, in response to a variety of pro-inflammatory stimuli. Therefore, targeting the CaSR by NAM, provides an upstream mechanism to reduce chronic inflammation, remodelling, and AHR associated with asthma pathogenesis. NAM could provide a mechanism through which multiple aberrant intracellular signalling pathways, associated with the pathogenesis of lung diseases, can be ameliorated, in a multitude of cell types, thereby providing an effective "all in one" therapeutic for sufferers of lung diseases, such as asthma.

5.5 Future Directions:

This chapter highlights the potential roles of the CaSR in airway cells, in response to exposure to innocuous stimuli, such as PM, however, further research is required to better understand the CaSR-mediated signalling

pathways activated by PM in the airways, to identify those underpinning CaSR-mediated and PM-induced effects, in the airways.

First, based on data provided in online repositories of sc-RNAseq data, and discussed in the previous chapter, the most abundant CaSR expressing cells in the airways are the ciliated cells (The Human Protein Atlas). Differentiation of basal NHBECs at the air-liquid interface results in generation of a pseudostratified epithelium which better recapitulates the human airway *in vivo* and is considered the gold standard of respiratory research. However, specialised, and unique exposure systems, such as the Inexpose™ system, are required to deliver PM to the ciliated cells, on the apical side of the layer, as these are the first to encounter inhaled innocuous stimuli such as PM. Therefore, as mentioned during the discussion of this chapter, I have forged a collaboration with Professor Hansbro at The University of Technology Sydney, where they have an established *in vitro* model of the human airway epithelium and an Inexpose™ system. Professor Hansbro and his laboratory are planning to carry out exposure of NHBECs (grown at the air-liquid interface) to PM ± NAM, to better assess the potential of NAM as an effective therapeutic for PM-induced or exacerbated lung diseases, such as asthma and COPD.

Secondly, it would be important to establish a simpler *in vitro* model of monocyte-derived macrophages and continue working with the monocyte-derived DCs and provide models which recapitulate both "normal" and inflamed environments, by altering extracellular Ca^{2+} levels and addition of mediators of inflammation, such as TNF-α and IL-1ß. These models would allow us to better understand whether previously determined CaSR-mediated effects in these cells, such as macropinocytosis and NLRP3 inflammasome activation, can be driven through direct activation of the CaSR by PM. This would be instrumental in deepening our understanding of the potential PM-induced and CaSR-mediated effects in these cells and provide more relevant

in vitro models which better recapitulate the *in vivo* environment. Moreover, to better understand the CaSR-mediated signalling pathways associated with key functions of macrophages, inhibition of specific downstream intracellular signalling pathways, such as RhoA, could be used to understand which intracellular signalling pathways associated with key functions of these cells are CaSR-mediated, by direct comparison with NAM. This would further knowledge into which CaSR-mediated signalling pathways underpin key functions of macrophages and DCs and therefore are potentially targetable by NAM, during the pathogenesis and acute exacerbations associated with lung diseases, such as asthma.

In addition, DCs provide a unique link between the innate and adaptive immune systems and therefore, using conditioned medium from PM ± NAM exposed DCs and applying this to T-cell populations would allow us to identify a potential role for the CaSR in mediating adaptive immune responses, as well as the innate immune responses revealed in this chapter. Finally, to validate our findings and to understand whether NAM could be an effective therapeutic for lung diseases, such as asthma, it would be important to corroborate the CaSR-mediated functions revealed in "healthy" cells and extend this to diseased cells, such as those from asthma or COPD patients, which have altered functions to their healthy counterparts. Together, this evidence could propose the CaSR as an upstream mechanism to effectively treat lung diseases, such as asthma and COPD, and provide a targetable mechanism for harmful PM-induced effects in the airways.

5.6 Conclusions:

This chapter reveals that the CaSR could play a multitude of roles, *in vivo,* during PM-induced airways inflammation, in a range of airway structural and immune cells. This data lays basis for further establishment of these *in vitro* models, to provide suitable models to further assess the roles of the CaSR in

mediating PM-induced effects in the airways and deepen our knowledge and understanding of the CaSR as a potential key regulator of inflammatory responses to inhaled noxious stimuli.

CHAPTER 6: GENERAL DISCUSSION, CONCLUSIONS AND FUTURE DIRECTIONS.

Exposure to PM is a major problem worldwide and contributes to acute exacerbations of lung diseases, such as asthma, COPD, and more recently, IPF (Atkinson *et al*. 2012; Winterbottom *et al*. 2018), however, the underlying mechanisms behind PM-induced responses are poorly understood. Given that the CaSR has been implicated in T2 and non-T2 asthma (Yarova *et al*. 2015; Yarova *et al*. 2016; Huang *et al*. 2019) and the presence of potential CaSR activators contained within PM, I hypothesised that the CaSR comprises one of the mechanisms which mediates PM-sensing and downstream pro-inflammatory responses, in a range of human cell types typically associated with the pathogenesis of asthma.

6.1 Key Findings:

1. PM directly activates the CaSR in HEK-CaSR cells, by increasing intracellular Ca^{2+}, an effect which can be abolished by co-treatment with NAM and that is not observed in HEK-0 cells, which lack the CaSR
2. The CaSR is expressed at the protein level in airway epithelial cells and lung- and blood-derived immune cells, involved in sensing and responding to inhaled PM, and in the pathogenesis of lung diseases which are exacerbated by exposure to PM
3. Undifferentiated basal NHBECs are characterised by low functional expression of the CaSR, using intracellular Ca^{2+} as a biological readout for CaSR activation
4. Exposure of PM to "Healthy" AMs does not affect efferocytosis, a key resolving function of AMs
5. The CaSR plays a key role in PM- and pro-inflammatory cytokine-induced maturation of DCs, and PM-induced cytokine secretion by DCs, effects which are reduced by NAM.

Together, my thesis proposes the CaSR as a key multimodal chemosensor for PM in the airways and potentially comprises one of the mechanisms underpinning PM-induced pro-inflammatory responses in a range of airways cells associated with inflammatory lung diseases. Moreover, NAM comprise a potential effective therapeutic to target pollution-induced exacerbations of lung diseases, such as asthma, especially those with difficult-to-treat, severe asthma.

6.2 The CaSR is Directly Activated by Particulate Matter:

In my thesis I demonstrated that the CaSR is directly activated by PM and caused an increase in intracellular Ca^{2+} in HEK-CaSR cells, an effect which was abolished by NAM and not observed in HEK-0 cells. These findings provided suitable premise to assess the potential of the airway CaSR as a key sensor and responder to inhaled PM during Chapters 4 and 5 of my thesis. To contribute to my findings, further work is required to assess the influence of PM on known downstream effectors of CaSR activation, such as: PI3K/Akt (Ward 2004; Zhang et al. 2020a), mTOR (Rybchyn *et al.* 2019), ERK/MAPK (Ward 2004; Physiology et al. 2008; Zhang et al. 2020) and RhoA (Min et al. 2002; Ward 2004; Zhang et al. 2017). These experiments would aid in our understanding of the roles of the CaSR in mediating PM-induced airways responses and assess the potential of NAM as an "all in one" therapeutic to reduce multiple pro-inflammatory signals during the pathogenesis of PM-exacerbated lung disease.

6.3 The CaSR is Expressed in Airway Epithelial and Lung- and Blood-Derived Immune Cells Associated with Particulate Matter-Exacerbated Lung Diseases:

During my studies, I demonstrated that the CaSR is expressed at the protein level in airway epithelial and tissue-resident and blood-derived immune cells involved in sensing and responding to inhaled PM and associated with the pathogenesis of lung diseases. These findings supported my hypothesis and

allowed for establishment of CaSR-expressing *in vitro* models to further test the role of the CaSR in mediating PM-induced cellular responses.

The CaSR has been implicated in the pathogenesis of T2 and non-T2 asthma, using *in vivo* models (Yarova *et al*. 2015; Huang *et al*. 2019) and the CaSR protein has been demonstrated to be increased in ASM cells obtained from mild-moderate asthmatic patients, compared to controls (Yarova *et al*. 2015). Therefore, better understanding of the differences in expression of the CaSR in different airways cell types during mild-moderate asthma and difficult-to-treat, severe asthma, would contribute to our assessment of the role of the CaSR during the pathogenesis of distinct endotypes of asthma. Understanding CaSR distribution during the pathogenesis of these lung diseases would also allow us to predict which endotypes of asthma patients would best respond to NAM treatment, according to the levels of the CaSR, which would aid in the clinical advancement of NAM for different endotypes of asthma.

Due to ongoing COVID-19 restrictions in our laboratory during 2020, I decided to apply for a long-term Research Fellowship with the European Respiratory Society (ERS), to visit world-renowned laboratories of asthma and PM research in Sydney, Australia. One of the aims was to assess the potential alterations to CaSR expression in distinct lung cell types of *in vivo* models of difficult-to-treat, severe asthma developed in the laboratory of Prof Hansbro (Horvat *et al*. 2007; Singanayagam *et al*. 2015; Hansbro *et al*. 2017) and PM-exposure (Chan *et al*. 2019), developed in the laboratory of Prof Brian Oliver. Despite me not obtaining the fellowship, an ongoing collaboration with Prof Hansbro will explore this aim during 2022, where we will maximise data output of lung scRNA-seq data repositories of past experiments using their world-renowned *in vivo* models of difficult-to-treat, severe asthma to determine whether CaSR expression is altered in these models.

6.4 The CaSR plays roles in PM-induced effects in key airways cells:

6.4.1 The CaSR is Not Functionally Expressed in An in vitro Model of Basal Normal Human Bronchial Epithelial Cells:

The *in vitro* model of basal NHBECs used during my studies demonstrated a lack of functional activity of the CaSR, assessed by increases to intracellular Ca^{2+}. However, previous studies have shown that NHBECs express functionally active CaSR (Cortijo et al. 2010) and respond to the PM used in my study (Pfeffer et al. 2018). Therefore, my findings suggest that PM-induced cellular responses are not due to CaSR-mediated increases to intracellular Ca^{2+} in this model. In future studies, further testing of alternative CaSR-mediated intracellular signals, such as activation of PI3K/Akt (Ward 2004; Zhang et al. 2020a), mTOR (Rybchyn *et al.* 2019), ERK/MAPK (Ward 2004; Physiology et al. 2008; Zhang et al. 2020) and RhoA (Min et al. 2002; Ward 2004; Zhang et al. 2017) in my *in vitro* model of basal NHBECs is required to better understand whether the CaSR is functionally active in these cells and assess its role in mediating PM-induced basal NHBEC responses.

To better assess the role of the CaSR in mediating PM-induced airway epithelial cell responses, future experiments should utilise a 3D *in vitro* model of the differentiated airway epithelium, such as HBEC ALI, with presence of CaSR-expressing ciliated epithelial cells (Wolffs *et al.* 2020). Furthermore, utilising a specialised exposure system to aerosolise PM would better recapitulate the airways exposure to PM *in vivo*.

Assessing the role of the airway epithelial CaSR in response to PM exposure, comprised one of the main aims of my ERS fellowship application. Due to our ongoing collaboration with Prof Hansbro's laboratory, experiments are planned for 2022 using their established HBEC ALI (healthy and asthmatic) and specialised exposure system as a relevant *in vitro* model uniquely available in his laboratory. In addition, experiments planned with Prof Brian Oliver

(University of Technology Sydney) will allow us to assess the *in vivo* efficacy of NAM against PM-induced airway epithelial cell responses, associated with asthma pathogenesis. Here we plan to use IHC analysis performed on lung tissue obtained from these animals and analysing these using our established quantitative image analysis platform (Yarova *et al.* 2021). These experiments would provide crucial understanding of the role of the CaSR during PM-induced cellular responses *in vitro* and *in vivo* and continue to propose NAM as an effective therapeutic for asthma and other PM-exacerbated lung diseases.

6.4.2 Particulate Matter Exposure to Alveolar Macrophages Does Not Alter Ability to Efferocytose Apoptotic Neutrophils:

I also demonstrated that PM does not alter the ability of AMs to efferocytose apoptotic neutrophils *in vitro*, an important resolving feature of AMs (reviewed in Greenlee-Wacker 2016), where my data add to the current conflicting evidence on the influence of PM on AM functions (Hiraiwa and Van Eeden 2013). Since my experiments did not reveal a role for the CaSR during this function, future experiments could investigate alternative known CaSR-mediated functions of macrophages such as macropinocytosis and activation of the NLRP3 inflammasome, where CaSR has been previously involved, and the dysregulation of which has been associated with the pathogenic features of lung diseases (Hiraiwa and Van Eeden 2013b; Canton *et al.* 2016b; Zheng *et al.* 2018; Wang *et al.* 2020).

6.4.3 The CaSR is a Mediator of Dendritic Cell Maturation in Response to Particulate Matter and Pro-Inflammatory Cytokines:

In line with previous findings (Matthews *et al.* 2016), I demonstrated that DC maturation induced by exposure to PM and to pro-inflammatory cytokines (TNF-α and IL-1ß). I also demonstrated that both PM- and TNF-α and IL-1ß-induced DC maturation was mediated via the CaSR using NAM as a

pharmacological tool to assess involvement of the CaSR in this function. In addition, I demonstrated that PM induces secretion of pro-inflammatory cytokines from DC, where NAM inhibited some, but not all the cytokines secreted in response to PM exposure.

Investigation of alternative DC responses induced by PM, were beyond the scope of my thesis, due to COVID-19 restrictions in Cardiff and Guy's Hospital. Therefore, further work is required to better understand the influence of PM on alternative known CaSR-mediated DC functions such as constitutive macropinocytosis (Canton et al. 2016) and NLRP3 inflammasome activation (Lee et al. 2012). Additionally, further work is required to assess the role of the CaSR in PM-induced functions of DC, such as generation of ROS and activation and expansion of T cells, which comprise part of the adaptive immune system (Matthews *et al.* 2016; Mann *et al.* 2017). These data would determine whether the CaSR comprises a master mediator of PM-induced pro-inflammatory responses in DC and continue to propose NAM as an effective therapeutic for PM-exacerbated lung diseases, such as asthma.

6.5 Proposed mechanisms of Particulate Matter-Induced Effects in the Airways and the Potential Involvement of the CaSR:

The CaSR is likely to represent one of several mechanisms behind PM-induced airways responses, therefore, in this section I provide a holistic view of the alternative mechanisms thought to underpin some PM-induced responses, such as the influence of extracellular Ca^{2+} during disease, activation of TLR by PM, and generation of ROS during PM-induced cellular responses, and link these to current knowledge regarding the potential roles of the CaSR in mediating some of these effects.

6.5.1 Potential Involvement of The CaSR in Mediating Effects of Elevated Extracellular Ca^{2+}, which Drives and Contributes to the Pathogenesis of Lung Diseases:

In humans, extracellular Ca^{2+} concentrations are tightly maintained within a range of 0.9 -1.7 mM (Vardhan and Hutchison 2017). Elevated serum Ca^{2+} levels are associated with chronic inflammation which primes airway cells to inhaled substances, during the pathogenesis of lung diseases (Kaslick et al. 1970; Robertson et al. 1981; Brancaccio et al. 2002; Rossol et al. 2012; Hendy and Canaff 2016; Shridhar et al. 2019). Interestingly, Ca^{2+} and other CaSR agonists were some of the most abundant metals contained within the PM used during my studies and I revealed that the CaSR could comprise an environmental sensor to exogenous stimuli, such as inhaled PM. Endogenous CaSR agonists include elevated serum Ca^{2+} levels during inflammation, which promotes partial activation of the CaSR, rendering airway cells to a hyperresponsive state, where the airways have increased sensitivity to inhaled stimuli which drive the pathogenesis and acute exacerbations of asthma (Yarova *et al.* 2015). Extracellular Ca^{2+} also drives chemotaxis of monocytes, a key function during pro-inflammatory responses to inhaled stimuli, such as PM. This was demonstrated to be mediated via the CaSR, as similar effects were observed with PAM (NPS R-467) (Olszak *et al.* 2000). These findings highlight a role for the CaSR during key pro-inflammatory functions, in a range of airways cell types. In addition, these findings promote NAM as an effective therapeutic to reduce PM-induced cellular responses associated with the pathogenesis and acute exacerbations of lung diseases.

Furthermore, activation of the CaSR has been demonstrated to promote NLRP3 inflammasome activation and release of inflammatory cytokines such as IL-6 and IL-1ß, in a range of cell types which contribute to the pathogenesis of lung diseases and have been associated with PM-exposure (Broide *et al.* 1992; Rossol *et al.* 2012a). In addition, both IL-6 and IL-1ß have been

demonstrated to drive upregulation of the CaSR, providing evidence that the CaSR is important in mediating and maintaining pro-inflammatory environments which contribute to the pathogenesis and acute exacerbations of lung diseases (Rossol et al. 2012; Yarova et al. 2015; Hendy and Canaff 2016).

6.5.2 Potential Involvement of The CaSR in Toll-like Receptor-Mediated Responses to Particulate Matter:

Recently, $PM_{2.5}$ specifically, has been demonstrated to directly activate TLR4, which culminates in activation of NF-κß, the NLRP3 inflammasome, and MAPK (Tang *et al.* 2019b; Nagappan *et al.* 2021), which are all downstream of CaSR activation (Ward 2004; Li et al. 2013). TLRs are expressed in airways cells involved in sensing and responding to PM, such as epithelial cells, AMs, and DCs (Kawasaki and Kawai 2014), which were shown to express the CaSR during my thesis and contribute to the pathogenesis of PM-exacerbated lung diseases. LPS-induced TLR4 mediated increases to IL-6 and TNF-α expression, has been shown to be Ca^{2+}-dependent (Tang et al. 2019), however, whether the CaSR plays a role in these LPS-induced cellular responses, is not yet known. LPS has been previously suggested to be a potential modulator of the CaSR in cardiomyocytes, where it drives increases to intracellular Ca^{2+} and CaSR expression levels (Wang *et al.* 2013). This evidence poses the question of potential convergence of downstream effectors of TLR4 and CaSR signalling in a range of cell types, which upon activation, could work synergistically to contribute to PM-induced pro-inflammatory responses and acute exacerbations of lung diseases, such as asthma.

Previous studies in our laboratory have shown that NAM (NPS89636) was effective at reducing LPS-induced lung inflammation, using an *in vivo* model of COPD, suggesting the CaSR mediates some LPS-induced cellular responses in airways cells (Yarova *et al.* 2016). Despite promise for TLR inhibitors during preclinical experiments to treat inflammatory disease, clinical development of

TLR inhibitors for diseases, such as asthma, have proved unsuccessful (Gao *et al.* 2017; Li *et al.* 2017). Therefore, NAM could provide an effective upstream therapeutic to reduce pro-inflammatory responses induced by exposure to PM and associated with the pathogenesis of asthma.

6.5.3 Potential Involvement of The CaSR in Particulate Matter-Induced Redox Imbalance:

Imbalance in redox status by generation of ROS is thought to contribute to imbalances in intracellular Ca^{2+} homeostasis (Deweirdt et al. 2017; Pfeffer et al. 2018; Dong et al. 2019; Valacchi et al. 2020) and the pathogenesis of lung diseases, such as asthma (Henricks and Nijkamp 2001). However, the upstream mechanisms underpinning redox imbalance in the airways during the pathogenesis of lung diseases remains somewhat unclear.

Synthesis of GSH has been demonstrated to be Ca^{2+} dependent in cell lines of macrophages and hepatocytes (which are the major source of GSH synthesis *in vivo*) (Pascoe *et al.* 1987; Teshima *et al.* 2000), however, whether the CaSR underpins this process in the airways is unknown. In addition, activation of the CaSR, by $GdCl_3$, enhances ROS generation in an ethylene glycol induced *in vivo* model of kidney stones (Li *et al.* 2021), highlighting the CaSR as a potential target for redox imbalance during inflammatory diseases. Moreover, both GSH and GSSG have been demonstrated to be allosteric modulators at the CaSR, therefore, redox imbalance (increased GSH or GSSG) could promote sensitisation of the CaSR to ligands such as increased serum Ca^{2+} levels and PM, thereby contributing to the pathogenesis and acute exacerbations of the symptoms of lung diseases (Conigrave *et al.* 2000; Goralski and Ram 2022).

Pulmonary arterial hypertension (PAH) comprises a disease in which is driven by pathological CaSR activation and redox imbalance is thought to be one of the key contributors to disease pathogenesis (Ghasemzadeh *et al.* 2014; Zhou *et al.* 2021). Targeting redox imbalance for the treatment of PAH, has been

postulated, and due to the potential links between redox imbalance and the CaSR, NAM could represent an effective therapeutic for redox imbalances during the pathogenesis of inflammatory diseases, such as asthma (Goralski and Ram 2022).

Finally, the contribution of PM to TLR signalling and oxidative stress are not the only mechanism by which PM induces its detrimental effects in the airways and contributes to acute exacerbations of lung diseases. Further work is required to better understand the intracellular signalling pathways induced by exposure to PM and mediated via the CaSR, in the key airway cells *in vitro* models investigated during my thesis and involved in the pathogenesis and acute exacerbations of asthma. Better understanding of the roles of the CaSR in these cells, would allow for further assessment of the potential of NAM as an effective upstream therapeutic for asthma, especially for those who are frequently exacerbated by continued exposure to inhaled stimuli, such as PM. Finally, NAM could comprise a therapeutic for patients with difficult-to-treat, severe asthma, with no effective treatment options currently available.

6.6 Limitations of My Studies:

The CaSR signals in a promiscuous manner, through activation of a variety of intracellular signalling pathways (Min et al. 2002; Ward 2004; Davies et al. 2006a; Molostvov et al. 2008; Rybchyn et al. 2019; Zhang et al. 2020). Although my thesis starts to lay the basis for testing whether the CaSR mediates PM-induced cellular responses, I did not test alternative CaSR-mediated signalling pathways associated with exposure to PM, providing limitations to my findings. In future studies, investigation of alternative CaSR-mediated intracellular signalling pathways associated with PM-exposure, such as activation of PI3K/Akt (Park *et al.* 2020) or mTOR (Zhang et al. 2020) signalling would aid better understanding of the roles of the CaSR in mediating PM-induced

cellular responses and contribution to the pathogenesis and acute exacerbations of lung diseases, such as asthma.

Additionally, during my thesis, I used a commercial reference standard of PM (NIST SRM1648a) to provide a well-characterised tool to assess the potential interactions between PM and the CaSR. This PM contained both fine (<2.5μm) and coarse (<10μm) particles, which recapitulates the urban environment in the USA during 1976-1977 and is widely used as a well-defined tool for PM research, in a range of *in vitro* models of airways structural and immune cells (Akhtar *et al.* 2010; Matthews *et al.* 2016; Mann *et al.* 2017; Pfeffer, Lu, *et al.* 2018b; Byun *et al.* 2019; Cooper and Loxham 2019; Mazuryk *et al.* 2020; Chang-Chien *et al.* 2021). This well-characterised PM allowed me to conduct all experiments with the same batch of PM which avoided potential limitations of mass and characterisation availability of most present-day PM samples. However, considerations need to be made regarding the use of this standard reference material of PM, due to its historic collection and changes in the modern ambient air composition.

During future studies, it would be important to understand whether distinct fractions of PM ($PM_{2.5}$ or PM_{10}) and whether distinct components of this PM contribute to differential activation of intracellular signalling pathways associated with the CaSR. Therefore, collection of present-day fractionated PM samples would be required to fully test the contribution of the CaSR to PM-induced cellular responses in the present-day environment. These experiments would contribute to our assessment of NAM as an effective "all in one" therapeutic for lung diseases, exacerbated by exposure to PM generated from a variety of sources across the globe.

Due to the low functional and molecular expression of the CaSR in the basal NHBEC 2D model used in my studies, further work is required to test the

potential of CaSR-mediation of PM-induced pro-inflammatory cellular responses, reported elsewhere (Pfeffer et al. 2018). Therefore, during future studies, utilising a 3D model of the airway epithelium, such as NHBEC ALI, containing ciliated epithelial cells, the most abundant CaSR expressing cells of the airways, would prove beneficial in assessing potential mediation of PM-induced responses by the CaSR.

In contrast, the *in vitro* models of AMs and DCs provided a valid tool for my studies as they expressed the CaSR at both the protein and mRNA level, however, these models posed issues with sample abundance (AMs) and patient-to-patient variability (DCs). Therefore, utilising an established cell line of macrophages and DCs, such as THP-1 cells, would potentially be beneficial to determine CaSR mediated signalling pathways in response to PM, in these cells (Deng et al 2020). Findings could be validated in the primary immune cell models, in collaboration with The University of Birmingham (AMs) and King's College London (DCs), forged during my PhD studies.

Finally, during future studies, we could explore the potential influence of crosstalk between airways cells during PM-induced responses by using co-culture *in vitro* systems of HBEC ALI, AMs and DCs. These experiments would more fully recapitulate the airways *in vivo* and assess the role of the CaSR in mediating PM-induced crosstalk between airways cells, such as HBEC ALI, AMs, and DCs during pro-inflammatory responses to inhaled stimuli, such as PM.

6.7 Concluding Remarks:

Together, my data suggest that the airway CaSR could play an important role in sensing and responding to PM by initiating and maintaining T2 and non-T2 pro-inflammatory responses, in a range of airways structural and immune cells, which contributes to the pathogenesis and acute exacerbations of asthma (Figure 6.1 A). Therefore, NAM has the potential to offer an "all in one"

therapeutic for patients with T2 and non-T2 asthma, by reducing pathogenic features and the exaggerated and sustained responses to inhaled stimuli, such as PM (Figure 6.1 B).

6.8 Graphical Abstract:

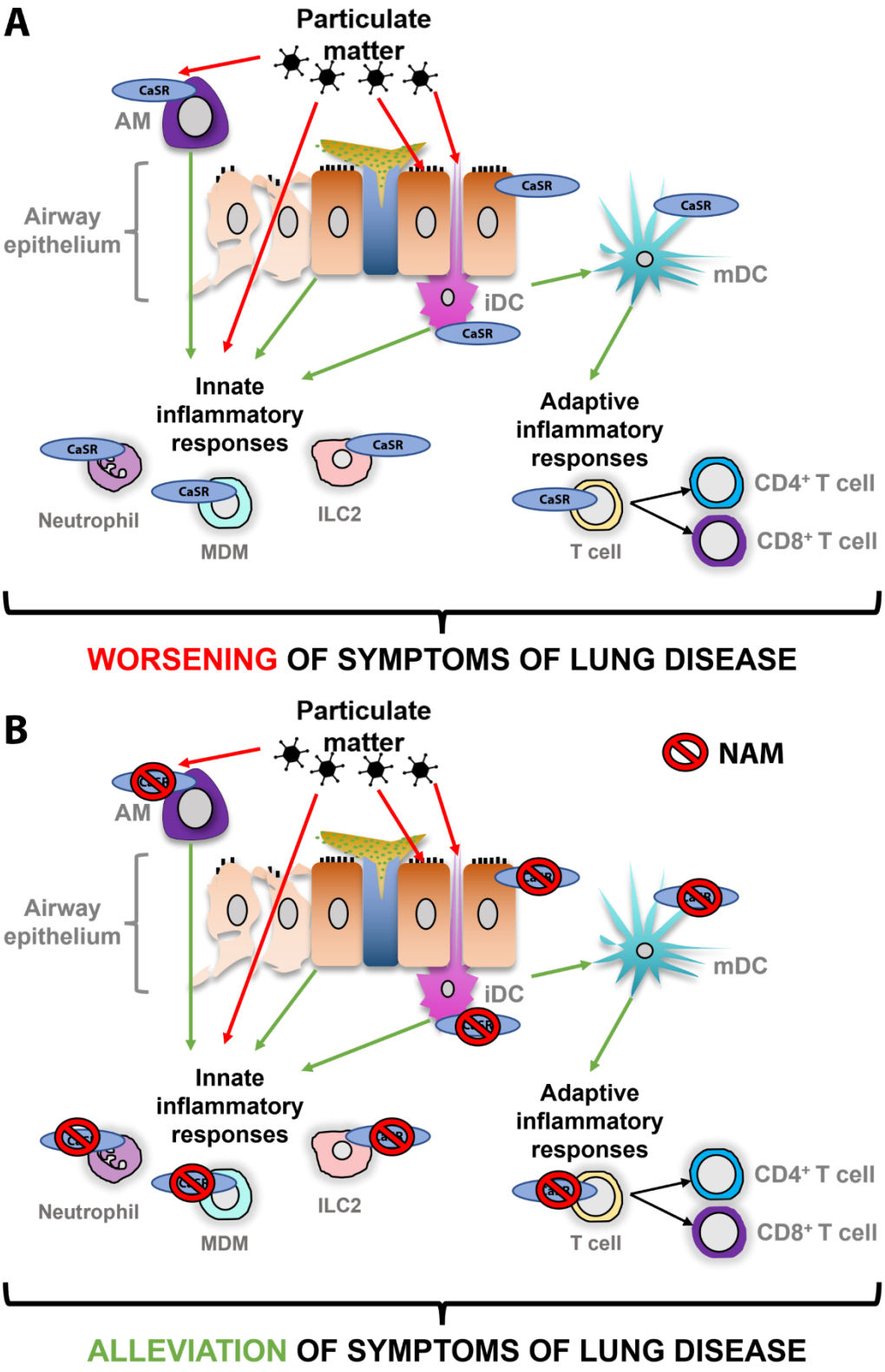

Figure 6.1: The calcium-sensing receptor (CaSR) comprises one of the potential mechanisms underpinning activation of innate and adaptive immunity associated with lung diseases, such as asthma and COPD in response to exposure to particulate matter (PM). PM, one of the major components of air pollution, is generated from a variety of sources and causes direct (red arrows) effects to alveolar macrophages (AM), airway epithelial cells and immature dendritic cells (iDC) (A & B). PM can also cross the airway epithelium, in spaces which have been damaged by continued exposure to PM, where the PM-induced responses (green arrows) produced by each cell type leads to initiation of innate immunity by activation of AM, airway epithelial cells, and iDC and also recruitment of blood- and tissue-derived immune cells such as neutrophils, monocyte-derived macrophages (MDM) and type 2 innate lymphoid cells (ILC2), potentially through activation of the CaSR, which contributes to the rapid response to inhaled PM, and its associated pro-inflammatory effects in the airways (A). Exposure of iDC to PM results in maturation of DC (mDC) and activation of adaptive immune responses through activation of T (lymphocyte) cells, into $CD4^+$ or $CD8^+$ T cell populations, to enhance the adaptive immune response to inhaled innocuous stimuli, such as PM, however, the role of the CaSR in these processes remains unclear. Together, these contribute to the worsening of the symptoms of lung diseases, such as asthma and COPD (A). However, a negative allosteric modulator at the CaSR (NAM) inhibits activation of the CaSR in a range of cell types, in response to a variety of pro-inflammatory stimuli, such as PM and downstream effectors of alternative PM-induced intracellular signalling, to comprise an effective therapeutic to alleviate the symptoms of lung diseases, such as asthma and COPD. NAM could act to directly counteract PM-induced effects in the airways and reduce chronic features associated with the airways of patients with lung diseases, such as asthma and COPD (B).

REFERENCES

Abdulnour-Nakhoul, S., Brown, K.L., Rabon, E.C., Al-Tawil, Y., Islam, M.T., Schmieg, J.J. and Nakhoul, N.L. (2015). Cytoskeletal changes induced by allosteric modulators of calcium-sensing receptor in esophageal epithelial cells. *Physiological Reports* **3**(11). doi: https://doi.org/10.14814/PHY2.12616.

Acciani, T.H., Brandt, E.B., Khurana Hershey, G.K. and Le Cras, T.D. (2013). Diesel exhaust particle exposure increases severity of allergic asthma in young mice. *Clinical and Experimental Allergy* **43**(12):1406–1418. doi: https://doi.org/10.1111/CEA.12200.

Adan, A., Alizada, G., Kiraz, Y., Baran, Y. and Nalbant, A. (2017). Flow cytometry: basic principles and applications. *Critical Reviews in Biotechnology* **37**(2):163–176. doi: https://doi.org/10.3109/07388551.2015.1128876.

Aguilera, R., Corringham, T., Gershunov, A. and Benmarhnia, T. (2021). Wildfire smoke impacts respiratory health more than fine particles from other sources: observational evidence from Southern California. *Nature Communications* **12**(1):1–8. doi: https://doi.org/10.1038/s41467-021-21708-0.

Akhtar, U.S., McWhinney, R.D., Rastogi, N., Abbatt, J.P.D., Evans, G.J. and Scott, J.A. (2010). Cytotoxic and proinflammatory effects of ambient and source-related particulate matter (PM) in relation to the production of reactive oxygen species (ROS) and cytokine adsorption by particles. *Inhalation Toxicology* **22**:37–47. doi: https://doi.org/10.3109/08958378.2010.518377.

Akizawa, T., Ikejiri, K., Kondo, Y., Endo, Y. and Fukagawa, M. (2020). Evocalcet: A New Oral Calcimimetic for Dialysis Patients With Secondary Hyperparathyroidism. *Therapeutic Apheresis and Dialysis* **24**(3):248. doi: https://doi.org/10.1111/1744-9987.13434.

Al-Alwan, M.M., Rowden, G., Lee, T.D.G. and West, K.A. (2001). Cutting Edge: The Dendritic Cell Cytoskeleton Is Critical for the Formation of the Immunological Synapse. *The Journal of Immunology* **166**(3):1452–1456. doi: https://doi.org/10.4049/JIMMUNOL.166.3.1452.

Ali, H., Du, Z., Li, X., Yang, Q., Zhang, Y.C., Wu, M., … Zhang, G. (2015). Identification of suitable reference genes for gene expression studies using quantitative polymerase chain reaction in lung cancer in vitro. *Molecular Medicine Reports* **11**(5):3767–3773. doi: https://doi.org/10.3892/mmr.2015.3159.

Almaraz-De-Santiago, J., Solis-Torres, N., Quintana-Belmares, R., Rodríguez-Carlos, A., Rivas-Santiago, B., Huerta-García, J., … Rivas-Santiago, C.E. (2021). Long-term exposure to particulate matter from air pollution alters airway β-defensin-3 and -4 and cathelicidin host defense peptides production in a murine model. *Peptides* **142**:170581. doi: https://doi.org/10.1016/J.PEPTIDES.2021.170581.

Anenberg, S.C., Henze, D.K., Tinney, V., Kinney, P.L., Raich, W., Fann, N., … Kuylenstierna, J.C.I. (2018). Estimates of the global burden of ambient PM2:5, ozone, and NO2 on asthma incidence and emergency room visits. *Environmental Health Perspectives* **126**(10). doi: https://doi.org/10.1289/EHP3766.

Angelidis, I., Simon, L.M., Fernandez, I.E., Strunz, M., Mayr, C.H., Greiffo, F.R., … Schiller, H.B. (2019). An atlas of the aging lung mapped by single cell transcriptomics and deep tissue proteomics. *Nature Communications* **10**(1):1–17. doi: https://doi.org/10.1038/s41467-019-08831-9.

Arya, M., Shergill, I.S., Williamson, M., Gommersall, L., Arya, N. and Patel, H.R.H. (2005). Basic principles of real-time quantitative PCR. *Expert Review of Molecular Diagnostics* **5**(2):209–219. doi: https://doi.org/10.1586/14737159.5.2.209.

Athari, S.S. (2019). Targeting cell signaling in allergic asthma. *Signal Transduction*

and Targeted Therapy 2019 4:1 **4**(1):1–19. doi: https://doi.org/10.1038/s41392-019-0079-0.

Atkinson, R.W., Ross Anderson, H., Sunyer, J., Ayres, J., Baccini, M., Vonk, J.M., … Katsouyanni, K. (2012). Acute Effects of Particulate Air Pollution on Respiratory Admissions. *Am J Respir Crit Care Med.* **164**(10 I):1860–1866. doi: https://doi.org/10.1164/AJRCCM.164.10.2010138.

Auffray, C., Sieweke, M.H. and Geissmann, F. (2009). Blood monocytes: development, heterogeneity, and relationship with dendritic cells. *Annual review of immunology* **27**:669–692. doi: https://doi.org/10.1146/ANNUREV.IMMUNOL.021908.132557.

Bagley, K.C., Abdelwahab, S.F., Tuskan, R.G. and Lewis, G.K. (2004). Calcium signaling through phospholipase C activates dendritic cells to mature and is necessary for the activation and maturation of dendritic cells induced by diverse agonists. *Clinical and Diagnostic Laboratory Immunology* **11**(1):77–82. doi: https://doi.org/10.1128/CDLI.11.1.77-82.2004.

Bai, M., Trivedi, S. and Brown, E.M. (1998). Dimerization of the extracellular calcium-sensing receptor (CaR) on the cell surface of CaR-transfected HEK293 cells. *The Journal of Biological Chemistry* **273**(36):23605–23610. doi: https://doi.org/10.1074/JBC.273.36.23605.

Barlow, P. (2021). Ella Kissi-Debrah. *Courts and Tribunal Judiciary - Prevention of Future Deaths*.

Barlow, P.G., Brown, D.M., Donaldson, K., MacCallum, J. and Stone, V. (2007). Reduced alveolar macrophage migration induced by acute ambient particle (PM10) exposure. *Cell Biology and Toxicology* **24**(3):243–252. doi: https://doi.org/10.1007/S10565-007-9033-Y.

Barnes, P.J. (1995). Inhaled glucocorticoids for asthma. *The New England Journal of Medicine* **332**(13):868–875. doi: https://doi.org/10.1056/NEJM199503303321307.

Barnes, P.J. (2002). Scientific rationale for inhaled combination therapy with long-acting beta2-agonists and corticosteroids. *The European Respiratory Journal* **19**(1):182–191. doi: https://doi.org/10.1183/09031936.02.00283202.

Barnes, P.J. (2011). Biochemical basis of asthma therapy. *The Journal of Biological Chemistry* **286**(38):32899–32905. doi: https://doi.org/10.1074/JBC.R110.206466.

Basil, M.C., Katzen, J., Engler, A.E., Guo, M., Herriges, M.J., Kathiriya, J.J., … Morrisey, E.E. (2020). The Cellular and Physiological Basis for Lung Repair and Regeneration: Past, Present, and Future. *Cell - Stem Cell* **26**(4):482–502. doi: https://doi.org/10.1016/J.STEM.2020.03.009.

Becker, S., Mundandhara, S., Devlin, R.B. and Madden, M. (2005). Regulation of cytokine production in human alveolar macrophages and airway epithelial cells in response to ambient air pollution particles: Further mechanistic studies. *Toxicology and Applied Pharmacology* **207**(2):269–275. doi: https://doi.org/10.1016/J.TAAP.2005.01.023.

Bell, M., Davis, D.L. and Fletcher, T. (2004). A retrospective assessment of mortality from the London smog episode of 1952: the role of influenza and pollution. *Environmental Health Perspectives* **112**(1):6. doi: https://doi.org/10.1289/EHP.6539.

Bender, A., Sapp, M., Schuler, G., Steinman, R.M. and Bhardwaj, N. (1996). Improved methods for the generation of dendritic cells from nonproliferating progenitors in human blood. *Journal of Immunological Methods* **196**(2):121–135. doi: https://doi.org/10.1016/0022-1759(96)00079-8.

Berridge, M.J. (1993). Inositol trisphosphate and calcium signalling. *Nature*

361(6410):315–325. doi: https://doi.org/10.1038/361315a0.

Bertani, F.R., Mozetic, P., Fioramonti, M., Iuliani, M., Ribelli, G., Pantano, F., … Rainer, A. (2017). Classification of M1/M2-polarized human macrophages by label-free hyperspectral reflectance confocal microscopy and multivariate analysis. *Scientific Reports 2017 7:1* **7**(1):1–9. doi: https://doi.org/10.1038/s41598-017-08121-8.

Beutler, B. (2009). TLRs and innate immunity. *The Journal of the American Society of Hematology***113**(7):1399-1407. doi: 10.1182/blood-2008-07-019307.

Bewley, M.A., Belchamber, K.B.R., Chana, K.K., Budd, R.C., Donaldson, G., Wedzicha, J.A., … COPDMAP (2016). Differential Effects of p38, MAPK, PI3K or Rho Kinase Inhibitors on Bacterial Phagocytosis and Efferocytosis by Macrophages in COPD Maus, U. A. (ed.). *PLOS ONE* **11**(9):e0163139. doi: https://doi.org/10.1371/journal.pone.0163139.

Bharat, A., Bhorade, S.M., Morales-Nebreda, L., McQuattie-Pimentel, A.C., Soberanes, S., Ridge, K., … Misharin, A. V. (2016). Flow cytometry reveals similarities between lung macrophages in humans and mice. *American Journal of Respiratory Cell and Molecular Biology* **54**(1):147–149. doi: https://doi.org/10.1165/RCMB.2015-0147LE/SUPPL_FILE/DISCLOSURES.PDF.

Blank, F., Rothen-Rutishauser, B. and Gehr, P. (2007). Dendritic Cells and Macrophages Form a Transepithelial Network against Foreign Particulate Antigens. *American Journal of Respiratory Cell and Molecular Biology* **36**(6):669–677. doi: https://doi.org/10.1165/rcmb.2006-0234OC.

Bleck, B., Ahsan, M.R., Tse, D.B., Grunig, G. and Reibman, J. (2011a). IL-33 Upregulate Myeloid DC Maturation Induced By Diesel-Exhaust Particle Treated Human Bronchial Epithelial Cells. *American Thoracic Society International Conference Meetings Abstracts*:A4267–A4267. doi:

https://doi.org/10.1164/AJRCCM-CONFERENCE.2011.183.1_MEETINGABSTRACTS.A4267.

Bleck, B., Ahsan, M.R., Tse, D.B., Grunig, G. and Reibman, J. (2011b). IL-33 Upregulate Myeloid DC Maturation Induced By Diesel-Exhaust Particle Treated Human Bronchial Epithelial Cells. *C31. INTERLEUKIN-33 BIOLOGY*. American Thoracic Society, pp. A4267–A4267.

Bleck, B., Tse, D.B., Curotto De Lafaille, M.A., Zhang, F. and Reibman, J. (2008). Diesel exhaust particle-exposed human bronchial epithelial cells induce dendritic cell maturation and polarization via thymic stromal lymphopoietin. *Journal of Clinical Immunology* **28**(2):147–156. doi: https://doi.org/10.1007/S10875-007-9149-0.

Bleck, B., Tse, D.B., Gordon, T., Ahsan, M.R. and Reibman, J. (2010). Diesel exhaust particle-treated human bronchial epithelial cells upregulate Jagged-1 and OX40L in myeloid dendritic cells via TSLP. *Journal of Immunology* **185**(11):6636. doi: https://doi.org/10.4049/JIMMUNOL.1000719.

Block, G.A., Bushinsky, D.A., Cheng, S., Cunningham, J., Dehmel, B., Drueke, T.B., … Chertow, G.M. (2017). Effect of Etelcalcetide vs Cinacalcet on Serum Parathyroid Hormone in Patients Receiving Hemodialysis With Secondary Hyperparathyroidism: A Randomized Clinical Trial. *JAMA* **317**(2):156–164. doi: https://doi.org/10.1001/JAMA.2016.19468.

Block, G.A., Martin, K.J., de Francisco, A.L.M., Turner, S.A., Avram, M.M., Suranyi, M.G., … Goodman, W.G. (2004). Cinacalcet for secondary hyperparathyroidism in patients receiving hemodialysis. *The New England Journal of Medicine* **350**(15):1516–1525. doi: https://doi.org/10.1056/NEJMOA031633.

Boada-Romero, E., Martinez, J., Heckmann, B.L. and Green, D.R. (2020). The

clearance of dead cells by efferocytosis. *Nature Reviews Molecular Cell Biology* **21**(7):398–414. doi: https://doi.org/10.1038/S41580-020-0232-1.

Bockaert, J. and Pin, J.P. (1999). Molecular tinkering of G protein-coupled receptors: an evolutionary success. *The EMBO Journal* **18**(7):1723–1729. doi: https://doi.org/10.1093/EMBOJ/18.7.1723.

Boers, J.E., Ambergen, A.W. and Thunnissen, F.B.J.M. (1999). Number and proliferation of clara cells in normal human airway epithelium. *American Journal of Respiratory and Critical Care Medicine* **159**(5 Pt 1):1585–1591. doi: https://doi.org/10.1164/AJRCCM.159.5.9806044.

Boers, J.E., Ambergen, A.W. and Thunnissen, F.B.J.M. (2012). Number and Proliferation of Basal and Parabasal Cells in Normal Human Airway Epithelium. *American Thoracic Society Journal* **157**(6 PART I):2000–2006. doi: https://doi.org/10.1164/AJRCCM.157.6.9707011.

Bourdin, A., Neveu, D., Vachier, I., Paganin, F., Godard, P. and Chanez, P. (2007). Specificity of basement membrane thickening in severe asthma. *The Journal of Allergy and Clinical Immunology* **119**(6):1367–1374. doi: https://doi.org/10.1016/J.JACI.2007.01.055.

Bouschet, T., Martin, S., Kanamarlapudi, V., Mundell, S. and Henley, J.M. (2007). The calcium-sensing receptor changes cell shape via a β-arrestin-1–ARNO–ARF6–ELMO protein network. *Journal of Cell Science* **120**(Pt 15):2489. doi: https://doi.org/10.1242/JCS.03469.

Bowatte, G., Lodge, C., Lowe, A.J., Erbas, B., Perret, J., Abramson, M.J., … Dharmage, S.C. (2015). The influence of childhood traffic-related air pollution exposure on asthma, allergy and sensitization: a systematic review and a meta-analysis of birth cohort studies. *Allergy* **70**(3):245–256. doi: https://doi.org/10.1111/ALL.12561.

Bradbury, R.A., Cropley, J., Kifor, O., Lovicu, F.J., De Iongh, R.U., Kable, E., … Conigrave, A.D. (2002). Localization of the Extracellular Ca2+-sensing Receptor in the Human Placenta. *Placenta* **23**(2–3):192–200. doi: https://doi.org/10.1053/PLAC.2001.0765.

Brancaccio, D., Tetta, C., Gallieni, M. and Panichi, V. (2002). Inflammation, CRP, calcium overload and a high calcium–phosphate product: a 'liaison dangereuse'. *Nephrology Dialysis Transplantation* **17**(2):201–203. doi: https://doi.org/10.1093/NDT/17.2.201.

Brandt, E.B., Bolcas, P.E., Ruff, B.P. and Khurana Hershey, G.K. (2020). TSLP contributes to allergic airway inflammation induced by diesel exhaust particle exposure in an experimental model of severe asthma. *Clinical and Experimental Allergy* **50**(1):121–124. doi: https://doi.org/10.1111/CEA.13512.

Brandt, E.B., Kovacic, M.B., Lee, G.B., Gibson, A.M., Acciani, T.H., Le Cras, T.D., … Khurana Hershey, G.K. (2013). Diesel exhaust particle induction of IL17A contributes to severe asthma. *The Journal of Allergy and Clinical Immunology* **132**(5). doi: https://doi.org/10.1016/J.JACI.2013.06.048.

Brauer, M., Amann, M., Burnett, R.T., Cohen, A., Dentener, F., Ezzati, M., … Thurston, G.D. (2012). Exposure assessment for estimation of the global burden of disease attributable to outdoor air pollution. *Environmental Science & Technology* **46**(2):652–660. doi: https://doi.org/10.1021/ES2025752.

Braun, M., Koger, F., Klingelhöfer, D., Müller, R. and Groneberg, D.A. (2019). Particulate Matter Emissions of Four Different Cigarette Types of One Popular Brand: Influence of Tobacco Strength and Additives. *International Journal of Environmental Research and Public Health* **16**(2). doi: https://doi.org/10.3390/IJERPH16020263.

Breitwieser, G.E. (2012). Minireview: The Intimate Link Between Calcium Sensing Receptor Trafficking and Signaling: Implications for Disorders of Calcium Homeostasis. *Molecular Endocrinology* **26**(9):1482. doi: https://doi.org/10.1210/ME.2011-1370.

Brennan, S.C., Thiem, U., Roth, S., Aggarwal, A., Fetahu, Irfete Sh, Tennakoon, S., … Kallay, E. (2013). Calcium sensing receptor signalling in physiology and cancer. *Biochimica et Biophysica Acta - Molecular Cell Research* **1833**(7):1732–1744. doi: https://doi.org/10.1016/j.bbamcr.2012.12.011.

Brennan, S.C., Thiem, U., Roth, S., Aggarwal, A., Fetahu, Irfete Sh., Tennakoon, S., … Kallay, E. (2013). Calcium sensing receptor signalling in physiology and cancer. *Biochimica et Biophysica Acta (BBA) - Molecular Cell Research* **1833**(7):1732–1744. doi: https://doi.org/10.1016/J.BBAMCR.2012.12.011.

Brennan, S.C., Wilkinson, W.J., Tseng, H.E., Finney, B., Monk, B., Dibble, H., … Riccardi, D. (2016). The extracellular calcium-sensing receptor regulates human fetal lung development via CFTR. *Scientific Reports* **6**. doi: https://doi.org/10.1038/SREP21975.

Briffa, J., Sinagra, E. and Blundell, R. (2020). Heavy metal pollution in the environment and their toxicological effects on humans. *Heliyon* **6**(9):e04691. doi: https://doi.org/10.1016/J.HELIYON.2020.E04691.

Broide, D.H., Lotz, M., Cuomo, A.J., Coburn, D.A., Federman, E.C. and Wasserman, S.I. (1992). Cytokines in symptomatic asthma airways. *The Journal of Allergy and Clinical Immunology* **89**(5):958–967. doi: https://doi.org/10.1016/0091-6749(92)90218-Q.

Brown, E., Enyedi, P., LeBoff, M., Rotberg, J., Preston, J. and Chen, C. (1987). High extracellular Ca2+ and Mg2+ stimulate accumulation of inositol phosphates in

bovine parathyroid cells. *FEBS Letters* **218**(1):113–118. doi: https://doi.org/10.1016/0014-5793(87)81029-3.

Brown, E.M. and Chen, C.J. (1989). Calcium, magnesium and the control of PTH secretion. *Bone and Mineral Research* **5**(3):249–257. doi: https://doi.org/10.1016/0169-6009(89)90003-2.

Brown, E.M., Gamba, G., Riccardi, D., Lombardi, M., Butters, R., Kifor, O., … Hebert, S.C. (1993). Cloning and characterization of an extracellular Ca2+-sensing receptor from bovine parathyroid. *Nature* **366**(6455):575–580. doi: https://doi.org/10.1038/366575a0.

Brown, E.M. and Macleod, R.J. (2001). Extracellular calcium sensing and extracellular calcium signaling. *Physiological Reviews* **81**(1):239–297. doi: https://doi.org/10.1152/PHYSREV.2001.81.1.239.

Brown, J.S., Gordon, T., Price, O. and Asgharian, B. (2013). Thoracic and respirable particle definitions for human health risk assessment. *Particle and Fibre Toxicology* **10**(1). doi: https://doi.org/10.1186/1743-8977-10-12.

Bruce, J.I.E., Yang, X., Ferguson, C.J., Elliott, A.C., Steward, M.C., Case, R.M. and Riccardi, D. (1999). Molecular and functional identification of a Ca2+ (polyvalent cation)-sensing receptor in rat pancreas. *The Journal of Biological Chemistry* **274**(29):20561–20568. doi: https://doi.org/10.1074/JBC.274.29.20561.

Brugha, R. and Grigg, J. (2014). Urban air pollution and respiratory infections. *Paediatric Respiratory Reviews* **15**(2):194–199. doi: https://doi.org/10.1016/J.PRRV.2014.03.001.

Bu, L., Michino, M., Wolf, R.M. and Brooks, C.L. (2008). Improved model building and assessment of the Calcium-sensing receptor transmembrane domain. *Proteins:*

Structure, Function and Genetics **71**(1):215–226. doi: https://doi.org/10.1002/PROT.21685.

Bukoski, R.D. (1998). The perivascular sensory nerve Ca2+ receptor and blood pressure regulation. *American Journal of Hypertension* **11**(9):1117–1123. doi: https://doi.org/10.1016/S0895-7061(97)00499-8.

Bullens, D.M.A., Truyen, E., Coteur, L., Dilissen, E., Hellings, P.W., Dupont, L.J. and Ceuppens, J.L. (2006). IL-17 mRNA in sputum of asthmatic patients: Linking T cell driven inflammation and granulocytic influx? *Respiratory Research* **7**(1):1–9. doi: https://doi.org/10.1186/1465-9921-7-135/FIGURES/3_526.

Burnett, Chen, Szyszkowicz, Fann, Hubbell, Pope, … Spadaro (2018). Global estimates of mortality associated with long-term exposure to outdoor fine particulate matter. *Proceedings of the National Academy of Sciences of the United States of America* **115**(38):9592–9597. doi: https://doi.org/10.1073/PNAS.1803222115.

Busse, W.W., Dahl, R., Jenkins, C. and Cruz, A.A. (2016). Long-acting muscarinic antagonists: a potential add-on therapy in the treatment of asthma? *European Respiratory Review* **25**(139):54–64. doi: https://doi.org/10.1183/16000617.0052-2015.

Bustamante-Marin, X.M. and Ostrowski, L.E. (2017). Cilia and Mucociliary Clearance. *Cold Spring Harbor Perspectives in Biology* **9**(4). doi: https://doi.org/10.1101/CSHPERSPECT.A028241.

Byers, D.E., Alexander-Brett, J., Patel, A.C., Agapov, E., Dang-Vu, G., Jin, X., … Holtzman, M.J. (2013). Long-term IL-33–producing epithelial progenitor cells in chronic obstructive lung disease. *The Journal of Clinical Investigation* **123**(9):3967. doi: https://doi.org/10.1172/JCI65570.

Byun, J., Song, B., Lee, Kyungwoo, Kim, B., Hwang, H.W., Ok, M.R., … Kim, T.H. (2019). Identification of urban particulate matter-induced disruption of human respiratory mucosa integrity using whole transcriptome analysis and organ-on-a chip. *Journal of Biological Engineering* **13**(1):1–12. doi: https://doi.org/10.1186/S13036-019-0219-7/FIGURES/5.

Cadelis, G., Tourres, R. and Molinie, J. (2014). Short-Term Effects of the Particulate Pollutants Contained in Saharan Dust on the Visits of Children to the Emergency Department due to Asthmatic Conditions in Guadeloupe (French Archipelago of the Caribbean). *PLoS ONE* **9**(3). doi: https://doi.org/10.1371/JOURNAL.PONE.0091136.

Caltabiano, S., Dollery, C.T., Hossain, M., Kurtinecz, M.T., Desjardins, J.P., Favus, M.J., … Fitzpatrick, L.A. (2013). Characterization of the effect of chronic administration of a calcium-sensing receptor antagonist, ronacaleret, on renal calcium excretion and serum calcium in postmenopausal women. *Bone* **56**(1):154–162. doi: https://doi.org/10.1016/J.BONE.2013.05.021.

Calvén, J., Ax, E. and Rådinger, M. (2020). The Airway Epithelium-A Central Player in Asthma Pathogenesis. *Molecular Sciences* **21**(23):8907. doi: https://doi.org/10.3390/ijms21238907.

Canaff, L. and Hendy, G.N. (2005). Calcium-sensing receptor gene transcription is up-regulated by the proinflammatory cytokine, interleukin-1beta. Role of the NF-kappaB PATHWAY and kappaB elements. *The Journal of Biological Chemistry* **280**(14):14177–14188. doi: https://doi.org/10.1074/JBC.M408587200.

Canaff, L., Petit, J.L., Kisiel, M., Watson, P.H., Gascon-Barré, M. and Hendy, G.N. (2001). Extracellular calcium-sensing receptor is expressed in rat hepatocytes. Coupling to intracellular calcium mobilization and stimulation of bile flow. *Journal*

of Biological Chemistry **276**(6):4070–4079. doi: https://doi.org/10.1074/jbc.M009317200.

Canaff, L., Zhou, X. and Hendy, G.N. (2008). The Proinflammatory Cytokine, Interleukin-6, Up-regulates Calcium-sensing Receptor Gene Transcription via Stat1/3 and Sp1/3. *Journal of Biological Chemistry* **283**(20):13586–13600. doi: https://doi.org/10.1074/jbc.M708087200.

Canton, J., Schlam, D., Breuer, C., Gütschow, M., Glogauer, M. and Grinstein, S. (2016a). Calcium-sensing receptors signal constitutive macropinocytosis and facilitate the uptake of NOD2 ligands in macrophages. doi: https://doi.org/10.1038/ncomms11284.

Canton, J., Schlam, D., Breuer, C., Gütschow, M., Glogauer, M. and Grinstein, S. (2016b). Calcium-sensing receptors signal constitutive macropinocytosis and facilitate the uptake of NOD2 ligands in macrophages. *Nature Communications* **7**(1):1–12. doi: https://doi.org/10.1038/ncomms11284.

Carp, H. and Janoff, A. (1978). Possible mechanisms of emphysema in smokers. In vitro suppression of serum elastase-inhibitory capacity by fresh cigarette smoke and its prevention by antioxidants. *American Review of Respiratory Disease* **118**(3):617–621. doi: https://doi.org/10.1164/ARRD.1978.118.3.617.

Carroll, F.Y., Stolle, A., Beart, P.M., Voerste, A., Brabet, I., Mauler, F., … Prézeau, L. (2001). BAY36-7620: A Potent Non-Competitive mGlu1 Receptor Antagonist with Inverse Agonist Activity. *Molecular Pharmacology* **59**(5):965–973. doi: https://doi.org/10.1124/MOL.59.5.965.

Centeno, P.P., Herberger, A., Mun, H.C., Tu, C., Nemeth, E.F., Chang, W., … Ward, D.T. (2019). Phosphate acts directly on the calcium-sensing receptor to stimulate parathyroid hormone secretion. *Nature Communications* **10**(1):1–12. doi:

https://doi.org/10.1038/s41467-019-12399-9.

Centers for Disease Control and Prevention (CDC) (2019). *Particle Pollution | Air | CDC.Particle Pollution*. Available at: https://www.cdc.gov/air/particulate_matter.html [Accessed: 4 October 2021].

Cernadas, M., Lu, J., Watts, G. and Brenner, M.B. (2009). CD1a expression defines an interleukin-12 producing population of human dendritic cells. *Clinical and Experimental Immunology* **155**(3):523. doi: https://doi.org/10.1111/J.1365-2249.2008.03853.X.

Cesaroni, G., Forastiere, F., Stafoggia, M., Andersen, Z.J., Badaloni, C., Beelen, R., … Peters, A. (2014). Long term exposure to ambient air pollution and incidence of acute coronary events: prospective cohort study and meta-analysis in 11 European cohorts from the ESCAPE Project. *BMJ* **348**. doi: https://doi.org/10.1136/BMJ.F7412.

Chakravarti, B., Chattopadhyay, N. and Brown, E.M. (2012). Signaling through the extracellular calcium-sensing receptor (CaSR). *Advances in experimental medicine and biology* **740**:103–142. doi: https://doi.org/10.1007/978-94-007-2888-2_5.

Chan, Y.L., Wang, B., Chen, H., Ho, K.F., Cao, J., Hai, G., … Oliver, B.G.G. (2019). Pulmonary inflammation induced by low-dose particulate matter exposure in mice. *American Journal of Physiology - Lung Cellular and Molecular Physiology* **317**(3):L424–L430. doi: https://doi.org/10.1152/AJPLUNG.00232.2019/ASSET/IMAGES/LARGE/ZH50091976820002.JPEG.

Chang-Chien, J., Huang, J.L., Tsai, H.J., Wang, S.L., Kuo, M.L. and Yao, T.C. (2021). Particulate matter causes telomere shortening and increase in cellular senescence markers in human lung epithelial cells. *Ecotoxicology and Environmental Safety*

222:112484. doi: https://doi.org/10.1016/J.ECOENV.2021.112484.

Chang, W., Tu, C., Chen, T.H., Bikle, D. and Shoback, D. (2008). The extracellular calcium-sensing receptor (CaSR) is a critical modulator of skeletal development. *Science Signaling* **1**(35):ra1. doi: https://doi.org/10.1126/scisignal.1159945.

Chattopadhyay, N., Vassilev, P.M. and Brown, E.M. (1997). Calcium-sensing receptor: roles in and beyond systemic calcium homeostasis. *Biological Chemistry* **378**(8):759–768.

Chen, L., Deng, H., Cui, H., Fang, J., Zuo, Z., Deng, J., … Zhao, L. (2018). Inflammatory responses and inflammation-associated diseases in organs. *Oncotarget* **9**(6):7204. doi: https://doi.org/10.18632/ONCOTARGET.23208.

Chiarini, A., Armato, U., Hu, P. and Dal Prà, I. (2020). CaSR Antagonist (Calcilytic) NPS 2143 Hinders the Release of Neuroinflammatory IL-6, Soluble ICAM-1, RANTES, and MCP-2 from Aβ-Exposed Human Cortical Astrocytes. *Cells* **9**(6). doi: https://doi.org/10.3390/CELLS9061386.

Chiba, Y., Nakazawa, S., Todoroki, M., Shinozaki, K., Sakai, H. and Misawa, M. (2009). Interleukin-13 augments bronchial smooth muscle contractility with an up-regulation of RhoA protein. *American Journal of Respiratory Cell and Molecular Biology* **40**(2):159–167. doi: https://doi.org/10.1165/RCMB.2008-0162OC.

Chirino, Y.I., García-Cuellar, C.M., García-García, C., Soto-Reyes, E., Osornio-Vargas, Á.R., Herrera, L.A., … Sánchez-Pérez, Y. (2017). Airborne particulate matter in vitro exposure induces cytoskeleton remodeling through activation of the ROCK-MYPT1-MLC pathway in A549 epithelial lung cells. *Toxicology Letters* **272**:29–37. doi: https://doi.org/10.1016/J.TOXLET.2017.03.002.

Choi, M.S., Jeon, H., Yoo, S.M. and Lee, M.S. (2021). Activation of the complement

system on human endothelial cells by urban particulate matter triggers inflammation-related protein production. *International Journal of Molecular Sciences* **22**(7). doi: https://doi.org/10.3390/IJMS22073336.

Churg, A., Brauer, M., del Carmen Avila-Casado, M., Fortoul, T.I. and Wright, J.L. (2003). Chronic exposure to high levels of particulate air pollution and small airway remodeling. *Environmental Health Perspectives* **111**(5):714. doi: https://doi.org/10.1289/EHP.6042.

Cohen, L., Xueping, E., Tarsi, J., Ramkumar, T., Horiuchi, T.K., Cochran, R., … Noel, P. (2007). Epithelial cell proliferation contributes to airway remodeling in severe asthma. *American Journal of Respiratory and Critical Care Medicine* **176**(2):138–145. doi: https://doi.org/10.1164/RCCM.200607-1062OC.

Collin, M. and Bigley, V. (2018). Human dendritic cell subsets: an update. *Immunology* **154**(1):3–20.

Collin, M., Mcgovern, N. and Haniffa, M. (2013). Human dendritic cell subsets. *Immunology* **140**(1):22–30.

Condon, T.V., Sawyer, R.T., Fenton, M.J. and Riches, D.W.H. (2011). Lung dendritic cells at the innate-adaptive immune interface. *Journal of Leukocyte Biology* **90**(5):883. doi: https://doi.org/10.1189/JLB.0311134.

Conigrave, A.D. (2016). The calcium-sensing receptor and the parathyroid: Past, present, future. *Frontiers in Physiology* **7**(DEC):563. doi: https://doi.org/10.3389/FPHYS.2016.00563/BIBTEX.

Conigrave, A.D., Quinn, S.J. and Brown, E.M. (2000). l-Amino acid sensing by the extracellular Ca2+-sensing receptor. *Proceedings of the National Academy of Sciences* **97**(9):4814–4819. doi: https://doi.org/10.1073/PNAS.97.9.4814.

Cooper, D.M. and Loxham, M. (2019). Particulate matter and the airway epithelium: the special case of the underground? *European Respiratory Review* **28**(153). doi: https://doi.org/10.1183/16000617.0066-2019.

Corinti, S., Albanesi, C., Sala, A. la, Pastore, S. and Girolomoni, G. (2001). Regulatory Activity of Autocrine IL-10 on Dendritic Cell Functions. *The Journal of Immunology* **166**(7):4312–4318. doi: https://doi.org/10.4049/JIMMUNOL.166.7.4312.

Cortijo, J., Milara, J., Mata, M., Donet, E., Gavara, N., Peel, S.E., … Morcillo, E.J. (2010a). Nickel induces intracellular calcium mobilization and pathophysiological responses in human cultured airway epithelial cells. *Chemico-Biological Interactions* **183**(1):25–33. doi: https://doi.org/10.1016/j.cbi.2009.09.011.

Cortijo, J., Milara, J., Mata, M., Donet, E., Gavara, N., Peel, S.E., … Morcillo, E.J. (2010b). Nickel induces intracellular calcium mobilization and pathophysiological responses in human cultured airway epithelial cells. *Chemico-Biological Interactions* **183**(1):25–33. doi: https://doi.org/10.1016/j.cbi.2009.09.011.

Cortijo, J., Milara, J., Mata, M., Donet, E., Gavara, N., Peel, S.E., … Morcillo, E.J. (2010). Nickel induces intracellular calcium mobilization and pathophysiological responses in human cultured airway epithelial cells. *Chemico-Biological Interactions* **183**(1):25–33. doi: https://doi.org/10.1016/j.cbi.2009.09.011.

Cosman, F., Gilchrist, N., McClung, M., Foldes, J., de Villiers, T., Santora, A., … Denker, A.E. (2016). A phase 2 study of MK-5442, a calcium-sensing receptor antagonist, in postmenopausal women with osteoporosis after long-term use of oral bisphosphonates. *Osteoporosis International* **27**(1):377–386. doi: https://doi.org/10.1007/S00198-015-3392-7.

Couper, K.N., Blount, D.G. and Riley, E.M. (2008). IL-10: The Master Regulator of Immunity to Infection. *The Journal of Immunology* **180**(9):5771–5777. doi:

https://doi.org/10.4049/JIMMUNOL.180.9.5771.

Crystal, R.G. (2014). Airway basal cells. The 'smoking gun' of chronic obstructive pulmonary disease. *American Journal of Respiratory and Critical Care Medicine* **190**(12):1355–1362. doi: https://doi.org/10.1164/RCCM.201408-1492PP.

Cua, D.J., Sherlock, J., Chen, Y., Murphy, C.A., Joyce, B., Seymour, B., … Sedgwick, J.D. (2003). Interleukin-23 rather than interleukin-12 is the critical cytokine for autoimmune inflammation of the brain. *Nature* **421**(6924):744–748. doi: https://doi.org/10.1038/nature01355.

Dales, R., Blanco-Vidal, C. and Cakmak, S. (2020). The Association Between Air Pollution and Hospitalization of Patients With Idiopathic Pulmonary Fibrosis in Chile: A Daily Time Series Analysis. *Chest* **158**(2):630–636. doi: https://doi.org/10.1016/J.CHEST.2020.02.017.

Davidson, D. and Patel, H. (2014). Cytokine-induced neutrophil chemotaxis assay. *Methods in Molecular Biology* **1172**:107–113. doi: https://doi.org/10.1007/978-1-4939-0928-5_9.

Davies, S.L., Gibbons, C.E., Vizard, T. and Ward, D.T. (2006a). Ca2+-sensing receptor induces Rho kinase-mediated actin stress fiber assembly and altered cell morphology, but not in response to aromatic amino acids. *American journal of physiology. Cell physiology* **290**(6). doi: https://doi.org/10.1152/AJPCELL.00482.2005.

Davies, S.L., Gibbons, C.E., Vizard, T. and Ward, D.T. (2006b). Ca^{2+} -sensing receptor induces Rho kinase-mediated actin stress fiber assembly and altered cell morphology, but not in response to aromatic amino acids. *American Journal of Physiology-Cell Physiology* **290**(6):C1543–C1551. doi: https://doi.org/10.1152/ajpcell.00482.2005.

Department for Environment, F. and R.A. (Defra) (2020). *Pollutant Information.About Air Pollution*. Available at: https://uk-air.defra.gov.uk/air-pollution/ [Accessed: 31 January 2022].

Deweirdt, J., Quignard, J., Crobeddu, B., Baeza-Squiban, A., Sciare, J., Courtois, A., … Baudrimont, I. (2017). Involvement of oxidative stress and calcium signaling in airborne particulate matter - induced damages in human pulmonary artery endothelial cells. *Toxicology in vitro* **45**(Pt 3):340–350. doi: https://doi.org/10.1016/J.TIV.2017.07.001.

Dhimal, M., Chirico, F., Bista, B., Sharma, S., Chalise, B., Dhimal, M.L., … Sofia, D. (2021). Impact of Air Pollution on Global Burden of Disease in 2019. *Processes* **9**(10):1719. doi: https://doi.org/10.3390/PR9101719.

Diociaiuti, M., Balduzzi, M., De Berardis, B., Cattani, G., Stacchini, G., Ziemacki, G., … Paoletti, L. (2001). The Two PM2.5 (Fine) and PM2.5–10 (Coarse) Fractions: Evidence of Different Biological Activity. *Environmental Research* **86**(3):254–262. doi: https://doi.org/10.1006/ENRS.2001.4275.

Dong, L., Sun, W., Li, F., Shi, M., Meng, X., Wang, C., … Song, L. (2019). The harmful effects of acute PM2.5 exposure to the heart and a novel preventive and therapeutic function of CEOs. *Scientific Reports 2019 9:1* **9**(1):1–12. doi: https://doi.org/10.1038/s41598-019-40204-6.

Drake, L.Y. and Kita, H. (2017). IL-33: biological properties, functions, and roles in airway disease. *Immunological Reviews* **278**(1):173–184.

Drexler, S. and Foxwell, B. (2010). The role of toll-like receptors in chronic inflammation. *The International Journal of Biochemistry & Cell Biology*.

Dvorak, M.M., Siddiqua, A., Ward, D.T., Carter, D.H., Dallas, S.L., Nemeth, E.F. and

Riccardi, D. (2004). Physiological changes in extracellular calcium concentration directly control osteoblast function in the absence of calciotropic hormones. *Proceedings of the National Academy of Sciences of the United States of America* **101**(14):5140–5145. doi: https://doi.org/10.1073/PNAS.0306141101/ASSET/7CFC1D15-B364-41B2-9DE3-CF23B3396110/ASSETS/GRAPHIC/ZPQ0130443700007.JPEG.

Ehlert, F.J. (2005). Analysis of Allosterism in Functional Assays. *Journal of Pharmacology and Experimental Therapeutics* **315**(2):740–754. doi: https://doi.org/10.1124/JPET.105.090886.

Embgenbroich, M. and Burgdorf, S. (2018). Current concepts of antigen cross-presentation. *Frontiers in Immunology* **9**(JUL):1643. doi: https://doi.org/10.3389/FIMMU.2018.01643/BIBTEX.

Falcon-Rodriguez, C.I., Osornio-Vargas, A.R., Sada-Ovalle, I. and Segura-Medina, P. (2016). Aeroparticles, composition, and lung diseases. *Frontiers in Immunology* **7**(JAN):3. doi: https://doi.org/10.3389/FIMMU.2016.00003/BIBTEX.

Fan, Y., Liu, W., Bi, R., Densmore, M.J., Sato, T., Mannstadt, M., … Lanske, B. (2018). Interrelated role of Klotho and calcium-sensing receptor in parathyroid hormone synthesis and parathyroid hyperplasia. *Proceedings of the National Academy of Sciences of the United States of America* **115**(16):E3749–E3758. doi: https://doi.org/10.1073/pnas.1717754115.

Farley, J.M. (1994). Airway Smooth Muscle Ion Channels. *Methods in Neurosciences* **19**(C):220–239. doi: https://doi.org/10.1016/B978-0-12-185287-0.50018-1.

Fetahu, I.S., Hummel, D.M., Manhardt, T., Aggarwal, A., Baumgartner-Parzer, S. and Kállay, E. (2014). Regulation of the calcium-sensing receptor expression by 1,25-dihydroxyvitamin D3, interleukin-6, and tumor necrosis factor alpha in colon

cancer cells. *The Journal of Steroid Biochemistry and Molecular Biology* **144**(PART A):228. doi: https://doi.org/10.1016/J.JSBMB.2013.10.015.

Finney, B.A., Del Moral, P.M., Wilkinson, W.J., Cayzac, S., Cole, M., Warburton, D., … Riccardi, D. (2008). Regulation of mouse lung development by the extracellular calcium-sensing receptor, CaR. *The Journal of Physiology* **586**(24):6007–6019. doi: https://doi.org/10.1113/JPHYSIOL.2008.161687.

Fitzpatrick, L.A., Dabrowski, C.E., Cicconetti, G., Gordon, D.N., Fuerst, T., Engelke, K. and Genant, H.K. (2012). Ronacaleret, a calcium-sensing receptor antagonist, increases trabecular but not cortical bone in postmenopausal women. *Journal of Bone and Mineral Research* **27**(2):255–262. doi: https://doi.org/10.1002/JBMR.554.

Fitzpatrick, L.A., Dabrowski, C.E., Cicconetti, G., Gordon, D.N., Papapoulos, S., Bone, H.G. and Bilezikian, J.P. (2011). The effects of ronacaleret, a calcium-sensing receptor antagonist, on bone mineral density and biochemical markers of bone turnover in postmenopausal women with low bone mineral density. *The Journal of Clinical Endocrinology and Metabolism* **96**(8):2441–2449. doi: https://doi.org/10.1210/JC.2010-2855.

Fox, S., Leitch, A.E., Duffin, R., Haslett, C. and Rossi, A.G. (2010). Neutrophil Apoptosis: Relevance to the Innate Immune Response and Inflammatory Disease. *J Innate Immun* **2**:216–227. doi: https://doi.org/10.1159/000284367.

Fujii, T., Hayashi, S., Hogg, J.C., Vincent, R. and Van Eeden, S.F. (2001). Particulate matter induces cytokine expression in human bronchial epithelial cells. *American Journal of Respiratory Cell and Molecular Biology* **25**(3):265–271. doi: https://doi.org/10.1165/AJRCMB.25.3.4445.

Fukao, T., Frucht, D.M., Yap, G., Gadina, M., O'Shea, J.J. and Koyasu, S. (2001). Inducible Expression of Stat4 in Dendritic Cells and Macrophages and Its Critical

Role in Innate and Adaptive Immune Responses. *The Journal of Immunology* **166**(7):4446–4455. doi: https://doi.org/10.4049/JIMMUNOL.166.7.4446.

Gafni, R.I., Hartley, I.R., Roszko, K.L., Nemeth, E.F., Pozo, K.A., Sani-Grosso, R., … Collins, M.T. (2021). The Effects of Encaleret (CLTX-305) on Mineral Physiology in Autosomal Dominant Hypocalcemia Type 1 (ADH1) Demonstrate Proof-of-Concept: Early Results From an Ongoing Phase 2b, Open-Label, Dose-Ranging Study. *Journal of the Endocrine Society* **5**(Suppl 1):A269. doi: https://doi.org/10.1210/JENDSO/BVAB048.545.

Gan, W.Q., FitzGerald, J.M., Carlsten, C., Sadatsafavi, M. and Brauer, M. (2013). Associations of ambient air pollution with chronic obstructive pulmonary disease hospitalization and mortality. *American Journal of Respiratory and Critical Care Medicine* **187**(7):721–727. doi: https://doi.org/10.1164/RCCM.201211-2004OC.

Ganguly, D., Haak, S., Sisirak, V. and Reizis, B. (2013). The role of dendritic cells in autoimmunity. *Nature Reviews Immunology* **13**(8):566–577. doi: https://doi.org/10.1038/nri3477.

Gao, W., Xiong, Y., Li, Q. and Yang, H. (2017). Inhibition of toll-like receptor signaling as a promising therapy for inflammatory diseases: A journey from molecular to nano therapeutics. *Frontiers in Physiology* **8**(JUL):508. doi: https://doi.org/10.3389/FPHYS.2017.00508/BIBTEX.

Garciá, S.R., Deprez, M., Lebrigand, K., Cavard, A., Paquet, A., Arguel, M.J., … Zaragosi, L.E. (2019). Novel dynamics of human mucociliary differentiation revealed by single-cell RNA sequencing of nasal epithelial cultures. *Development* **146**(20). doi: https://doi.org/10.1242/DEV.177428.

Genchi, G., Carocci, A., Lauria, G., Sinicropi, M.S. and Catalano, A. (2020). Nickel: Human Health and Environmental Toxicology. *International Journal of*

Environmental Research and Public Health **17**(3). doi: https://doi.org/10.3390/IJERPH17030679.

Gerspacher, M., Altmann, E., Beerli, R., … T.B.-B.& medicinal and 2010, U. (2010). Penta-substituted benzimidazoles as potent antagonists of the calcium-sensing receptor (CaSR-antagonists). *Elsevier* **20**(17):5161–5164.

Ghasemzadeh, N., Patel, R.S., Eapen, D.J., Veledar, E., Kassem, H. Al, Manocha, P., … Quyyumi, A.A. (2014). Oxidative stress is associated with increased pulmonary artery systolic pressure in humans. *Hypertension* **63**(6):1270–1275. doi: https://doi.org/10.1161/HYPERTENSIONAHA.113.02360.

Giannone, G., Dubin-Thaler, B.J., Döbereiner, H.G., Kieffer, N., Bresnick, A.R. and Sheetz, M.P. (2004). Periodic lamellipodial contractions correlate with rearward actin waves. *Cell* **116**(3):431–443. doi: https://doi.org/10.1016/S0092-8674(04)00058-3.

Giri, A. and Sundar, I.K. (2022). Evaluation of stable reference genes for qPCR normalization in circadian studies related to lung inflammation and injury in mouse model. *Scientific Reports* **12**(1764).

Glencross, D.A., Ho, T.R., Camiña, N., Hawrylowicz, C.M. and Pfeffer, P.E. (2020). Air pollution and its effects on the immune system. *Free Radical Biology and Medicine* **151**:56–68. doi: https://doi.org/10.1016/J.FREERADBIOMED.2020.01.179.

Global Burden of Disease (2019). *Global Health Metrics*.

Gold, D.R., Litonjua, A., Schwartz, J., Lovett, E., Larson, A., Nearing, B., … Verrier, R. (2000). Ambient pollution and heart rate variability. *Circulation* **101**(11):1267–1273. doi: https://doi.org/10.1161/01.CIR.101.11.1267.

Gómez, J., Borràs, F.E., Singh, R., Rajananthanan, P., English, N., Knight, S.C. and

Navarrete, C. V. (2004). Differential up-regulation of HLA-DM, invariant chain, and CD83 on myeloid and plasmacytoid dendritic cells from peripheral blood. *Tissue Antigens* **63**(2):149–157. doi: https://doi.org/10.1111/J.1399-0039.2004.00159.X.

González-Flecha, B. (2004). Oxidant mechanisms in response to ambient air particles. *Molecular Aspects of Medicine* **25**(1–2):169–182. doi: https://doi.org/10.1016/J.MAM.2004.02.017.

Goossens, J., Jonckheere, A.C., Dupont, L.J. and Bullens, D.M.A. (2021). Air Pollution and the Airways: Lessons from a Century of Human Urbanization. *Atmosphere 2021, Vol. 12, Page 898* **12**(7):898. doi: https://doi.org/10.3390/ATMOS12070898.

Goralski, T. and Ram, J.L. (2022). Extracellular Calcium Receptor as a Target for Glutathione and Its Derivatives. *International Journal of Molecular Sciences* **23**(2). doi: https://doi.org/10.3390/IJMS23020717.

Gras, D., Martinez-Anton, A., Bourdin, A., Garulli, C., De Senneville, L., Vachier, I., … Chanez, P. (2017). Human bronchial epithelium orchestrates dendritic cell activation in severe asthma. *European Respiratory Journal* **49**(3). doi: https://doi.org/10.1183/13993003.02399-2016.

Green, R.H., Brightling, C.E., Woltmann, G., Parker, D., Wardlaw, A.J. and Pavord, I.D. (2002). Analysis of induced sputum in adults with asthma: identification of subgroup with isolated sputum neutrophilia and poor response to inhaled corticosteroids. *Thorax* **57**(10):875–879. doi: https://doi.org/10.1136/THORAX.57.10.875.

Greenlee-Wacker, M.C. (2016). Clearance of apoptotic neutrophils and resolution of inflammation. *Immunological Reviews* **273**(1):357. doi: https://doi.org/10.1111/IMR.12453.

Gregory, K.J., Kufareva, I., Keller, A.N., Khajehali, E., Mun, H.C., Goolam, M.A., … Leach, K. (2018). Dual action calcium-sensing receptor modulator unmasks novel mode-switching mechanism. *ACS Pharmacology and Translational Science* **1**(2):96–109. doi: https://doi.org/10.1021/ACSPTSCI.8B00021.

De Grove, K.C., Provoost, S., Brusselle, G.G., Joos, G.F. and Maes, T. (2018). Insights in particulate matter-induced allergic airway inflammation: Focus on the epithelium. *Clinical and Experimental Allergy* **48**(7):773–786. doi: https://doi.org/10.1111/CEA.13178.

Gu, J., Dai, S., Liu, Y., Liu, H., Zhang, Y., Ji, X., … Shi, H. (2018). Activation of Ca2+-sensing receptor as a protective pathway to reduce Cadmium-induced cytotoxicity in renal proximal tubular cells. *Scientific Reports* **8**(1):1092. doi: https://doi.org/10.1038/s41598-018-19327-9.

Guaita, R., Pichiule, M., Mate, T., Linares, C. and Diaz, J. (2011). Short-term impact of particulate matter (PM2.5) on respiratory mortality in Madrid. *International Journal of Environmental Health Research* **21**(4):260–274. doi: https://doi.org/10.1080/09603123.2010.544033.

Guillot, L., Nathan, N., Tabary, O., Thouvenin, G., Le Rouzic, P., Corvol, H., … Clement, A. (2013). Alveolar epithelial cells: master regulators of lung homeostasis. *The International Journal of Biochemistry & Cell Biology* **45**(11):2568–2573. doi: https://doi.org/10.1016/J.BIOCEL.2013.08.009.

Guo, H., Kota, S.H., Chen, K., Sahu, S.K., Hu, J., Ying, Q., … Zhang, H. (2018). Source contributions and potential reductions to health effects of particulate matter in India. *Atmospheric Chemistry and Physics* **18**(20):15219–15229. doi: https://doi.org/10.5194/ACP-18-15219-2018.

Hajj, R., Baranek, T., Le Naour, R., Lesimple, P., Puchelle, E. and Coraux, C. (2007).

Basal cells of the human adult airway surface epithelium retain transit-amplifying cell properties. *Stem cells (Dayton, Ohio)* **25**(1):139–148. doi: https://doi.org/10.1634/STEMCELLS.2006-0288.

Hallgren, O., Rolandsson, S., Andersson-Sjöland, A., Nihlberg, K., Wieslander, E., Kvist-Reimer, M., … Westergren-Thorsson, G. (2012). Enhanced ROCK1 dependent contractility in fibroblast from chronic obstructive pulmonary disease patients. *Journal of Translational Medicine* **10**(1):1–11. doi: https://doi.org/10.1186/1479-5876-10-171/FIGURES/7.

Halse, J., Greenspan, S., Cosman, F., Ellis, G., Santora, A., Leung, A., … Denker, A.E. (2014). A phase 2, randomized, placebo-controlled, dose-ranging study of the calcium-sensing receptor antagonist MK-5442 in the treatment of postmenopausal women with osteoporosis. *The Journal of Clinical Endocrinology and Metabolism* **99**(11):E2207–E2215. doi: https://doi.org/10.1210/JC.2013-4009.

Hamanaka, R.B. and Mutlu, G.M. (2020). The airway epithelial response to air pollution: It's not just inflammation. *American Journal of Respiratory Cell and Molecular Biology* **63**(2):139–140. doi: https://doi.org/10.1165/RCMB.2020-0116ED/SUPPL_FILE/DISCLOSURES.PDF.

Handlogten, M.E., Shiraishi, N., Awata, H., Huang, C. and Miller, R.T. (2000a). Extracellular Ca2+-sensing receptor is a promiscuous divalent cation sensor that responds to lead. *American Journal of Physiology - Renal Physiology* **279**(6 48-6). doi: https://doi.org/10.1152/AJPRENAL.2000.279.6.F1083.

Handlogten, M.E., Shiraishi, N., Awata, H., Huang, C. and Miller, R.T. (2000b). Extracellular Ca2+-sensing receptor is a promiscuous divalent cation sensor that responds to lead. *American Journal of Physiology - Renal Physiology* **279**(6 48-6). doi: https://doi.org/10.1152/ajprenal.2000.279.6.f1083.

Hannan, F.M., Gorvin, C.M., Babinsky, V.N., Olesen, M.K., Stewart, M., Wells, S., … Thakker, R. V. (2020). Calcilytic NPSP795 Increases Plasma Calcium and PTH in an Autosomal Dominant Hypocalcemia Type 1 Mouse Model. *JBMR Plus* **4**(10). doi: https://doi.org/10.1002/JBM4.10402.

Hansbro, P.M., Kim, R.Y., Starkey, M.R., Donovan, C., Dua, K., Mayall, J.R., … Horvat, J.C. (2017). Mechanisms and treatments for severe, steroid-resistant allergic airway disease and asthma. *Immunological Reviews* **278**(1):41–62. doi: https://doi.org/10.1111/IMR.12543.

Haslett, C., Savill, J.S. and Meagher, L. (1989). The neutrophil. *Current Opinion in Immunology* **2**(1):10–18. doi: https://doi.org/10.1016/0952-7915(89)90091-5.

Hauser, A.S., Chavali, S., Masuho, I., Jahn, L.J., Martemyanov, K.A., Gloriam, D.E. and Babu, M.M. (2018). Pharmacogenomics of GPCR Drug Targets. *Cell* **172**(1–2):41-54.e19. doi: https://doi.org/10.1016/J.CELL.2017.11.033.

Havenith, C.E.G., Breedijk, A.J., Van Miert, P.P.M.C., Blijleven, N., Calame, W., Beelen, R.H.J. and Hoefsmit, E.C.M. (1993). Separation of alveolar macrophages and dendritic cells via autofluorescence: phenotypical and functional characterization. *Journal of Leukocyte Biology* **53**(5):504–510. doi: https://doi.org/10.1002/JLB.53.5.504.

Hendy, Geoffrey N and Canaff, L. (2016). Calcium-sensing receptor, proinflammatory cytokines and calcium homeostasis. *Seminars in Cell & Developmental Biology* **49**:37–43. doi: https://doi.org/10.1016/j.semcdb.2015.11.006.

Hendy, Geoffrey N. and Canaff, L. (2016). Calcium-sensing receptor gene: Regulation of expression. *Frontiers in Physiology* **7**(SEP).

Henricks, P.A.J. and Nijkamp, F.P. (2001). Reactive oxygen species as mediators in asthma. *Pulmonary Pharmacology & Therapeutics* **14**(6):409–421. doi: https://doi.org/10.1006/PUPT.2001.0319.

Henry, P.J., Mann, T.S. and Goldie, R.G. (2005). A Rho kinase inhibitor, Y-27632 inhibits pulmonary eosinophilia, bronchoconstriction and airways hyperresponsiveness in allergic mice. *Pulmonary Pharmacology & Therapeutics* **18**(1):67–74. doi: https://doi.org/10.1016/J.PUPT.2004.10.002.

Henson, P.M., Bratton, D.L. and Fadok, V.A. (2001). Apoptotic cell removal. *Current Biology* **11**(19):R795–R805. doi: https://doi.org/10.1016/S0960-9822(01)00474-2.

Hiasa, M., Abe, M., Nakano, A., Oda, A., Amou, H., Kido, S., … Matsumoto, T. (2009). GM-CSF and IL-4 induce dendritic cell differentiation and disrupt osteoclastogenesis through M-CSF receptor shedding by up-regulation of TNF-alpha converting enzyme (TACE). *Blood* **114**(20):4517–4526. doi: https://doi.org/10.1182/BLOOD-2009-04-215020.

Hilligan, K.L. and Ronchese, F. (2020). Antigen presentation by dendritic cells and their instruction of CD4+ T helper cell responses. *Cellular & Molecular Immunology 2020 17:6* **17**(6):587–599. doi: https://doi.org/10.1038/s41423-020-0465-0.

Hiraiwa, K. and Van Eeden, S.F. (2013a). Contribution of lung macrophages to the inflammatory responses induced by exposure to air pollutants. *Mediators of Inflammation* **2013**. doi: https://doi.org/10.1155/2013/619523.

Hiraiwa, K. and Van Eeden, S.F. (2013b). Contribution of Lung Macrophages to the Inflammatory Responses Induced by Exposure to Air Pollutants. *Mediators of Inflammation* **2013**. doi: https://doi.org/10.1155/2013/619523.

Hirota, J.A., Hirota, S.A., Warner, S.M., Stefanowicz, D., Shaheen, F., Beck, P.L., …

Knight, D.A. (2012). The airway epithelium nucleotide-binding domain and leucine-rich repeat protein 3 inflammasome is activated by urban particulate matter. *Journal of Allergy and Clinical Immunology* **129**(4):1116-1125.e6. doi: https://doi.org/10.1016/J.JACI.2011.11.033.

Hitzfeld, B., Friedrichs, K.H., Ring, J. and Behrendt, H. (1997). Airborne particulate matter modulates the production of reactive oxygen species in human polymorphonuclear granulocytes. *Toxicology* **120**(3):185–195. doi: https://doi.org/10.1016/S0300-483X(97)03664-0.

Holder, A.L., Goth-Goldstein, R., Lucas, D. and Koshland, C.P. (2012). Particle-induced artifacts in the MTT and LDH viability assays. *Chemical Research in Toxicology* **25**(9):1885–1892. doi: https://doi.org/10.1021/tx3001708.

Holt, P.G., Schon-Hegrad, M.A. and McMenamin, P.G. (1990). Dendritic cells in the respiratory tract. *International Reviews of Immunology* **6**(2–3):139–49.

Hong, K.U., Reynolds, S.D., Giangreco, A., Hurley, C.M. and Stripp, B.R. (2001). Clara cell secretory protein-expressing cells of the airway neuroepithelial body microenvironment include a label-retaining subset and are critical for epithelial renewal after progenitor cell depletion. *American Journal of Respiratory Cell and Molecular Biology* **24**(6):671–681. doi: https://doi.org/10.1165/AJRCMB.24.6.4498.

Hong, K.U., Reynolds, S.D., Watkins, S., Fuchs, E. and Stripp, B.R. (2004). Basal Cells Are a Multipotent Progenitor Capable of Renewing the Bronchial Epithelium. *The American Journal of Pathology* **164**(2):577. doi: https://doi.org/10.1016/S0002-9440(10)63147-1.

Horak, F., Studnicka, M., Gartner, C., Spengler, J.D., Tauber, E., Urbanek, R., … Frischer, T. (2002). Particulate matter and lung function growth in children: a 3-yr follow-up study in Austrian schoolchildren. *European Respiratory Journal*

19(5):838–845. doi: https://doi.org/10.1183/09031936.02.00512001.

Horvat, J.C., Beagley, K.W., Wade, M.A., Preston, J.A., Hansbro, N.G., Hickey, D.K., … Hansbro, P.M. (2007). Neonatal chlamydial infection induces mixed T-cell responses that drive allergic airway disease. *American Journal of Respiratory and Critical Care Medicine* **176**(6):556–564. doi: https://doi.org/10.1164/RCCM.200607-1005OC.

Horwitz, K.B., Jackson, T.A., Bain, D.L., Richer, J.K., Takimoto, G.S. and Tung, L. (1996). Nuclear receptor coactivators and corepressors. *Molecular Endocrinology* **10**(10):1167–1177. doi: https://doi.org/10.1210/MEND.10.10.9121485.

Htwe, S.S., Cha, B.H., Yue, K., Khademhosseini, A., Knox, A.J. and Ghaemmaghami, A.M. (2017). Role of Rho-Associated coiled-coil forming kinase isoforms in regulation of stiffness-induced myofibroblast differentiation in lung fibrosis. *American Journal of Respiratory Cell and Molecular Biology* **56**(6):772–783. doi: https://doi.org/10.1165/RCMB.2016-0306OC/SUPPL_FILE/DISCLOSURES.PDF.

Hu, J., Jiang, J., Costanzi, S., Thomas, C., … W.Y.-J. of B. and 2006, U. (2006). A missense mutation in the seven-transmembrane domain of the human Ca2+ receptor converts a negative allosteric modulator into a positive allosteric. *Journal of Biological Chemistry* **281**(30):21558–21565.

Huang, K.P. (1989). The mechanism of protein kinase C activation. *Trends in Neurosciences* **12**(11):425–432. doi: https://doi.org/10.1016/0166-2236(89)90091-X.

Huang, P., Mansfield, B., Du, X., Huang, Q., Wang, W., William, F., … Riccardi, D. (2019). Therapeutic effects of topical calcilytic in IgE/Th2 and alarmin-driven surrogates of human asthma. *European Respiratory Journal* **54**(suppl 63):OA4958. doi: https://doi.org/10.1183/13993003.CONGRESS-2019.OA4958.

Huynh, M.L.N., Malcolm, K.C., Kotaru, C., Tilstra, J.A., Westcott, J.Y., Fadok, V.A. and Wenzel, S.E. (2005). Defective apoptotic cell phagocytosis attenuates prostaglandin E2 and 15-hydroxyeicosatetraenoic acid in severe asthma alveolar macrophages. *American Journal of Respiratory and Critical Care Medicine* **172**(8):972–979. doi: https://doi.org/10.1164/RCCM.200501-035OC.

Iamartino, L., Elajnaf, T., Gall, K., David, J., Manhardt, T., Heffeter, P., … Kallay, E. (2020). Effects of pharmacological calcimimetics on colorectal cancer cells over-expressing the human calcium-sensing receptor. *Biochimica et Biophysica Acta (BBA) - Molecular Cell Research* **1867**(12):118836. doi: https://doi.org/10.1016/J.BBAMCR.2020.118836.

IARC (2016). *Sources of Air Pollutants*.*Working Group on the Evaluation of Carcinogenic Risks to Humans*. Available at: https://www.ncbi.nlm.nih.gov/books/NBK368029/ [Accessed: 4 October 2021].

Iijima, K., Kobayashi, T., Hara, K., Kephart, G.M., Ziegler, S.F., McKenzie, A.N. and Kita, H. (2014). IL-33 and Thymic Stromal Lymphopoietin Mediate Immune Pathology in Response to Chronic Airborne Allergen Exposure. *Journal of Immunology* **193**(4):1549. doi: https://doi.org/10.4049/JIMMUNOL.1302984.

Invernizzi, R., Lloyd, C.M. and Molyneaux, P.L. (2020). Respiratory microbiome and epithelial interactions shape immunity in the lungs. *Immunology* **160**(2):171–182. doi: https://doi.org/10.1111/IMM.13195.

Ishii, H., Hayashi, S., Hogg, J.C., Fujii, T., Goto, Y., Sakamoto, N., … van Eeden, S.F. (2005). Alveolar macrophage-epithelial cell interaction following exposure to atmospheric particles induces the release of mediators involved in monocyte mobilization and recruitment. *Respiratory Research* **6**(1). doi: https://doi.org/10.1186/1465-9921-6-87.

Islam, H., Chamberlain, T.C., Mui, A.L. and Little, J.P. (2021). Elevated Interleukin-10 Levels in COVID-19: Potentiation of Pro-Inflammatory Responses or Impaired Anti-Inflammatory Action? *Frontiers in Immunology* **12**:2485. doi: https://doi.org/10.3389/FIMMU.2021.677008/BIBTEX.

Israel, E. and Reddel, H.K. (2017). Severe and difficult-to-treat asthma in adults Drazen, J. M. (ed.). *New England Journal of Medicine* **377**(10):965–976.

Italiani, P. and Boraschi, D. (2014). From monocytes to M1/M2 macrophages: Phenotypical vs. functional differentiation. *Frontiers in Immunology* **5**(OCT):514. doi: https://doi.org/10.3389/FIMMU.2014.00514/BIBTEX.

Ito, H., Yamashita, Y., Tanaka, T., Takaki, M., Le, M.N., Yoshida, L.-M. and Morimoto, K. (2020). Cigarette smoke induces endoplasmic reticulum stress and suppresses efferocytosis through the activation of RhoA. *Scientific Reports* **10**:12620. doi: https://doi.org/10.1038/s41598-020-69610-x.

Jafari, A., Rajabi, A., Gholian-Aval, M., Peyman, N., Mahdizadeh, M. and Tehrani, H. (2021). National, regional, and global prevalence of cigarette smoking among women/females in the general population: a systematic review and meta-analysis. *Environmental Health and Preventive Medicine* **26**(1). doi: https://doi.org/10.1186/S12199-020-00924-Y.

Jaguin, M., Fardel, O. and Lecureur, V. (2015). Exposure to Diesel Exhaust Particle Extracts (DEPe) Impairs Some Polarization Markers and Functions of Human Macrophages through Activation of AhR and Nrf2. *PLOS ONE* **10**(2):e0116560. doi: https://doi.org/10.1371/JOURNAL.PONE.0116560.

Jahnsen, F.L., Strickland, D.H., Thomas, J.A., Tobagus, I.T., Napoli, S., Zosky, G.R., … Holt, P.G. (2006). Accelerated antigen sampling and transport by airway mucosal dendritic cells following inhalation of a bacterial stimulus. *Journal of Immunology*

177(9):5861–5867. doi: https://doi.org/10.4049/JIMMUNOL.177.9.5861.

Jain, V. (2018). Role of Polyamines in Asthma Pathophysiology. *Medical Sciences* **6**(1). doi: https://doi.org/10.3390/MEDSCI6010004.

Jheng, Y.T., Putri, D.U., Chuang, H.C., Lee, K.Y., Chou, H.C., Wang, S.Y. and Han, C.L. (2021). Prolonged exposure to traffic-related particulate matter and gaseous pollutants implicate distinct molecular mechanisms of lung injury in rats. *Particle and Fibre Toxicology* **18**(1):1–16. doi: https://doi.org/10.1186/S12989-021-00417-Y/FIGURES/6.

Jiménez-Uribe, A.P., Valencia-Martínez, H., Carballo-Uicab, G., Vallejo-Castillo, L., Medina-Rivero, E., Chacón-Salinas, R., … Pérez-Tapia, S.M. (2019). CD80 Expression Correlates with IL-6 Production in THP-1-Like Macrophages Costimulated with LPS and Dialyzable Leukocyte Extract (Transferon®). *Journal of Immunology Research* **2019**. doi: https://doi.org/10.1155/2019/2198508.

John, M.R., Harfst, E., Loeffler, J., Belleli, R., Mason, J., Bruin, G.J.M., … Kneissel, M. (2014). AXT914 a novel, orally-active parathyroid hormone-releasing drug in two early studies of healthy volunteers and postmenopausal women. *Bone* **64**:204–210. doi: https://doi.org/10.1016/J.BONE.2014.04.015.

Josephs, T.M., Keller, A.N., Khajehali, E., DeBono, A., Langmead, C.J., Conigrave, A.D., … Leach, K. (2020). Negative allosteric modulators of the human calcium-sensing receptor bind to overlapping and distinct sites within the 7-transmembrane domain. *British Journal of Pharmacology* **177**(8):1917–1930. doi: https://doi.org/10.1111/BPH.14961.

Kadiiska, M.B., Mason, R.P., Dreher, K.L., Costa, D.L. and Ghio, A.J. (1997). In vivo evidence of free radical formation in the rat lung after exposure to an emission source air pollution particle. *Chemical Research in Toxicology* **10**(10):1104–1108.

doi: https://doi.org/10.1021/TX970049R.

Kaku, Y., Imaoka, H., Morimatsu, Y., Komohara, Y., Ohnishi, K., Oda, H., … Hoshino, T. (2014). Overexpression of CD163, CD204 and CD206 on Alveolar Macrophages in the Lungs of Patients with Severe Chronic Obstructive Pulmonary Disease. *PLoS ONE* **9**(1):87400. doi: https://doi.org/10.1371/JOURNAL.PONE.0087400.

Kapellos, T.S., Bonaguro, L., Gemünd, I., Reusch, N., Saglam, A., Hinkley, E.R. and Schultze, J.L. (2019). Human monocyte subsets and phenotypes in major chronic inflammatory diseases. *Frontiers in Immunology* **10**(AUG):2035. doi: https://doi.org/10.3389/FIMMU.2019.02035/BIBTEX.

Kaplan, A., FitzGerald, J.M., Buhl, R., Vogelberg, C. and Hamelmann, E. (2020). Comparing LAMA with LABA and LTRA as add-on therapies in primary care asthma management. *npj Primary Care Respiratory Medicine 2020 30:1* **30**(1):1–11. doi: https://doi.org/10.1038/s41533-020-00205-9.

Kasahara, Y., Tuder, R.M., Cool, C.D., Lynch, D.A., Flores, S.C. and Voelkel, N.F. (2001). Endothelial cell death and decreased expression of vascular endothelial growth factor and vascular endothelial growth factor receptor 2 in emphysema. *American Journal of Respiratory and Critical Care Medicine* **163**(3 Pt 1):737–744. doi: https://doi.org/10.1164/AJRCCM.163.3.2002117.

Kaslick, R.S., Chasens, A.I., Mandel, I.D., Weinstein, D., Waldman, R., Pluhar, T. and Lazzara, R. (1970). Quantitative Analysis of Sodium, Potassium and Calcium in Gingival Fluid from Gingiva in Varying Degrees of Inflammation. *Journal of Periodontology* **41**(2):93–97. doi: https://doi.org/10.1902/JOP.1970.41.2.93.

Kawasaki, T. and Kawai, T. (2014). Toll-like receptor signaling pathways. *Frontiers in Immunology* **5**(SEP):461. doi: https://doi.org/10.3389/FIMMU.2014.00461/BIBTEX.

Kearley, J., Silver, J.S., Sanden, C., Liu, Z., Berlin, A.A., White, N., … Humbles, A.A. (2015). Cigarette smoke silences innate lymphoid cell function and facilitates an exacerbated type I interleukin-33-dependent response to infection. *Immunity* **42**(3):566–579. doi: https://doi.org/10.1016/J.IMMUNI.2015.02.011.

Keet, C.A., Keller, J.P. and Peng, R.D. (2018). Long-term coarse particulate matter exposure is associated with asthma among children in medicaid. *American Journal of Respiratory and Critical Care Medicine* **197**(6):737–746. doi: https://doi.org/10.1164/RCCM.201706-1267OC/SUPPL_FILE/DISCLOSURES.PDF.

Keller, A., Kufareva, I., Josephs, T., Diao, J., … V.M.-M. and 2018, U. (2018). Identification of global and ligand-specific calcium sensing receptor activation mechanisms. *ASPET* **93**(6):619–630.

Kelly, F.J. and Fussell, J.C. (2015). Air pollution and public health: emerging hazards and improved understanding of risk. *Environmental Geochemistry and Health* **37**(4):631–649. doi: https://doi.org/10.1007/S10653-015-9720-1/FIGURES/5.

Kelly, J.C., Lungchukiet, P. and John MacLeod, R. (2011). Extracellular Calcium-Sensing Receptor Inhibition of Intestinal EpithelialTNF Signaling Requires CaSR-Mediated Wnt5a/Ror2 Interaction. *Frontiers in Physiology* **2**. doi: https://doi.org/10.3389/FPHYS.2011.00017.

Kenakin, T. (2017). A Scale of Agonism and Allosteric Modulation for Assessment of Selectivity, Bias, and Receptor Mutation. *Molecular Pharmacology* **92**(4):414–424. doi: https://doi.org/10.1124/MOL.117.108787.

Khan, M.A. and Conigrave, A.D. (2010). Mechanisms of multimodal sensing by extracellular Ca 2+-sensing receptors: A domain-based survey of requirements for binding and signalling. *British Journal of Pharmacology* **159**(5):1039–1050. doi: https://doi.org/10.1111/J.1476-5381.2009.00603.X.

Khreis, H., Kelly, C., Tate, J., Parslow, R., Lucas, K. and Nieuwenhuijsen, M. (2017). Exposure to traffic-related air pollution and risk of development of childhood asthma: A systematic review and meta-analysis. *Environment International* **100**:1–31. doi: https://doi.org/10.1016/J.ENVINT.2016.11.012.

Kifor, O., Macleod, R.J., Diaz, R., Bai, M., Yamaguchi, T., Yao, T., … Brown, E.M. (2001). Regulation of MAP kinase by calcium-sensing receptor in bovine parathyroid and CaR-transfected HEK293 cells. *American Journal of Physiology - Renal Physiology* **280**(2). doi: https://doi.org/10.1152/AJPRENAL.2001.280.2.F291.

Kim, M.J., Kim, J.H., Jeong, G.J., Park, K.Y., Lee, M.K. and Seo, S.J. (2019). Particulate matter induces pro-inflammatory cytokines via phosphorylation of p38 MAPK possibly leading to dermal inflammaging. *Experimental Dermatology* **28**(7):809–815. doi: https://doi.org/10.1111/EXD.13943.

Komuves, L., Oda, Y., Tu, C.L., Chang, W.H., Ho-Pao, C.L., Mauro, T. and Bikle, D.D. (2002). Epidermal expression of the full-length extracellular calcium-sensing receptor is required for normal keratinocyte differentiation. *Journal of Cellular Physiology* **192**(1):45–54. doi: https://doi.org/10.1002/JCP.10107.

Kruse, M., Rosorius, O., Krätzer, F., Bevec, D., Kuhnt, C., Steinkasserer, A., … Hauber, J. (2000). Inhibition of CD83 cell surface expression during dendritic cell maturation by interference with nuclear export of CD83 mRNA. *The Journal of Experimental Medicine* **191**(9):1581–1589. doi: https://doi.org/10.1084/JEM.191.9.1581.

Kunishima, N., Shimada, Y., Tsuji, Y., Sato, T., Yamamoto, M., Kumasaka, T., … Morikawa, K. (2000). Structural basis of glutamate recognition by a dimeric metabotropic glutamate receptor. *Nature* **407**(6807):971–977. doi: https://doi.org/10.1038/35039564.

Lambrecht, B.N., Hammad, H. and Fahy, J. V (2019). The Cytokines of Asthma.

Immunity **50**:975–991. doi: https://doi.org/10.1016/j.immuni.2019.03.018.

Langrish, C.L., Chen, Y., Blumenschein, W.M., Mattson, J., Basham, B., Sedgwick, J.D., … Cua, D.J. (2005). IL-23 drives a pathogenic T cell population that induces autoimmune inflammation. *Journal of Experimental Medicine* **201**(2):233–240. doi: https://doi.org/10.1084/JEM.20041257.

Larsen, S.B., Cowley, C.J. and Fuchs, E. (2020). Epithelial cells: liaisons of immunity. *Current Opinion in Immunology* **62**:45. doi: https://doi.org/10.1016/J.COI.2019.11.004.

Laumbach, R., Meng, Q. and Kipen, H. (2015). What can individuals do to reduce personal health risks from air pollution? *Journal of Thoracic Disease* **7**(1):96. doi: https://doi.org/10.3978/J.ISSN.2072-1439.2014.12.21.

Lavreysen, H., Janssen, C., Bischoff, F., Langlois, X., Leysen, J.E. and Lesage, A.S.J. (2003). [3H]R214127: A Novel High-Affinity Radioligand for the mGlu1 Receptor Reveals a Common Binding Site Shared by Multiple Allosteric Antagonists. *Molecular Pharmacology* **63**(5):1082–1093. doi: https://doi.org/10.1124/MOL.63.5.1082.

Leach, K., Gregory, K., Kufareva, I., Khajehali, E., Research, A.C.-C. and 2016, U. (2016). Towards a structural understanding of allosteric drugs at the human calcium-sensing receptor. *Nature* **26**:574–592.

Leach, K., Hannan, F.M., Josephs, T.M., Keller, A.N., Møller, T.C., Ward, D.T., … Bräuner-Osborne, H. (2020). International Union of Basic and Clinical Pharmacology. CVIII. Calcium-Sensing Receptor Nomenclature, Pharmacology, and Function. *Pharmacological Reviews* **72**(3):558–604. doi: https://doi.org/10.1124/pr.119.018531.

Leach, K., Sexton, P.M., Christopoulos, A. and Conigrave, A.D. (2014). Engendering biased signalling from the calcium-sensing receptor for the pharmacotherapy of diverse disorders. *British Journal of Pharmacology* **171**(5):1142–1155. doi: https://doi.org/10.1111/BPH.12420.

LeBoff, M.S., Shoback, D., Brown, E.M., Thatcher, J., Leombruno, R., Beaudoin, D., … Marynick, S. (1985). Regulation of parathyroid hormone release and cytosolic calcium by extracellular calcium in dispersed and cultured bovine and pathological human parathyroid cells. *The Journal of Clinical investigation* **75**(1):49–57. doi: https://doi.org/10.1172/JCI111696.

Lee, G.S., Subramanian, N., Kim, A.I., Aksentijevich, I., Goldbach-Mansky, R., Sacks, D.B., … Chae, J.J. (2012a). The calcium-sensing receptor regulates the NLRP3 inflammasome through Ca2+ and cAMP. *Nature* **492**(7427):123–127. doi: https://doi.org/10.1038/NATURE11588.

Lee, G.S., Subramanian, N., Kim, A.I., Aksentijevich, I., Goldbach-Mansky, R., Sacks, D.B., … Chae, J.J. (2012b). The calcium-sensing receptor regulates the NLRP3 inflammasome through Ca2+ and cAMP. *Nature* **492**(7427):123–127.

Lee, J.W., Park, J.W., Kwon, O.K., Lee, H.J., Jeong, H.G., Kim, J.H., … Ahn, K.S. (2017). NPS2143 Inhibits MUC5AC and Proinflammatory Mediators in Cigarette Smoke Extract (CSE)-Stimulated Human Airway Epithelial Cells. *Inflammation* **40**(1):184–194. doi: https://doi.org/10.1007/S10753-016-0468-2.

Lee, T.A., Pickard, A.S., Au, D.H., Bartle, B. and Weiss, K.B. (2008). Risk for death associated with medications for recently diagnosed chronic obstructive pulmonary disease. *Annals of Internal Medicine* **149**(6):380–390. doi: https://doi.org/10.7326/0003-4819-149-6-200809160-00004.

Lefrançais, E., Roga, S., Gautier, V., Gonzalez-de-Peredo, A., Monsarrat, B., Girard,

J.P. and Cayrol, C. (2012). IL-33 is processed into mature bioactive forms by neutrophil elastase and cathepsin G. *Proceedings of the National Academy of Sciences of the United States of America* **109**(5):1673–1678. doi: https://doi.org/10.1073/PNAS.1115884109/-/DCSUPPLEMENTAL.

Lefrançais, E., Duval, A., Mirey, E., Roga, S., Espinosa, E., Cayrol, C. and Girard, J.P. (2014). Central domain of IL-33 is cleaved by mast cell proteases for potent activation of group-2 innate lymphoid cells. *Proceedings of the National Academy of Sciences of the United States of America* **111**(43):15502–15507. doi: https://doi.org/10.1073/PNAS.1410700111/-/DCSUPPLEMENTAL.

Leikauf, G.D., Kim, S.H. and Jang, A.S. (2020). Mechanisms of ultrafine particle-induced respiratory health effects. *Experimental & Molecular Medicine 2020 52:3* **52**(3):329–337. doi: https://doi.org/10.1038/s12276-020-0394-0.

Lelieveld, J., Evans, J.S., Fnais, M., Giannadaki, D. and Pozzer, A. (2015). The contribution of outdoor air pollution sources to premature mortality on a global scale. *Nature* **525**(7569):367–371. doi: https://doi.org/10.1038/nature15371.

Lelieveld, J., Pozzer, A., Pö Schl, U., Fnais, M., Haines, A. and Mü Nzel, T. (2020). Loss of life expectancy from air pollution compared to other risk factors: a worldwide perspective. *Cardiovascular Research* **116**(11):1910–1917. doi: https://doi.org/10.1093/cvr/cvaa025.

Lelieveld, J., Pozzer, A., Pöschl, U., Fnais, M., Haines, A. and Münzel, T. (2020). Loss of life expectancy from air pollution compared to other risk factors: a worldwide perspective. *Cardiovascular Research* **116**(11):1910–1917. doi: https://doi.org/10.1093/CVR/CVAA025.

Li, J., Liao, P., Wang, K., Miao, Z., Xiao, R., Zhu, L. and Hu, Q. (2020). Calcium Sensing Receptor Inhibits Growth of Human Lung Adenocarcinoma Possibly via the

GSK3β/Cyclin D1 Pathway. *Frontiers in Cell and Developmental Biology* **8**. doi: https://doi.org/10.3389/FCELL.2020.00446.

Li, M., Wang, Z.N., Yang, L.F., Yan, Y., Cai, L.M., Li, Y.T., … Chen, Z.G. (2017). TLR4 antagonist suppresses airway remodeling in asthma by inhibiting the T-helper 2 response. *Experimental and Therapeutic Medicine* **14**(4):2911–2916. doi: https://doi.org/10.3892/ETM.2017.4898.

Li, T., Sun, M., Yin, X., Wu, C., Wu, Q., Feng, S., … Sun, Y. (2013). Expression of the calcium sensing receptor in human peripheral blood T lymphocyte and its contribution to cytokine secretion through MAPKs or NF-κB pathways. *Molecular Immunology* **53**(4):414–420. doi: https://doi.org/10.1016/J.MOLIMM.2012.09.010.

Li, X., Chen, S., Feng, D., Fu, Y., Wu, H., Lu, J. and Bao, J. (2021). Calcium-sensing receptor promotes calcium oxalate crystal adhesion and renal injury in Wistar rats by promoting ROS production and subsequent regulation of PS ectropion, OPN, KIM-1, and ERK expression. *Renal Failure* **43**(1):465–476. doi: https://doi.org/10.1080/0886022X.2021.1881554.

Li, Z., Ju, X., Silveira, P.A., Abadir, E., Hsu, W.H., Hart, D.N.J. and Clark, G.J. (2019). CD83: Activation marker for antigen presenting cells and its therapeutic potential. *Frontiers in Immunology* **10**(JUN):1312. doi: https://doi.org/10.3389/FIMMU.2019.01312/BIBTEX.

Lim, T.S., Goh, J.K.H., Mortellaro, A., Lim, C.T., Hämmerling, G.J. and Ricciardi-Castagnoli, P. (2012). CD80 and CD86 Differentially Regulate Mechanical Interactions of T-Cells with Antigen-Presenting Dendritic Cells and B-Cells. *PLoS ONE* **7**(9). doi: https://doi.org/10.1371/JOURNAL.PONE.0045185.

Lindberg, J.S., Culleton, B., Wong, G., Borah, M.F., Clark, R. V., Shapiro, W.B., … Coburn, J.W. (2005). Cinacalcet HCl, an Oral Calcimimetic Agent for the Treatment

of Secondary Hyperparathyroidism in Hemodialysis and Peritoneal Dialysis: A Randomized, Double-Blind, Multicenter Study. *Journal of the American Society of Nephrology* **16**(3):800–807. doi: https://doi.org/10.1681/ASN.2004060512.

Lipscomb, M.F., Lyons, C.R., Nunez, G., Ball, E.J., Stastny, P., Vial, W., … Miller, L.M. (1986). Human alveolar macrophages: HLA-DR-positive macrophages that are poor stimulators of a primary mixed leukocyte reaction. *The Journal of Immunology* **136**(2).

Liu, C., Li, Y., Yu, J., Feng, L., Hou, S., Liu, Y., … Ma, C. (2013). Targeting the Shift from M1 to M2 Macrophages in Experimental Autoimmune Encephalomyelitis Mice Treated with Fasudil. *PLoS ONE* **8**(2):e54841. doi: https://doi.org/10.1371/JOURNAL.PONE.0054841.

Liu, D.W., Chen, S.T. and Liu, H.P. (2005). Choice of endogenous control for gene expression in nonsmall cell lung cancer. *European Respiratory Journal* **26**(6):1002 LP – 1008. doi: https://doi.org/10.1183/09031936.05.00050205.

Liu, Y., Pan, J., Zhang, H., Shi, C., Li, G., Peng, Z., … Zhang, L. (2019). Short-Term Exposure to Ambient Air Pollution and Asthma Mortality. *American Journal of Respiratory and Critical Care Medicine* **200**(1):24–32. doi: https://doi.org/10.1164/RCCM.201810-1823OC.

Liu, Z. and Roche, P.A. (2015). Macropinocytosis in phagocytes: Regulation of MHC class-II-restricted antigen presentation in dendritic cells. *Frontiers in Physiology* **6**(JAN):1. doi: https://doi.org/10.3389/FPHYS.2015.00001/BIBTEX.

Livak, K.J. and Schmittgen, T.D. (2001). Analysis of relative gene expression data using real-time quantitative PCR and the 2(-Delta Delta C(T)) Method. *Methods (San Diego, Calif.)* **25**(4):402–408. doi: https://doi.org/10.1006/METH.2001.1262.

Löndahl, J., Massling, A., Pagels, J., Swietlicki, E., Vaclavik, E. and Loft, S. (2007). Size-resolved respiratory-tract deposition of fine and ultrafine hydrophobic and hygroscopic aerosol particles during rest and exercise. *Inhalation Toxicology* **19**(2):109–116. doi: https://doi.org/10.1080/08958370601051677.

Luo, H.R., Li, Y., Jia, Y., Harris, C., Williams, D.A., Mondal, S., … Loison, F. (2011). PTEN Negatively Regulates Engulfment of Apoptotic Cells by Modulating Activation of Rac GTPase. *Journal of Immunology* **187**(11):5783–94. doi: https://doi.org/10.4049/jimmunol.1100484.

Lupardus, P.J. and Garcia, K.C. (2008). The structure of Interleukin-23 reveals the molecular basis of p40 subunit sharing with IL-12. *Journal of Molecular Biology* **382**(4):931. doi: https://doi.org/10.1016/J.JMB.2008.07.051.

Lüthi, A.U., Cullen, S.P., McNeela, E.A., Duriez, P.J., Afonina, I.S., Sheridan, C., … Martin, S.J. (2009). Suppression of interleukin-33 bioactivity through proteolysis by apoptotic caspases. *Immunity* **31**(1):84–98. doi: https://doi.org/10.1016/J.IMMUNI.2009.05.007.

Ma, D.Y. and Clark, E.A. (2009). The role of CD40 and CD40L in Dendritic Cells. *Seminars in Immunology* **21**(5):265. doi: https://doi.org/10.1016/J.SMIM.2009.05.010.

MacKay, C.E., Shaifta, Y., Snetkov, V. V., Francois, A.A., Ward, J.P.T. and Knock, G.A. (2017). ROS-dependent activation of RhoA/Rho-kinase in pulmonary artery: Role of Src-family kinases and ARHGEF1. *Free Radical Biology and Medicine* **110**:316–331. doi: https://doi.org/10.1016/j.freeradbiomed.2017.06.022.

Magno, A.L., Ward, B.K. and Ratajczak, T. (2011). The Calcium-Sensing Receptor: A Molecular Perspective. *Endocrine Reviews* **32**(1):3–30. doi: https://doi.org/10.1210/er.2009-0043.

Mahida, R.Y., Scott, A., Parekh, D., Lugg, S.T., Hardy, R.S., Lavery, G.G., … Thickett, D.R. (2021). Acute Respiratory Distress Syndrome is associated with impaired alveolar macrophage efferocytosis. *European Respiratory Journal* **58**(3). doi: https://doi.org/10.1183/13993003.00829-2021.

Majewski, S. and Piotrowski, W.J. (2020). Air Pollution—An Overlooked Risk Factor for Idiopathic Pulmonary Fibrosis. *Journal of Clinical Medicine 2021, Vol. 10, Page 77* **10**(1):77. doi: https://doi.org/10.3390/JCM10010077.

Majolée, J., Pronk, M.C.A., Jim, K.K., van Bezu, J.S.M., van der Sar, A.M., Hordijk, P.L. and Kovačević, I. (2019). CSN5 inhibition triggers inflammatory signaling and Rho/ROCK-dependent loss of endothelial integrity. *Scientific Reports 2019 9:1* **9**(1):1–12. doi: https://doi.org/10.1038/s41598-019-44595-4.

Maldonado-Pérez, Breitwieser, Gama, Elliott, Ward and Riccardi (2003). Human calcium-sensing receptor can be suppressed by antisense sequences. *Biochemical and Biophysical Research Communications* **311**(3):610–617. doi: https://doi.org/10.1016/J.BBRC.2003.10.041.

Mamillapalli, R., VanHouten, J., Zawalich, W. and Wysolmerski, J. (2008). Switching of G-protein usage by the calcium-sensing receptor reverses its effect on parathyroid hormone-related protein secretion in normal versus malignant breast cells. *The Journal of Biological Chemistry* **283**(36):24435–24447. doi: https://doi.org/10.1074/JBC.M801738200.

Mamillapalli, R. and Wysolmerski, J. (2010). The calcium-sensing receptor couples to Galpha(s) and regulates PTHrP and ACTH secretion in pituitary cells. *The Journal of Endocrinology* **204**(3):287–297. doi: https://doi.org/10.1677/JOE-09-0183.

Mann, E.H., Ho, T.R., Pfeffer, P.E., Matthews, N.C., Chevretton, E., Mudway, I., … Hawrylowicz, C.M. (2017). Vitamin D counteracts an IL-23-dependent IL-17A1IFN-

g1 response driven by urban particulate matter. *American Journal of Respiratory Cell and Molecular Biology* **57**(3):355–366. doi: https://doi.org/10.1165/RCMB.2016-0409OC/SUPPL_FILE/DISCLOSURES.PDF.

Mann, J.S., Howarth, P.H. and Holgate, S.T. (1984). Bronchoconstriction induced by ipratropium bromide in asthma: relation to hypotonicity. *British Medical Journal* **289**(6443):469–469. doi: https://doi.org/10.1136/BMJ.289.6443.469.

Mansfield, B., Ho, T.-R., Mudway, I., Lugg, S.T., Corrigan, C.J., Ward, J.P.T., … Riccardi, D. (2020). Calcium-sensing receptor antagonists, calcilytics, prevent activation of human dendritic and epithelial cells by urban particulate matter. *European Respiratory Journal*. European Respiratory Society (ERS), p. 1970.

Manzano-León, N., Serrano-Lomelin, J., Sánchez, B.N., Quintana-Belmares, R., Vega, E., Vázquez-López, I., … Osornio-Vargas, A.R. (2016). TNFα and IL-6 Responses to Particulate Matter in Vitro: Variation According to PM Size, Season, and Polycyclic Aromatic Hydrocarbon and Soil Content. *Environmental Health Perspectives* **124**(4):406. doi: https://doi.org/10.1289/EHP.1409287.

Marini, M., Vittori, E., Hollemborg, J. and Mattoli, S. (1992). Expression of the potent inflammatory cytokines, granulocyte-macrophage-colony-stimulating factor and interleukin-6 and interleukin-8, in bronchial epithelial cells of patients with asthma. *The Journal of Allergy and Clinical Immunology* **89**(5):1001–1009. doi: https://doi.org/10.1016/0091-6749(92)90223-O.

Marsh, A. (1963). Journal of the Air Pollution Control Association The December Smog. A First Survey. *Journal of the Air Pollution Control Association* **13**(8):384–387. doi: https://doi.org/10.1080/00022470.1963.10468197.

Martinez-Gonzalez, I., Mathä, L., Steer, C.A., Ghaedi, M., Poon, G.F.T. and Takei, F. (2016). Allergen-Experienced Group 2 Innate Lymphoid Cells Acquire Memory-like

Properties and Enhance Allergic Lung Inflammation. *Immunity* **45**(1):198–208. doi: https://doi.org/10.1016/J.IMMUNI.2016.06.017.

Matsuda Futamura, A., Hashimoto, N., Matsumoto, K., Akiko Yagami, H., Orihara, K. and Morita, H. (2019). Human Lung Tissue Cells IL-33 Mediates Inflammatory Responses in. *J Immunol References* **185**:5743–5750. doi: https://doi.org/10.4049/jimmunol.0903818.

Matthews, N.C., Faith, A., Pfeffer, P., Lu, H., Kelly, F.J., Hawrylowicz, C.M. and Lee, T.H. (2014). Urban particulate matter suppresses priming of T helper type 1 cells by granulocyte/macrophage colony-stimulating factor-activated human dendritic cells. *American journal of respiratory cell and molecular biology* **50**(2):130906123417006. doi: https://doi.org/10.1165/RCMB.2012-0465OC.

Matthews, N.C., Pfeffer, P.E., Mann, E.H., Kelly, F.J., Corrigan, C.J., Hawrylowicz, C.M. and Lee, T.H. (2016). Urban particulate matter-activated human dendritic cells induce the expansion of potent inflammatory Th1, Th2, and Th17 effector cells. *American Journal of Respiratory Cell and Molecular Biology* **54**(2):250–262. doi: https://doi.org/10.1165/rcmb.2015-0084OC.

Mazuryk, O., Stochel, G. and Brindell, M. (2020). Variations in Reactive Oxygen Species Generation by Urban Airborne Particulate Matter in Lung Epithelial Cells—Impact of Inorganic Fraction. *Frontiers in Chemistry* **8**:1132. doi: https://doi.org/10.3389/FCHEM.2020.581752/BIBTEX.

Mercer, B.A., Kolesnikova, N., Sonett, J. and D'Armiento, J. (2004). Extracellular Regulated Kinase/Mitogen Activated Protein Kinase Is Up-regulated in Pulmonary Emphysema and Mediates Matrix Metalloproteinase-1 Induction by Cigarette Smoke *. *Journal of Biological Chemistry* **279**(17):17690–17696. doi: https://doi.org/10.1074/JBC.M313842200.

Miedlich, S., Gama, L., Seuwen, K., … R.W.-J. of B. and 2004, U. (2004). Homology modeling of the transmembrane domain of the human calcium sensing receptor and localization of an allosteric binding site. *Journal of Biological Chemistry* **279**(8):7254–63.

Milara, J., Mata, M., Serrano, A., Peiró, T., Morcillo, E.J. and Cortijo, J. (2010). Extracellular calcium-sensing receptor mediates human bronchial epithelial wound repair. *Biochemical Pharmacology* **80**(2):236–246. doi: https://doi.org/10.1016/j.bcp.2010.03.035.

Mills, C.D. (2012). M1 and M2 Macrophages: Oracles of Health and Disease. *Critical Reviews in Immunology* **32**(6):463–488. doi: https://doi.org/10.1615/CRITREVIMMUNOL.V32.I6.10.

Min, P.I., Spurney, R.F., Qisheng, T.U., Hinson, T. and Darryl Quarles, L. (2002). Calcium-sensing receptor activation of rho involves filamin and rho-guanine nucleotide exchange factor. *Endocrinology* **143**(10):3830–3838. doi: https://doi.org/10.1210/EN.2002-220240.

Minshawi, F., Lanvermann, S., McKenzie, E., Jeffery, R., Couper, K., Papoutsopoulou, S., … Muller, W. (2020). The Generation of an Engineered Interleukin-10 Protein With Improved Stability and Biological Function. *Frontiers in Immunology* **11**:1794. doi: https://doi.org/10.3389/FIMMU.2020.01794/BIBTEX.

Mitkus, R.J., Powell, J.L., Zeisler, R. and Squibb, K.S. (2013). Comparative physicochemical and biological characterization of NIST Interim Reference Material PM2.5 and SRM 1648 in human A549 and mouse RAW264.7 cells. *Toxicology in Vitro* **27**(8):2289–2298. doi: https://doi.org/10.1016/J.TIV.2013.09.024.

Mitsi, E., Kamng'ona, R., Rylance, J., Solórzano, C., Jesus Reiné, J., Mwandumba, H.C., … Jambo, K.C. (2018). Human alveolar macrophages predominately express

combined classical M1 and M2 surface markers in steady state. *Respiratory Research* **19**(1). doi: https://doi.org/10.1186/S12931-018-0777-0.

Mohning, M.P., Thomas, S.M., Barthel, L., Mould, K.J., McCubbrey, A.L., Frasch, S.C., … Janssen, W.J. (2018). Phagocytosis of microparticles by alveolar macrophages during acute lung injury requires merTK. *American Journal of Physiology - Lung Cellular and Molecular Physiology* **314**(1):L69–L82. doi: https://doi.org/10.1152/AJPLUNG.00058.2017/ASSET/IMAGES/LARGE/ZH50111773430008.JPEG.

Molostvov, G., Fletcher, S., Bland, R. and Zehnder, D. (2008). Extracellular Calcium-Sensing Receptor Mediated Signalling is Involved in Human Vascular Smooth Muscle Cell Proliferation and Apoptosis. *Cell Physiol Biochem* **22**:413–422.

Mölter, A., Agius, R.M., de Vocht, F., Lindley, S., Gerrard, W., Lowe, L., … Simpson, A. (2013). Long-term exposure to PM10 and NO2 in association with lung volume and airway resistance in the MAAS birth cohort. *Environmental Health Perspectives* **121**(10):1232–1238. doi: https://doi.org/10.1289/EHP.1205961.

Monaco, G., Lee, B., Xu, W., Mustafah, S., Hwang, Y.Y., Carré, C., … Larbi, A. (2019). RNA-Seq Signatures Normalized by mRNA Abundance Allow Absolute Deconvolution of Human Immune Cell Types. *Cell Reports* **26**(6):1627-1640.e7. doi: https://doi.org/10.1016/J.CELREP.2019.01.041.

Moon, H., Min, C., Kim, G., Kim, D., Kim, K., Lee, S.A., … Park, D. (2020). Crbn modulates calcium influx by regulating Orai1 during efferocytosis. *Nature* **11**(1):1–13. doi: https://doi.org/10.1038/s41467-020-19272-0.

Moreira, A.R., de Castro, T.B.P., Kohler, J.B., Ito, J.T., de França Silva, L.E., Lourenço, J.D., … dos Santos Lopes, F.D.T.Q. (2020). Chronic exposure to diesel particles worsened emphysema and increased M2-like phenotype macrophages in a PPE-

induced model. *PLOS ONE* **15**(1):e0228393. doi: https://doi.org/10.1371/JOURNAL.PONE.0228393.

Murphy, J., Summer, R., Wilson, A.A., Kotton, D.N. and Fine, A. (2012). The Prolonged Life-Span of Alveolar Macrophages. *Mediators of Inflammation* **38**(4):380–385. doi: https://doi.org/10.1165/RCMB.2007-0224RC.

Muto, T., Tsuchiya, D., Morikawa, K. and Jingami, H. (2007). Structures of the extracellular regions of the group II/III metabotropic glutamate receptors. *Proceedings of the National Academy of Sciences of the United States of America* **104**(10):3759–3764. doi: https://doi.org/10.1073/PNAS.0611577104.

Næss, Ø., Nafstad, P., Aamodt, G., Claussen, B. and Rosland, P. (2007). Relation between concentration of air pollution and cause-specific mortality: four-year exposures to nitrogen dioxide and particulate matter pollutants in 470 neighborhoods in Oslo, Norway. *American Journal of Epidemiology* **165**(4):435–443. doi: https://doi.org/10.1093/AJE/KWK016.

Nagappan, A., Park, S.B., Lee, S.J. and Moon, Y. (2021). Mechanistic Implications of Biomass-Derived Particulate Matter for Immunity and Immune Disorders. *Toxics* **9**(2):1–22. doi: https://doi.org/10.3390/TOXICS9020018.

Nagarkar, D.R., Poposki, J.A., Tan, B.K., Comeau, M.R., Peters, A.T., Hulse, K.E., … Kato, A. (2013). Thymic stromal lymphopoietin activity is increased in nasal polyps of patients with chronic rhinosinusitis. *The Journal of Allergy and Clinical Immunology* **132**(3). doi: https://doi.org/10.1016/J.JACI.2013.04.005.

National Institute of Standards & Technology (2020). *Standard Reference Material 1648a Certificate of Analysis*. Available at: https://www-s.nist.gov/srmors/certificates/1648A.pdf [Accessed: 28 May 2022].

Nemeth, E.F. and Scarpa, A. (1986). Cytosolic Ca2+ and the regulation of secretion in parathyroid cells. *FEBS letters* **203**(1):15–19. doi: https://doi.org/10.1016/0014-5793(86)81427-2.

Nemeth, E.F. and Scarpa, A. (1987). Rapid mobilization of cellular Ca2+ in bovine parathyroid cells evoked by extracellular divalent cations. Evidence for a cell surface calcium receptor. *Journal of Biological Chemistry* **262**(11):5188–5196. doi: https://doi.org/10.1016/S0021-9258(18)61172-X.

Nemeth, E.F., Steffey, M.E., Hammerland, L.G., Hung, B.C.P., Van Wagenen, B.C., DelMar, E.G. and Balandrin, M.F. (1998). Calcimimetics with potent and selective activity on the parathyroid calcium receptor. *Proceedings of the National Academy of Sciences of the United States of America* **95**(7):4040. doi: https://doi.org/10.1073/PNAS.95.7.4040.

Neves, S.R., Ram, P.T. and Iyengar, R. (2002). G Protein Pathways. *Science* **296**(5573):1636–1639. doi: https://doi.org/10.1126/SCIENCE.1071550.

Newton, K. and Dixit, V.M. (2012). Signaling in Innate Immunity and Inflammation. *Cold Spring Harbor Perspectives in Biology* **4**(3). doi: https://doi.org/10.1101/CSHPERSPECT.A006049.

Nguyen, K.D., Vanichsarn, C. and Nadeau, K.C. (2010). TSLP directly impairs pulmonary Treg function: association with aberrant tolerogenic immunity in asthmatic airway. *Allergy, Asthma, and Clinical Immunology* **6**(1). doi: https://doi.org/10.1186/1710-1492-6-4.

Nguyen, L.P., Al-Sawalha, N.A., Parra, S., Pokkunuri, I., Omoluabi, O., Okulate, A.A., … Bond, R.A. (2017). β 2-Adrenoceptor signaling in airway epithelial cells promotes eosinophilic inflammation, mucous metaplasia, and airway contractility. *Proceedings of the National Academy of Sciences of the United States of America*

114(43):E9163–E9171. doi: https://doi.org/10.1073/PNAS.1710196114.

Nitschké, M., Aebischer, D., Abadier, M., Haener, S., Lucic, M., Vigl, B., … Halin, C. (2012). Differential requirement for ROCK in dendritic cell migration within lymphatic capillaries in steady-state and inflammation. *Blood* **120**(11):2249–2258. doi: https://doi.org/10.1182/BLOOD-2012-03-417923.

Nouno, T., Okamoto, M., Ohnishi, K., Kaieda, S., Tominaga, M., Zaizen, Y., … Hoshino, T. (2019). Elevation of pulmonary CD163+ and CD204+ macrophages is associated with the clinical course of idiopathic pulmonary fibrosis patients. *Journal of Thoracic Disease* **11**(9):4005. doi: https://doi.org/10.21037/JTD.2019.09.03.

Nwaru, B.I., Ekström, M., Hasvold, P., Wiklund, F., Telg, G. and Janson, C. (2020). Overuse of short-acting β2-agonists in asthma is associated with increased risk of exacerbation and mortality: a nationwide cohort study of the global SABINA programme. *European Respiratory Journal* **55**(4). doi: https://doi.org/10.1183/13993003.01872-2019.

Olszak, I.T., Poznansky, M.C., Evans, R.H., Olson, D., Kos, C., Pollak, M.R., … Scadden, D.T. (2000). Extracellular calcium elicits a chemokinetic response from monocytes in vitro and in vivo. *Journal of Clinical Investigation* **105**(9):1299–1305. doi: https://doi.org/10.1172/JCI9799.

Oltmanns, U., Chung, K.F., Walters, M., John, M. and Mitchell, J.A. (2005). Cigarette smoke induces IL-8, but inhibits eotaxin and RANTES release from airway smooth muscle. *Respiratory Research* **6**(1):1–10. doi: https://doi.org/10.1186/1465-9921-6-74.

Oppmann, B., Lesley, R., Blom, B., Timans, J.C., Xu, Y., Hunte, B., … Kastelein, R.A. (2000). Novel p19 Protein Engages IL-12p40 to Form a Cytokine, IL-23, with

Biological Activities Similar as Well as Distinct from IL-12. *Immunity* **13**(5):715–725. doi: https://doi.org/10.1016/S1074-7613(00)00070-4.

Ostro, B., Feng, W.Y., Broadwin, R., Green, S. and Lipsett, M. (2007). The Effects of Components of Fine Particulate Air Pollution on Mortality in California: Results from CALFINE. *Environmental Health Perspectives* **115**(1):13. doi: https://doi.org/10.1289/EHP.9281.

Palm, N.W. and Medzhitov, R. (2009). Pattern recognition receptors and control of adaptive immunity. *Immunological Reviews* **227**(1):221–233. doi: https://doi.org/10.1111/J.1600-065X.2008.00731.X.

Pappas, R.S., Fresquez, M.R., Martone, N. and Watson, C.H. (2014). Toxic Metal Concentrations in Mainstream Smoke from Cigarettes Available in the USA. *Journal of Analytical Toxicology* **38**(4):204. doi: https://doi.org/10.1093/JAT/BKU013.

Park, J.-H., Shin, J.-M., Yang, H.-W., Kim, T.H., Lee, S.H., Lee, H.-M., … Park, I.-H. (2020). Cigarette Smoke Extract Stimulates MMP-2 Production in Nasal Fibroblasts via ROS/PI3K, Akt, and NF-κB Signaling Pathways. *Antioxidants* **9**(8):739. doi: https://doi.org/10.3390/ANTIOX9080739.

Park, S.-J., Nakagawa, T., Kitamura, H., Atsumi, T., Kamon, H., Sawa, S., … Hirano, T. (2004). IL-6 regulates in vivo dendritic cell differentiation through STAT3 activation. *Journal of Immunology* **173**(6):3844–3854. doi: https://doi.org/10.4049/JIMMUNOL.173.6.3844.

Pascoe, G.A., Fariss, M.W., Olafsdottir, K. and Reed, D.J. (1987). A role of vitamin E in protection against cell injury. Maintenance of intracellular glutathione precursors and biosynthesis. *European Journal of Biochemistry* **166**(1):241–247. doi: https://doi.org/10.1111/J.1432-1033.1987.TB13508.X.

Patel, J. and Bridgeman, M.B. (2018). Etelcalcetide (Parsabiv) for Secondary Hyperparathyroidism in Adults With Chronic Kidney Disease on Hemodialysis. *Pharmacy and Therapeutics* **43**(7):396.

Peacock, M., Bilezikian, J.P., Klassen, P.S., Guo, M.D., Turner, S.A. and Shoback, D. (2005). Cinacalcet hydrochloride maintains long-term normocalcemia in patients with primary hyperparathyroidism. *The Journal of Clinical Endocrinology and Metabolism* **90**(1):135–141. doi: https://doi.org/10.1210/JC.2004-0842.

Peng, J., Yang, X.O., Chang, S.H., Yang, J. and Dong, C. (2010). IL-23 signaling enhances Th2 polarization and regulates allergic airway inflammation. *Cell Research* **20**(1):62. doi: https://doi.org/10.1038/CR.2009.128.

Penn, R.B. (2008). Embracing emerging paradigms of G protein-coupled receptor agonism and signaling to address airway smooth muscle pathobiology in asthma. *Naunyn-Schmiedeberg's Archives of Pharmacology* **378**(2):149–169. doi: https://doi.org/10.1007/S00210-008-0263-1.

Perera, F. (2018). Pollution from Fossil-Fuel Combustion is the Leading Environmental Threat to Global Pediatric Health and Equity: Solutions Exist. *International Journal of Environmental Research and Public Health* **15**(1). doi: https://doi.org/10.3390/IJERPH15010016.

Pérez-Ricart, A., Galicia-Basart, M., Alcalde-Rodrigo, M., Segarra-Medrano, A., Suñé-Negre, J.M. and Montoro-Ronsano, J.B. (2016). Effectiveness of Cinacalcet in Patients with Chronic Kidney Disease and Secondary Hyperparathyroidism Not Receiving Dialysis. *PLOS ONE* **11**(9):e0161527. doi: https://doi.org/10.1371/JOURNAL.PONE.0161527.

Perez, J.F. and Sanderson, M.J. (2005). The contraction of smooth muscle cells of intrapulmonary arterioles is determined by the frequency of Ca2+ oscillations

induced by 5-HT and KCl. *The Journal of General Physiology* **125**(6):555–567. doi: https://doi.org/10.1085/JGP.200409217.

Perlman, H., Pagliari, L.J., Georganas, C., Mano, T., Walsh, K. and Pope, R.M. (1999). Flice-Inhibitory Protein Expression during Macrophage Differentiation Confers Resistance to FAS-Mediated Apoptosis. *The Journal of Experimental Medicine* **190**(11):1679. doi: https://doi.org/10.1084/JEM.190.11.1679.

Petrel, C., Kessler, A., Dauban, P., … R.D.-J. of B. and 2004, U. (2004). Positive and negative allosteric modulators of the Ca2+-sensing receptor interact within overlapping but not identical binding sites in the transmembrane. *Journal of Biological Chemistry*.

Petrel, C., Kessler, A., Maslah, F., … P.D.-J. of B. and 2003, U. (2003). Modeling and mutagenesis of the binding site of Calhex 231, a novel negative allosteric modulator of the extracellular Ca2+-sensing receptor. *Journal of Biological Chemistry*.

Pfeffer, P.E., Ho, T.R., Mann, E.H., Kelly, F.J., Sehlstedt, M., Pourazar, J., … Hawrylowicz, C.M. (2018). Urban particulate matter stimulation of human dendritic cells enhances priming of naive CD8 T lymphocytes. *Immunology* **153**(4):502–512. doi: https://doi.org/10.1111/IMM.12852.

Pfeffer, P.E., Lu, H., Mann, E.H., Chen, Y.-H., Ho, T.-R., Cousins, D.J., … Hawrylowicz, C.M. (2018a). Effects of vitamin D on inflammatory and oxidative stress responses of human bronchial epithelial cells exposed to particulate matter Loukides, S. (ed.). *PLOS ONE* **13**(8):e0200040. doi: https://doi.org/10.1371/journal.pone.0200040.

Pfeffer, P.E., Lu, H., Mann, E.H., Chen, Y.-H., Ho, T.-R., Cousins, D.J., … Hawrylowicz, C.M. (2018b). Effects of vitamin D on inflammatory and oxidative stress responses of human bronchial epithelial cells exposed to particulate matter. *PLOS ONE*

13(8):e0200040. doi: https://doi.org/10.1371/JOURNAL.PONE.0200040.

Pidasheva, S., Canaff, L., Simonds, W.F., Marx, S.J. and Hendy, G.N. (2005). Impaired cotranslational processing of the calcium-sensing receptor due to signal peptide missense mutations in familial hypocalciuric hypercalcemia. *Human Molecular Genetics* **14**(12):1679–1690. doi: https://doi.org/10.1093/HMG/DDI176.

Prazma, C.M. and Tedder, T.F. (2008). Dendritic cell CD83: A therapeutic target or innocent bystander? *Immunology Letters* **115**(1):1–8. doi: https://doi.org/10.1016/J.IMLET.2007.10.001.

Prechtel, A.T. and Steinkasserer, A. (2007). CD83: an update on functions and prospects of the maturation marker of dendritic cells. *Archives of Dermatological Research 2007 299:2* **299**(2):59–69. doi: https://doi.org/10.1007/S00403-007-0743-Z.

Préfontaine, D., Nadigel, J., Chouiali, F., Audusseau, S., Semlali, A., Chakir, J., … Hamid, Q. (2010). Increased IL-33 expression by epithelial cells in bronchial asthma. *The Journal of Allergy and Clinical Immunology* **125**(3):752–754. doi: https://doi.org/10.1016/J.JACI.2009.12.935.

Quarles, L.D. (2005). Cinacalcet HCl: A novel treatment for secondary hyperparathyroidism in stage 5 chronic kidney disease. *Kidney International* **68**:S24–S28. doi: https://doi.org/10.1016/S0085-2538(15)51229-5.

Quinn, S.J., Ye, C.P., Diaz, R., Kifor, O., Bai, M., Vassilev, P. and Brown, E. (1997). The Ca2+-sensing receptor: A target for polyamines. *American Journal of Physiology - Cell Physiology* **273**(4 42-4):1315–1323. doi: https://doi.org/10.1152/AJPCELL.1997.273.4.C1315/ASSET/IMAGES/LARGE/ACEL0103211.JPEG.

Raeiszadeh Jahromi, S., Mahesh, P.A., Jayaraj, B.S., Madhunapantula, S.R. V., Holla, A.D., Vishweswaraiah, S. and Ramachandra, N.B. (2014). Serum levels of IL-10, IL-17F and IL-33 in patients with asthma: a case-control study. *The Journal of Asthma* **51**(10):1004–1013. doi: https://doi.org/10.3109/02770903.2014.938353.

Rahman, Q., Abidi, P., Afaq, F., Schiffmann, D., Mossman, B.T., Kamp, D.W. and Athar, M. (1999). Glutathione redox system in oxidative lung injury. *Critical Reviews in Toxicology* **29**(6):543–568. doi: https://doi.org/10.1080/10408449991349276.

Rasschaert, J. and Malaisse, W.J. (1999). Expression of the Calcium-Sensing Receptor in Pancreatic Islet B-Cells. *Biochemical and Biophysical Research Communications* **264**(3):615–618. doi: https://doi.org/10.1006/BBRC.1999.1577.

Ray, K. and Northup, J.-J. (2002). Evidence for distinct cation and calcimimetic compound (NPS 568) recognition domains in the transmembrane regions of the human Ca2+ receptor. *Journal of Biological Chemistry* **277**(21):18908–13.

Reinhardt, R.L., Hong, S., Kang, S.-J., Wang, Z. and Locksley, R.M. (2006). Visualization of IL-12/23p40 In Vivo Reveals Immunostimulatory Dendritic Cell Migrants that Promote Th1 Differentiation. *The Journal of Immunology* **177**(3):1618–1627. doi: https://doi.org/10.4049/JIMMUNOL.177.3.1618.

Ren, Z., Yang, K., Zhao, M., Liu, W., Zhang, Xin, Chi, J., … Yin, X. (2020). Calcium-Sensing Receptor on Neutrophil Promotes Myocardial Apoptosis and Fibrosis After Acute Myocardial Infarction via NLRP3 Inflammasome Activation. *The Canadian Journal of Cardiology* **36**(6):893–905. doi: https://doi.org/10.1016/J.CJCA.2019.09.026.

Rhen, T. and Cidlowski, J.A. (2009). Antiinflammatory Action of Glucocorticoids — New Mechanisms for Old Drugs. *New England Journal of Medicine* **353**(16):1711–1723. doi: https://doi.org/10.1056/NEJMRA050541.

Riccardi, D., Brennan, S.C. and Chang, W. (2013). The extracellular calcium-sensing receptor, CaSR, in fetal development. *Best Practice & Research. Clinical Endocrinology & Metabolism* **27**(3):443–453. doi: https://doi.org/10.1016/J.BEEM.2013.02.010.

Riccardi, D., Park, J., Lee, W. Sen, Gamba, G., Brown, E.M. and Hebert, S.C. (1995). Cloning and functional expression of a rat kidney extracellular calcium/polyvalent cation-sensing receptor. *Proceedings of the National Academy of Sciences of the United States of America* **92**(1):131–135. doi: https://doi.org/10.1073/PNAS.92.1.131.

Rider, P., Voronov, E., Dinarello, C.A., Apte, R.N. and Cohen, I. (2017). Alarmins: Feel the Stress. *Journal of Immunology* **198**(4):1395–1402. doi: https://doi.org/10.4049/JIMMUNOL.1601342.

Ritchie, H. and Roser, M. (2019). *Outdoor Air Pollution*.*Our World In Data*. Available at: https://ourworldindata.org/outdoor-air-pollution#citation [Accessed: 17 May 2022].

Ritter, C., Haughey, B., … H.A.-T.J. of steroid and 2012, U. (2012). Distribution and regulation of the 25-hydroxyvitamin D3 1α-hydroxylase in human parathyroid glands. *Elsevier*.

Roberts, M.S., Gafni, R.I., Brillante, B., Guthrie, L.C., Streit, J., Gash, D., … Collins, M.T. (2019). Treatment of Autosomal Dominant Hypocalcemia Type 1 With the Calcilytic NPSP795 (SHP635). *Journal of Bone and Mineral Research* **34**(9):1609–1618. doi: https://doi.org/10.1002/JBMR.3747.

Robertson, W.G., Marshall, R.W. and Bowers, G.N. (1981). Ionized calcium in body fluids. *Critical Reviews in Clinical Laboratory Sciences* **15**(2):85–125. doi: https://doi.org/10.3109/10408368109105869.

Rock, J.R., Onaitis, M.W., Rawlins, E.L., Lu, Y., Clark, C.P., Xue, Y., … Hogan, B.L.M. (2009). Basal cells as stem cells of the mouse trachea and human airway epithelium. *Proceedings of the National Academy of Sciences of the United States of America* **106**(31):12771–12775. doi: https://doi.org/10.1073/PNAS.0906850106/SUPPL_FILE/0906850106SI.PDF.

Rossol, M., Pierer, M., Raulien, N., Quandt, D., Meusch, U., Rothe, K., … Wagner, U. (2012a). Extracellular Ca2+ is a danger signal activating the NLRP3 inflammasome through G protein-coupled calcium sensing receptors. *Nature* **3**:1329. doi: https://doi.org/10.1038/ncomms2339.

Rossol, M., Pierer, M., Raulien, N., Quandt, D., Meusch, U., Rothe, K., … Wagner, U. (2012b). Extracellular Ca2+ is a danger signal activating the NLRP3 inflammasome through G protein-coupled calcium sensing receptors. *Nature* **3**(1):1–9. doi: https://doi.org/10.1038/ncomms2339.

Rowe, B.H., Bota, G.W., Fabris, L., Therrien, S.A., Milner, R.A. and Jacono, J. (1999). Inhaled Budesonide in Addition to Oral Corticosteroids to Prevent Asthma Relapse Following Discharge From the Emergency Department: A Randomized Controlled Trial. *JAMA* **281**(22):2119–2126. doi: https://doi.org/10.1001/JAMA.281.22.2119.

Ruat, M., Molliver, M.E., Snowman, A.M. and Snyder, S.H. (1995). Calcium sensing receptor: molecular cloning in rat and localization to nerve terminals. *Proceedings of the National Academy of Sciences of the United States of America* **92**(8):3161. doi: https://doi.org/10.1073/PNAS.92.8.3161.

Rubins, J.B. (2003). Alveolar Macrophages. *American Journal of Respiratory and Critical Care Medicine* **167**(2):103–104. doi: https://doi.org/10.1164/rccm.2210007.

Rybchyn, M.S., Islam, K.S., Brennan-Speranza, T.C., Cheng, Z., Brennan, S.C., Chang, W., … Conigrave, A.D. (2019). Homer1 mediates CaSR-dependent activation of

mTOR complex 2 and initiates a novel pathway for AKT-dependent β-catenin stabilization in osteoblasts. *Journal of Biological Chemistry* **294**(44):16337–16350. doi: https://doi.org/10.1074/JBC.RA118.006587/ATTACHMENT/F783B47E-81DB-475C-8004-BFA3B91656CD/MMC1.ZIP.

Salter, B.M., Oliveria, J.P., Nusca, G., Smith, S.G., Watson, R.M., Comeau, M., … Gauvreau, G.M. (2015). Thymic stromal lymphopoietin activation of basophils in patients with allergic asthma is IL-3 dependent. *The Journal of Allergy and Clinical Immunology* **136**(6):1636–1644. doi: https://doi.org/10.1016/J.JACI.2015.03.039.

Sander, J., Schmidt, S. V., Cirovic, B., McGovern, N., Papantonopoulou, O., Hardt, A.L., … Schultze, J.L. (2017). Cellular Differentiation of Human Monocytes Is Regulated by Time-Dependent Interleukin-4 Signaling and the Transcriptional Regulator NCOR2. *Immunity* **47**(6):1051. doi: https://doi.org/10.1016/J.IMMUNI.2017.11.024.

Schmiedel, B.J., Singh, D., Madrigal, A., Valdovino-Gonzalez, A.G., White, B.M., Zapardiel-Gonzalo, J., … Vijayanand, P. (2018). Impact of Genetic Polymorphisms on Human Immune Cell Gene Expression. *Cell* **175**(6):1701-1715.e16. doi: https://doi.org/10.1016/J.CELL.2018.10.022.

Schwende, H., Fitzke, E., Ambs, P. and Dieter, P. (1996). Differences in the state of differentiation of THP-1 cells induced by phorbol ester and 1 ,25-dihydroxyvitamin D3. *Journal of Leukocyte Biology* **59**.

Shadie, A.M., Herbert, C. and Kumar, R.K. (2014). Ambient particulate matter induces an exacerbation of airway inflammation in experimental asthma: role of interleukin-33. *Clinical and Experimental Immunology* **177**(2):491–499. doi: https://doi.org/10.1111/CEI.12348.

Shannon, J., Ernst, P., Yamauchi, Y., Olivenstein, R., Lemiere, C., Foley, S., … Martin,

J.G. (2008). Differences in airway cytokine profile in severe asthma compared to moderate asthma. *Chest* **133**(2):420–426. doi: https://doi.org/10.1378/CHEST.07-1881.

Shapiro, S.D. (2004). The search for biological truth using imperfect models in an imperfect world. *American Journal of Respiratory Cell and Molecular Biology* **31**(5):479. doi: https://doi.org/10.1165/rcmb.F283.

Shikotra, A., Choy, D.F., Ohri, C.M., Doran, E., Butler, C., Hargadon, B., … Bradding, P. (2012). Increased expression of immunoreactive thymic stromal lymphopoietin in patients with severe asthma. *The Journal of Allergy and Clinical Immunology* **129**(1). doi: https://doi.org/10.1016/J.JACI.2011.08.031.

Shorte, S.L., Stafford, S.J.V., Collett, V.J. and Schofield, J.G. (1995). Simultaneous measurement of [Ca2+]i and secretion-coupled membrane turnover, by single cell fluorescence microscopy. *Cell Calcium* **18**(5):440–454. doi: https://doi.org/10.1016/0143-4160(95)90059-4.

Shridhar, K., Kinra, S., Gupta, R., Khandelwal, S., D, P., Cox, S.E. and Dhillon, P.K. (2019). Serum Calcium Concentrations, Chronic Inflammation and Glucose Metabolism: A Cross-Sectional Analysis in the Andhra Pradesh Children and Parents Study (APCaPS). *Current Developments in Nutrition* **3**(3). doi: https://doi.org/10.1093/CDN/NZY085.

Singanayagam, A., Glanville, N., Walton, R.P., Aniscenko, J., Pearson, R.M., Pinkerton, J.W., … Johnston, S.L. (2015). A short-term mouse model that reproduces the immunopathological features of rhinovirus-induced exacerbation of COPD. *Clinical Science* **129**(3):245–258. doi: https://doi.org/10.1042/CS20140654.

De Smedt, T., Van Mechelen, M., De Becker, G., Urbain, J., Leo, O. and Moser, M.

(1997). Effect of interleukin-10 on dendritic cell maturation and function. *European Journal of Immunology* **27**(5):1229–1235. doi: https://doi.org/10.1002/EJI.1830270526.

Sokol, C.L. and Luster, A.D. (2015). The chemokine system in innate immunity. *Cold Spring Harbor Perspectives in Biology* **7**(5):1–20. doi: https://doi.org/10.1101/CSHPERSPECT.A016303.

Sousa and Caetano (2006). Dendritic cells in a mature age. *Nature Reviews Immunology* **6**(6):476–483. doi: https://doi.org/10.1038/nri1845.

Sriram, K. and Insel, P.A. (2018). G Protein-Coupled Receptors as Targets for Approved Drugs: How Many Targets and How Many Drugs? *Molecular Pharmacology* **93**(4):251–258. doi: https://doi.org/10.1124/MOL.117.111062.

Steinbrink, K., Graulich, E., Kubsch, S., Knop, J. and Enk, A.H. (2002). CD4(+) and CD8(+) anergic T cells induced by interleukin-10-treated human dendritic cells display antigen-specific suppressor activity. *Blood* **99**(7):2468–2476. doi: https://doi.org/10.1182/BLOOD.V99.7.2468.

Steinman, R.M. and Hemmi, H. (2006). Dendritic cells: translating innate to adaptive immunity. *Current Topics in Microbiology and Immunology* **311**:17–58. doi: https://doi.org/10.1007/3-540-32636-7_2.

Sung, S.-S.J., Fu, S.M., Rose, C.E., Gaskin, F., Ju, S.-T. and Beaty, S.R. (2006). A major lung CD103 (alphaE)-beta7 integrin-positive epithelial dendritic cell population expressing Langerin and tight junction proteins. *Journal of Immunology* **176**(4):2161–2172. doi: https://doi.org/10.4049/JIMMUNOL.176.4.2161.

Takeda, K., Kaisho, T. and Akira, S. (2003). Toll-like receptors. *Annual Review of Immunology* **21**:335–376. doi:

https://doi.org/10.1146/ANNUREV.IMMUNOL.21.120601.141126.

Tang, Q., Huang, K., Liu, J., Wu, S., Shen, D., Dai, P. and Li, C. (2019a). Fine particulate matter from pig house induced immune response by activating TLR4/MAPK/NF-κB pathway and NLRP3 inflammasome in alveolar macrophages. *Chemosphere* **236**:124373. doi: https://doi.org/10.1016/J.CHEMOSPHERE.2019.124373.

Tang, Q., Huang, K., Liu, J., Wu, S., Shen, D., Dai, P. and Li, C. (2019b). Fine particulate matter from pig house induced immune response by activating TLR4/MAPK/NF-κB pathway and NLRP3 inflammasome in alveolar macrophages. *Chemosphere* **236**. doi: https://doi.org/10.1016/J.CHEMOSPHERE.2019.124373.

Tata, P.R., Mou, H., Pardo-Saganta, A., Zhao, R., Prabhu, M., Law, B.M., … Rajagopal, J. (2013). Dedifferentiation of committed epithelial cells into stem cells in vivo. *Nature* **503**(7475):218–223. doi: https://doi.org/10.1038/NATURE12777.

Tato, C.M. and Cua, D.J. (2008). Reconciling id, ego, and superego within interleukin-23. *Immunological Reviews* **226**(1):103–111. doi: https://doi.org/10.1111/J.1600-065X.2008.00715.X.

Teng, M.W.L., Bowman, E.P., McElwee, J.J., Smyth, M.J., Casanova, J.L., Cooper, A.M. and Cua, D.J. (2015). IL-12 and IL-23 cytokines: from discovery to targeted therapies for immune-mediated inflammatory diseases. *Nature Medicine* **21**(7):719–729. doi: https://doi.org/10.1038/nm.3895.

Tennakoon, S., Aggarwal, A. and Kállay, E. (2016). The calcium-sensing receptor and the hallmarks of cancer. *Biochimica et Biophysica Acta - Molecular Cell Research* **1863**(6 Pt B):1398–1407. doi: https://doi.org/10.1016/J.BBAMCR.2015.11.017.

Teshima, K., Yamamoto, A., Yamaoka, K., Honda, Y., Honda, S., Sasaki, T. and Kojima, S. (2000). Involvement of calcium ion in elevation of mRNA for gamma-glutamylcysteine synthetase (gamma-GCS) induced by low-dose gamma-rays. *International Journal of Radiation Biology* **76**(12):1631–1639. doi: https://doi.org/10.1080/09553000050201127.

Thomsen, A.R.B., Worm, J., Jacobsen, S.E., Stahlhut, M., Latta, M. and Braüner-Osborne, H. (2012). Strontium is a biased agonist of the calcium-sensing receptor in rat medullary thyroid carcinoma 6-23 cells. *Journal of Pharmacology and Experimental Therapeutics* **343**(3):638–649. doi: https://doi.org/10.1124/jpet.112.197210.

Thurston, G.D., Balmes, J.R., Garcia, E., Gilliland, F.D., Rice, M.B., Schikowski, T., … White, C.W. (2020). Outdoor Air Pollution and New-Onset Airway Disease. An Official American Thoracic Society Workshop Report. *Annals of American Thoracic Society* **17**(4):387–398. doi: https://doi.org/10.1513/ANNALSATS.202001-046ST.

Travaglini, K.J., Nabhan, A.N., Penland, L., Sinha, R., Gillich, A., Sit, R. V., … Krasnow, M.A. (2020). A molecular cell atlas of the human lung from single-cell RNA sequencing. *Nature* **587**(7835):619–625. doi: https://doi.org/10.1038/s41586-020-2922-4.

Tsuchiya, D., Kunishima, N., Kamiya, N., Jingami, H. and Morikawa, K. (2002). Structural views of the ligand-binding cores of a metabotropic glutamate receptor complexed with an antagonist and both glutamate and Gd3+. *Proceedings of the National Academy of Sciences of the United States of America* **99**(5):2660–2665. doi: https://doi.org/10.1073/PNAS.052708599.

Usmani, O.S., Ito, K., Maneechotesuwan, K., Ito, M., Johnson, M., Barnes, P.J. and Adcock, I.M. (2012). Glucocorticoid Receptor Nuclear Translocation in Airway Cells

after Inhaled Combination Therapy. *American Journal of Respiratory and Critical Care Medicine* **172**(6):704–712. doi: https://doi.org/10.1164/RCCM.200408-1041OC.

Vaeth, M., Zee, I., Concepcion, A.R., Maus, M., Shaw, P., Portal-Celhay, C., … Feske, S. (2015). Ca2+ signaling but not store-operated Ca2+ entry (SOCE) is required for the function of macrophages and dendritic cells. *Journal of Immunology* **195**(3):1202. doi: https://doi.org/10.4049/JIMMUNOL.1403013.

Valacchi, G., Magnani, N., Woodby, B., Ferreira, S.M. and Evelson, P. (2020). Particulate Matter Induces Tissue OxInflammation: From Mechanism to Damage. *Antioxidants and Redox Signalling* **33**(4):308–326. doi: https://doi.org/10.1089/ARS.2019.8015.

Valavanidis, A., Fiotakis, K. and Vlachogianni, T. (2008). Airborne particulate matter and human health: toxicological assessment and importance of size and composition of particles for oxidative damage and carcinogenic mechanisms. *Journal of Environmental Science and Health* **26**(4):339–362. doi: https://doi.org/10.1080/10590500802494538.

van EEDEN, S.F., TAN, W.C., SUWA, T., MUKAE, H., TERASHIMA, T., FUJII, T., … HOGG, J.C. (2001). Cytokines Involved in the Systemic Inflammatory Response Induced by Exposure to Particulate Matter Air Pollutants (PM_{10}). *American Journal of Respiratory and Critical Care Medicine* **164**(5):826–830. doi: https://doi.org/10.1164/ajrccm.164.5.2010160.

Vardhan, A. and Hutchison, A.J. (2017). Peritoneal Dialysis Solutions. *Handbook of Dialysis Therapy* **5**:408-417.e1. doi: https://doi.org/10.1016/B978-0-323-39154-2.00032-1.

Vaughan, A. (2021). 'Ella's law' for clean air would honour her. *New Scientist*

249(3316):14. doi: https://doi.org/10.1016/S0262-4079(21)00007-5.

Verdijk, P., van Veelen, P.A., de Ru, A.H., Hensbergen, P.J., Mizuno, K., Koerten, H.K., … Mommaas, A.M. (2004). Morphological changes during dendritic cell maturation correlate with cofilin activation and translocation to the cell membrane. *European Journal of Immunology* **34**(1):156–164. doi: https://doi.org/10.1002/EJI.200324241.

Vieira Braga, F.A., Kar, G., Berg, M., Carpaij, O.A., Polanski, K., Simon, L.M., … Teichmann, S.A. (2019). A cellular census of human lungs identifies novel cell states in health and in asthma. *Nature Medicine* **25**(7):1153–1163. doi: https://doi.org/10.1038/s41591-019-0468-5.

Virchow, J.C., Kuna, P., Paggiaro, P., Papi, A., Singh, D., Corre, S., … Canonica, G.W. (2019). Single inhaler extrafine triple therapy in uncontrolled asthma (TRIMARAN and TRIGGER): two double-blind, parallel-group, randomised, controlled phase 3 trials. *The Lancet* **394**(10210):1737–1749. doi: https://doi.org/10.1016/S0140-6736(19)32215-9.

Vohra, K., Vodonos, A., Schwartz, J., Marais, E.A., Sulprizio, M.P. and Mickley, L.J. (2021). Global mortality from outdoor fine particle pollution generated by fossil fuel combustion: Results from GEOS-Chem. *Environmental Research* **195**:110754. doi: https://doi.org/10.1016/J.ENVRES.2021.110754.

Walker, J.K.L., Penn, R.B., Hanania, N.A., Dickey, B.F. and Bond, R.A. (2011). New perspectives regarding β(2) -adrenoceptor ligands in the treatment of asthma. *British journal of pharmacology* **163**(1):18–28. doi: https://doi.org/10.1111/J.1476-5381.2010.01178.X.

Walters, M.J., Paul-Clark, M.J., McMaster, S.K., Ito, K., Adcock, I.M. and Mitchell, J.A. (2005). Cigarette Smoke Activates Human Monocytes by an Oxidant-AP-1 Signaling Pathway: Implications for Steroid Resistance. *Molecular Pharmacology*

68(5):1343–1353. doi: https://doi.org/10.1124/MOL.105.012591.

Wang, H.Y., Liu, X.Y., Han, G., Wang, Z.Y., Li, X.X., Jiang, Z.M. and Jiang, C.M. (2013). LPS induces cardiomyocyte injury through calcium-sensing receptor. *Molecular and Cellular Biochemistry* **379**(1):153. doi: https://doi.org/10.1007/S11010-013-1637-3.

Wang, L., Chitano, P., Paré, P.D. and Seow, C.Y. (2020). Upregulation of smooth muscle Rho-kinase protein expression in human asthma. *The European Respiratory Journal* **55**(3). doi: https://doi.org/10.1183/13993003.01785-2019.

Wang, M., Aaron, C.P., Madrigano, J., Hoffman, E.A., Angelini, E., Yang, J., … Barr, R.G. (2019). Association Between Long-term Exposure to Ambient Air Pollution and Change in Quantitatively Assessed Emphysema and Lung Function. *JAMA* **322**(6):546–556. doi: https://doi.org/10.1001/JAMA.2019.10255.

Wang, Y.L., Gao, W., Li, Y. and Wang, Y.F. (2017). Concentration-dependent effects of PM2.5 mass on expressions of adhesion molecules and inflammatory cytokines in nasal mucosa of rats with allergic rhinitis. *European Archives of Oto-Rhino-Laryngology* **274**(8):3221–3229. doi: https://doi.org/10.1007/s00405-017-4606-8.

Wang, Z., Zhou, Y., Zhang, Y., Huang, X., Duan, X., Chen, D., … Ran, P. (2021). Association of change in air quality with hospital admission for acute exacerbation of chronic obstructive pulmonary disease in Guangdong, China: A province-wide ecological study. *Ecotoxicology and Environmental Safety* **208**:111590. doi: https://doi.org/10.1016/J.ECOENV.2020.111590.

Ward, D.T. (2004). Calcium receptor-mediated intracellular signalling. *Cell calcium* **35**(3):217–228. doi: https://doi.org/10.1016/J.CECA.2003.10.017.

Ward, D.T., Brown, E.M. and Harris, H.W. (1998). Disulfide bonds in the extracellular calcium-polyvalent cation-sensing receptor correlate with dimer formation and its

response to divalent cations in vitro. *The Journal of Biological Chemistry* **273**(23):14476–14483. doi: https://doi.org/10.1074/JBC.273.23.14476.

Ward, D.T., McLarnon, S.J. and Riccardi, D. (2002). Aminoglycosides increase intracellular calcium levels and ERK activity in proximal tubular OK cells expressing the extracellular calcium-sensing receptor. *Journal of the American Society of Nephrology : JASN* **13**(6):1481–1489. doi: https://doi.org/10.1097/01.ASN.0000015623.73739.B8.

Wasserman, K., Subklewe, M., Pothoff, G., Banik, N. and Schell-Frederick, E. (1994). Expression of surface markers on alveolar macrophages from symptomatic patients with HIV infection as detected by flow cytometry. *Chest* **105**(5):1324–1334. doi: https://doi.org/10.1378/CHEST.105.5.1324.

Weston, A.H., Absi, M., Ward, D.T., Ohanian, J., Dodd, R.H., Dauban, P., … Edwards, G. (2005). Evidence in favor of a calcium-sensing receptor in arterial endothelial cells: studies with calindol and Calhex 231. *Circulation Research* **97**(4):391–398. doi: https://doi.org/10.1161/01.RES.0000178787.59594.A0.

Whitsett, J.A. (2018). Airway Epithelial Differentiation and Mucociliary Clearance. *Annals of the American Thoracic Society* **15**(Suppl 3):S143–S148. doi: https://doi.org/10.1513/ANNALSATS.201802-128AW.

WHO, W.H.O.- (2018). *9 out of 10 People Worldwide Breathe Polluted Air, but More Countries Are Taking Action.9 out of 10 people worldwide breathe polluted air, but more countries are taking action*. Available at: https://www.who.int/news-room/detail/02-05-2018-9-out-of-10-people-worldwide-breathe-polluted-air-but-more-countries-are-taking-action.

Winterbottom, C.J., Shah, R.J., Patterson, K.C., Kreider, M.E., Panettieri, R.A., Rivera-Lebron, B., … Christie, J.D. (2018). Exposure to Ambient Particulate Matter Is

Associated With Accelerated Functional Decline in Idiopathic Pulmonary Fibrosis. *Chest* **153**(5):1221. doi: https://doi.org/10.1016/J.CHEST.2017.07.034.

Wolffs, K.L., Mansfield, B., Bruce, R.T., Huang, P., Schepelmann, M., Brennan, S.C., … Riccardi, D. (2020). Calcium-sensing receptor antagonism as a novel therapeutic for pulmonary fibrosis. *medRxiv*:2020.03.12.20034751. doi: https://doi.org/10.1101/2020.03.12.20034751.

World Health Organization (2013). *Health Effects of Particulate Matter.http://www.euro.who.int/pubrequest*. Available at: http://www.euro.who.int/pubrequest [Accessed: 25 April 2022].

World Heath Organisation (2018). *Ambient Air Pollution*. Available at: https://www.who.int/teams/environment-climate-change-and-health/air-quality-and-health/ambient-air-pollution [Accessed: 28 May 2022].

Wu, J.-Z., Ge, D.-D., Zhou, L.-F., Hou, L.-Y., Zhou, Y. and Li, Q.-Y. (2018). Effects of particulate matter on allergic respiratory diseases. *Chronic Diseases and Translational Medicine* **4**(2):95–102. doi: https://doi.org/10.1016/j.cdtm.2018.04.001.

Wu, X., Verschut, V., Woest, M.E., Ng-Blichfeldt, J.P., Matias, A., Villetti, G., … Kistemaker, L.E.M. (2021). Rho-Kinase 1/2 Inhibition Prevents Transforming Growth Factor-β-Induced Effects on Pulmonary Remodeling and Repair. *Frontiers in Pharmacology* **11**:2363. doi: https://doi.org/10.3389/FPHAR.2020.609509/BIBTEX.

Yamaguchi, T., Kifor, O., Chattopadhyay, N., Bai, M. and Brown, E.M. (1998). Extracellular calcium (Ca2+o)-sensing receptor in a mouse monocyte-macrophage cell line (J774): potential mediator of the actions of Ca2+o on the function of J774 cells. *Journal of Bone and Mineral Research* **13**(9):1390–1397. doi: https://doi.org/10.1359/JBMR.1998.13.9.1390.

Yamaguchi, T., Olozak, I., Chattopadhyay, N., Butters, R.R., Kifor, O., Scadden, D.T. and Brown, E.M. (1998). Expression of Extracellular Calcium (Ca2+o)-Sensing Receptor in Human Peripheral Blood Monocytes. *Biochemical and Biophysical Research Communications* **246**(2):501–506. doi: https://doi.org/10.1006/bbrc.1998.8648.

Yan, J., Lai, C.H., Lung, S.C.C., Chen, C., Wang, W.C., Huang, P.I. and Lin, C.H. (2017). Industrial PM 2.5 cause pulmonary adverse effect through RhoA/ROCK pathway. *The Science of the Total Environment* **599**–**600**:1658–1666. doi: https://doi.org/10.1016/J.SCITOTENV.2017.05.107.

Yang, X., Zhang, Y., Zhan, X., Xu, Xuchen, Li, S., Xu, Xuefeng, … Chen, Z. (2021). Particulate matter exposure is highly correlated to pediatric asthma exacerbation. *Aging (Albany NY)* **13**(13):17818. doi: https://doi.org/10.18632/AGING.203281.

Yarova, P.L., Davies, C., Price, S.A., Huang, Q., Graca, J.A., Maleki-toyserkani, S., … Prakash, Y.S. (2016). Inhaled Calcilytics : Effects on Airway Inflammation and Remodeling. *Respiratory Drug Delivery*:1–12.

Yarova, P.L., Huang, P., Schepelmann, M.W., Bruce, R., Ecker, R., Nica, R., … Riccardi, D. (2021). Characterization of Negative Allosteric Modulators of the Calcium-Sensing Receptor for Repurposing as a Treatment of Asthma. *Journal of Pharmacology and Experimental Therapeutics* **376**(1):51–63. doi: https://doi.org/10.1124/JPET.120.000281.

Yarova, P.L., Huang, P., Schepelmann, M.W., Bruce, R., Ecker, R., Nica, R., … Riccardi, D. (2020). Characterisation of negative allosteric modulators of the calcium-sensing receptor, CaSR, for repurposing as a treatment for asthma . *Journal of Pharmacology and Experimental Therapeutics*:JPET-AR-2020-000281. doi: https://doi.org/10.1124/jpet.120.000281.

Yarova, P.L., Stewart, A.L., Sathish, V., Britt, R.D., Thompson, M.A., Lowe, A.P.P., … Riccardi, D. (2015). Calcium-sensing receptor antagonists abrogate airway hyperresponsiveness and inflammation in allergic asthma. *Science Translational Medicine* **7**(284):284ra58. doi: https://doi.org/10.1126/scitranslmed.aaa0282.

Ying, S., O'Connor, B., Ratoff, J., Meng, Q., Fang, C., Cousins, D., … Corrigan, C.J. (2008). Expression and cellular provenance of thymic stromal lymphopoietin and chemokines in patients with severe asthma and chronic obstructive pulmonary disease. *Journal of Immunology* **181**(4):2790–2798. doi: https://doi.org/10.4049/JIMMUNOL.181.4.2790.

Ying, S., O'Connor, B., Ratoff, J., Meng, Q., Mallett, K., Cousins, D., … Corrigan, C. (2005). Thymic stromal lymphopoietin expression is increased in asthmatic airways and correlates with expression of Th2-attracting chemokines and disease severity. *Journal of Immunology* **174**(12):8183–8190. doi: https://doi.org/10.4049/JIMMUNOL.174.12.8183.

Yokoyama, K., Shimazaki, R., Fukagawa, M., Akizawa, T., Maeda, Y., Ueki, K., … Ogawa, H. (2019). Long-Term Efficacy and Safety of Evocalcet in Japanese Patients with Secondary Hyperparathyroidism Receiving Hemodialysis. *Scientific Reports 2019 9:1* **9**(1):1–11. doi: https://doi.org/10.1038/s41598-019-42017-z.

Yu, Y.R.A., O'Koren, E.G., Hotten, D.F., Kan, M.J., Kopin, D., Nelson, E.R., … Gunn, M.D. (2016). A Protocol for the Comprehensive Flow Cytometric Analysis of Immune Cells in Normal and Inflamed Murine Non-Lymphoid Tissues. *PLOS ONE* **11**(3):e0150606. doi: https://doi.org/10.1371/JOURNAL.PONE.0150606.

Zanin, S., Lidron, E., Rizzuto, R. and Pallafacchina, G. (2019). Methods to Measure Intracellular Ca 2+ Concentration Using Ca 2+-Sensitive Dyes. *Methods in Molecular Biology* **1925**:43–58. doi: https://doi.org/10.1007/978-1-4939-9018-4_4.

Zhai, T.Y., Cui, B.H., Zou, L., Zeng, J.Y., Gao, S., Zhao, Q., … Sun, Y.H. (2017). Expression and Role of the Calcium-Sensing Receptor in Rat Peripheral Blood Polymorphonuclear Neutrophils. *Oxidative Medicine and Cellular Longevity* **2017**. doi: https://doi.org/10.1155/2017/3869561.

Zhang, C., Qin, S., Qin, L., Liu, L., Sun, W., Li, X., … Wang, X. (2016). Cigarette smoke extract-induced p120-mediated NF-κB activation in human epithelial cells is dependent on the RhoA/ROCK pathway. *Scientific Reports 2016 6:1* **6**(1):1–12. doi: https://doi.org/10.1038/srep23131.

Zhang, F., Ma, H., Wang, Z.L., Li, W.H., Liu, H. and Zhao, Y.X. (2020). The PI3K/AKT/mTOR pathway regulates autophagy to induce apoptosis of alveolar epithelial cells in chronic obstructive pulmonary disease caused by PM2.5 particulate matter. *The Journal of International Medical Research* **48**(7). doi: https://doi.org/10.1177/0300060520927919.

Zhang, L., Ji, T., Wang, Q., Meng, K., Zhang, R., Yang, H., … Jiao, J. (2017). Calcium-Sensing Receptor Stimulation in Cultured Glomerular Podocytes Induces TRPC6-Dependent Calcium Entry and RhoA Activation. *Cellular Physiology and Biochemistry* **43**(5):1777–1789. doi: https://doi.org/10.1159/000484064.

Zhang, M.J., Ntranos, V. and Tse, D. (2020). Determining sequencing depth in a single-cell RNA-seq experiment. *Nature* **11**(1):1–11. doi: https://doi.org/10.1038/s41467-020-14482-y.

Zhang, Y., Wang, Z., Cao, Y., Zhang, L., Wang, G., Dong, F., … Su, S. (2021). The effect of consecutive ambient air pollution on the hospital admission from chronic obstructive pulmonary disease in the Chengdu region, China. *Air Quality, Atmosphere and Health* **14**(7):1049–1061. doi: https://doi.org/10.1007/S11869-021-00998-9/FIGURES/5.

Zhao, W., Zhang, Z., Zheng, L., You, C., Chi, H., Zhang, T. and Xu, G. (2020). Calcium-sensing receptor activating ERK1/2 and PI3K-Akt pathways to induce the proliferation of osteosarcoma cells. *Clinical and Experimental Pharmacology & Physiology* **47**(3):517–519. doi: https://doi.org/10.1111/1440-1681.13209.

Zheng, R., Tao, L., Jian, H., Chang, Y., Cheng, Y., Feng, Y. and Zhang, H. (2018). NLRP3 inflammasome activation and lung fibrosis caused by airborne fine particulate matter. *Ecotoxicology and Environmental Safety* **163**:612–619. doi: https://doi.org/10.1016/J.ECOENV.2018.07.076.

Zheng, X.Y., Ding, H., Jiang, L.N., Chen, S.W., Zheng, J.P., Qiu, M., … Guan, W.J. (2015). Association between Air Pollutants and Asthma Emergency Room Visits and Hospital Admissions in Time Series Studies: A Systematic Review and Meta-Analysis. *PLOS ONE* **10**(9):e0138146. doi: https://doi.org/10.1371/JOURNAL.PONE.0138146.

Zhou, M.Y., Cheng, L., Chen, L., Gu, Y.J. and Wang, Y. (2021). Calcium-sensing receptor in the development and treatment of pulmonary hypertension. *Molecular Biology Reports* **48**(1):975–981. doi: https://doi.org/10.1007/S11033-020-06065-3.

Ziegelstein, R.C., Xiong, Y., He, C. and Hu, Q. (2006). Expression of a functional extracellular calcium-sensing receptor in human aortic endothelial cells. *Biochemical and Biophysical Research Communications* **342**(1):153–163. doi: https://doi.org/10.1016/J.BBRC.2006.01.135.

Zimmermann, J., Radbruch, A. and Chang, H.D. (2015). A Ca2+ concentration of 1.5 mM, as present in IMDM but not in RPMI, is critical for maximal response of Th cells to PMA/ionomycin. *European Journal of Immunology* **45**(4):1270. doi: https://doi.org/10.1002/EJI.201445247.

A

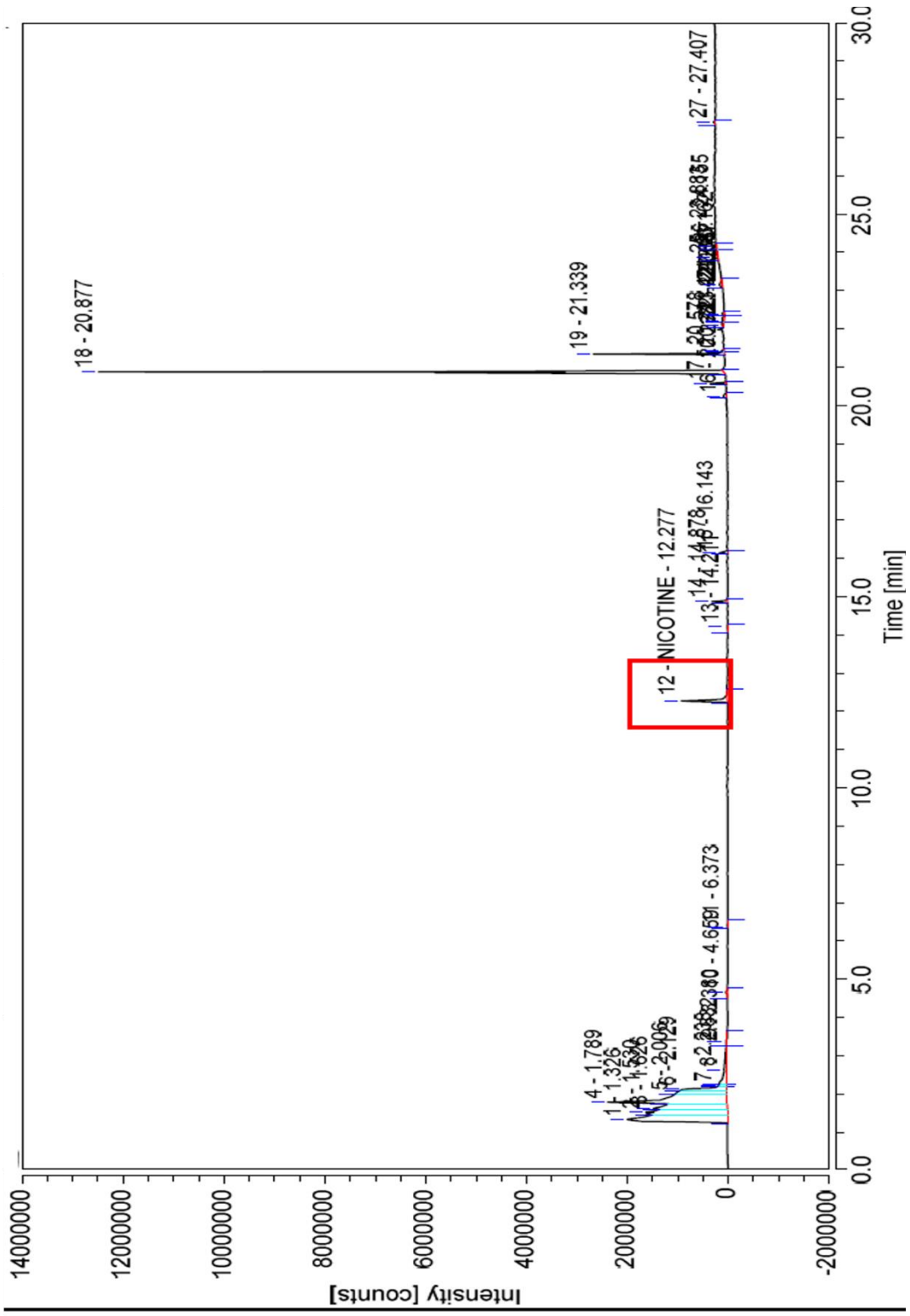
Intensity [counts]
14000000
12000000
10000000
8000000
6000000
4000000
2000000
0
-2000000
0.0
5.0
10.0
15.0
20.0
25.0
30.0
Time [min]
18 - 20.877
19 - 21.339
27 - 27.407
12 - NICOTINE - 12.277
16.143
4 - 1.789
1.326
6.373

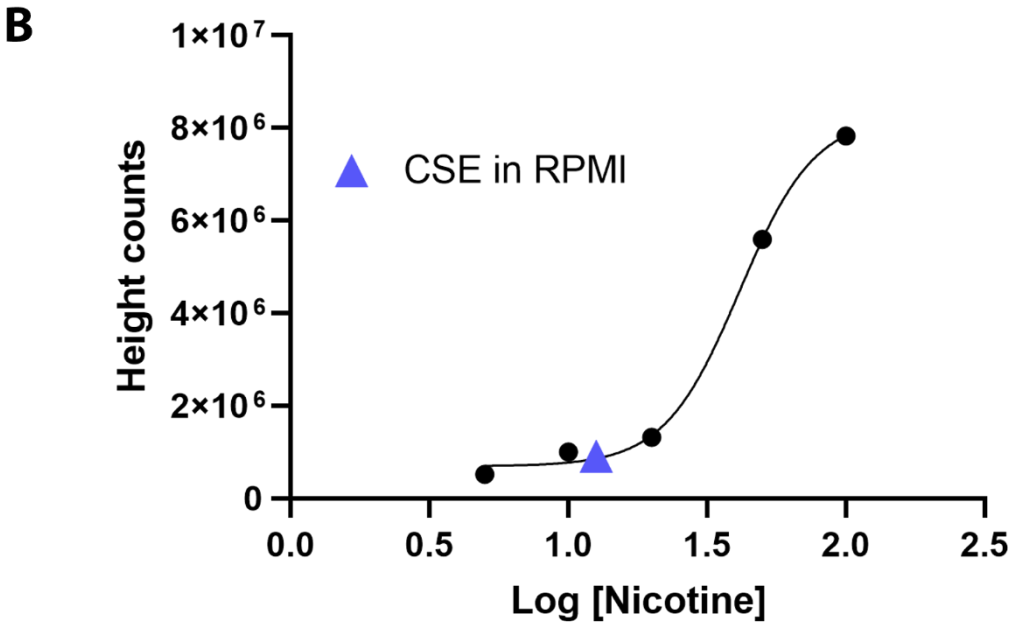

Appendix 1: Cigarette Smoke Extract (CSE) generated in the lab contains nicotine. Representative image of presence of nicotine in CSE extracted in-house into RPMI culture medium then solid phase micro extraction (SPME) of CS extracted into RPMI cell culture medium followed by gas chromatography and mass spectrometry (GC/MS), using the Thermo Scientific™ TSQ™ 8000 GC/MS machine. The chromatogram demonstrates the wide range of components present in CSE, shown y peaks at specific retention times (time taken from sample injection to the end of the GC run), where the height of the peak represents the response of the detector within the GC/MS machine (intensity counts, y axis). Nicotine contained with CSE had a retention time of 12.277 minutes where the corresponding peak is shown in the red box within the figure (A). Increasing nicotine concentration (5-100 ng/ml, x axis) resulted in increased Height counts (y axis, representing amounts of compounds measured within CSE). Standard curves were generated from known concentrations of nicotine prepared in RPMI and data were plotted with a sigmoidal non-linear regression fit where unknown values of nicotine present in CSE were interpolated from the graph using the Chromeleon Software (Thermofisher Scientific). An average of 9.3005 ng/ml nicotine was contained within the CSE generated in house from 2 separate SPME and GC/MS experimental runs (purple triangle) (B).

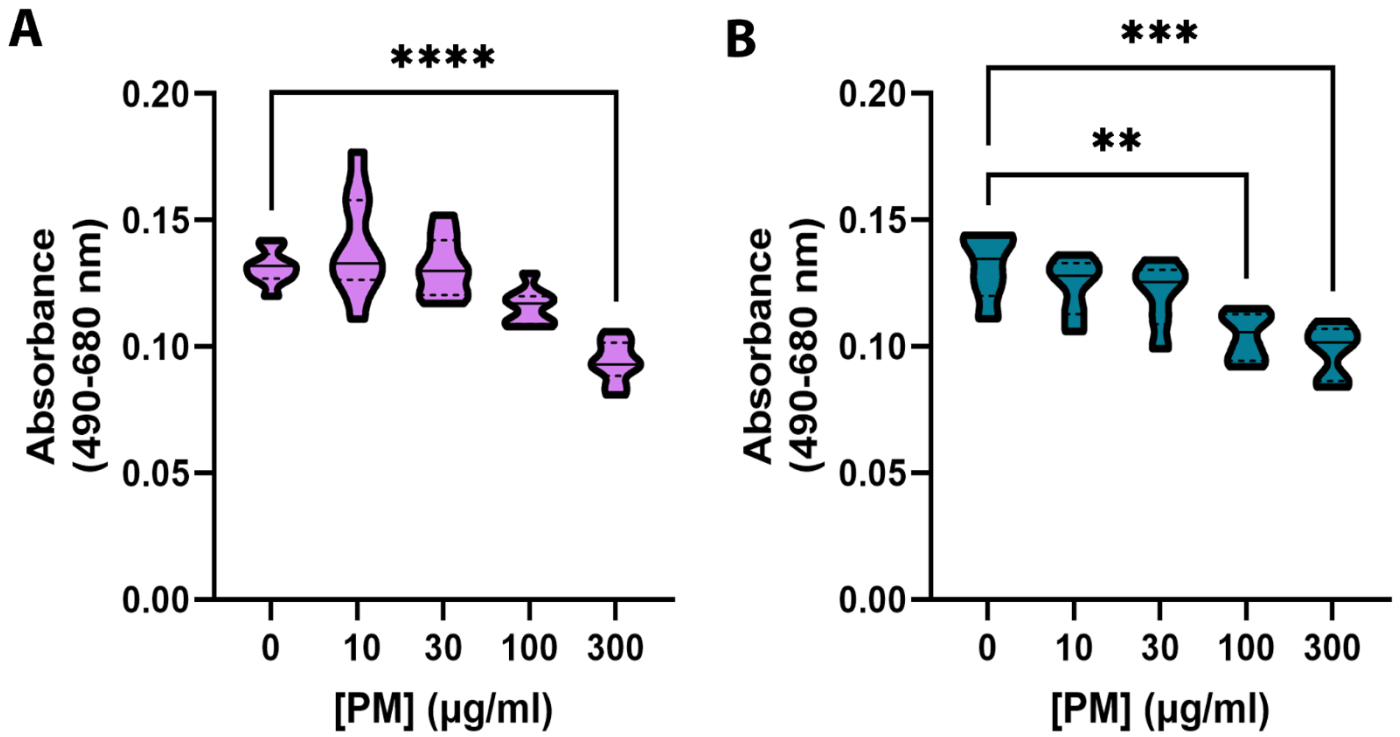
A
****
0.20
0.15
0.10
0.05
0.00
Absorbance (490-680 nm)
0
10
30
100
300
[PM] (µg/ml)
B
***
**
0.20
0.15
0.10
0.05
0.00
Absorbance (490-680 nm)
0
10
30
100
300
[PM] (µg/ml)

Appendix 2: Particulate matter (PM) exposure to human embryonic kidney cells stably expressing the human calcium-sensing receptor (HEK-CaSR) appears to enhance HEK-CaSR viability, in a concentration-dependent manner. HEK-CaSR cells exposed to PM for 4 (A) and 24 hrs (B) results in a significant reduction in release of lactate dehydrogenase (LDH), used as an indicator of cytotoxicity. Data presented as violin plots where the solid line within the plot is the median and dotted lines within the plot are the upper and lower quartiles. N=3 p**** (0 vs 300) in 4hr = <0.0001, p** (0 vs 100) in 24hr = 0.0029 and p*** (0 vs 300) = 0.0003. One way ANOVA with Tukey's MC test

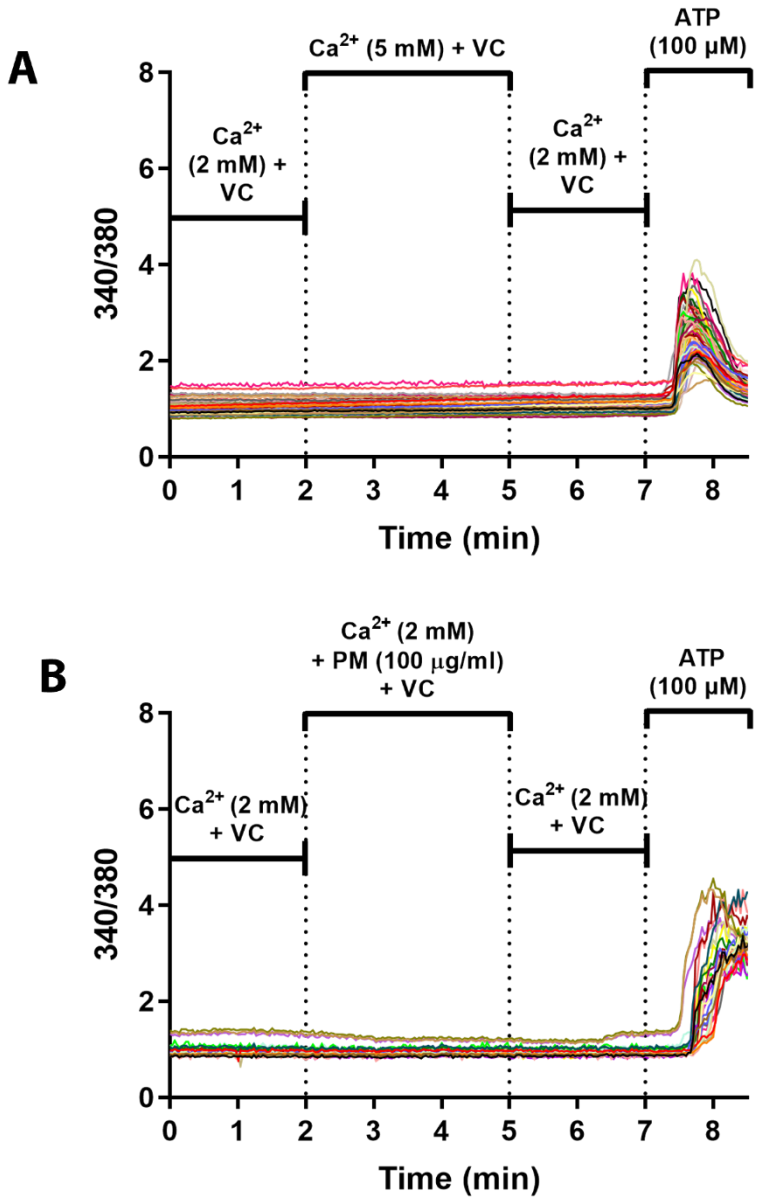

Appendix 3: Intracellular calcium mobilisation is not affected upon exposure to calcium-sensing receptor (CaSR) agonists in normal human bronchial epithelial cells (NHBECs). Representative traces of NHBECs loaded with the Ca^{2+}-sensitive fluorescent dye, Fura-2AM to measure changes in intracellular Ca^{2+} concentration as one of the biological readouts for CaSR activation. In all experiments, NHBECs were acutely exposed to extracellular Ca^{2+} (5 mM) in Vehicle Control (VC, 0.01% DMSO). At the end of each experiment, NHBECs were stimulated with 100µM ATP, a positive control for cell viability and proper functioning of the G-protein coupled receptor machinery. N=3 (A) and N=2 (B) per trace and n=29-61 cells per treatment condition.

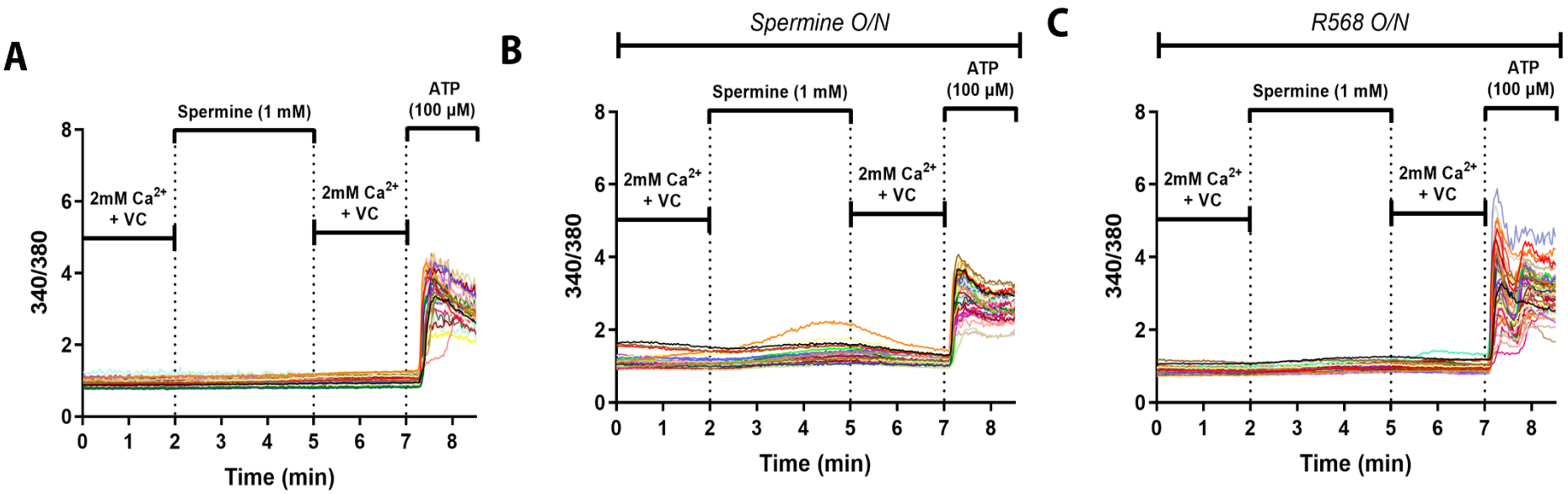

Appendix 4: Pharmacochaperoning the calcium-sensing receptor (CaSR) to the plasma membrane of normal human bronchial epithelial cells (NHBECs) does not enhance spermine induced intracellular calcium mobilisation. Representative traces of NHBECs loaded with the Ca^{2+}-sensitive fluorescent dye, Fura-2AM to measure changes in intracellular Ca^{2+} concentration as one of the biological readouts for CaSR activation. Exposure of NHBECs to spermine (1 mM) induces no alterations to intracellular Ca^{2+} levels (A). Pharmacochaperoning the CaSR using overnight exposure of NHBECs to spermine (100 µM, B) or a positive allosteric modulator at the CaSR (R568, 100 nM, C), does not alter potential of spermine-induced changes to intracellular Ca^{2+} levels. In all experiments, NHBECs were acutely exposed to spermine (1 mM in 0.01% DMSO). At the end of each experiment, NHBECs were stimulated with 100µM ATP, a positive control for cell viability and proper functioning of the G-protein coupled receptor machinery. N=3 per treatment condition and n=22-56 cells per treatment condition.

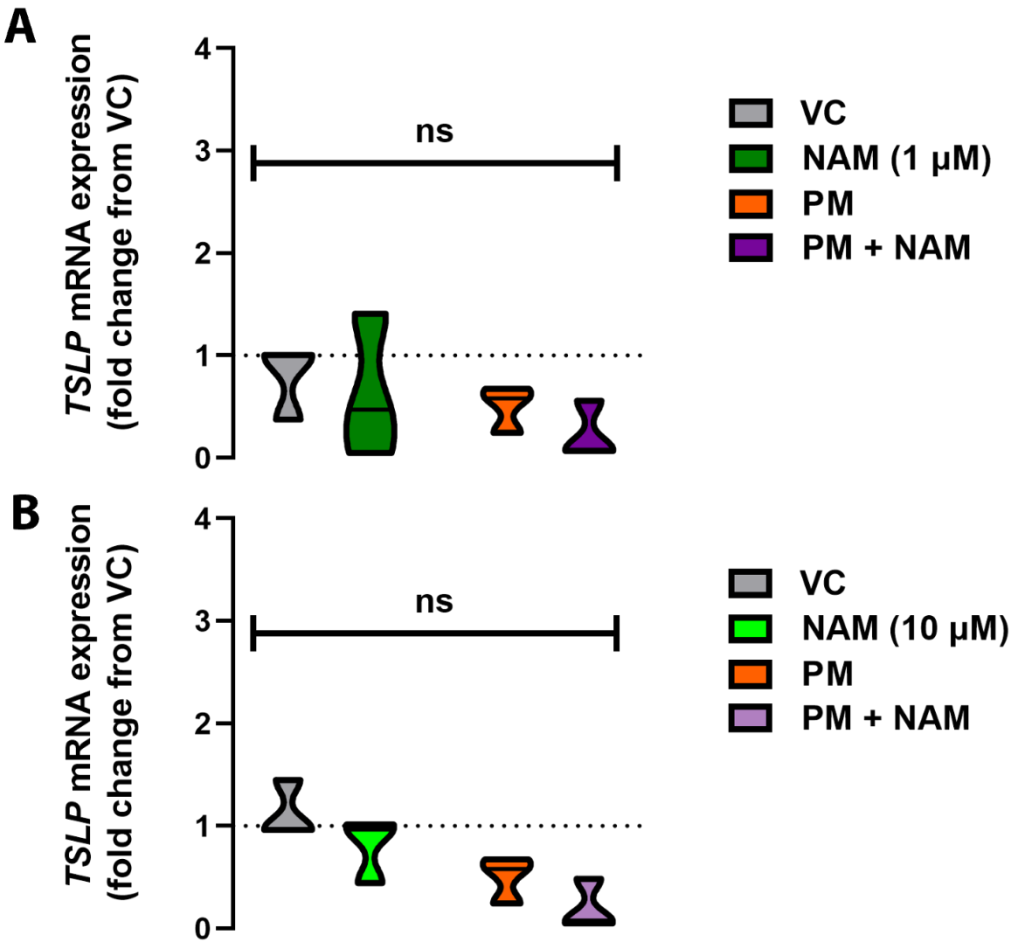

Appendix 5: Exposure of basal human bronchial epithelial cells (NHBECs) to urban particulate matter (PM) has no effect on mRNA expression of thymic stromal lymphopoietin (TSLP). 4hr treatment of HBECs with PM (50 µg/ml) ± negative allosteric modulator at the calcium-sensing receptor (NAM, NPS2143) at 1 µM (A) or 10 µM (B) induces no alterations to TSLP mRNA expression. Data are represented as violin plots with the solid line representing the median expression from N=3 NHBEC donors, analysed by 2-way ANOVA and Sidak's Multiple Comparisons Test where ns=not significant.

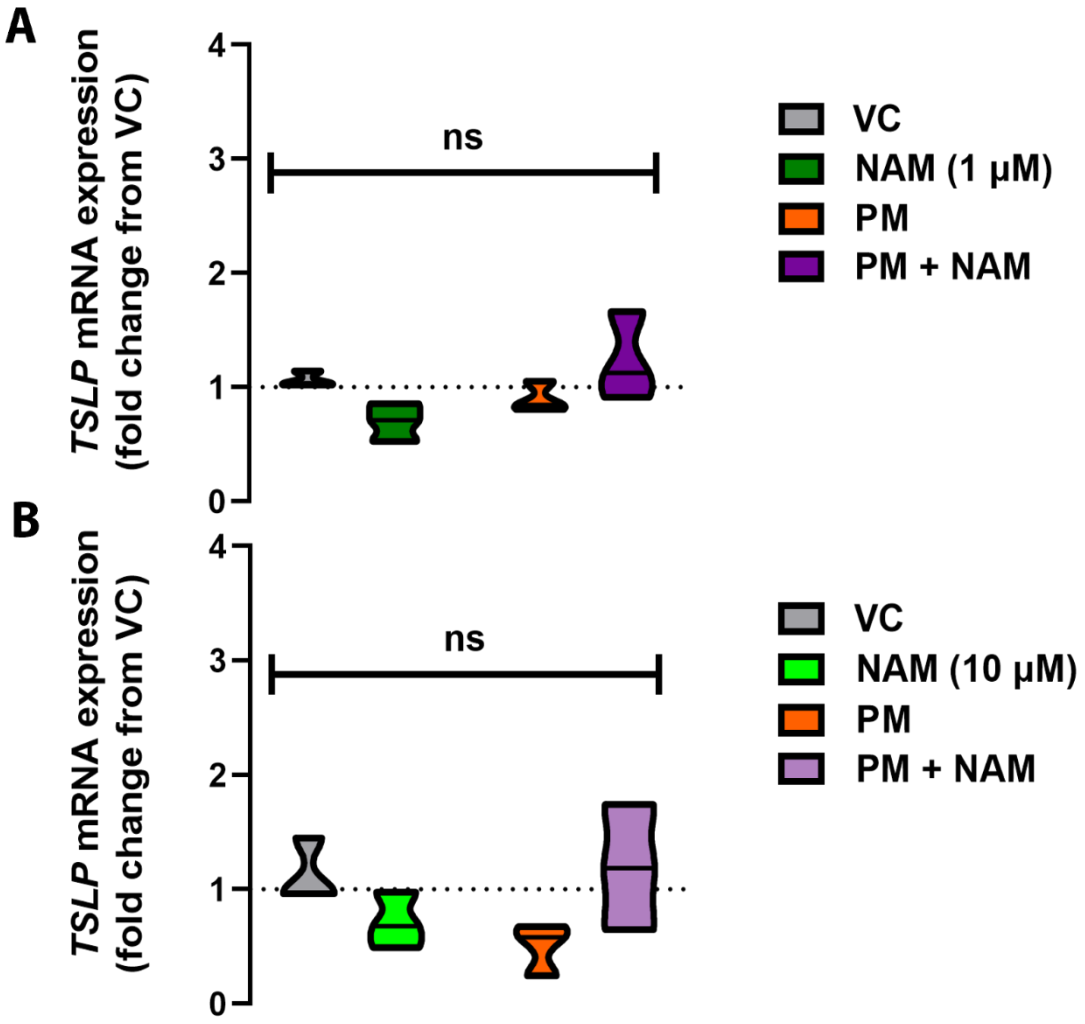

Appendix 6: Exposure of basal human bronchial epithelial cells (NHBECs) to urban particulate matter (PM) has no effect on mRNA expression of thymic stromal lymphopoietin (TSLP). 24hr treatment of HBECs with PM (50 µg/ml) ± negative allosteric modulator at the calcium-sensing receptor (NAM, NPS2143) at 1 µM (A) or 10 µM (B) induces no alterations to TSLP mRNA expression. Data represents 2^ΔΔCT as fold change (dotted line at 1 = no change). Data are represented as violin plots with the solid line representing the median expression from N=3 NHBEC donors, analysed by 2-way ANOVA and Sidak's Multiple Comparisons Test where ns=not significant.

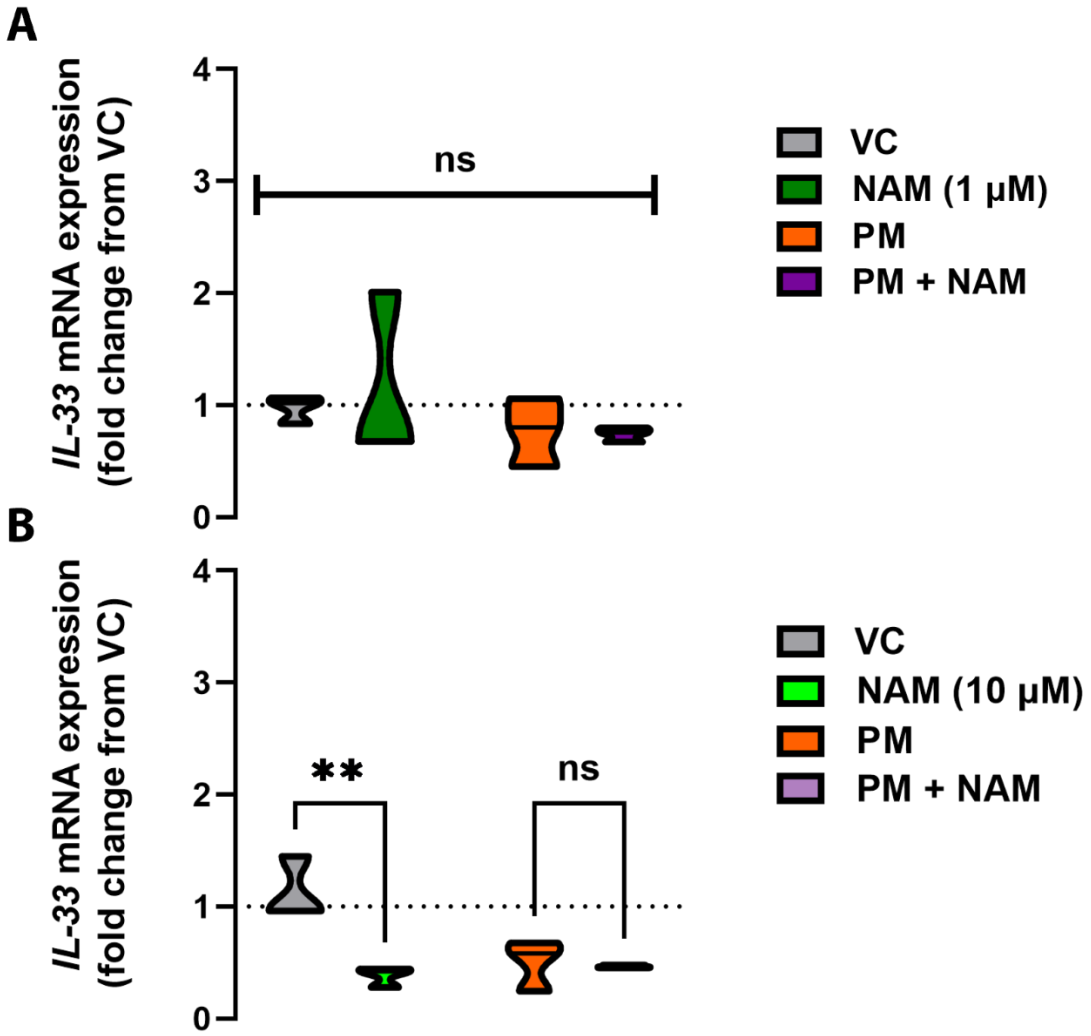

Appendix 7: Exposure of basal human bronchial epithelial cells (NHBECs) to urban particulate matter (PM) has no effect on mRNA expression of interleukin (IL)-33, however, a negative allosteric modulator at the calcium-sensing receptor (CaSR) induces a significant decrease in IL-33 mRNA expression. 4hr treatment of HBECs with PM (50 µg/ml) ± NAM (NPS2143) at 1 µM (A) induces no alterations to IL-33 mRNA expression. However, treatment with 10 µM NAM (B), induces a significant decrease in IL-33 mRNA expression. Data represents 2^ΔΔCT as fold change (dotted line at 1 = no change). Data are represented as violin plots with the solid line representing the median expression from N=3 NHBEC donors, analysed by 2-way ANOVA and Sidak's Multiple Comparisons Test where ** p=0.0024 and ns=not significant.

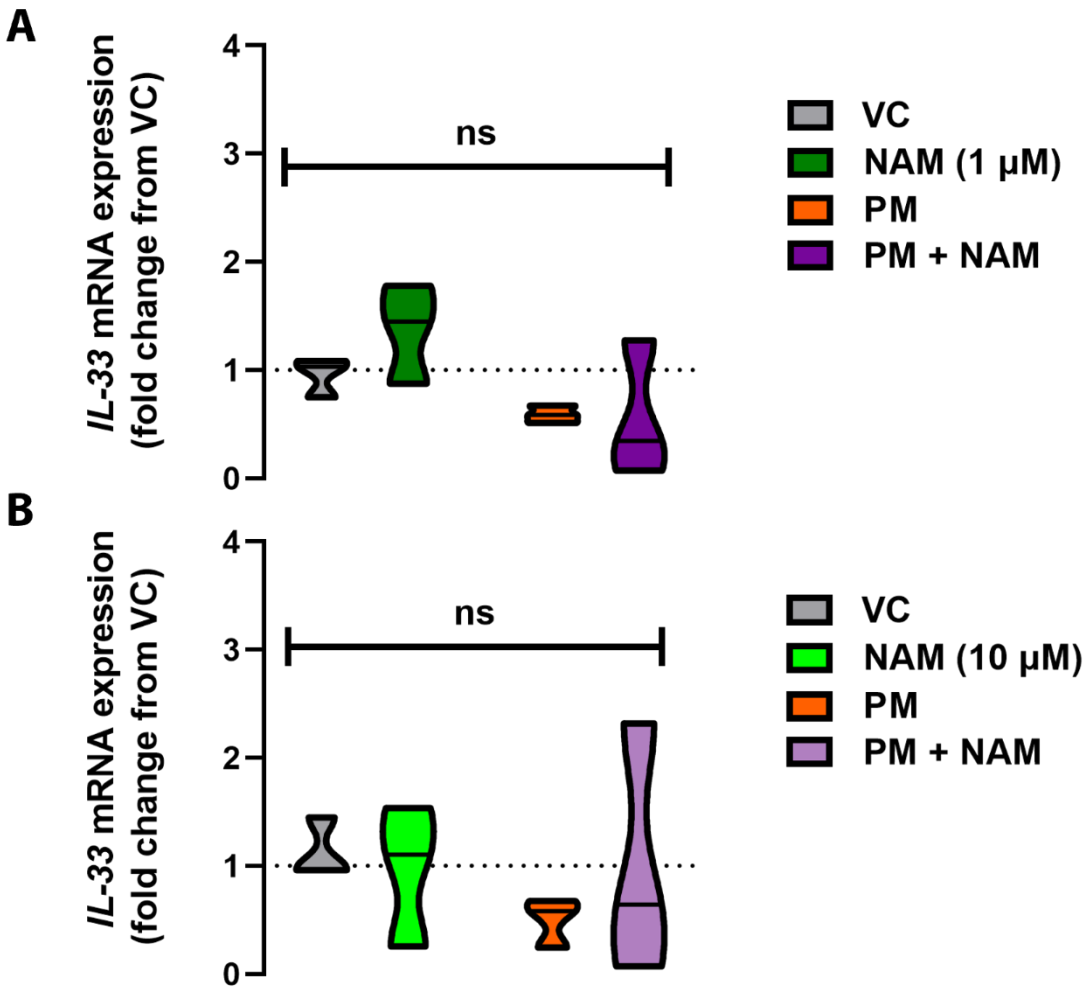

Appendix 8: Exposure of basal human bronchial epithelial cells (NHBECs) to urban particulate matter (PM) has no effect on mRNA expression of interleukin (IL)-33. 24hr treatment of HBECs with PM (50 µg/ml) ± NAM (NPS2143) at 1 µM (A) or 10 µM (B) induces no alterations to IL-33 mRNA expression. Data represents 2^ΔΔCT as fold change (dotted line at 1 = no change). Data are represented as violin plots with the solid line representing the median expression from N=3 NHBEC donors, analysed by 2-way ANOVA and Sidak's Multiple Comparisons Test where ns=not significant.

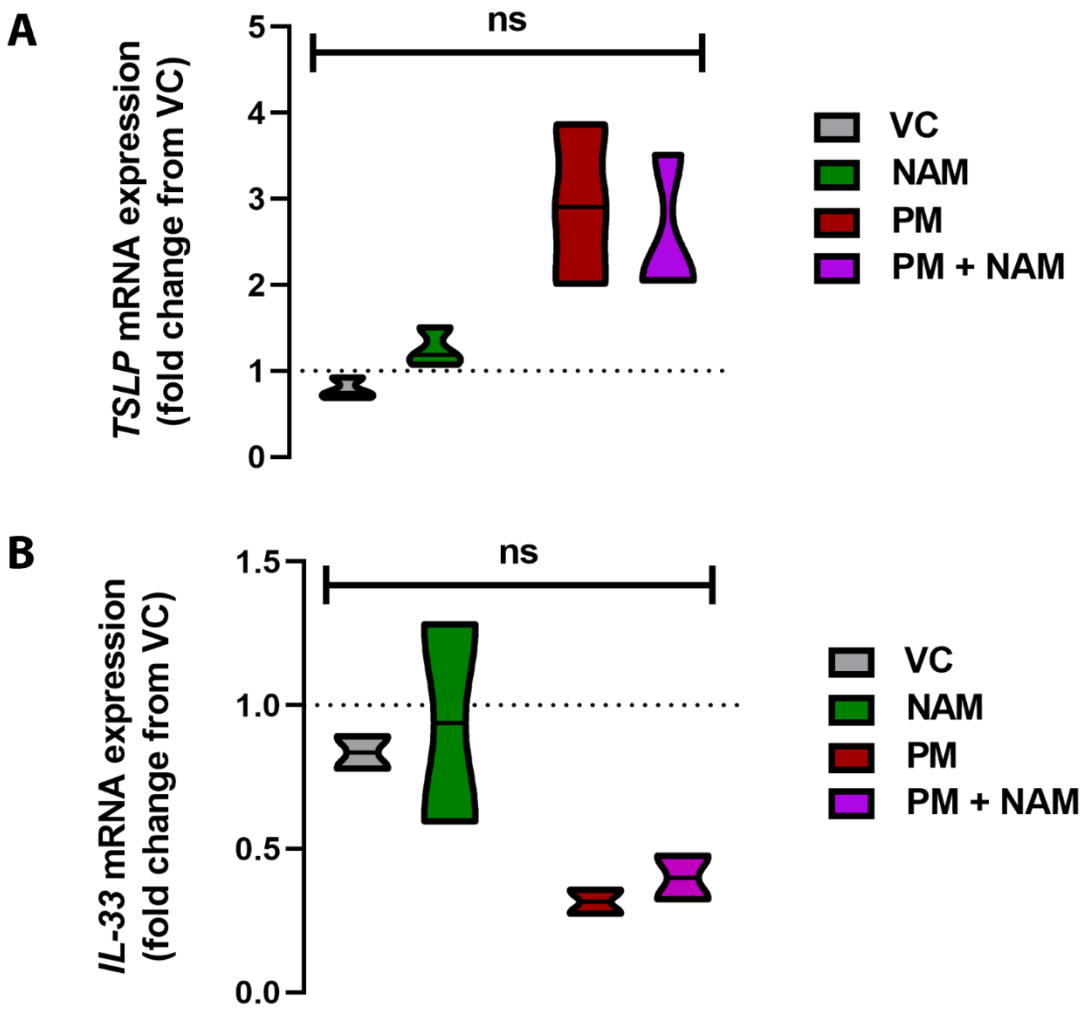

Appendix 9 Urban particulate matter (PM) exposure to submerged basal human bronchial epithelial cells (NHBECs) induces no significant alterations to alarmin mRNA expression. Exposure of NHBECs to UPM (100 µg/ml) for 24hrs results in no significant alterations to thymic stromal lymphopoietin (TSLP) or interleukin (IL)-33 (alarmin) mRNA expression. Data are represented as violin plots and within each plot, solid line represents the median and dotted lines represent the upper and lower quartiles. Data represents 2^ΔΔCT as fold change (dotted line at 1 = no change) and analysed with 2-way ANOVA & Sidak's Multiple Comparisons test from N=3 donors where ns=not significant.

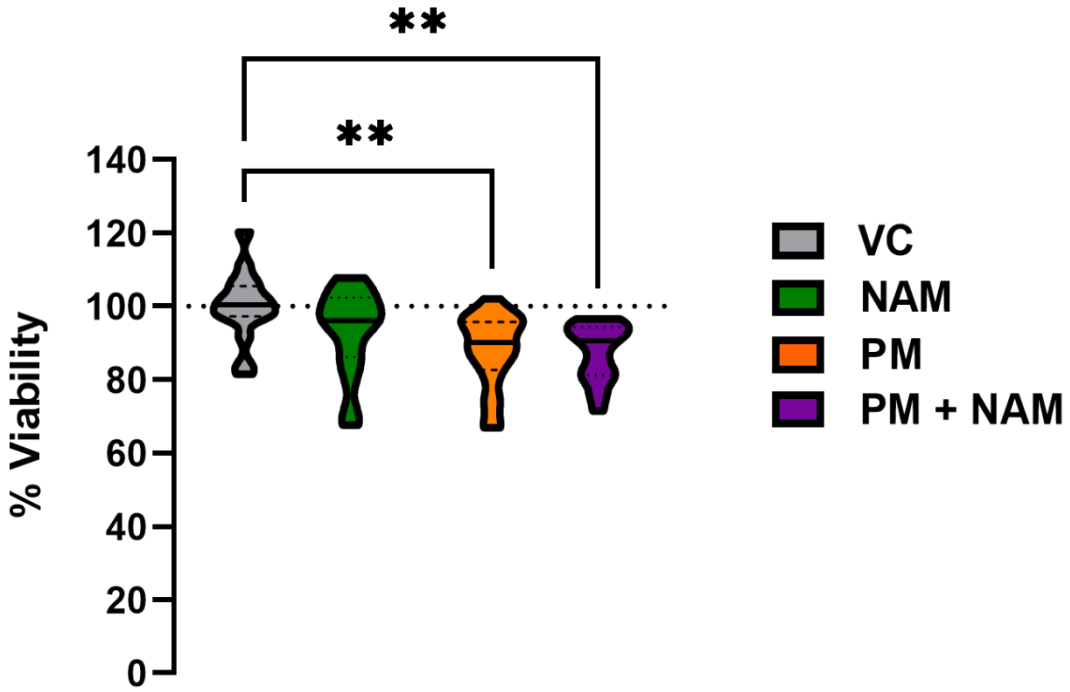

Appendix 10: Urban Particulate Matter (PM) exposure induces a significant decrease in viability of submerged basal human bronchial epithelial cells (NHBECs). 24hr exposure of NHBECs to PM (100 µg/ml) ± negative allosteric modulator at the calcium-sensing receptor (NAM, NPS2143, 1 µM) significantly decreases viability of NHBECs, whereas the vehicle control (VC, 0.01% DMSO) or NAM alone, induced no significant changes. Viability was measured using the Vialight assay (Lonza) which measures ATP levels in lysed cells from each treatment condition where data are expressed as a percentage of untreated NHBECs (cell culture medium only, set at 100% within each experiment) from NHBECs from N=3 donors. Data were analysed by analysed by 2-way ANOVA with Tukey multiple comparisons test. ** (0.01% DMSO vs. PM + 0.01% DMSO) p=0.0020 and ** (0.01% DMSO vs. PM + NAM) p=0.0014.

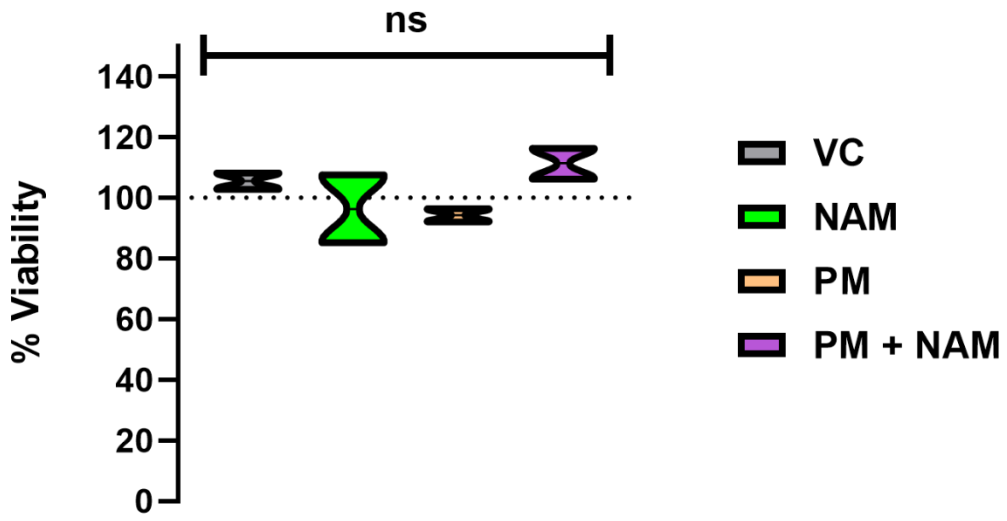

Appendix 11: Urban Particulate Matter (PM) exposure induces no significant alterations to viability of primary alveolar macrophages (AMs). 6hr exposure of AMs to vehicle control (VC, 0.01% DMSO), negative allosteric modulator at the calcium-sensing receptor (NAM, NPS2143, 5 μM) and PM (30 μg/ml) ± NAM, induced no significant alterations to AM viability. Viability was measured using the Vialight assay (Lonza) which measures ATP levels in lysed cells from each treatment condition where data are expressed as a percentage of untreated AMs (cell culture medium only, set at 100% within each experiment) from AMs from N=4 donors. Data were analysed by analysed by 2-way ANOVA with Tukey multiple comparisons test, where ns=not significant.

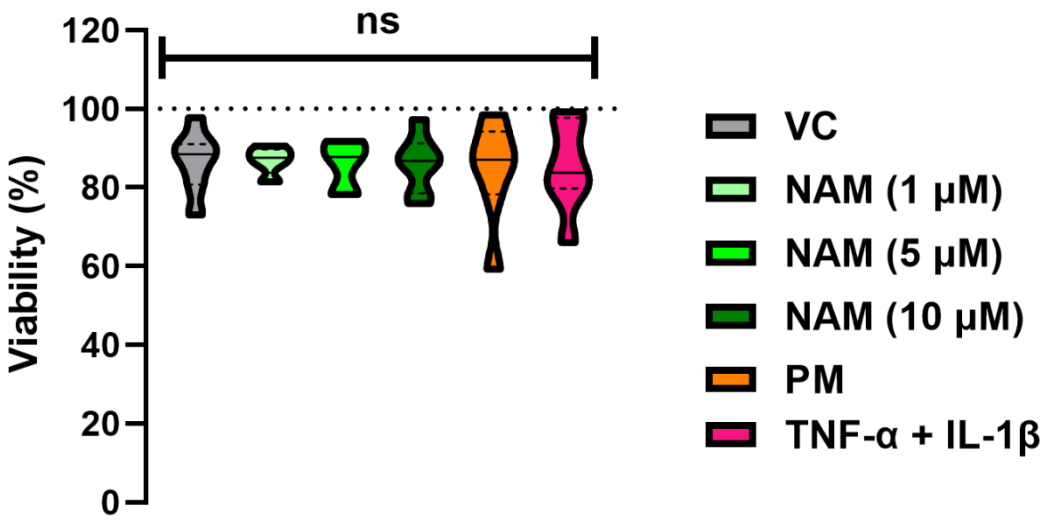

Appendix 12: Urban Particulate Matter (PM), negative allosteric modulator at the calcium-sensing receptor (NAM) or tumour necrosis factor-α (TNF-α) and interleukin (IL)-1ß exposure induces no significant alterations to viability of monocyte-derived dendritic cells (DCs). 24 hr exposure of DCs to vehicle control (VC, 0.01% DMSO), NAM, NPS2143, 1 5 and 10 µM), PM (10 µg/ml) and TNF-α and IL-1ß, induced no significant alterations to DC viability. % Viability was obtained by taking the % of live cells in each condition, gated by the viability dye Alexafluor 780. Data are expressed as a percentage of untreated DCs (cell culture medium only, set at 100% within each experiment) from AMs from N=4 donors. Data were analysed by analysed by One-way ANOVA with Tukey multiple comparisons test, where ns=not significant.